Two Novel Assays for the Readout of Total and Active FoxO1 in Single Cells

John Simpson

Doctor of Philosophy

—

Institute of Chemical Biology, Department of Chemistry

—

Imperial College London

Abstract

COPD is the third most prevalent disease globally and is poorly diagnosed. Methods to better understand the proteomic markers and disease progression are highly sought after but pose a technical challenge. Current standards are relatively rudimentary and will often overlap with other diseases or environmental factors such as smoking. Analysis at the proteomic level is challenging and collection of patient samples is typically highly invasive, and the current tests provide poor levels of data economy. The ability to ask proteomic questions on any disease state at a highly accurate level is a key tool to develop for a greater understanding of these diseases. Furthermore, the ability to use non-invasively derived patient samples, and obtain reliable data, opens new avenues for rapid and safe patient analysis.

The MAC chip is quantitative single molecule sensitive protein assay which can accurately evaluate absolute protein copy number in single cells. This thesis shows the design of two new assays to analyse the FoxO1 transcription factor total copy number and active copy number subpopulation. The works shows the two assays being validated on 3 cell lines. Followed with optimisations to the assays mid-way through the project to ensure they are robust and reliable for use with patient samples. Building on the creation of these novel assays, the assays are multiplexed within the MAC chip device to provide in tandem readouts of total and active FoxO1 copy number in two patient sample types. This thesis demonstrates the use of the assays on lung resection tissues and then on non-invasive sputum samples. The sputum samples demonstrate the ability of the MAC chip to isolate specific cell types with 100% accuracy from highly heterogenous samples. The use of patient samples in general shows the feasibility of utilising highly accurate and data rich single cell techniques with clinical materials.

Declaration of Originality

All the work presented within is entirely my own with the following exceptions:

- The single molecule counting algorithms were written by Alastair Magness.
- The printing programs and MAC chip structures were designed by Alastair Magness.

Copyright Declaration

The copyright of this thesis rests with the author and is made available under a Creative Com-mons Attribution Non-Commercial No Derivatives licence. Researchers are free to copy, dis-tribute or transmit the thesis on the condition that they attribute it, that they do not use it for commercial purposes and that they do not alter, transform or build upon it. For any reuse or redistribution, researchers must make clear to others the licence terms of this work.

Acknowledgements

I would like to thank my supervisors for the opportunity to undertake this PhD, providing me an opportunity to make an ever so slight dent in the scientific field. I wish to express my deepest gratitude to Professor John Barnes and his group at the NHLI for their collaboration and kindness to allow access to their highly precious clinical samples. Without this collaboration and guidance this project would not have achieved half as much as it has. Thank you to the patients whom participated in these clinical trials who enabled this work.

Secondly, I wish to thank my friends and colleagues past and present, Alastair, Jim, Mike, Hugh, Max, Paul, Stuart and everyone else. Whose warm smiles, infinite kindness and most importantly full pints made the hard parts easier and the easy parts a joyful collection of memories. I could not have asked for a better group to battle the beast of chemical biology with. Thank you also to many others who are unnamed but were still of immeasurable help to me. I extend thanks to my two co-founders Alex and Rob where together we have founded a new venture, which I am excited to call my next journey. Thank you to my family also, who have always offered a warm meal and bed during the harder times. Lastly, I thank Kate, as she's pretty cool too, and more impressively has managed to cope with my stresses and hardest moments. I cannot thank these people and many more enough.

List of Abbreviations

Akt	Protein kinase B
APTES	(3-aminopropyl)triethoxysilane
ASMI	Average single molecule intensity
BNO	Baseline noise offset
BSA	Bovine serum albumin
CTC	Circulating tumour cell
DMEM	Dulbecco's Modified Eagle's Medium
DMSO	Dimethylsulfoxide
DNA	Deoxyribonucleic acid
ELISA	Enzyme-linked immunosorbent assay
EM-CCD	Electron multiplying charged coupled device
EpCAM	Epithelial cell adhesion molecule
ER	Estrogen receptor
FACS	Fluorescence activated cell sorting
FBS	Foetal bovine serum
FoxO	Forkhead Box Transcription Factor Protein O
GPTS	(3-glycidyloxypropyl)trimethoxysilane
IgG	Immunoglobulin G
JNK	c-Jun N-terminal kinases
K_D	Dissociation constant
LOD	Limit of detection
MAC chip	Microfluidic affinity capture chip
MCF7	Human estrogen receptor-positive breast cancer cell line

MST1	Macrophage-stimulating protein 1
NA	Numerical aperture
NES	Nuclear export domain
NLS	Nuclear localisation domain
PALM	Photoactivatable localisation microscopy
PBS	Phosphate buffered saline
PBSA	Bovine serum albumin in phosphate buffered saline
PCR	Polymerase chain reaction
PDMS	Polydimethylsiloxane
PEG	Polyethylene glycol
PI3K	Phosphoinositide 3-kinase
PTM	Post-translational modification
SDS	Sodium dodecyl sulphate
SDS-PAGE	SDS polyacrylamide gel electrophoresis
SIRT1	Sirtuin 1
SNR	Signal to noise ratio
SSC	Saline sodium citrate
TIRF	Total internal reflection fluorescence

Table of Contents

1. Introduction 17

1.1 Proteomics 17

1.2 The Single Cell Regime 19

1.2.1 Single Cell Analysis 21

1.3 Microfluidics 25

1.4 Fox Transcription Factor Proteins 26

1.5 FoxO Transcriptional Outputs 27

1.6 FoxO Regulatory Mechanisms 29

1.6.1 Phosphorylation Regulation by Insulin/IFG Signalling and Growth Factors 31

1.6.2 Phosphorylation Regulation by MST1 and JNK1 33

1.6.3 Dephosphorylation of FoxO to Permit Relocalisation Back into the Nucleus 34

1.6.4 Acetylation/Deacetylation by CBP, p300 and SIRT Proteins 34

1.6.5 Mono- and Polyubiquitination of FoxO Proteins 37

1.6.6 Hierarchy of PTMs That Lead to Complex Transcriptional Activities 38

1.7 FoxO DNA Binding 39

1.7.1 FoxO DNA Binding in Relation to Total vs Active Copy Number 42

1.8 Chronic Obstructive Pulmonary Disease 43

1.9 Chronic Obstructive Pulmonary Disease and FoxO1 45

1.10 Haploinsufficiency and the effect on Copy Number Experiments 47

1.11 Thesis Overview and Aims 48

2 Microfluidic Affinity Capture (MAC) Chip 50

2.1 MAC Chip Overview 50

2.2 Microfluidics Introduction 53

2.3 Surface Chemistry Introduction 54

2.3.1 Orientation of Capture Agents Using Surface Chemistries 55

2.4 Readout and Data Analysis using TIRF Microscopy 56

3 Methods 59
3.1 MAC Chip Experimental Overview 59
3.2 Design and Manufacture 59
3.2.2 MAC Chip Manufacture 60
3.2.3 Microarray Printing 62
3.2.4 Final Device Bonding of Microfluidic Architecture with Functionalised Coverslip 63
3.2.5 Device Filling and Cell Loading 64
3.2.6 Localisation Counting Algorithm 66
3.2.7 Non-congested Counting 68
3.2.8 Congested Counting 72
3.2.9 Data presentation 73
3.3 Cell Culture Techniques 73
3.3.1 Toledo Cell Line 73
3.3.2 MCF7 Cell Line 74
3.3.3 Beas-2b Cell Line 74
3.3.4 Lung Resection Culture 74
3.3.5 Sputum Freezing 74
3.4 Other Methods 75
3.4.1 Western Blot 75
3.4.2 Western Blot Imaging 75
3.4.3 Bulk Cell Lysis for Western Blots 75
3.4.4 Fluorescent Labelling of Antibodies 75
3.4.5 DNA Hybridisation 76
3.5 Patient Sample Specific Methods 76
3.5.1 Lung Resection Tissues 76
3.5.2 Sputum Processing and Cell Isolation 77
3.5.3 On-Chip Cell Selection and Sorting 78

3.6 Equipment and Vendor List.....80
4 Identification and characterisation of FoxO1 antibodies and Capture Agents.....82
4.1 Outline.....82
4.2 Introduction.....82
4.3 Validation Protocol.....85
4.4 Antibody Based Assay Development.....89
4.4.1 Antibody Conjugation Strategies.....89
4.4.2 Open Chip Validation Studies.....90
4.4.3 Bimolecular Binding Tests.....93
4.4.4 MAC Chip Calibration.....95
4.5 DNA Based Assay Development.....97
4.5.1 DNA Immobilisation Strategies.....100
4.5.2 Biotin modified Capture Agent Assay Development.....103
5 Validation of Assays Using Single Cell MAC Chip Experiments.....108
5.1 Outline.....108
5.2 Introduction.....108
5.3 Toledo Cell Line Antibody Studies.....109
5.3.1 DU1071 Basal FoxO1 Distributions.....109
5.3.2 ZSTK474 Treated Experiments with DU1071.....111
5.3.3 mAb5939 Basal FoxO1 Distributions.....113
5.3.4 ZSTK474 Treated Experiments with mAb5939.....115
5.3.5 Glucose Treated Experiments with mAb5939 + EP927Y Pair.....116
5.4 Toledo Cell Line DNA Capture Agent 7 Studies.....118
5.4.1 CA7 Basal FoxO1 Distributions.....119
5.4.2 ZSTK474 Treated Experiments with Capture Agent 7 + EP927Y Pair.....120
5.4.3 Glucose Treated Experiments with Capture Agent 7 + EP927Y pair.....122
5.5 MCF7 Cell Line Validation Studies.....124

5.5.1 mAb5939 + EP927Y Basal FoxO1 Distributions 125
5.5.2 ZSTK474 Treated Experiments with mAb5939 + EP927Y pair 126
5.5.3 Glucose Treated Experiments with mAb5939 + EP927Y Pair 128
5.6 MCF7 Cell Line DNA Capture Agent 7 + EP927Y Studies 129
5.6.1 Capture Agent 7 + EP927Y pair Basal FoxO1 Distributions 129
5.6.2 PI3K Inhibitor ZSTK474 Treated Experiments with Capture Agent 7 + EP927Y pair 131
5.6.3 Glucose Treated Experiments with Capture Agent 7 + EP927Y pair 132
5.7 Beas-2b Cell Line Validation Studies 133
5.7.1 Initial Basal Beas-2b mAb5939 + EP927Y Experiments 134
5.7.2 Glucose Treated Experiments with mAb5939 + EP927Y pair 136
5.7.3 Initial Basal Capture Agent 7 + EP927Y Pair Experiments 138
5.7.4 Glucose Treated Experiments with Capture Agent 7 + EP927Y pair 139
5.8 Discussion of Total and Active FoxO1 Cell Assay Validations 140
6 Assay Optimisation and Troubleshooting 142
6.1 Outline 142
6.2 Introduction 142
6.3 Analysis of Assay Reagents 147
6.4 Effects of the Reagent Concentrations on Assay Sensitivity 152
6.4.1 Increasing the Concentration of Printed Capture Agent 7 153
6.4.2 Increasing the Concentration of Printed mAb5939 155
6.4.3 Increasing the Concentration of Secondary EP927Y in the Capture Agent 7 Assay 156
6.4.4 Beas-2b Cell Validation Studies using 500 ng/mL EP927Y + CA7 Assay 159
6.4.5 Increasing the Concentration of Secondary EP927Y in the mAb5939 Assay 160
6.4.6 Beas-2b Cell Validation Studies using 500 ng/mL EP927Y + mAb5939 Assay 162
6.4.7 T-Test Validation of 50ng/mL EP927Y Assays 163
6.5 Discussions on Optimisation and Repair of the Total and Active FoxO1 Assays 165

7 Multiplexed Single Cell Total and Active FoxO1 Protein Expression Analysis in Lung Resection Tissues Using the MAC Chip 168
7.1 Overview 168
7.2 Introduction 168
7.3 Experimental Setup 169
7.3.1 Lung Tissue Resection and Processing 170
7.4 Results 171
7.4.1 mAb5939 Total FoxO1 Measurements 171
7.4.2 CA7 Active FoxO1 Measurements 173
7.4.3 Student T-test Analysis of the Multiplexed Assays 177
7.4.4 Discussion 178
8 Use of Clinically Derived Sputum in FoxO1 Multiplexed MAC Chip Analysis 180
8.1 Overview 180
8.2 Introduction 181
8.3 Experimental Set Up 182
8.4 Results 182
8.4.1 Optimising Cell Freezing Protocol 183
8.4.2 mAb5939 Total FoxO1 Measurements in Sputum Derived T-cells 184
8.4.3 CA7 Active FoxO1 Measurements in Sputum Derived T-cells. 186
8.4.4 Discussion of FoxO1 Measurements in Sputum Derived T-cells 189
8.4.5 mAb5939 Total FoxO1 Measurements in Sputum Derived Epithelial Cells 190
8.4.6 CA7 Active FoxO1 Measurements in Sputum Derived Epithelial Cells 192
8.4.7 Discussion of FoxO1 Measurements in Sputum Derived Epithelial Cells 195
9 Conclusions and Future Work 197
9.1 General Conclusions 197
9.2 Assay Design and Optimisation 197
9.3 Assay Validation 198

9.4 Lung Resection Studies 198
9.5 Sputum Sample Studies 199
9.6 Future Work 199
10 References 202
11 Appendix: 221
11.1 Antibody and DNA Capture Agents Sequences 221
11.2 Western Blots 222
11.3 Origin Overlap Function 223

List of Figures

Figure 1.1 Example of the loss of information with bulk average, ensemble measurements 21
Figure 1.2 Scheme showing the primary structure of FoxO proteins with their shared domain organisation containing the forkhead DBD, NLS, NES and TA domain in sequence. 27
Figure 1.3 The general range of FoxO transcriptional functions 28
Figure 1.4 Diagram showing some of the major players in FoxO control via post-translational modifications and the difficulty in assigning a determined effect to FoxO activity 30
Figure 1.5 Simple schematic showing FoxO1 inactivation by PI3K-Akt/SGK phosphorylation at T24, S256 and S319 31
Figure 1.6 Simple schematic showing the activation of FoxO1 by MST1 mediated phosphorylation at Ser212, Ser218, Ser234 and Ser235 33
Figure 1.7 Simple schematic showing the complex outcome of acetylation of FoxO1 by CBP at K242, K245 and K262. 34
Figure 1.8 Simple schematic showing the probable activation of FoxO1 pathways by SIRT1 at K242, K245 and K262 36
Figure 1.9 A figure demonstrating SIRT1 interaction and its function of switching FoxO1 output from apoptosis to stress resistance with FoxO deacetylation 36
Figure 1.10 Simple schematic showing polyubiquitination of FoxO1 leading to tagging for proteasome degradation by Skp2 complex association 37
Figure 1.11 Simple schematic showing the monoubiquitination sites of FoxO1 which augment the response of FoxO4 activity by USP7 at K199 and K211 38
Figure 1.12 A simplified scheme of the 'FoxO code' 39

Figure 1.13 A stereoview of the interactions between the key recognition helix H3 and a DNA sequence which included the consensus sequences for FoxO1 41
Figure 1.14 Comparison of healthy and COPD lung airway obstruction 44
Figure 2.1 The MAC Chip..... 51
Figure 2.2 Top: A workflow of the MAC chip process to obtain single cell analysis. 52
Figure 2.3 Diagram of a TIRF set up showing the total internal reflection and the evanescent field and its limited depth of penetration. Taken from Shashkova et al.[134] 57
Figure 3.1 Workflow of how a MAC chip is fabricated for single cell analysis..... 59
Figure 3.2 Printed microarray spot inside of the standard 4.5 nL [300X300X50 µM] MAC chamber. . 63
Figure 3.3 The MAC chip bespoke alignment rig 64
Figure 3.4 Example of non-congested (top) and congested (bottom) images and their reconstructions 67
Figure 3.5 Flowchart of the image processing steps for the single molecule counting algorithm. 68
Figure 3.6 Illustration of the Baseline noise offset 71
Figure 3.7 A selection of images showing typical sputum derived cell trapping and identification 79
Figure 4.1 Schematic of the 'Open Chip' format. 86
Figure 4.2 A map showing the range of antibodies available for purchase and their documented epitope binding sites..... 88
Figure 4.3 Images demonstrating the colour classifications in all subsequent heat maps. Red demonstrates no binding, yellow some binding and green a high degree of binding. 91
Figure 4.4 Bimolecular analysis of the potential Capture Agents mAb5939 and DU1071 against fluorescently tagged recombinant FoxO1 94
Figure 4.5 4.5nL MAC chip Calibration..... 96
Figure 4.6 Images (above) and calculated SM count (below) showing an increase in relation to the increase in DNA print concentration.. 98
Figure 4.7 Left shows the levels of non specific binding seen using GPTES slides, where single molecules are homogenously spread across the image, the right shows a perfect situation with little if no non-specific binding. 100
Figure 4.8 Simplified diagram of the strained ring Click chemistry reaction 102
Figure 4.9 Calibration curve of Capture Agent 7 using azide and strained alkyne attachment methodologies 103
Figure 4.10 Biotinylated Capture Agent 7 4.5 nL MAC chip calibration. 105
Figure 4.11 Biotinylated Capture Agent 7 with spacer addition in 4.5 nL MAC chip calibration attempt. 106

Figure 5.1 Histogram showing the single molecule distributions of FoxO1 in 135 untreated Toledo cells, compiled of 3 separate experiments. 110
Figure 5.2 Assay validation test of DU1071 using Toledo cells treated with ZSTK474 showing the expected increase in total FoxO1 copy number 112
Figure 5.3 Histogram showing the single molecule distributions of FoxO1 in 135 untreated Toledo cells with the mAb5939 + EP927Y antibody assay pairing..... 114
Figure 5.4 Assay validation test of mAb5939 using Toledo cells treated with 10 µM ZSTK474 showing the expected increase in total FoxO1 copy number. 115
Figure 5.5 Assay validation test of mAb5939 using 135 Toledo cells, across 3 experimental repeats, treated with 20 mM glucose showing the expected decrease in total FoxO1 copy number. 117
Figure 5.6 Histogram showing the single molecule distributions of FoxO1 in 135 untreated Toledo cells over 3 experimental repeats, with DNA Capture Agent 7 + EP927Y assay in 4.5 nL volume chambers, data is combined over 3 MAC chips. 120
Figure 5.7 Assay validation test of CA7 using 135 Toledo cells over 3 experimental repeats, treated with 10 µM ZSTK474 showing the expected increase in total FoxO1 copy number. 121
Figure 5.8 Assay validation test of Capture Agent 7 using 135 Toledo cells, treated with 20 mM glucose showing the expected decrease in active FoxO1 copy number. 123
Figure 5.9 Histogram showing the single molecule distributions of FoxO1 in 90 untreated MCF7 cells with the mAb5939 + EP927Y antibody assay pairing. Compiled from 2 experiments and 90 cells.... 125
Figure 5.10 Images of MCF7 (left) and Toledo cells (right) in MAC chip chambers with a calibrated scale bar to show the differences in cell radius and diameter 126
Figure 5.11 Assay validation test of mAb5939 using 95 MCF7 cells treated with 10 µM ZSTK474 showing the expected increase in total FoxO1 copy number 127
Figure 5.12 Assay validation test of Capture Agent 7 using 90 MCF7 cells treated with 20 mM glucose showing the expected decrease in total FoxO1 copy number. 128
Figure 5.13 Assay validation test of CA7 using 90 untreated MCF7 cells showing the basal level of active FoxO1. Collected over 2 repeats and 90 single cells. 130
Figure 5.14 Assay validation test of CA7 using 90 MCF7 cells treated with 10 µM ZSTK474 showing the expected increase in total FoxO1 copy number. Collected over 2 repeats and 90 single cells. .. 131
Figure 5.15 Assay validation test of Capture Agent 7 using 90 MCF7 cells treated with 20 mM glucose showing the expected decrease in total FoxO1 copy number. 132
Figure 5.16 94 Untreated Beas-2b cells analysed in the standard MAC chip format with the mAb5939 + EP927Y showing a questionably lowered single molecule count for total FoxO1 compared to what was expected 135

Figure 5.17 100 Beas-2b cells treated with 20 mM glucose over 3 MAC chip experiments, the results showed negligible, if any FoxO1 capture. 137
Figure 5.18 135 Untreated Beas-2b cells analysed in the standard MAC chip format over 3 experiments with the Capture Agent 7 + EP927Y showing a questionably lowered single molecule count for active FoxO1 compared to what was expected. 138
Figure 5.19 100 Beas-2b cells treated with 20 mM glucose over 2 MAC chip experiments and 100 cells, the results showed negligible, if any FoxO1 capture. 139
Figure 6.1 Combined histogram plots showing the distribution of total and active FoxO1 shown in each plot respectively 144
Figure 6.2 Box Hill plots demonstrating that the restock of EP927Y was unsuccessful in recovering the optimal single molecule distribution of FoxO1 in both assays using Toledo cells, the top shows the drop in the mAb5939 antibody total FoxO1 with the bottom showing the drop in the CA7 active FoxO1 assay. 146
Figure 6.3 A comparison of the printing quality for the different pins used 149
Figure 6.4 Figure taken from Salehi-Reyhani et al.[35] and shows how the LOD will vary as a function of chamber volume for a range of spot radii 151
Figure 6.5 A plot showing the effect of DNA printing concentration on the single molecule count of DNA tethered to the surface 154
Figure 6.6 A comparison of a random selection of experiments from across the assay validation experiments, the left plot shows the observed background binding seen with a 250 ng/mL concentration of EP927Y secondary antibody and its consistency across multiple experiments. 157
Figure 6.7 Compiled MAC Chip experiments on Toledo cells showing basal level expression (in blue) along with perturbation studies using 20 mM glucose (in red) and 10 µM ZSTk474 (in green) to bring a decrease and increase in active FoxO1 levels respectively 158
Figure 6.8 Compiled MAC Chip experiments on Beas-2b cells showing basal level expression (blue) along with perturbation studies using 20 mM glucose (red) and 10 µM ZSTk474 (green) to bring a decrease and increase in active FoxO1 levels respectively 159
Figure 6.9 A comparison of a random selection of experiments from across the assay validation experiments, the left plot shows the observed background binding seen with a 250 ng/mL concentration of EP927Y secondary antibody and its consistency across multiple experiments 160
Figure 6.10 Compiled MAC Chip experiments on Toledo cells showing basal level expression (blue) along with perturbation studies using 20 mM glucose (red) and 10 µM ZSTk474 (green) to bring a decrease and increase in total FoxO1 levels respectively 161

Figure 6.11 Compiled MAC Chip experiments on Beas-2b cells showing basal level expression (blue) along with perturbation studies using 20 mM glucose (red) and 10 µM ZSTk474 (green) to bring a decrease and increase in total FoxO1 levels respectively 162
Figure 7.1 Image of a multiplexed chamber. 170
Figure 7.2 Total FoxO1 expression in 4 healthy (n = 120) and 4 COPD (n= 115) samples compiled and compared 172
Figure 7.3 Active FoxO1 expression in 4 healthy (n=120) and 4 COPD (n=115) samples compiled and compared 174
Figure 7.4 A scatter plot comparing the two assays of FoxO1 direct comparison to show the ability of the bimultiplexed assay to distinguish healthy from COPD patient samples 175
Figure 8.1 Total FoxO1 expression in 3 healthy and 3 COPD sputum derived T-cell samples compiled and compared 185
Figure 8.2 Active FoxO1 expression in 3 healthy and 3 COPD sputum derived T-cell samples compiled and compared 187
Figure 8.3 A scatter plot comparing the two assays of FoxO1 direct comparison to show the overlap of the bimultiplexed assay with healthy and COPD sputum derived T-cell patient samples 188
Figure 8.4 Total FoxO1 expression in 3 healthy and 3 COPD sputum derived epithelial samples compiled and compared. 191
Figure 8.5 Active FoxO1 expression in 3 healthy and 3 COPD sputum derived epithelial samples compiled and compared 193
Figure 8.6 A scatter plot comparing the two assays of FoxO1 direct comparison to show the overlap of the bimultiplexed assay with healthy and COPD sputum derived epithelial cell patient samples. 194
Figure 11.1 Western blots for the two most used antibodies in this project 222

1. Introduction

1.1 Proteomics

The *proteome* is defined simply as the combination of proteins expressed at certain times whilst under defined conditions.[1] Proteomics is the term for the study of the proteome. Assuming there are no localised cell mutations, every cell within an organism is genetically identical as they share the same *genome*. However, there will be clear and distinguishable differences in the phenotype of the different cells. This alteration in phenotype is still observable in cells within the same tissues because each cell in that tissue may be in a slightly different environment and responding to that environment differently. Furthermore, alterations can occur to the individual's proteome as the cell goes through the cell cycle. There is around 20,000 protein-encoding genes within the human genome and any one of these genes may be activated by the transcription of their mRNA at any time.[2] This process of active transcription has complex regulatory mechanisms which elicit a range of protein expression patterns. The control of the total protein copy number expressed can be regulated by factors such as; varying the amount of mRNA for the specific gene, several mRNA silencing mechanisms and also nuclear export mechanisms.[3] For the majority of proteins, dysregulation of their copy number will have significant implications on the outcome of the biological pathways involving those proteins. The under- and over-expression of proteins are the key effectors in most disease states and cell dysregulating processes, including cancer.[4]

To further complicate proteomic studies further there are protein isoforms, which are different forms of the same protein. Isoforms arise from alternate splicing, from heterozygous genes, mutations of the genome and/or post-translational modifications.[1] As a result of this, the proteome of a human cell consists of hundreds of thousands of isoforms rather than the 20,000 that are expected from genomic profiling alone.[2,5] Due to there being many isoforms of the same protein, and with several isoforms causing activation or hyperactivation of a protein, it is important to look beyond the genome when probing biological theories. This is especially important when considering pathways where the proteome is involved, such as cancers, antibiotic resistances and differential drug responses in several other disease states.

Proteomic analysis can be generalised into either qualitative or quantitative proteomics. Qualitative proteomics concerns itself with looking at large changes in the expression of a protein of interest, with the analysis usually observing if a protein is present or absent. The most common techniques for this analysis are western blots and in-gel fluorescence. On the other hand, quantitative

proteomics utilises methods with higher resolutions in an attempt to achieve relative or absolute quantification of a particular protein and its isoforms. This yields a greater quality of data and can quantify both the total copy number as well as the activated (or inactivated) isoforms of a protein of interest. The most widely used methods for this analysis are quantitative Western blots, 2D gel electrophoresis, LC-MS/MS and mass cytometry.[6]

Quantitative methods can provide greater accuracy in the data but there are limitations to the current methods. The use of many of the techniques, such as Western Blots, requires high quality antibodies and so the experiments often suffer from a limited range of linearity. Gel electrophoresis methods, such as difference gel electrophoresis (DIGE) can only determine relative expression levels and it is limited in its ability to study post-translational modifications, as the protein content is not excluded by size.

The technology with the most potential for proteomic studies is the use of LC-MS/MS because it can resolve both total copy number as well as protein isoforms including post-translational modifications. The ability to resolve to such a fine detail is crucial for understanding changes in the proteome in diseased and/or drugged states. LC-MS/MS can help to understand in greater detail the importance of diseased states and how they arise. However, there are still limitations, such as the need for highly sophisticated equipment which is expensive. Furthermore, much of the work uses isotopically enriched cell media to aid in the protein observation, which will only provide relative and not absolute quantification. Therefore, the use of current quantitative methods are still relatively limited. Currently, the majority of studies still use simpler non-quantitative methods such as 1D gel electrophoresis and qualitative Western blotting.[2,7,8]

In this project, we are analysing the copy number of a specific protein. The ability to analyse the copy numbers of specific proteins is important because disease states often arise from dysregulated copy numbers of proteins that leads to the hyperactivation or inactivation of their pathways.[4,9] Understanding the balance of protein copy numbers will help to learn more about the disease state of interest and inform clinicians as to important pathway. Therefore, the development of new tools and techniques that can observe and analyse copy numbers with high sensitivity are highly sought after. Furthermore, techniques that can analyse specific protein isoforms will bring a further level of detail to the analysis of proteins and their implication in diseases.

1.2 The Single Cell Regime

In this project, we are going to be using a technique that analyses samples at a single cell level. There are many benefits to working within a single cell regime. The three most prevalent examples of how working within a single cell regime is beneficial are:

1. The cell sample size is extremely small and conventional bulk techniques would not yield accurate results with such a small sample size.
2. The cell samples of interest are rare and severely limited in quantity.
3. The user wishes to remove the effects of averaging that bulk measurements cause and instead look at the distributions present in a specific population of cells.

The first example corresponds to cell types that are uncommon or hard to obtain or if you wish to have high data economy from a small sample size. This example is best described by considering invasive and even non-invasive patient biopsies. Most biopsy techniques are considered highly invasive, with several requiring operative procedures by specialists. Biopsies are challenging to obtain for using in the context of medical research, due to the need to use the samples for diagnostic efforts in the clinic. Furthermore, these biopsies are typically analysed with ensemble averaging methods using traditional biochemical techniques. While these traditional techniques do provide results, they are commonly a 'one shot' experiment and the whole sample of 50,000 to 500,000 cells are used in just the one experiment. Methods to increase biopsy data economy that allow one sample to be run in several unique tests are highly sought after. Therefore, single cell analytical techniques are perfectly positioned to tackle this problem. Several single cell techniques can offer a comparable level of diagnostic power while utilising magnitudes lower amounts of cells. For example, the MAC chip method that will be utilised in this project, only requires 50 cells or less to determine the same results as seen in patient sample western blots requiring 50,000 cells or more.

The second example can be explained by cell types that are difficult to isolate, such as circulating tumour cells (CTCs). Over 90% of cancer deaths are linked to the formation of secondary and tertiary tumours in a process called metastasis.[10] CTCs originate from metastasis, which occurs when cells from the primary tumour are shed into the blood stream and will eventually reseed into organs at a different location in the patient. This process is intrinsically complex and it is extremely challenging to study how these CTCs migrate around the body through the blood stream.[11,12] The major hurdle for analysing CTCs is their scarcity within the bloodstream, with a typical 7.5 mL blood sample typically containing around 5 CTCs amongst the millions of other cells present within the sample.[13]

This frequency of these cells in an already heterogenous sample is far too small for the traditional method to be applicable. However, single cell methodology allows for isolation and accurate analysis of each individual CTC to give an accurate result from a rare sample.

The third example highlights one of the greatest advantages of the single cell regime – the removal of averaging from a cell population. As previously mentioned, the traditional biochemical methods currently used, such as a western blot or even flow cytometry to an extent, can be defined as ensemble or bulk techniques. Their input is a large amount of biological material and the output is an average measurement of the sample. In terms of a western blot, the measurement is a relative quantification of the amount of protein present with respect to a standard, thus the output is at best semi quantitative.

One of the best analogies for the importance of the single cell regime came from Michael Barclay.[14] His analogy was to imagine a crowded stadium, within this stadium the only outputted data is the averaged crowd noise from the tens of thousands of people present. With this data it is possible to obtain some useful information, such as when the crowd is loud and when it is quiet. This information can be correlated to certain events, such as the crowd being louder when a goal is scored and quieter at half time.

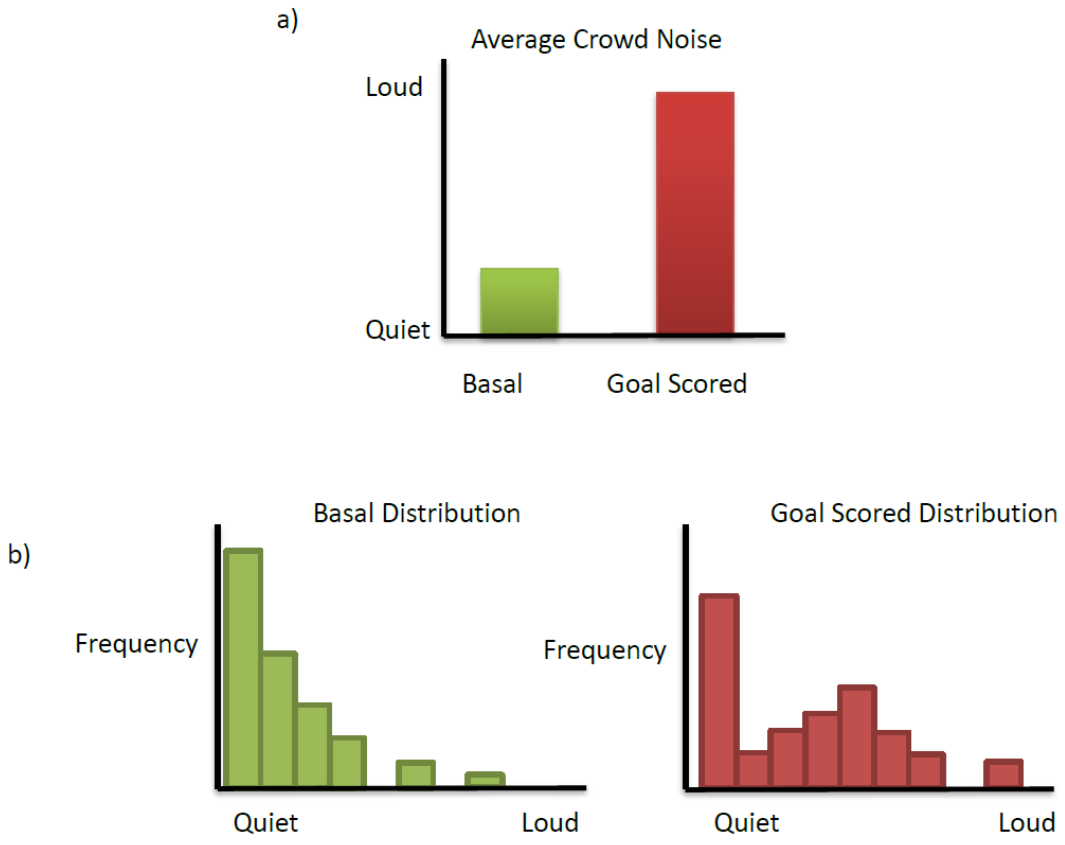


Figure 1.1 Example of the loss of information with bulk average, ensemble measurements. a) demonstrates the bulk measurement of the averaged crowd noise at the basal level and after a goal is scored. b) demonstrates the same crowd population but the sound is recorded from each individual crowd member. The important point to note is the continued existence of a quiet population even with the 'Goal Scored Distribution'. Taken with permission from Michael Barclay.[14]

Figure 1.1 shows the importance of resolving population data to a fine detail. Even though the averaged bulk measurements do show the general pattern of the crowd being louder when there is a goal, it fails to show that half the crowd support the other team and thus are not louder. The individual analysis of the crowd can yield a wider range of data, such as how many people support each team or how many people are simply perpetually loud. This data is entirely lost with the bulk measurements. Therefore, the above analogy demonstrates the importance of the single cell regime.

If we go back to the Western Blot comparison, you could imagine an experiment to measure the change in protein copy number in response to a novel drug treatment. The experiment itself would take tens of thousands (or even more) cells to produce a lysate and show either an increase or decrease in the protein copy number with respect to a basal control cell lysate. This increase or decrease in copy number could then be correlated with the external stimulus of the drug treatment. This is similar to the above analogy, although the stimulus has changed from 'a goal' to the 'drug treatment'. This shows, along with the stadium analogy, that Western Blot experiments lead to a vast amount of data being lost. Also, this method is unable to identify the presence of any subpopulations or the importance and size of the subpopulations that may be present in the experiment. For example, there may only be 40% of the cells in a sample showing a dramatic increase in protein copy number amongst 60% of the cells showing a similar distribution to the basal measurement. This means that important information on the efficacy of the drug will be missed, as the smaller highly responsive population of the cells towards the treatment will mask the information that the majority of the cells are non-responsive. The ability to observe non-responsive cells is particularly important in many disease states. For example, in cancer it is crucial to understand whether the toxic therapeutics that are being used are targeting the correct protein and whether the cells are responding to that treatment effectively.

1.2.1 Single Cell Analysis

As detailed in Section 1.1, studying at the single cell level is important to help the understanding of how cellular regulatory networks work. This section will detail some of the trends around single cell proteomics. Due to the inherent complexity of biological regulatory networks it is challenging to

achieve comprehensive molecular profiling. One of the largest challenges is finding tools for multiplexed analysis, which will help improve the understanding of altered expression and activation in diseases. Recently, several technologies have been developed to allow single cell analysis of proteins, DNA and RNA. While there are many methods for nucleic acid analysis, they fail to provide information on protein isotopes and their importance in disease states. For this reason, several novel single cell proteomic tools have been developed. These methods all have different strengths and weaknesses and can allow the user to study expression, localisation, transportation, PTMs and protein-protein interactions (PPIs).[6]

As signalling networks are complex and highly interconnected, they are spatially dependent in nature and often rely on low-abundance molecules to produce stochastic behaviours that underpin heterogeneity in cellular systems.[15] The ability to measure the noise in specific protein copy numbers of low abundance proteins will help to isolate the relationship between biological heterogeneity and signalling pathway regulation which likely results in disease states and is therefore critical to understand to drive novel therapeutic interventions.[16] The largest challenge for single cell protein analysis is the low abundance of proteins in individual cells and the inability to amplify their copy number. This means to accurately detect the proteins extremely sensitive assays are needed. This places limitations on many methods used in single cell analysis such as LC-MS.[17] If the detection sensitivity is insufficient, the single cell variations in expression and activation will be masked. Several methods have been developed to enable greater utility around single cell proteomic analysis. Microfluidic methods have been developed to allow the isolation and capture of single cells.[18–20] These isolation techniques allow for *in situ* proteomic methods, which in turn provides the opportunity for comprehensive protein profiling in their native spatial contexts.

One of the largest advances in proteomic analysis is the single-cell barcode chip (SCBC) form James Heaths group, which allows for highly multiplexed proteomic analysis.[18] This method uses microfluidic techniques to isolate up to 1,000 cells simultaneously. Each individual chamber contains an arrayed barcode of immobilised antibodies which capture secreted proteins from the isolated cells. When the target proteins are isolated, a secondary antibody tagged fluorescently or with biotin is used to stain the captured protein and this can be analysed by total fluorescence or by MS. Fluorescent calibration curves can give relative abundances and MS can be used to quantify protein isoforms if desired. Heaths group would analyse cancer cell lines with a generally high throughput (around 100-200 cells), though this method is limited by needing a homogenous cell sample and the lysis techniques are limited. Also, MS is an expensive tool not available to all. This method is currently being improved to accommodate cell lysis techniques, such as electrophysiological

methods printed to the chip. This would allow further proteomic analysis to be possible with this method and not just be used for secreted proteins.[19] Even with these improvements, the analysis is limited by its multiplexing capacity, due to there being a trade off with the multiplexing capacity and the detection sensitivity. This means that to multiplex for analysis of higher numbers of proteins, there is an important requirement for high affinity and high-quality capture agents.

Antibody crosstalk is one of the main issues in single cell proteomics, thus the Herr group developed the use of single cell western blots (scWesterns).[21] This method also uses many microwells patterned with polyacrylamide gel on a standard microscope slide. The cells are isolated into the microwells and then lysed and denatured, much like with a traditional western blot. Akin to a standard western blot, the proteins are then separated along the gel according to their mass using electrophoresis, this spatial separation lowers cross-reactivity to enable clear discrimination of on-target signals. The targeted proteins are detected by sequential diffusion of primary and fluorescently labelled secondary antibodies. A key advantage of this method is that the proteins are covalently bonded to the gels and thus the antibodies can be stripped and the gel retreated with different antibody probes to allow a multiplexed analysis. The main disadvantage of this method is that many of the proteins present can be lost during the lysing process and the antibody recycling process. This means scWesterns can have limited detection sensitivity. The primary study of the scWestern technique is on rat neural stem cells (NSCs) and the studies were able to measure and analyse two isoforms of putative nestin (NEST) isoforms and link these isoforms to the NSCs transitioning from the immature state.[21]

Another detailed example in the most recent methods of single cell analysis is utilising mass cytometry. This method is a fusion of both flow cytometry and MS which takes both their advantages to provide multiplexed protein analysis with high cell throughput.[22] Antibodies that bind to specific protein targets are coupled to metal isotopes and incubated with cells. The cells are then sprayed as single cell droplets and transported into plasma by a laminar flow of argon gas. This vaporisation allows the cells to be atomised, ionised and analysed with time-of-flight (TOF) MS to quantify these ions. The abundances of each target protein can be analysed from the single cells due to the high shift in mass from the metal isotope attached to the antibodies that will be bound to the protein of interest. The method can allow for thousands of cells to be analysed every second, making it one of the highest throughput single cell techniques. The disadvantages are the use of the metal isotopes that contain 1% metal impurities, which can lead to misleading background signals. Furthermore, as the mass cytometry method is only able to successfully analyse 30–40% of the captured cells, it is unable to analyse samples with small total cell numbers effectively. This makes

this method unsuitable for studying many precious patient samples. As the cells are atomised it also means this is a 'one shot test'; a characteristic shared with the western blot method.

A final example is the most current methods which involve in-situ proteomic technologies. These techniques have the ability to analyse cells at a precise location which is a critical component for effective cell-cell and thus biomolecule-biomolecule analysis. Some examples of the importance of where spatial context is critical is with how neurons develop and interact with their axons and how the signal transmissions between presynaptic to postsynaptic alter biological pathways. Another example is how biomolecules can mislocate in cancer[23] and how the position of stem cells can determine their terminal fates.[24] To allow in-situ analysis, the two developed techniques utilise mass spectroscopy and cyclic immunofluorescence respectively. The mass spectroscopy imaging methods utilise metal labelled antibodies and a laser ion beam to yield a spatial resolution, as the specimen can be converted to a stream of particles for analysis in a spatial fashion and subsequently analysed. Next computational methods can reconstruct this information into a two-dimensional image. This method has the ability to avoid high background signals, although it also takes 8hrs to analyse a 1 mm^2 sample so it suffers from low throughput.[25] Furthermore it requires high resolution mass spectrometers which are expensive and rare to find in academia, which limits the broad applications of this technique.[6] The other spatial technique is to use cyclic immunofluorescence which uses three main steps. The first is to label the protein targets with antibodies which each have distinct fluorophores, next fluorescence images of each antibodies are captured under their respective fluoresce channel and this process is cycled with different targets.[26,27] As this method is of image capture is faster than MS analysis there is a higher throughput as a full data collection can be achieved in milliseconds to seconds, it also uses less costly equipment making the technique easily adoptable.[27] Cyclic immunofluorescence does have disadvantages, the main critical requirement for this technique is to remove the previous fluorescence signals before the next cycle whilst maintaining the integrity of the cell and protein targets. The main method used was developed by the Schubert group which utilizes a photobleaching method to achieve a signal removal process for subsequent cycles.[26] There are also chemical treatment processes using peroxide to remove antibodies but these may damage the cell and protein epitopes and therefore reduce the quality of the results.[28]

These methods all share similar strengths and limitations. The key strengths of the described methods that have driven this area of work have been the ability to analyse a high number of single cells and to accurately quantify protein copy number and isoform expression. However, one cannot usually come with the other, with the highest cell throughput techniques often suffering from the

accuracy in their measurements. Similarly, the studies with the greatest refinement of protein copy number and isoform distribution usually have lower cell throughput. The major bottleneck in this area of research at this time is the low multiplexing capability, with only dozens of proteins being able to be quantified at one time, which represents a minute fraction of the proteome. The current strategies are also limited by their typically low detection sensitivities. Nearly all the techniques used require labelled primary or secondary antibodies to capture and detect the target antigen proteins of interest. These assays can usually have their signals amplified using enzymatic steps in traditional fixing and staining immunofluorescent techniques.[29] However, with single cell proteomics no signal enrichment is possible. A final limitation with these techniques is that they often require a homogenous sample of cells. While there are methods being developed to isolate specific cell types in heterogenous samples, they are still in their infancy and they can still only isolate a fraction of the heterogenous sample and thus require a large cell number.[30]

1.3 Microfluidics

Microfluidics describe any device which flow fluid through channels that are at the micrometre scale. The term microfluidics is the generalised term related to a plethora of miniaturised 'Lab on a chip' devices that use microfluidic channels for a specific experimental purpose. Microfluidics represent a widespread field with applications in organic chemistry through to single cell proteomics.[18,20,31] There are key benefits for operating within the microfluidic regime; firstly, these devices can be produced in-house for specific requirements. Secondly, the number of reagents used is heavily reduced compared to operating in a microfluidic environment, which saves on costs and allows for greater reproducibility, as well as the devices themselves being relatively cheap to produce. By confining the volume of the devices to micrometre sizes the volumes are significantly reduced, thus experiments that usually need millilitres of reagent now use minute amounts at the picolitre level.

The key use of microfluidics in this project lie with their use in bioassays and subsequently single cell analysis.[32,33] A key advantage of reducing the volume of analysis chambers is that it enhances the effective concentration of the analytes and Capture Agents. This is because the confined volumes and capture of the limited number of analyte present drives the equilibrium towards a bound state.[34] Driving the equilibrium towards higher binding increases detection capability. This is due to the effects a confining volume has on the diffusion times, which helps to both speed the time to reach bound equilibrium but also improves the limits of detection.[35]

Microfluidic single cell analysis has been used previously in several techniques, some of which are included in Section 1.2.1. Single cell microfluidic methods were first developed for genomic applications, which then led to the field evolving into transcriptomics and eventually proteomics.[36,37] These fields rapidly led onto the field of single cell proteomics with the majority focusing on the use of antibody-based detection methods for specific isolation of the target protein analyte of choice. The several leaders (e.g. Heath et al.) of the field are discussed in Section 1.2.1, and their microfluidic uses include cell sorting and the single cell barcode chip. The technology used in this project, the Microfluidic Affinity Capture (MAC) Chip is described in detail in Section 2.1.

1.4 Fox Transcription Factor Proteins

The target protein of interest we are looking at in the project is FoxO1. This section will detail the role of the Fox transcription factor proteins and more specifically the role of FoxO and FoxO1. The section will also detail the posttranslational regulation along with the various signalling pathways and protein-protein interactions that are involved. This will provide a grounded breakdown of the innate biology of FoxO1, which is important to understand for when we come to analyse the experiments detailed in the results section.

The Forkhead box (Fox) family of transcriptional regulators are named after an evolutionally ancient gene family named after *the Drosophila melanogaster* gene fork head (*fkh*). The Fox family is extremely widespread and can be found in many species ranging from yeasts to humans. Fox transcription factors are a wide family of proteins involved in a plethora of cell pathways; the most notable of which are cell growth, proliferation, differentiation, and longevity. However, the pathways also extend to niche roles such as placental development and inner ear formation. Mutations within the class have often been implicated in various human diseases with the phenotypic responses ranging from speech impediments to inflammatory disorders and defective T cell differentiation.[38,39] The three main classes are: FoxO, FoxA and FoxP, with each class divided by their important biological aspects in this gene family. The unifying feature of Fox proteins is the forkhead (FKH) DNA-binding domain that is a highly conserved ~100 residue sequence found across all members of the Fox family.[40]

Their discovery was first documented in 1989 with a remarkable convergence of two discoveries around the world with the *fork head* domain phenotype being cloned in *D. melanogaster*, despite it bearing no resemblance to any documented motif at that time. Soon after, the protein now known as FoxA1 was cloned in a rat that at the time had no known similarity to other nuclear receptors or

known transcription factors (including zinc-fingers). Over the coming years, the DNA-binding region of FoxA1 was delimited to amino acids 124–288 by Lai,[41] which showed remarkable similarity to the central 110 amino acids of the *D. melanogaster* and mammalian Fox proteins seen by Weigle and Jäckle[42]. Eventually, Lai came to suggest the name forkhead domain for this newly discovered DNA-binding motif.

The FKH domain consists of three α-helices, three β-sheets and two 'wing' regions flanking the third β-sheet.[40] When bound to DNA, the FKH domain adopts a 'butterfly like' winged structure, which is termed the winged helix domain. The primary structure of all FoxO proteins is shared with the same organisation of domains. The key domains characterising the FoxO family are; the forkhead DNA-binding domain (DBD), nuclear localisation signal (NLS), nuclear export sequence (NES) and the transactivation domain (TA), which is shown in Figure 1.2.

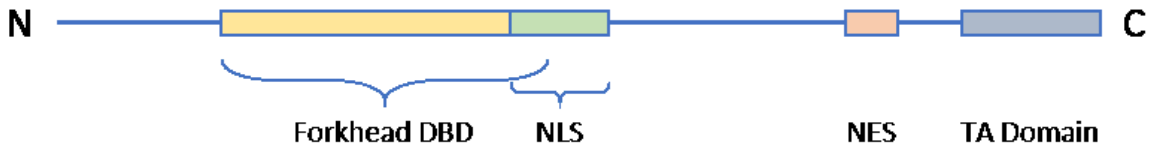


Figure 1.2 Scheme showing the primary structure of FoxO proteins with their shared domain organisation containing the forkhead DBD, NLS, NES and TA domain in sequence.

1.5 FoxO Transcriptional Outputs

FoxO transcriptional output is highly varied depending on the cellular environment and the response to different stimuli, such as oxidative stress, growth factor deprivation and metabolic stress. The FoxO family interact with several upstream pathways and are capable of integrating these several stimuli to respond and counteract the environmental changes. One of FoxOs crucial roles is the ability to adapt to nutrient availability. Another key pathway for the FoxO family is to control glucose homeostasis. FoxO1 in particular is activated to increase the expression of PEPCK and G6PC.[43] Also, the roles FoxOs play on homeostasis and maintenance will change depending on cell type. In hepatic tissues FoxOs are seen to control several metabolic processes for senescence[44], whereas stress and starvation in muscle tissues will activate both lysosomal and proteasomal degradation.[45] The plethora of potential responses the FoxO family mediates makes it a challenging transcription factor to unravel.

One of the key activities of FoxO proteins is a specific function in the immune system to regulate antimicrobial peptides (AMPs), among other functions of the innate immune response.[46] In

mammalian tissues, the role of FoxOs is far more complex and these transcription factors are involved in tightly controlling the proliferation, differentiation and apoptosis of different cell populations to yield an 'appropriate' immune response. The FoxO family does not only regulate immune response outputs but is also involved in T and B cell life cycles. FoxOs will promote the survival of naïve T cells and will aid the progression of B cells from pro to pre-B cells.[47] FoxOs also show several extra roles in the context of T and B cell biology; ranging from promoting recombination of B cells through to locating lymphocytes to certain tissues, potentially regulating the anti-viral responses of macrophages and the transcription of specific FoxO gene targets.[39]

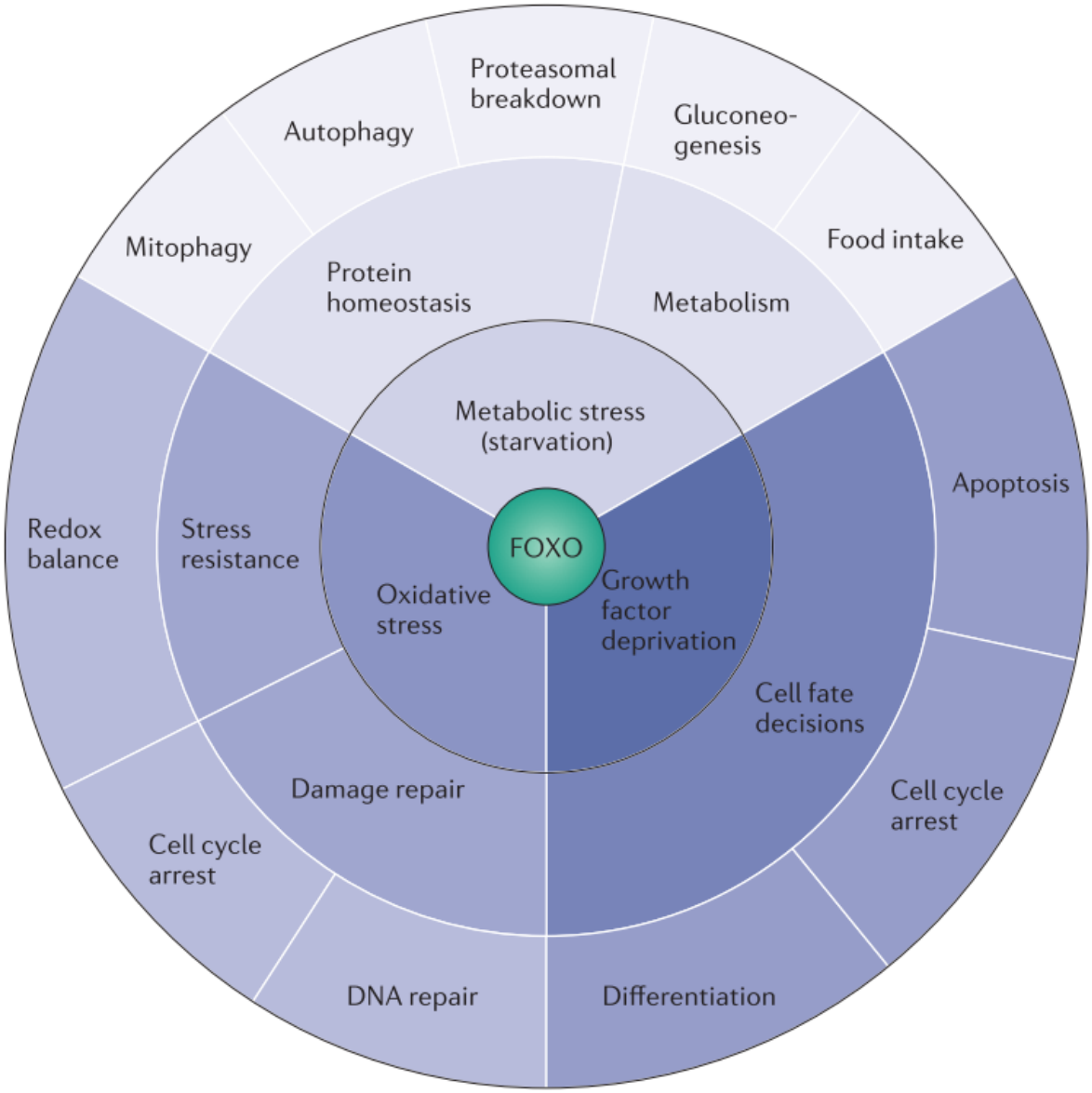


Figure 1.3 The general range of FoxO transcriptional functions. This diagram shows the processes in which FoxOs are implicated in and better highlights the range of processes in which FoxOs are important in controlling. Diagram taken from Burgering et al.[39]

Figure 1.3 shows the wide range of FoxO outputs in response to several upstream stimuli. This does not factor in certain specific gene outputs, because given the wide range of transcriptional activity, there is a wide range of genes to cover. This figure elucidates the importance of FoxO output with respect to certain upstream regulators. A better statement for FoxOs is that, in general, they act to counteract external changes that disturb homeostasis, which can arise from metabolic and oxidative stress along with growth factor deprivation. Discerning the specific targets of FoxO-induced gene programmes provides an over complication to the roles of FoxO, since several programmes are only one 'piece of the puzzle' to several homeostatic mechanisms.

1.6 FoxO Regulatory Mechanisms

In all species, FoxO activity is tightly regulated at the posttranslational level. There are several pathways that influence FoxOs activity and regulation; many of which will form covalent modifications and protein-protein interactions. This section will detail the most crucial pathways and their effect on FoxOs activity and copy number. The range of modifications elicit a modicum of different outcomes including FoxO localisation, stability and DNA binding efficiency.[48] In order to unravel the different PTMs and modifications, they will be broken down into separate subsections. The complexity of the combination of modifications and the dynamic range of responses that can arise from these interactions makes these modifications a challenge to unravel. The large number of modifications of this family has led to a proposed 'FoxO Code'. The FoxO code tries to unravel how single PTMs and combinations of interactions can lead to a range of different FoxO gene expressions and protein binding partners. This 'FoxO Code' is detailed by Calnan and Brunet among many others.[38,49]

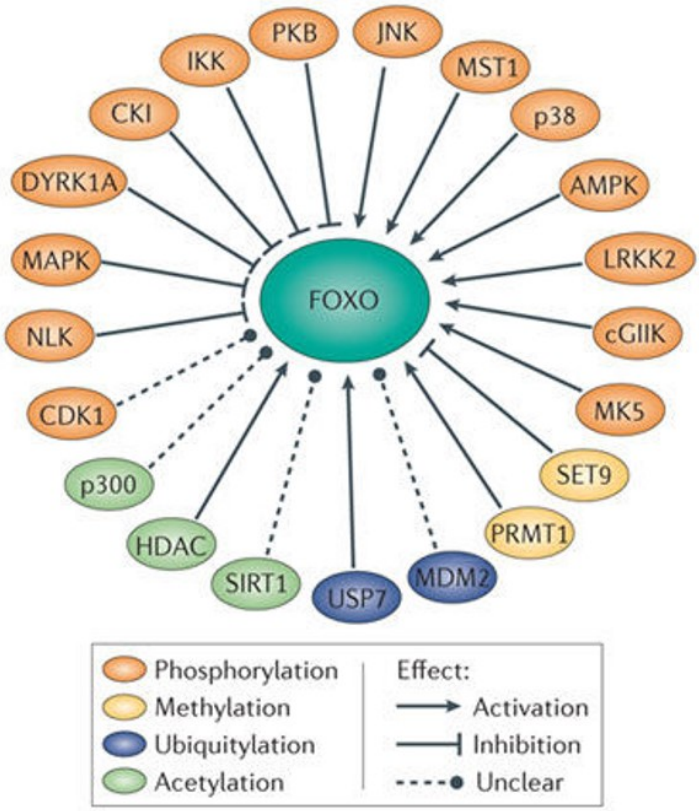


Figure 1.4 Diagram showing some of the major players in FoxO control via post-translational modifications and the difficulty in assigning a determined effect to FoxO activity. There are many phosphorylation events, although many are believed to act via the same upstream regulators. Figure taken from M. T. Burgering et al.[39]

There are many interactions that alter the activity of FoxO proteins and some are shown in Figure 1.4. In this introduction, only the most pertinent interactions for this project are discussed in detail. These interactions are discussed in terms of their biological relevance and their effects on the upregulation or downregulation. This project relies on changes in the copy numbers of both the total and 'active' form of the FoxO1 protein and the following sections detail how the protein is upregulated (higher copy number) or downregulated (lowered copy number) as well as how the 'active' protein is regulated. These pathways are detailed in terms of upregulation and downregulation, though this is readily directly applicable to changes in copy number.

1.6.1 Phosphorylation Regulation by Insulin/IFG Signalling and Growth Factors

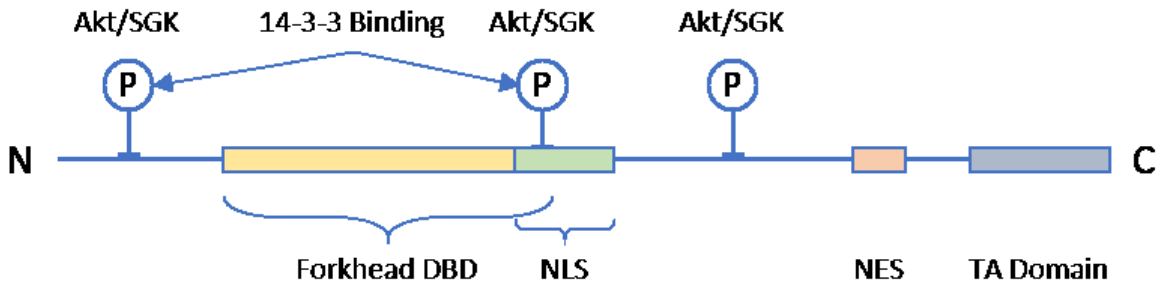


Figure 1.5 Simple schematic showing FoxO1 inactivation by PI3K-Akt/SGK phosphorylation at T24, S256 and S319. DBD=Drosophila binding domain; NES=nuclear export sequence; NLS=nuclear localisation sequence; P=phosphorylation; SGK= serum and glucocorticoid-induced kinase; TA=transactivation.

Insulin and insulin-like growth factor (IGF) proteins are known to regulate a variety of cellular functions across several tissues which include; metabolism, growth, cognition, and proteostasis. Insulin and IGF receptors are membrane-bound receptors that include intracellular tyrosine kinase domains.[50] Insulin, IGF and other growth factors typically act through the PI3K/Akt axis.

PI3K activation works by phosphorylation of the 3-hydroxyl group of phosphoinositide (4,5) bisphosphate (PIP2 or PI (4,5)P_2), which is a minor phospholipid component of cell membranes. This phosphorylation generates the second-messenger phosphoinositide (3,4,5) trisphosphate (PIP3 or (PI (3,4,5)P_3). PIP3 is able to bind to the pleckstrin homology (PH) domains that are expressed on a range of proteins, which subsequently causes the translocation and activation of Akt with PIP3 acting as a membrane tether.[51–53] Akt, also called Protein Kinase B (PKB), is involved in a plethora of cellular processes including the phosphorylation and subsequent inactivation of FoxO transcription factors.[51]

The PI3K/Akt axis is an extensively studied signalling pathway that responds to insulin, insulin-like growth factors, various other growth factors and neutrophic factors.[50,54,55] This pathway will negatively regulate all members of the FoxO family via phosphorylation by Akt and SGK (serum and glucocorticoid-induced kinase) at three conserved sites. These sites are T24, S256 and S319 for FoxO1 (which are labelled **P** in Figure 1.5).[56] The phosphorylation at these three sites cause the sequestration of the FoxO factors to the cytoplasm. Sequestration of FoxO to the cytoplasm indirectly inactivates FoxO activity, because FoxOs are then unable to transactivate their target genes.[47–50] The key event to cause this cytoplasmic sequestration is the phosphorylation causing a change in the physicochemical properties of FoxO1, as well as catalysing the binding to specific protein partners. Two of the Akt phosphorylation sites are T24 and S256, which importantly create binding sites for the chaperone protein 14-3-3 when phosphorylated.[57,58] This interaction leads to

the active export of FoxO1 from the nucleus and is hypothesised to be caused by the phosphorylation exposing the nuclear export sequence (NES).[59] Furthermore, the phosphorylation at S256 introduces a negative charge, which further inhibits FoxO1 activity by preventing nucleus re-entry. This mechanism works by blocking the stretch of residues that form the nuclear localization signal (NLS).[60] The phosphorylation at S256 also introduces a negative charge within the positively charged DNA-binding domain, which is shown in *in vitro* studies to inhibit DNA binding with FoxO1.[61,62] Another effect of Akt-mediated phosphorylation and 14-3-3 binding is that the 14-3-3 binding alters the flexibility of the FoxO NLS. By altering the flexibility of this region, it also leads to inhibition of FoxO entering the nucleus.[61,63] The insulin/growth factor pathway also triggers the degradation of FoxO proteins via Akt, by promoting the interaction with E3 ubiquitin ligase. This ligase is responsible for FoxO1 polyubiquitination and marks FoxO1 for proteasome degradation.[63,64] These several factors, mediated by insulin/growth factor stimulation, show the methods the PI3K-Akt/SGK axis will control FoxO activity and copy number in cells.

The PI3K/Akt pathway is widely recognised to be the most important phosphorylation pathway affecting FoxO1. For FoxO1, there are three additional phosphorylation sites of S249, S322 and S325 that also respond to FoxO1 cytoplasmic shuttling. This phosphorylation occurs after Akt phosphorylation at S319. S319 phosphorylation subsequently creates a binding epitope for casein kinase 1 (CK1) and this will cause sequential FoxO1 phosphorylation at S322 and S325. This phosphorylation cluster controls the interaction of FoxO1 with the Ran-containing protein complex, which is the key mediator for nuclear export to the cytoplasm.[65,66] The additional phosphorylation site at S249 is mediated by cyclin dependent kinases 1 and 2 (CDK1/2), which has also been shown to induce nuclear export and shown to directly inhibit transcriptional activity.[67]

There are several phosphorylation-based mechanisms that lead to the shuttling of FoxO1 from the nucleus into the cytoplasm. These multiple phosphorylation mechanisms are likely to form a sort of 'fail safe' to ensure the total inactivation of FoxO1 transcription. Due to the multiple phosphorylation sites and their different mediating proteins, it is likely that these mechanisms are used to control the kinetics of FoxO inactivation and subcellular localisation. The interplay serves to fine tune the exact level of FoxO1 activity, by altering the quantity of FoxO present in the nucleus.[49] Therefore, these phosphorylation sites serve as an 'on/off' switch for FoxO1 and will regulate the level of FoxO1 activity by control of the copy number and the localisation of FoxO1. Importantly, the PI3K pathway is pivotal to facilitate ubiquitination of FoxO1 and the subsequent degradation, thus reduction, in total copy number of FoxO1.

1.6.2 Phosphorylation Regulation by MST1 and JNK1

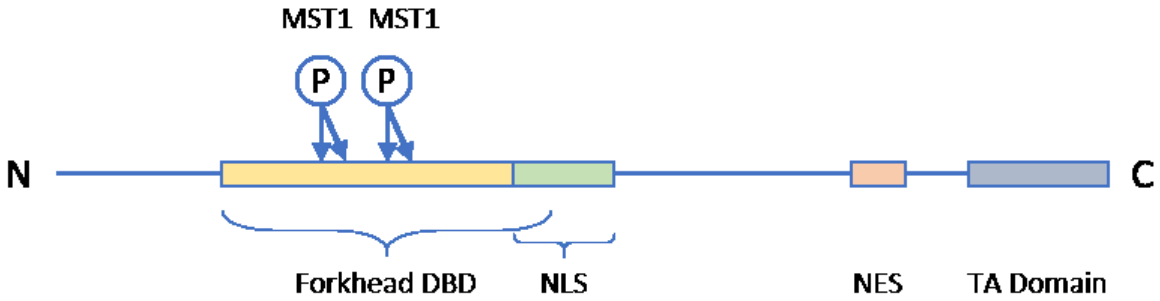


Figure 1.6 Simple schematic showing the activation of FoxO1 by MST1 mediated phosphorylation at Ser212, Ser218, Ser234 and Ser235. DBD=Drosophila binding domain; MST1=mammalian Ste20-like kinase; NES=nuclear export sequence; NLS=nuclear localisation sequence; P=phosphorylation; TA=transactivation.

The phosphorylation events described in section 1.6.1 all lead to the reduced activity of the FoxO proteins. Persistent PI3K activation would suggest that the general pool of FoxO proteins are found in the cytoplasm waiting for nuclear localisation and reactivation. One important factor for relocalisation to the nucleus is stress stimuli, even with the typical growth factor interactions present.[68,69] Studies show that even without dephosphorylation of the Akt/SGK sites, FoxO proteins can be relocalised into the nucleus in response to oxidative stress and other stress stimuli via the mammalian Ste20-like kinase (MST1) and c-Jun kinase (JNK) pathways.[63,70,71] MST1 has been observed to phosphorylate FoxO3 at an evolutionary conserved site of the FoxO family, which subsequently disrupts 14-3-3 binding. Blocking 14-3-3 binding in turn triggers the relocalisation of FoxO into the nucleus, thus allowing FoxO activity. The MST1 FoxO1 phosphorylation sites are located at Ser212, Ser218, Ser234 and Ser235, as observed by X-ray crystallography.[71] The JNK pathway directly phosphorylates 14-3-3 proteins at Ser184, which inhibits their interaction with FoxO proteins and further drives FoxO nuclear relocalisation.[72] Furthermore, MST1 has been observed to activate the JNK pathway in mammalian cells; thus, MST1 FoxO regulation may show their interactions through JNK-dependent pathways.[73]

The importance of this FoxO interaction is that oxidative stress stimuli will directly oppose the insulin/growth factor PI3K-Akt/SGK pathways in order to relocate FoxO back into the nucleus. This is a key pathway interaction that is one of the strongest cases showing the dynamic range of FoxO interactions and outcomes. The ability of MST1 and JNK to promote the relocalisation of FoxO to the nucleus and override PI3K signalling is believed to be linked to extended lifespan.[74,75] This override of PI3K also suggests a hierarchy of signalling cascades where certain interacting pathways have greater efficacy on the activity and copy number of FoxO1 by the inhibition of PI3K.

1.6.3 Dephosphorylation of FoxO to Permit Relocalisation Back into the Nucleus

The subcellular localisation of FoxO is the key regulatory mechanism, which suggests that there is a cytoplasmic pool of FoxO ready to be activated. Another mechanism for the relocalisation of FoxO to the nucleus is dephosphorylation, although some of the phosphorylation sites have not been entirely characterised (Akt/SGK sites have little data on them). There has been some anecdotal data suggesting that both protein phosphatase 2A and protein phosphatase 4 both dephosphorylate FoxO. One important and less researched area for phosphatase regulation of FoxO is the rates at which these proteins permit the nuclear influx of FoxO proteins. One study suggests this occurs as quickly as 20 minutes in exposure to Leptomycin B, which targets and eliminates nuclear efflux, thus allowing the measurement of FoxO1 influx to the nucleus using time course immunofluorescence studies.[76] However, this study did use GFP-tagged FoxO1 and 3a, which might lead to the blocking of certain endogenous events.

The studies of dephosphorylation events are less common with respect to the other interactions mentioned in this chapter. However, it seems that these events play an important role in keeping the active nuclear to cytosolic pool ratios fine-tuned to ensure the regulation of FoxO-mediated transcription.

1.6.4 Acetylation/Deacetylation by CBP, p300 and SIRT Proteins

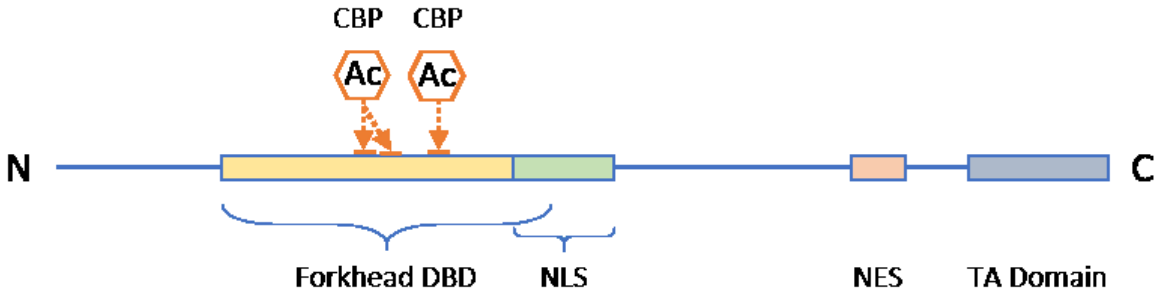


Figure 1.7 Simple schematic showing the complex outcome of acetylation of FoxO1 by CBP at K242, K245 and K262. The outcome of CBP and p300 acetylation is not as simple as 'activation' and is more a method of fine-tuning the transcriptional activity of FoxO1. Ac=acetylation; CBP=CREB-binding protein; DBD=Drosophila binding domain; NES=nuclear export sequence; NLS=nuclear localisation sequence; TA=transactivation.

The acetylation and deacetylation of FoxO proteins is also observed as a response to oxidative stress stimuli and these events also affect the subcellular localization. Acetylation of FoxO1 provides

another layer of complexity for FoxO transcription control. The levels of acetylation are controlled by opposing actions of protein acetylases CREB-binding protein (CBP) and p300 and the protein deacetylases sirtuin (silent mating type information regulation 2 homolog) 1 (SIRT1) and Sir2.[71,77–79] FoxO1 is acetylated at the lysine K242, K245 and K262 sites in response to oxidative stress by CBP.[80] This acetylation subsequently leads to the relocalisation of FoxO1 into the nucleus and more specifically to the PML nuclear bodies via the interaction of FoxO1 with PML (promyelocytic leukaemia protein). This acetylation will increase the local concentrations of FoxO1 into nuclear subcompartments that are already densely packed with several proteins, which also may play roles on FoxO regulation and activity.[81]

Acetylation of the FoxO family is a complex pathway that is further compounded by the complexity of the interplaying phosphorylation events. One example of the complexity is that FoxO1 stress-induced acetylation is shown to increase FoxO1 stability by inhibiting FoxO1 polyubiquitination pathways.[69] Despite this appearing to be a positive feedback for FoxO1 activity, the same acetylation is also seen to interfere with DNA binding for both FoxO1 and FoxO3.[62,80] While acetylation events appear to conserve a nuclear pool of FoxO proteins, this PTM also seems to hold FoxO in a state of inactivation. Furthermore, acetylated FoxO1 has enhanced interaction with Akt causing phosphorylation at S253, which deceases DNA binding via the introduction of a negative charge into the DNA binding domain.[82] While acetylation of FoxO factors by p300 and CBP does inhibit FoxO activity by reducing DNA binding, it also plays an important role in controlling the transcriptional output of the cell by initiating co-activator complex formations. The physical interaction of FoxO with p300/CBP allows for the recruitment of a co-activator complex that seems to initiate the transcription of certain genes.[83] These complex processes could act to fine tune the output of FoxO activity and regulate the expression of certain FoxO target genes. Presently, little work has been presented on the temporal aspects of these interactions. The apparent inhibitory effects seen with acetylating interactions may occur at later stages of FoxO regulation in order to terminate the activity of FoxO transcription events after transcription of target genes has occurred.[49]

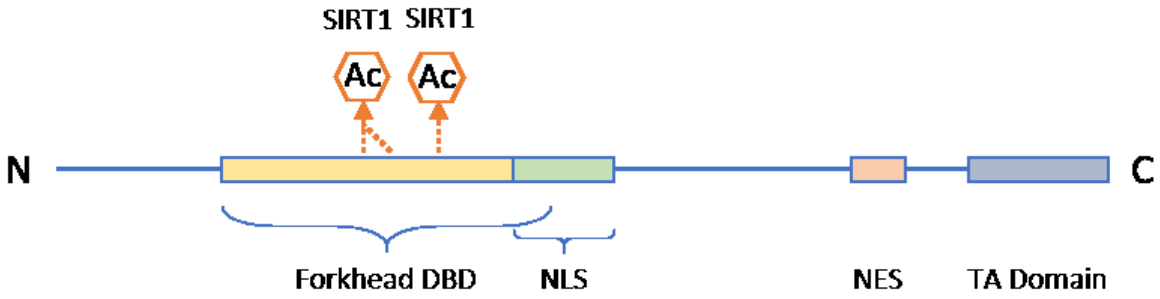


Figure 1.8 Simple schematic showing the probable activation of FoxO1 pathways by SIRT1 at K242, K245 and K262. The outcome of SIRT1 and Sir2 deacetylation is not as simple as 'activation' and is more a method of fine-tuning the transcriptional activity of FoxO1. Ac=acetylation; DBD=Drosophila binding domain; NES=nuclear export sequence; NLS=nuclear localisation sequence; SIRT1=sirtuin 1; TA=transactivation.

The deacetylases Sir2 and SIRT1 have been shown to counteract the effects of CBP/p300 and are observed to show enhanced longevity in a range of species.[82,84,85] Interestingly, the role of SIRT1 seems to regulate the target genes of FoxO1 and modify FoxO1 transcription from inducing apoptotic genes into enhancing the expression of stress resistant and cell cycle arrest genes.[77] The SIRT1 mechanism to cause this switch in gene expression is complex. A possible theory is that SIRT1 also deacetylates at histone sites, which increases FoxO binding to DNA at other promoter sites. Furthermore, the pattern of deacetylation that SIRT1 mediates may cause this alteration of FoxO binding to specific transcription promoters.

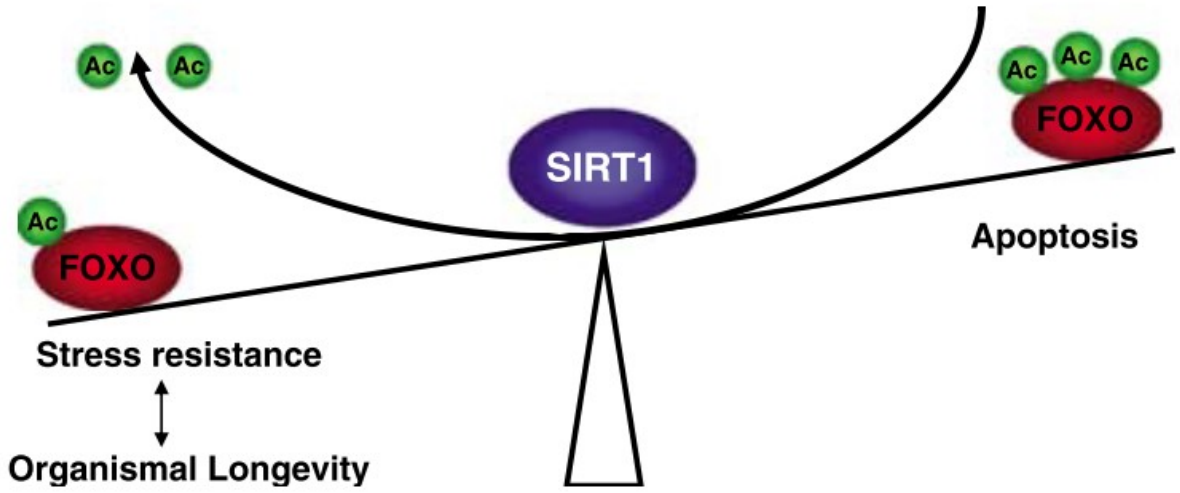


Figure 1.9 A figure demonstrating SIRT1 interaction and its function of switching FoxO1 output from apoptosis to stress resistance with FoxO deacetylation. Image taken from Brunet et al.[86] Ac=acetylation; FOXO=Forkhead box protein; SIRT1=sirtuin 1.

The role of acetylation is challenging to elucidate fully. Acetylation of the FoxO family and various targets seems to modulate FoxO activity rather than be a simple 'on/off' switch, which is observed with kinases.[48] For each mention of an inactivating pathway by acetylation, there is one stating activation of different FoxO downstream targets. One example is the p300 acetylation of FoxO3 that results in enhanced transcriptional activity and conversely this acetylation is reversed with subsequent deacetylation by SIRT1.[87] In contrast, there are observations of CBP acetylation inhibiting FoxO transcriptional activity in oxidative stress environments, which can be reversed by SIRT1 deacetylation.[84] However, in the context of oxidative stress there are many different results. One study shows that FoxO4-CBP interacting in high oxidative stress environments causes stabilisation by forming a cysteine disulphide bridge.[79] This bridge formation inhibited FoxO4 cell cycle inhibition

transcription, whilst also inducing FoxO4 apoptotic protein transcription. There are many other examples of the interplay between acetylases and deacetylases, which often show contradictory results and effects of acetylation on the FoxO family. The general consensus is the varieties of acetylation patterns will hone the exact transcriptional products of FoxO activity.[71,80,88] The complexity of the role of acetylation is even harder to unravel when considering the wider role of acetylases and histone acetylation. Acetylation at certain histone sites is also likely to play a part in the specific transcription events of FoxO.[48]

1.6.5 Mono- and Polyubiquitination of FoxO Proteins

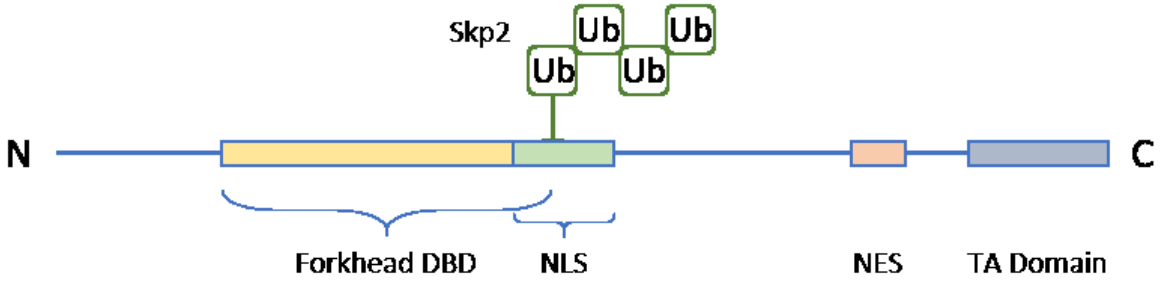


Figure 1.10 Simple schematic showing polyubiquitination of FoxO1 leading to tagging for proteasome degradation by Skp2 complex association. DBD=Drosophila binding domain; NES=nuclear export sequence; NLS=nuclear localisation sequence; SIRT1=sirtuin 1; Skp2= S-Phase Kinase-Associated Protein 2; TA=transactivation; Ub=ubiquitination.

The effects of mono- and polyubiquitination are detailed briefly in the section 1.6.1, as PI3K mediated phosphorylation drives ubiquitination and a drop in FoxO1 copy number. These two modification states have opposing effects, with polyubiquitination tagging FoxO proteins for degradation in the proteasome and monoubiquitination leading to FoxO nuclear localisation and augmented transcriptional activity.[63] The polyubiquitination studies on the FoxO family are quite robust, with many suggesting that the proteasome-mediated degradation via polyubiquitination is dependent on Akt signalling and subsequent S-Phase Kinase-Associated Protein 2 (Skp2) ubiquitin complex association.[89,90] Ubiquitination is the pivotal post-translational modification to tag FoxO for degradation, although it is more important to discuss the upstream regulators of this process in respect to this project. Nevertheless, it is important to recognise that this is the key and pivotal post-translational modification for causing a decrease in copy number of FoxO1.

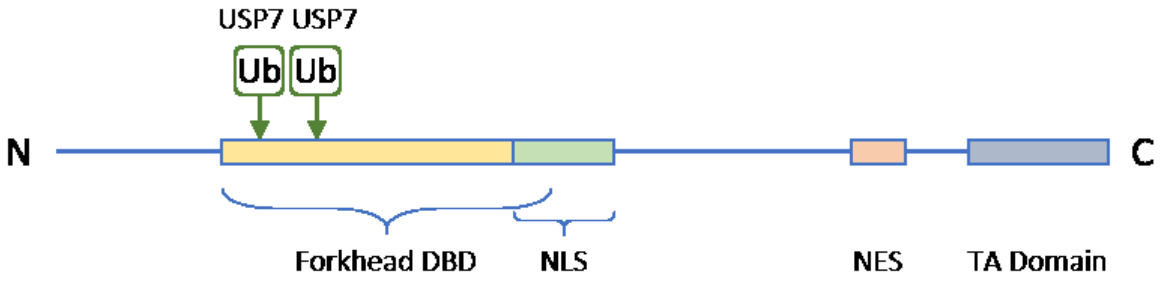


Figure 1.11 Simple schematic showing the monoubiquitination sites of FoxO1 which augment the response of FoxO4 activity by USP7 at K199 and K211. DBD=Drosophila binding domain; NES=nuclear export sequence; NLS=nuclear localisation sequence; SIRT1=sirtuin 1; TA=transactivation; Ub=ubiquitination; USP7=ubiquitin specific peptidase 7.

Monoubiquitination by ubiquitin specific peptidase 7 (USP7) has been observed to enhance the response of FoxO4 activity in response to oxidative stress by inducing nuclear localisation and enhancing transcriptional activity.[91] Various studies have shown two conserved lysine residues at K199 and K211 are the targets of USP7-mediated monoubiquitination.[91] Monoubiquitination has so far only been seen on K199 and K211 of FoxO4, but since these are two conserved lysine residues there is good evidence to assume the same enhancement of activity is seen across the other FoxO family members.[91]

1.6.6 Hierarchy of PTMs That Lead to Complex Transcriptional Activities

The previous sections describe the detailed complexity of FoxO regulatory and activation systems. There are also several PTMs which interplay with separate and shared upstream activators that will all tailor FoxO localisation and activation. The role of phosphorylation seems to control activity in a binary 'on/off' fashion by controlling the localisation and interactions of FoxO proteins. The chronic signalling of PI3K under 'normal cellular conditions' means that the FoxO family is kept in an inactive state by the negative regulation of PI3K-Akt/SGK signalling.[39] Nevertheless, there is a hierarchy to these interactions, where PI3K-Akt/SGK phosphorylation is overridden by phosphorylation by MST1 and JNK phosphorylation. The activation by MST1 and JNK bypasses the need for dephosphorylases to counter the PI3K-Akt/SGK signalling, which might explain the rapid response of the FoxO family to stress stimuli. While phosphorylation interacts as a 'on/off switch', the role of acetylation is far more complex. Acetylation seems to fine-tune the exact transcriptional activity of FoxO proteins. Depending on the pattern of acetylation, both on the FoxO family and on the histone environment, will tailor the transcription of the exact target proteins in response to the several upstream processes of FoxOs and acetylases alike. Coupling these paths with other less mentioned processes

such as ubiquitination shows the range of interactions and their importance in eliciting the appropriate response to stress resistance, oxidative stress and regulation of homeostasis.

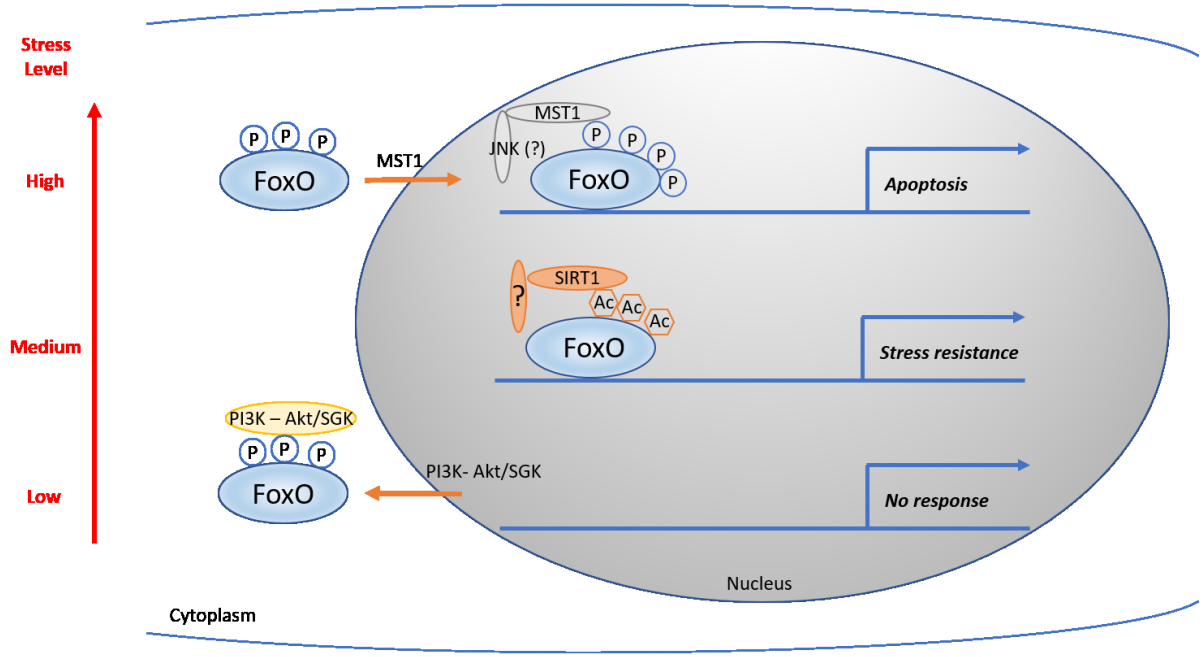


Figure 1.12 A simplified scheme of the 'FoxO code'. The scheme shows how the pattern and combination of FoxO modifications can elicit differential responses of the FoxO family. The primary example is how MST1 (Macrophage Stimulating 1) phosphorylation is able to circumvent PI3K (Phosphoinositide 3-kinase) -Akt/SGK to reactivate and return FoxO to the nucleus. The acetylation states are also shown although the complexity of the biology and response is less detailed.

1.7 FoxO DNA Binding

FoxO transcription factors contain an approximate 110-amino-acid winged helix DNA binding domain (DBD), which is termed the forkhead domain.[42,71,92] This domain is both directly and indirectly regulated by several PTMs. DNA binding is also controlled by FoxO localisation. The effects of the PTMs within or near the DBD regulate FoxO interaction with DNA both directly or through subsequent protein-protein interactions. The forkhead domain of the FoxO family binds to the conserved DNA consensus 5'-GTAAACAA-3' known as the DAF-16 family member-binding element.[42,93,94] This is conserved across all FoxO family members and furthermore, this sequence contains the core sequence 5'-(A/C)AA(C/T)A-3' that is recognised by all forkhead proteins.[95] While this sequence is shared with all FoxO proteins, the proteins can all play different roles depending on their PTM interactions and localisations (e.g. FoxO6 is only found within neuronal tissues).[63] The FoxO proteins are also documented to bind the insulin-responsive sequence found in the IGFBP-1

promoter region. This sequence is 5'-(C/A)(A/C)AAA(C/ T)AA-3' and also shares the shared sequence of all forkhead recognition but can differ in the first two bases.[96,97]

There have been several structural studies on the forkhead and FoxO family, utilising both X-ray crystallography and solution nuclear magnetic resonance, that have shown the similarities of the forkhead domains of Fox proteins.[92,94,98] There are highly conserved residues in recognition helix H3 of the DBD, which are integral to make certain hydrogen bonding and Van der Waals interactions with the DNA consensus sequences' major groove. The key interactions theorised to be preserved for DNA binding are between the methyl groups on the thymine bases and the Arg211, His212 and Ser215 side chains to ensure recognition.[94] Substitutions of these interactions in the H3 region show loss of DNA binding interactions. The C-terminus region is also observed to make key contacts with the phosphate backbone of the DNA consensus. Mutagenetic studies revealed that inserting negatively charged residues would reduce DNA binding.[94] This is backed by the fact certain phosphorylation PTMs in the DBD, which also introduce a negative charge near the DBD, reduce DNA binding. Modelling and deletion analysis has shown similar importance for the N-terminus region, which is further corroborated by studies on wider *fox* family members.[99] The major factor for DNA binding is the H3 helix in the DBD which forms the key interactions with the major groove of the consensus motif, the C and N-terminals along with the H2 region. These interactions provide a fine-tuning of sequence specificity and DBD-DNA stability across the FoxO family.

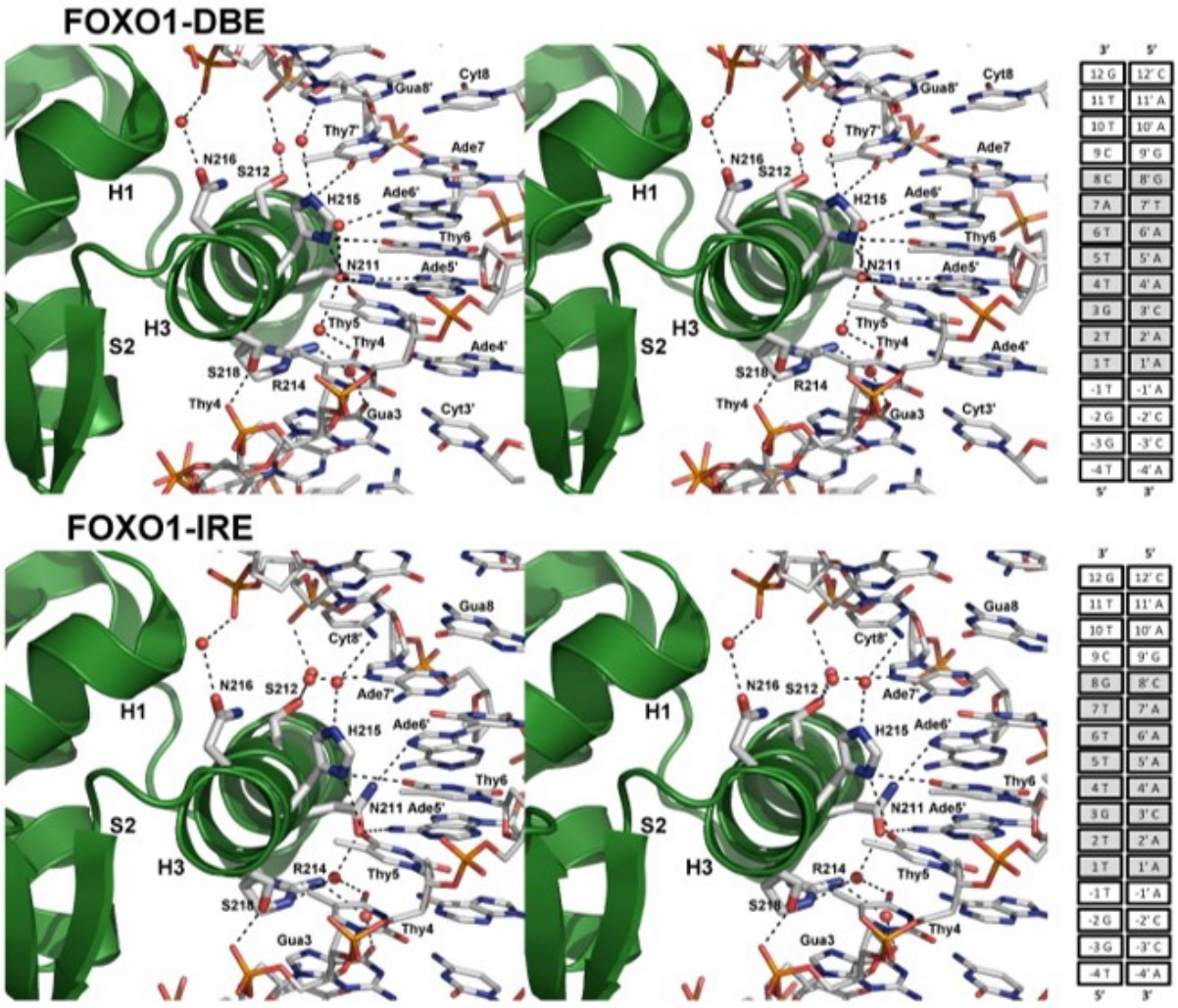


Figure 1.13 A stereoview of the interactions between the key recognition helix H3 and a DNA sequence which included the consensus sequences for FoxO1. The top scheme shows the interactions of H3 with the DBE (DAF16-family binding element) motif which includes the core sequence 5'-GTAAACA-3. The bottom scheme shows the interactions between FoxO1 with the IRE motif including the core sequence 5'-CAAAACA-3'. It is clear to see a larger number of interactions between H3 and DBE compared to the IRE (insulin response element), which shows FoxO1s higher affinity for the DBE. Image modified from T. Obsil et al.[98]

The solved crystal structures for FoxO1 provide a greater understanding of the basis of DNA recognition and shows the interactions have key contact points for H3 and the DNA sequences. The side chains of N211 and H215 give all the direct base-specific contacts for the FoxO1-DBE and IRE structures. For side chain H215 in the FoxO1-IRE binding, there are less specific contacts between the amino acid and the DNA sequence, which results in lowered affinity for FoxO1 and the IRE sequence.[98] Furthermore, studies have shown that a 5-fold increase in DBE binding affinity can be achieved by the addition of thymine rich 3' flanking bases to the consensus motif.[71] As the consensus motif is well documented, it was decided that study of DNA-based capture approaches to analyse the sub population of active FoxO1 should be a promising capture agent.

1.7.1 FoxO DNA Binding in Relation to Total vs Active Copy Number

DNA as a capture agent can be seen as a method of binding an 'active' subpopulation of the total copy number of FoxO. However, in reality this is not the only aspect that dictates transcriptional activity. For full transcriptional activity there is also a need for specific combinations of PTMs to bind the consensus motifs and the required protein partners to give a full transcriptional output.[48,57] For ease of discussion, the terminology in this thesis will define the copy number analysis of FoxO1 as total copy number against 'active' copy number. This active copy number is only analysing the FoxO subpopulation that is able to bind DNA, which in itself, is actually only one key piece of the puzzle.

This section has detailed the pathways FoxO1 is involved in and the methods used to validate the total and active copy number of FoxO1. This is not an exhaustive list of pathways that will modify the copy number of FoxO1, but they are the most important and well-studied pathways for this project.[84,100] One of the main pathways of FoxO1 is PI3K phosphorylation, which is the upstream mediator to tag FoxO1 for ubiquitination and subsequent degradation. This pathway of degradation via ubiquitination is the most essential pathway for perturbations to total FoxO1 copy number. The active copy number subpopulations are also affected by the PI3K degradation pathway, but also a range of other processes which will impact DNA binding and therefore activity.

1.8 Chronic Obstructive Pulmonary Disease

The protein of interest, FoxO1's key pathways are implicated within the disease Chronic Obstructive Pulmonary Disease (COPD), such as the PI3K and JNK pathways. This link suggests that FoxO1 might prove to be an indirect marker of COPD and was one of the key considerations when choosing FoxO1 as our protein of interest in this project.

Chronic obstructive pulmonary disease (COPD) is a major global health issue. COPD is currently the third leading cause of death worldwide, has a cumulative lifetime risk potentially as high as 25%, effects both genders equally and is ranked fifth with respect to disease burden.[101] COPD is described, *not defined* as a 'a common preventable and treatable disease … [that] is characterised by persistent airflow limitation that is usually progressive and associated with an enhanced chronic inflammatory response in the airways and the lung to noxious particles or gases. Exacerbations and comorbidities contribute to the overall severity in individual patients' by the Global Initiative for Chronic Obstructive Lung Disease (GOLD).[102] The fact COPD can only be described by these terms and not defined, shows there is a failure to use clear definitions for the disease. Often the term COPD is confused and used to describe people with low forced expiratory volumes, people with alterations in CT scans from emphysema or also similar symptoms arising from chronic lung disease and a history of smoking. Due to these confusions, COPD is greatly underdiagnosed and is often only diagnosed at late stages. This has led to concerted efforts to encourage methods, such as spirometry, to attempt to diagnose patients with increased speed and accuracy.[103]

At the research level, the current techniques incorporated for understanding the biological pathways are the traditional, gold standard methods. These methods include immunofluorescence, western blots and flow cytometry and many others. Although all these suffer from limited data output as they require high cell counts for accurate analysis and require homogenous samples.[104,105] Thus, the use of single cell techniques would be highly advantageous to understand the biological paths of COPD to a greater level.

COPD is mostly caused by smoking and exposure to environmental tobacco smoke, followed by a history of tuberculosis and next pollution.[105] COPD is also linked to low income countries and regions with low gross national incomes. This trend is seen with UK regions, where lower income regions in the north show a higher prevalence for COPD.[106] There are also genetic risk factors, as observed in family and twin studies against unrelated studies which showed that COPD risk was increased with twin siblings.[107] There was also significant heritability and a three-fold risk increase in developing COPD for first-degree relatives of COPD diagnosed patients.[105] Given there is a genetic risk factor

involved, it highlights that there are perturbed protein paths that are compromised in COPD patients. In brief, the pathophysiology of COPD seems to have several underlying mechanisms which can arise from distinct overlapping phenotypes. Given that COPD can occur in non-smokers it shows there are susceptibility mechanisms which likely come from genetic, epigenetic and environmental factors in combinations that are poorly understood. Recent papers have said 'A better understanding of the complex cellular mechanisms and molecular pathways involved in COPD might lead to improved therapies in the future.'[105]

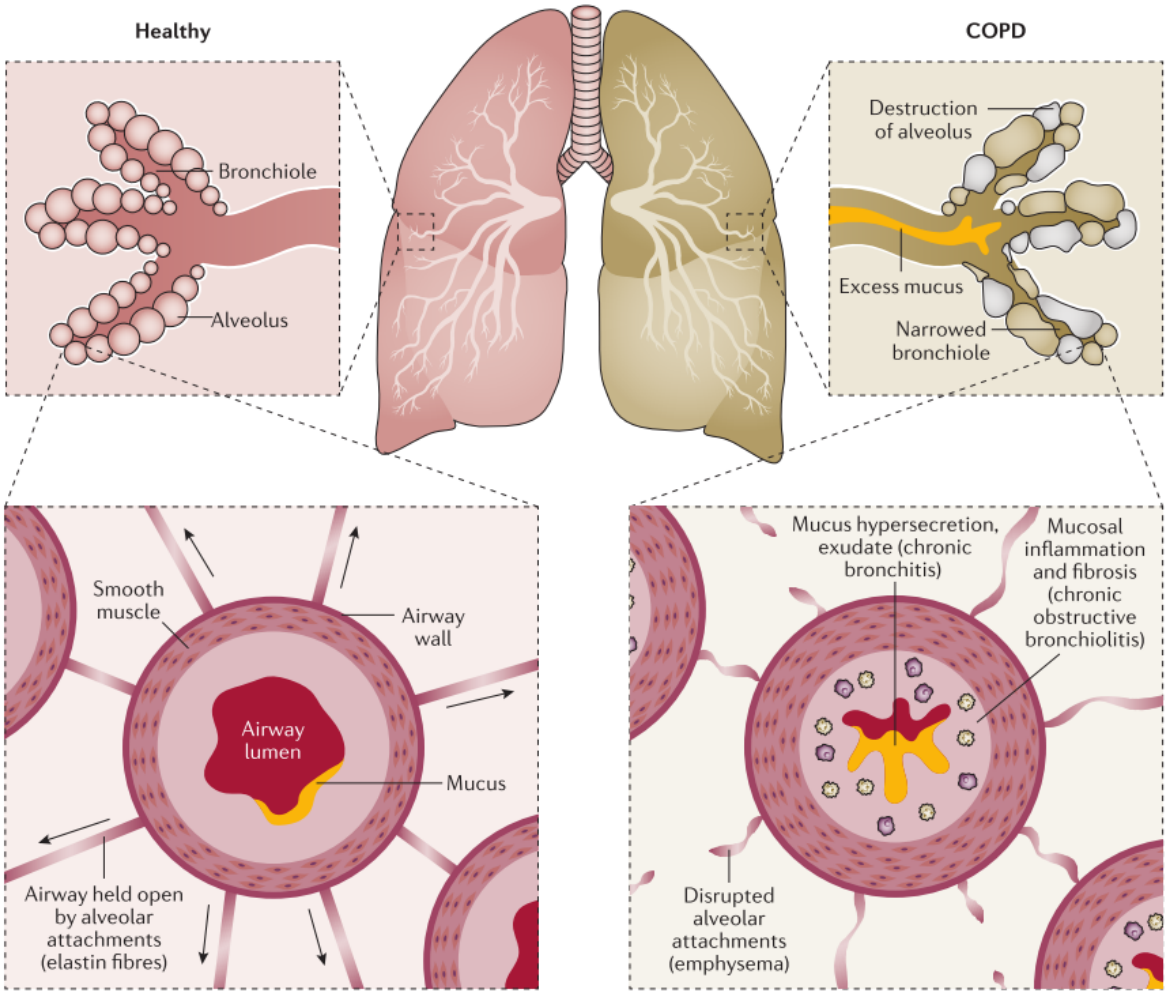


Figure 1.14 Comparison of healthy and COPD lung airway obstruction. In the healthy images (left), the alveolar wall attachments can hold open the bronchioles with elastin fibres and a healthy level of mucus is generated. In the COPD images (right), the bronchioles are clearly narrowed by the thickening of the periphery wall from inflammation, fibrosis and damage to the alveolar wall attachments resulting from emphysema and other factors, there is also mucus hypersecretion. Image taken from Barnes et al.[105]

The key features of COPD are obstructive bronchiolitis (fibrotic airway disease, or sometimes termed 'popcorn lung'), emphysema (small airway destruction) and in many cases mucosal hypersecretion (excessive mucus production). Although these are the key features, the relative contribution can vary between patients, with small airway destruction still present in even early-to-mid stage COPD

cases. These pathological paths of COPD have clear overlap with inflammatory cellular responses and the dysregulation of cellular senescence pathways. The severity of the features, such as chronic cough, occurrence of respiratory tract infections and dyspnea (difficulty breathing) are typically observed through spirometry, which provides the GOLD classification of COPD. The GOLD classifications run from 1–4 with 4 being the most severe. The primary practical test is observing forced expiratory volume in 1 second (FEV), with below 30% being classified as most severe.[108] Otherwise, initial tests for COPD are assessment of symptoms using a Modified British Medical Research Council (mMRC) Questionnaire which relates several COPD factors along with historical data of the patient. While these methods are thorough, they are still inaccurate and often lead to poor diagnosis or a lack of diagnosis of COPD.

There are many factors that describe COPD and given the combination of these factors and how COPD can occur with varying severities of these factors, it makes it a difficult disease to diagnose effectively and accurately. There is a call to determine new, more accurate methods to help increase the certainty in diagnosis of COPD in a simple, yet accurate fashion. The use of single cell assays is widely regarded as a growing field that can provide a novel method for the determination of disease states and such a tool for COPD would be of great benefit to the clinical field. Therefore, COPD ,alongside FoxO1 as a clinical marker for COPD, will be investigated in this project using the MAC chip.

1.9 Chronic Obstructive Pulmonary Disease and FoxO1

The studies of FoxO1 in direct relation to COPD are sparse and uncommon with little direct analysis of FoxO1s involvement in the disease state. Despite this, there are clear links to the disease and the activities and indications of FoxO1, the most prevalent being the involvement of dysregulated inflammatory responses and a loss of cellular senescence in moderate to severe COPD. Furthermore, as mentioned many key pathways of FoxO1 are implicated with COPD, suggesting that FoxO1 might prove to be an indirect marker of COPD. However, given the many inputs that lead to a COPD diagnosis it is important to understand the several factors that implicate FoxO1 with COPD.

One widely studied pathway linked to COPD is that of the pro-inflammatory transcription factor nuclear factor kB (NF-κB), which is observed to be hyperactivated in COPD-related inflammation. This pro-inflammatory cytokine is activated in oxidative stress environments and its activation is linked to the PI3K pathway. Studies on diabetes have shown that activation of the PI3K pathway will activate NF-κB along with a reduction of FoxO1.[109] The PI3K pathway is also activated in COPD

relevant oxidative stress to give rise to several downstream processes, such as a drop in FoxO1 activity and also, in severe cases, a drop in SIRT1 activity.[110] The activity of the PI3K pathway, as mentioned in Section 1.6.1, is a key regulator of FoxO1 by reducing the activity by Akt-driven phosphorylation of FoxO1 to cause nuclear sequestration. This would suggest that total levels of FoxO1 will be lowered in patients with COPD.

There is overwhelming evidence that oxidative stress and the subsequent damage play a pivotal role in COPD pathogenesis.[111] The source is closely linked to environmental exposures with the most abundant source coming from cigarette smoke and air pollutants. These sources lead to both reactive oxygen species (ROS) and reactive nitrogen species (RNS) being released into the lungs, by macrophages, in response to environmental factors. These released reactive species are reported in several papers to have varying effects on FoxO, and more importantly FoxO1 response. The wider body of literature has reported FoxO transcription factors to promote both apoptosis as well as cell survival, which are two contrary responses. Different methods of analysis and different experimental set ups can seemingly yield opposing results of FoxO in the context of oxidative stress. It is well documented that there is activation of the JNK pathway in response to oxidative stress in the context of COPD. As mentioned in Section 1.6.2, the activation of the JNK pathway will have indirect effects leading to the increase in FoxO1 activity and a drop in the degradation of FoxO proteins. Furthermore, the activation of the JNK and MST1 pathways is also known to override PI3K signalling. Therefore, an increase in FoxO1 activity can be hypothesised.

The other pathway which implicates both FoxO1 and COPD is SIRT1, which is again linked to ROS generation. ROS species are shown to reduce the expression and activity of SIRT1. This reduction is observed in COPD patient studies and is a theorised reason for the drop in genomic stability, dysregulation in cellular senescence and thus advanced cellular aging.[112] Despite a drop in SIRT1 activity being reported, this does not mean a drop in FoxO1 activity, rather an alteration in FoxO1 output that likely switches FoxO activity from cell survival to apoptosis. Given the variety of responses that FoxO1 mediates, this PTM is likely not a negative or positive regulator in the context of COPD, rather a moderator of responses seen in COPD. While it seems there is a juxtaposition of transcriptional activity, given the theory of the 'FoxO code' exists, it is a fair statement to assume FoxO1 activity will not be reduced from a lowered SIRT1 interaction but instead switch transcriptional output. Both the current understanding and diagnosis of COPD and the response of FoxO1 could vary patient to patient with respect to the severity of the disease. Due to the lack of direct comparisons between COPD and FoxO1, an assay investigating the two could be integral to elucidating a new way of diagnosing COPD.

As detailed in this section, there is a clear need for better methods to diagnose and understand the biological pathways implicated in COPD. Single cell proteomics offers a unique tool to accommodate this need by allowing the analysis of several proteins (as the MAC chip progresses) in tandem with high data economy compared to the traditional methods. By being able to use small samples of cells to achieve the same data through put of conventional techniques without the need for highly invasive biopsies. Which provides a clear need for the project detailed in this thesis.

1.10 Haploinsufficiency and the effect on Copy Number Experiments

Mammalian cells are diploid organisms, meaning the cells possess two functional copies of the same gene in their genome. Typical cellular function relies on both copies of each gene being functional, so they are able to be transcribed to protein and thus produce the wild-type phenotype. Haploinsufficiency is a mechanism of action in which a diploid organism loses a copy of a particular gene.[113] This loss of a particular gene usually comes from a mutation, which can be from a base substitution, deletion or insertion.

Haploinsufficiency is a prevalent mechanism in several cancer states, which is due to it resulting in a loss of wild type phenotypic function from the loss of one copy of that gene.[114] Therefore, haploinsufficiency often leads to cancerous phenotypes.[114] Haploinsufficiency is also prevalent in several other diseases.[115] Importantly, it will halve the copy number of the protein effected and thus is an important factor to keep in mind when undertaking proteomic analysis. If studies are undertaken on cancer cells, or cells from other disease states, it is important to determine if there may be a haploinsufficiency of the protein of interest compared to a wild type cell.

In the work presented throughout this thesis, there was nothing in the literature to suggest the cells used in the studies showed haploinsufficiency for the protein of interest – FoxO1. Even if there was a documented endogenous haploinsufficiency in the cell lines utilised, this would show the assays sensitivity is sufficient for a reduced copy number of FoxO1. There are several studies which show that knockout of FoxO1 and induced haploinsufficiency in mice has a clear phenotypic effect.[116,117] The haploid insufficiency studies resulted in the restoration of insulin sensitivity in insulin-resistant mice. This result further highlights the importance of FoxO1 interactions with the PI3K/Akt axis as detailed in Section 1.6.1.

1.11 Thesis Overview and Aims

The overall goal of the presented research is to apply the MAC chip technology to directly measure FoxO1 protein copy number in clinically-derived materials, with a focus on utilising non-invasive sputum samples from control and COPD patients. The MAC chip technology was chosen because, as mentioned in the previous section, most of the current single cell technology is incapable of processing heterogenous samples and the methods that can, require a significant number of cells for accurate analysis, which sputum cannot provide.

In order to achieve the overall goal, various assay agents will be tested and analysed to validate the ability of the MAC chip to detect FoxO1. The assay will be validated with two different capture agents – an antibody capture agent and also a DNA capture agent that will capture a subsection of FoxO1. A DNA capture agent is of interest here to selectively capture 'transcriptionally active' FoxO1. Therefore, 'total' copy number can be captured by the antibody capture agent, while the 'transcriptionally active' FoxO1 will be selectively capture with the DNA capture agent. The binding of 'transcriptionally active' FoxO1 with DNA is an over simplification and further details have been given in Chapter 1.4. However, for the sake of simplicity in the plots, the work is often described as total vs active copy number when comparing the data. The development of the MAC chip assays is detailed in Chapter 4.

Once the development of the two new assays to analyse FoxO1 is achieved, the next step will be to prove the assays ability to detect perturbations in FoxO1 copy number. The perturbations will be tested by growing various cell lines in conditions that are known to alter FoxO1 expression levels. The results of these assays will act as a control and provide evidence when using the assays developed on clinically derived samples. With COPD patient samples, there is only a hypothesis as to what should occur to the total and active copy numbers of FoxO1 in the disease state and therefore, correlating the results to these control assays will provide confidence in the results obtained. The perturbation studies are detailed in Chapter 5.

Before bringing the novel assay through to testing clinical samples, it will be necessary to analyse the reagents needed for a MAC chip experiment and determine which are most pivotal to achieving a successful experiment. This work will help optimise the MAC chip experiments for future use. The optimisation studies and the challenges that were faced while developing an optimal assay are detailed in Chapter 6.

Following the successful design of new MAC chip assays, the plan will be to optimise the assay using clinically-derived samples. In order to do this, lung and sputum samples from patients who were deemed healthy will be obtained and compared with samples from patients diagnosed with COPD. For this purpose, collaboration with the Peter Barnes group at the National Heart and Lung Institute (NHLI) was set up to provide access to patient samples. FoxO1 is not often used as a biomarker for COPD, and therefore the work outlined in this thesis is a proof-of-concept study. The main aim of this project is to provide evidence that the MAC chip can be used to utilise clinically-relevant samples for diagnosis of a disease state (in this case the disease state of interest is COPD). The expectation is to show that the MAC chip is a potential tool for bringing single cell proteomics into the clinic. The greatest advantages of the MAC chips are their ability to process small cell numbers accurately, provide an accurate readout and to be able to sort cells within heterogenous samples. The analysis of lung resection tissues and sputum is detailed in Chapters 7 and 8 respectively.

To summarise, the aims of this project will be to develop two new assays to analyse copy numbers of total and 'active' FoxO1. The main aim of this project is to produce a valid assay that can analyse clinically-derived samples. This is scientifically relevant as single cell diagnostics is always in need of new methods and tools.

2 Microfluidic Affinity Capture (MAC) Chip

2.1 MAC Chip Overview

The MAC chip is a microfluidic platform which is suited for the quantitative proteomic analysis of single cells and was first published in 2011 by Salehi-Reyhani et al.[118] The device utilises an all-optical approach for the isolation, lysis and subsequent protein quantification of single cells. The analysis itself consists of a miniaturised ELISA assay contained in a microfluidic environment. The microfluidic chamber volume assists in achieving a highly sensitive fluorescent TIRF readout to directly measure protein content within a single cell. The MAC chips unique place in the field of single cell proteomics is its ability to provide fully quantitative data on cellular protein copy numbers by calibration with recombinant protein standards. Another unique advantage of the MAC chip over other single cell techniques is the ability to actively isolate cells of interest in heterogenous patient (or cell line) samples, which allows quantification of a particular cell type of interest with absolute certainty.

The first MAC chip was developed to study the tumour suppressor protein p53. At the time of writing this thesis it is still the only successfully published assay utilizing the MAC chip method. To become a robust and useful analytical platform there was a need to expand the number of potential target analytes that can be analysed in the MAC chip regime. To achieve this, several previous attempts were undertaken by other PhD students including Gemma Milman's, Alastair Magness' and Ryan Lu's PhD theses, 2016, 2017, 2018 respectively, to design and develop assays for several protein targets of significance. In this project, the task was to take the MAC chip method and develop an assay for the Forkhead Box Transcription Factor O1 (FoxO1) which is a widely studied protein in several disease states.

The MAC chip method has been shown to be an effective platform in the relative and absolute quantification of p53 in single cell studies of cell lines.[20,33] What is of interest are the several features which make the MAC chip a highly useful platform for the processing of rare and precious clinical material. The key characteristics of the MAC chip for clinical material analysis are: 1) the isolation of cells allows high selectivity of viable and specific cell types, as surface specific markers can be used to ensure a cell type of interest is captured in heterogenous samples, viability staining is also possible to ensure only viable cells are analysed; 2) as the platform requires no fixation step, this means that the cells are viable until the point of analysis and thus functional and dynamic studies of proteins can be undertaken; 3) there is a low requirement for total number of primary cells, this allows for high data economy for a single patient sample. Currently bulk methods require a

minimum of around 50,000 cells for a semiquantitative measurement, whilst the MAC chip requires 50 single cells per experiment. So even if several chips must be run for an accurate conclusion, the total amount of cells is still greatly reduced. This would increase patient sample economy allowing several tests to be undertaken. It would also open the door to very small biopsies being sufficient for diagnosis, which leads to less invasive methods being used to generate the same diagnostic efficiency as current gold standards in the clinic. These characteristics drive the usefulness of the MAC chip in analysing precious samples which other single cell techniques do not utilise. FoxO1 is a robust biomarker for several disease states which makes it an obvious candidate for the MAC chip assay.

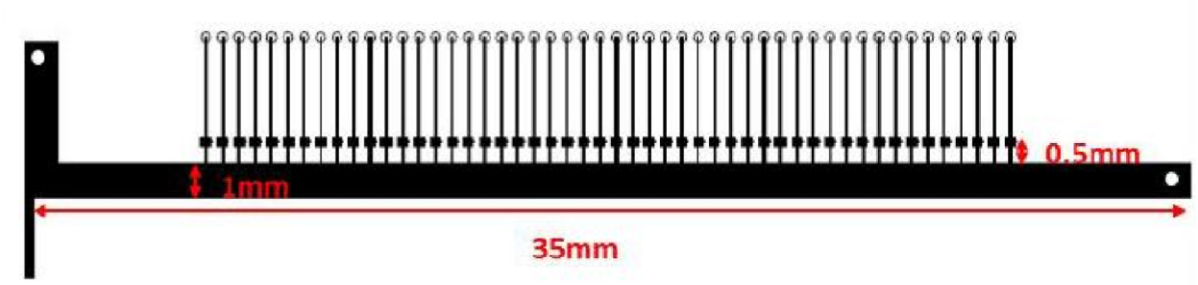
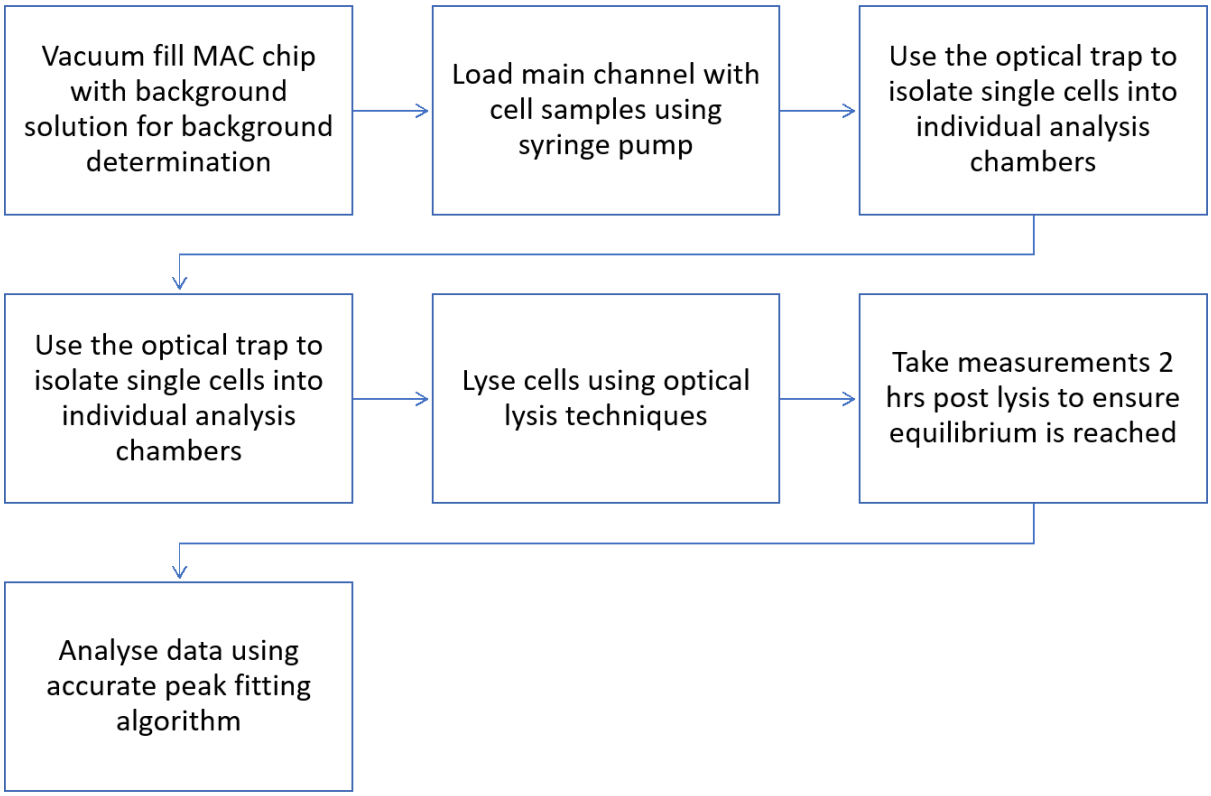


Figure 2.1 The MAC Chip. The design of the MAC chip shows 50 analysis chambers connected perpendicularly to the large main channel where the cells are loaded into the chip. This image is reproduced from Barclay and Magness et al.[14,119]

Two workflows show the experimental process of a MAC chip experiment, followed by the method of fabrication of a MAC chip and a breakdown of the tools used for analysis.



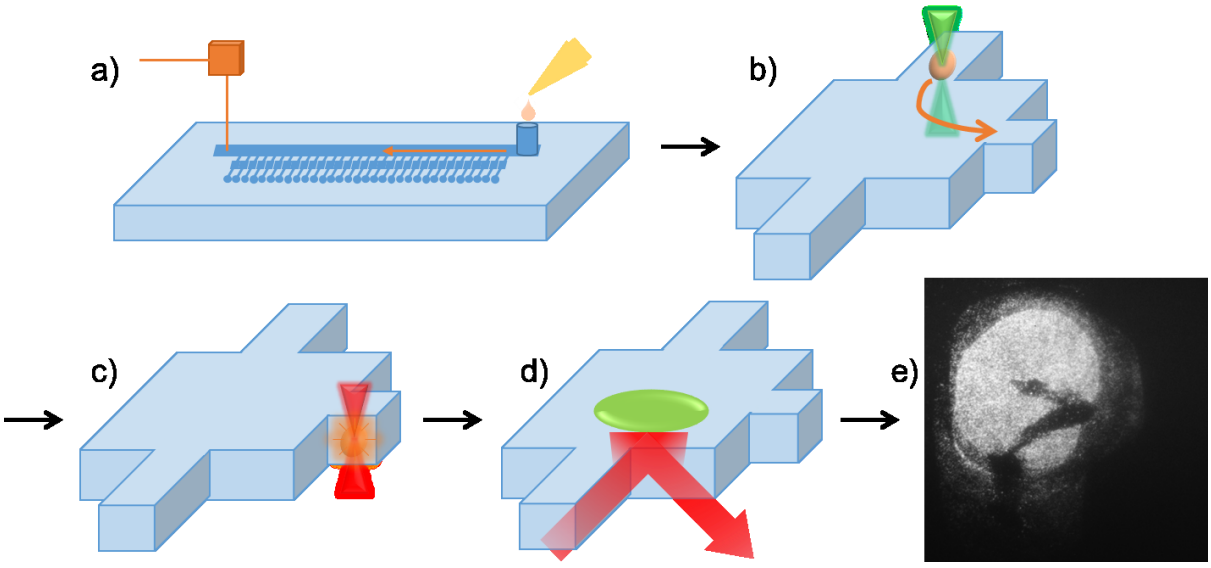


Figure 2.2 Top: A workflow of the MAC chip process to obtain single cell analysis. Bottom: Picture schematic of the MAC chip workflow. a) shows the loading of the 45-50 cells into the input of the device, where the cells are then drawn through to the outlet using a microfluidic pump, b) shows the trapping and isolation of the cells into the individual analysis chambers, c) shows the lysis of the cell using the high energy pulsed laser, d) shows the readout of the protein content of the single cell using single molecule TIRF microscopy techniques, e) shows a typical readout image of the printed Capture Agent spot and the protein of interested being bound to the spot and secondly to the fluorescent secondary antibody to generate single molecule fluorescence for each capture protein.

2.2 Microfluidics Introduction

Microfluidics is the science that deals with the flow of liquids in channels of micrometre sizes. Microfluidic chips are made of a set of micro-channels moulded into a material; these channels are connected in customised ways to give a desired function such as mixing, pumping and redirecting cells and many more.[30]

The most commonly used material for these devices is PDMS (Poly-DiMethylSiloxane) due to its optimal properties of being: transparent, biocompatible, deformable, inexpensive and easy to mould and bond to glass.[120] PDMS is widely regarded as the optimal material to make microfluidic devices due to the above properties as well as offering nanometre resolution[121], access to delicate structures such as integrated valves[122] and is well suitable for long term cell culture due to its gas permeability.[123]

Microfluidics are an optimal choice for use in single cell proteomics due to the channels having the same size as many of the cells of interest, allowing simple single cell manipulation. Also the low volumes used provide low equilibration times and quick binding of biomarkers to the glass surface.[120]

While PDMS and elastomers considered the most effective material for microfluidics in bioresearch including screenings and biochemical assays,[123,124] they still have unwanted properties associated with them. Whilst being extremely versatile for most biological applications it does have limitations. PDMS is limited to only aqueous solutions due to its organic solvent incompatibility[124], it suffers greatly from adsorption of biomaterials to the device walls[35,118], there are issues with water evaporation and concentration gradients forming.[124]

Other materials have been widely researched and reviewed[124] as the first generation of glass and silicon microfluidic chips as these chips suffered from a high cost of manufacture and limitations in biocompatibility.[124] This led to the research into new materials such as PDMS, as well as thermosets and thermoplastics. Thermosets proved to be limited in application due to their high cost and stiffness despite their solvent resistance and high strength.[125] Thermoplastics in general suffered from similar issues due to low gas permeability limiting cell studies and difficulties in forming valves and poor compatibility with other surfaces.[126] Although most thermoplastics are limited in function, perfluorinated polymers such as Teflon have proven to be extremely inert. This allows good solvent and chemical compatibility whilst also being able to access delicate structures and be gas permeable and thus compatible with cell culture.[127] Hydrogels have also been studied recently and show good

compatibility with most cells, though this varies depending on whether the gel is animal or plant derived. Their advantages lay in good compatibility for tissue cultures and simple fabrication techniques, but can only be fabricated into lower resolution structures.[128] One of the newest materials in development is paper. These paper methods must be refined and current applications at this time are limited and do suffer from low sensitivity. Though paper materials offer a cheap platform that has a promising future especially for commercial purposes.[129]

2.3 Surface Chemistry Introduction

For any sensitive adsorbent based assay, the chemistries of the capture surface must be considered to ensure the efficient and reproducible capture and detection of the target analyte. The use of untreated and unclean borosilicate glass is unsuitable for direct use in assays, as the glass will bind both hydrophobic and hydrophilic molecules. This non-specific binding leads to high levels of background binding and a poor signal to noise ratio (SNR).[130] Furthermore, the use of untreated glass gives a very heterogenous surface and so fluorophores will bind at varying magnitudes with respect to the local environment, which leads to a poor reproducibility for each chamber and intra-chip variability. Finally, microscopic pieces of dirt and dust can lie on the chip and bring their own autofluorescence which yields poor quality images. Given the need for high sensitivity, especially for a single cell regime, it is important to mitigate these issues. There are several methods for cleaning the slides to remove impurities which usually involve using base and non-polar solvent washes along with sonication to dislodge any and all organic and inorganic matter on the glass. Though this will only remove impurities and it does not generate a homogenous surface. Thus, non-specific binding of biological molecules is still a large issue. Hindering the unwanted binding of biological molecules is important to maintain a high signal to noise ratio. The process of trying to hinder non-specific binding is termed ‘passivation’ which aims to create a homogenous surface which also hinders non-specific binding.[131]

The MAC chip utilises one of the most popular surface chemistry passivation methods to achieve the necessary level of surface passivation. Firstly, the glass is coated in a series of polyethylene glycol (PEG) species of a high molecular weight of 5 kDa, these PEG chains are capped with a methyl to yield low biological molecule attachment properties. This is added along with another PEG species which has a biotin functionality. The added biotin functionality allows for the binding of Neutravidin which is a highly inert protein which further hinders unwanted biological binding. The final step for

passivation comes from flowing in background solutions of 4% BSA which further passivates the surface.

2.3.1 Orientation of Capture Agents Using Surface Chemistries

The printing of antibodies for use in the MAC chip affords what is known as a 'random orientation' adsorption. While this has advantages of a rapid and simple printing process, it also means a proportion of the deposited antibody lies on the surface in an orientation which is unable to bind the target analyte. This inability comes from the active site becoming masked or fully blocked by interactions with the neighbouring antibodies or with the coverslip itself. A simplified analogy is to picture the antibody as a cube, with only one side of the cube containing the active site which can bind the target analyte. This 'cube' is deposited randomly on the surface meaning, in the simplest terms, only a sixth of the antibody is deposited in an optimal fashion to successfully bind the target analyte. This is a simplified analogy but does demonstrate the disadvantage of a random printing method.

If the random printing method is not desirable, there are methods to attempt to orient the antibody, which has the added benefit of covalent, or near covalent binding it to the glass coverslip. As antibodies have several relatively active moieties there are several bioconjugation strategies which can exploit these moieties. Antibodies have surface lysines, cysteines and glycosides which are labile to react with different bioconjugation methods.[132] These methods will provide a relatively orientated and covalent print, although if these amino acids are present in the antibodies variable region and binding site, there is a chance of totally inactivating the antibody if the covalent attachment utilises amino acids in this region. While these methods do typically provide a greater capture efficiency, it cannot ever achieve a 100% capture.[30] Therefore, for this project it was decided not to use these methods as they offered little improvement over random adsorption methods currently used.

DNA orientation is comparatively far simpler, as DNA can be synthesised with a reactive functional group such as a maleimide, succinimide or a biotin at the terminal ends of the DNA sequence. This added functional group which is then able to react with a thiol, amine or neutravidin surface respectively to provide orientation of the DNA sequence. These methods are highly robust and as there is only one active moiety on each DNA molecule it provides a highly effective print strategy. These are discussed in Section 4.5

2.4 Readout and Data Analysis using TIRF Microscopy

As previously mentioned, the readout of the MAC chip is achieved using single-molecule total internal reflection fluorescence (TIRF) microscopy. Given the need for high sensitivity when working in the single cell regime the TIRF readout is well suited for single molecule detection for the MAC chip. Using TIRF microscopy greatly enhances the signal to noise ratio in the readout by greatly reducing the excitation region of the sample compared to similar techniques such as widefield microscopy.[133]

TIRF microscopy produces a fluorescent image of only a thin cross-section of a sample at the interface with a surface. In brief, the illuminating light hits the coverslip and media boundary at a large angle (compared to the epifluorescent regime where the light is perpendicular) and almost all the light is reflected off the sample interface. From this reflected light, a small amount of energy is transmitted as an evanescent wave to the sample where it can illuminate any fluorophores in close proximity to the interface. The evanescent wave relies on the incident light being totally internally reflected at the glass-media interface. The evanescent wave electromagnetic field decays exponentially from the incident light interface, meaning it only penetrates typically 100 nm into the sample. This gives a key advantage of inhibiting the illumination of unbound fluorophores in the bulk solution. This allows the user to load solutions with relatively high concentrations of fluorescent molecules that would otherwise cause a detrimentally high background signal if used in confocal or widefield microscopy.

The total internal reflection will occur at the interface between two medias with different refractive indexes (RI), for the MAC chip this is between glass and water. Depending on the RI of the two materials, the critical angle required to achieve total internal reflection will change. This critical angle is described by Snell's law in Equation 1.

Equation 1 Snell's Law equation. where n_1 and n_2 are the refractive indexes of the two materials.

$$\theta_c = sin^{-1}(\frac{n_2}{n_1})$$

The method of total internal reflection has the majority of the light reflect off the interface, though a small amount termed the evanescent wave will penetrate the sample to a small depth. The depth of penetration decays exponentially following the z axis. This is described in Equation 2.

Equation 2 Equation describing the depth of penetration for an evanescent wave. d represents the penetration depth with I(z) being the light intensity at a perpendicular distance, z, from the interface, I_0 with I_0 being the light intensity at the interface.

$$I(z) = I_0 e^{-z/d}$$

This exponential decay means that the evanescent wave can penetrate to depths as thin as 100 nm, therefore only fluorophores extremely close to the surface will be excited. This has the benefit of reducing background fluorescence as the ELISA style method of the MAC chip means only protein captured by the Capture Agent, thus is close to the surface, with secondary fluorescent antibody bound will be excited.

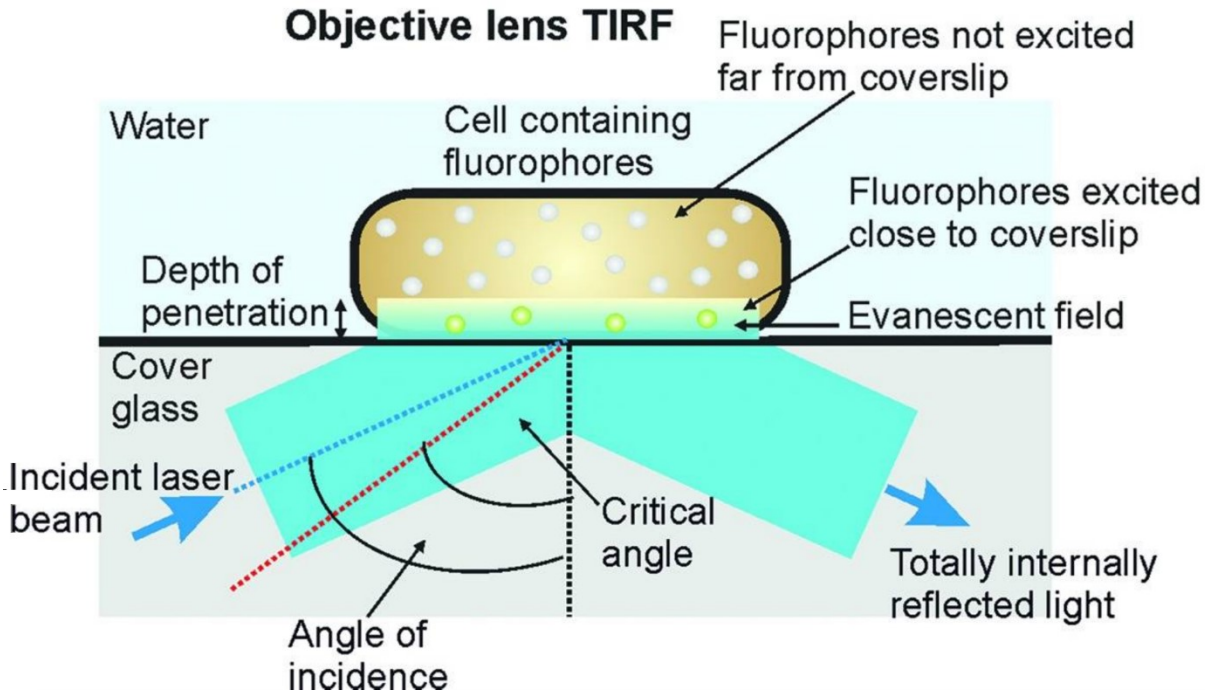


Figure 2.3 Diagram of a TIRF set up showing the total internal reflection and the evanescent field and its limited depth of penetration. Taken from Shashkova et al.[134]

Figure 2.3 above shows the general principle of TIRF microscopy and the method of placing the beam above a critical angle so as to yield totally internally reflected light. This means only the evanescent field will penetrate into the sample and the bulk volume is not illuminated, thus no excitement of background and unbound fluorophores.

The raw data obtained from the MAC chip TIRF set up is a sequence of single molecule fluorescent images. The fluorescence observed is from the secondary antibody bound to the analyte, FoxO1 in this project, captured down to the printed primary capture spot. Thus, each single fluorescent molecule observed corresponds to one captured analyte, assume that monoclonal antibodies are used. The images can be taken as a time-course, which shows the increase in fluorescence over time, or as a single time-points taken once the assay is at equilibrium. These images are analysed using the localisation counting algorithms detailed in Section 3.2.6. These algorithms can rapidly measure the

exact number of single molecule fluorescent events present in the image once fed simple parameters. These algorithms are discussed in Section 3.2.6.

3 Methods

3.1 MAC Chip Experimental Overview

The design of the standard MAC chip is covered in the original paper by Salehi Reyhani et al.[118] The design itself consists of a large main reservoir channel where the suspension of single cells is loaded via a micropump. Perpendicular to this main channel are typically 50 smaller channels which lead to individual analysis chambers of a fixed volume. The stepwise process of the workflow is detailed in the following subsections before a breakdown of the methods of fabrication for the MAC chip device itself.

3.2 Design and Manufacture

This section and subsequent subsections will introduce and detail the methods for the fabrication of the MAC chip in detail and all necessary processes are discussed.

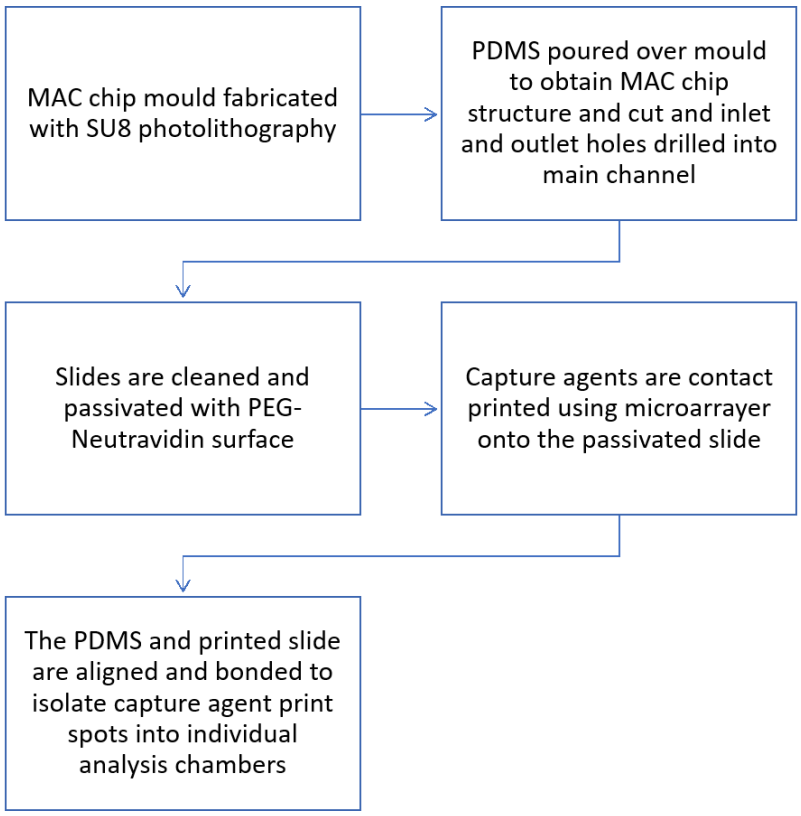


Figure 3.1 Workflow of how a MAC chip is fabricated for single cell analysis.

3.2.1.1 Microfluidic Mask and MAC Chip Fabrication

The MAC Chip mould was fabricated using SU-8-based soft-lithography techniques for PDMS.[127] Negative photoresist SU-8 [SU-8 Photoresist, Microchem, UK] was used to generate a positive imprint/mould of the design. The SU-8 masters were prepared as described by the manufacturers [SU-8 50, Elveflow, France]. Briefly, the silicon wafers were cleaned in 200 mL distilled water and then 200 mL ethanol and baked to dry. Approximately 1 mL of SU-8 was spin coated onto the wafer at a ramp rate between 100 rpm/sec to 500 rpm/sec to spread the SU-8 50, then increased after 5 mins to 3000 rpm at 300 rpm/sec to generate 40 µM thick layer. This was then soft baked for 5 min at 65 °C, then 15 min at 95 °C. The negative CAD design was then placed over the device and exposed to UV light at 350 nm for 45 seconds at a power of 250 mJ/cm^2. The wafer was then post baked for 2 min at 65 °C and subsequently 4 min at 95 °C. Un-polymerised SU-8 50 was then removed through the use of EC solvent developer and the wafer placed in a beaker. EC solvent (a developer) was then added to the wafer and the solution agitated through swirling. The Si-wafer surface was passivated by vapour-deposition of (tridecafluoro-1,1,2,2-tetrahydrooctyl)trichlorosilane) [(tridecafluoro-1,1,2,2-tetrahydrooctyl)trichlorosilane), Sigma-Aldrich, UK] under vacuum to enable easy lift-off of cured PDMS. Once this mould is made, it was possible to start mass production of the chips from this mould.[135]

3.2.1.2 PDMS Curing Closed and Open Chip

A mixture of PDMS and crosslinking agent [Sylguard, Sigma, UK] was mixed at 10:1 (typically 40.0 mL: 4.0 mL for a single mould respectively) and poured into the mould and left to cure.[118] Once the mould was set (≥24 hours), a microchannel replica on the PDMS block was obtained. The final steps were to punch in the inputs and outputs and sometimes the PDMS was treated with plasma to bind it to the glass slide finally sealing the chip.[135] This then yielded a closed chip.

An open chip was cured in the same way and then a sterile scalpel was used to cut out wells to line up with the printed arrays on the glass slide.

3.2.2 MAC Chip Manufacture

The MAC chip manufacture was separated into two components: (i) the microfluidic architecture, which was provided by a PDMS chip to provide the channels and the analysis chambers and (ii) the chemically passivated glass coverslip that gives the base of the device where the primary Capture

Agents are printed onto. The PDMS microfluidic architecture and the passivated glass slide were fabricated separately and combined shortly before an experiment.

MAC chips microfluidic properties were manufactured using the well-established photolithographic and soft lithographic techniques using the PDMS elastomer. Prior to the PDMS fabrication, a master template was designed using auto CAD or similar software that created the wanted architecture, and then could be translated to a master silicon wafer baseplate. A SU-8 negative resist is an epoxy resin and was crosslinked by UV light onto a commercially available photomask that created the master template. The PDMS elastomer was poured over the master template and left to cure and set the PDMS architecture of the master template. Once cured, the PDMS microfluidic was removed and two holes were drilled at the ends of the main channel to provide the inlets and outlets. The soft lithography process is well described in the literature.[14,119,136]

3.2.2.1 Surface Chemistry Methods

To clean and prepare glass slides for subsequent functionalisation, the slides were placed in a slide staining jar and treated sequentially with: 1.0 M KOH (20 min), MilliQ Water (5 min), acetone [Acetone 99% Analr, Sigma, UK] (15 min), MilliQ (5 min), 1.0 M KOH Solution (20 min), MilliQ (5 min) and finally acetone (10 min).[137] At each step, the slides were rinsed with each solution 3 times and each time placed in a sonicator at each wash step. The cleaned slides were then dried with nitrogen.

GPTES functionalisation was performed on cleaned slides by initial treatment in the plasma oven [Harrick Plasma] for 2 min and being immediately placed into a solution comprised of 50.0 mL ethanol, 50.0 mL GPTES [GPTES, Sigma, UK] solution and 5.0 mL acetic acid [Acetic acid, VWR, UK] for 20 min with a 1 min sonication halfway through. The treated slides were then washed with ethanol 3 times before being dried with nitrogen.[138]

The next step in the process was the PEG functionalisation step.[139] Firstly, cleaned slides were placed in a solution of 100 mL ethanol, 5.0 mL acetic acid [Acetic acid, VWR, UK] and 2.5 mL (3-Aminopropyl)triethoxysilane (APTES) [APTES, Sigma, UK] for 20 min with a 1 min sonication mid-way to facilitate the PEGylation of the slides. The slides were then rinsed 3 times with MeOH [MeOH, Sigma, UK], 3 times with deionised water and subsequently dried with nitrogen. Subsequent PEG/PEG-biotin-SVA functionalisation was performed by mixing 5–15 mg of PEG-biotin-SVA 5000 mW [PEG-biotin-SVA 5000, Laysanbio, USA] with 50 mg of mPEG-SVA 5000 mW [mPEG-SVA 5000, LaysanBio, USA] in 400.0 µL of 1 mM sodium bicarbonate buffer [Sigma, UK]. After the PEG solution was mixed, 80.0 µL of this was pipetted onto an APTES-treated coverslip and sandwiched with another prepared slide before incubation in darkness at room temperature in a humidity chamber

for 2–3 hours. The derivatised coverslips were then removed, rinsed copiously with deionised water and stored in the dark at room temperature until required.

Immediately before printing the slides were further functionalised with NeutrAvidin®, 80.0 µL of NeutrAvidin® at 0.1 mg/mL in Dulbecco's phosphate buffered saline [DPBS, PAA Laboratories GmbH, USA] was pipetted onto the PEGylated coverslips and incubated in the dark for 1 h at room temperature. Coverslips were again copiously washed with MilliQ water, dried with nitrogen and used immediately for printing.[118]

3.2.3 Microarray Printing

One of the most widely used methods for protein capture in assays is microarray printing. There are now several different biosensors available in microarray formats. These microarrays utilise several Capture Agent molecules, such as DNA, antibodies and small molecules such as therapeutic drugs or aptamer or affimer molecules.[140] These methods are highly robust and several arrays can characterise hundreds of thousands of proteins simultaneous when measuring bulk samples (i.e. tissue or cell lysates). The MAC chip is analogous to a larger ELISA assay as it uses a Capture Agent for the target of interest (for this thesis the Capture Agent is either an antibody or a DNA capture sequence) to the surface of a passivated glass slide. These printed Capture Agents can isolate and bind a target analyte to the surface, which is then sandwiched with a fluorescently tagged 'secondary' antibody to allow the detection of the target analyte. Using microfluidics, the printed spots are isolated within the individual analysis chambers of a confined volume which provides the sensitivity required to allow single cell protein resolution.

3.2.3.1 Microarray Printing Method

The MAC chip Capture Agents were printed onto the passivated coverslips using an Omnigrid digital microarrayer [Omnigrid digital microarrayer, ArrayIt, USA].[33] This microarrayer allowed for several coverslips to be printed in a pre-made pattern where the printed Capture Agent spots align with the microfluidic architecture, so the printed spots line up with the individual analysis chambers of the microfluidics. The Capture Agents were diluted 1:1 with the print buffer 3XSSC [SSC, Sigma, UK] 1.5 M betaine [20xBetaine, Sigma, UK] (final concentration), which gave a final printing concentration of 0.5 mg/mL for antibody printing and 50.0 µM for DNA printing (unless otherwise specified in the Results sections). This print buffer was used as it is known to be among the best printing buffers for both antibody and DNA microarray printing both in the literature.[141]

ArrayIt 946MP2 [ArrayIt 946MP2, ArrayIt, USA] contact printing pins were used for printing the Capture Agent, which were developed originally for use in DNA microarray fabrication – but are equally applicable to protein microarray fabrication. They have a spot diameter of 62.5 µM, an uptake volume of 250.0 nL and a delivery volume of 500.0 pL (dependant on print solution and printing conditions).

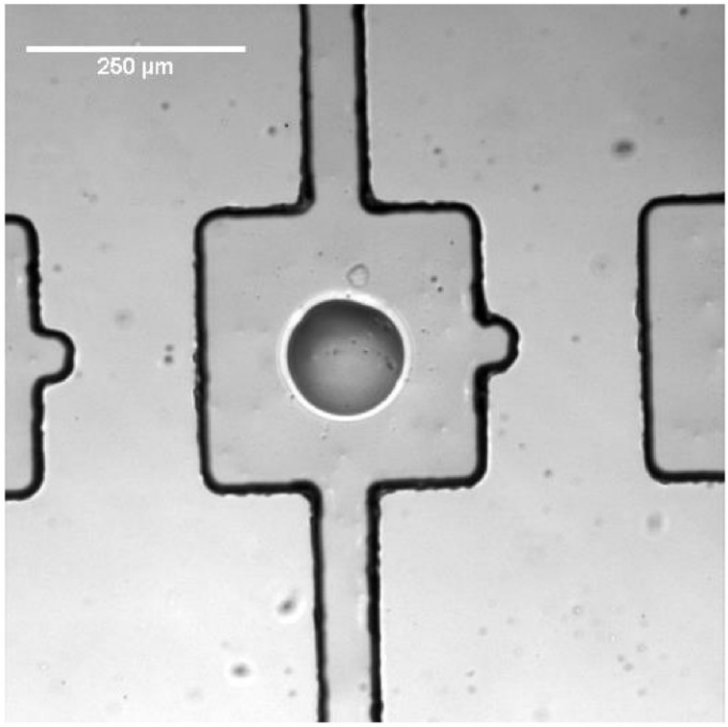


Figure 3.2 Printed microarray spot inside of the standard 4.5 nL [300X300X50 µM] MAC chamber.

3.2.4 Final Device Bonding of Microfluidic Architecture with Functionalised Coverslip

The final step of the device fabrication was to align the PDMS microfluidic architecture with the printed microarray of Capture Agent spots.[33] This was achieved using a bespoke alignment rig that allows the movement of the PDMS chip with respect to the static functionalised coverslip in the x,y and z dimensions, along with rotation in the x,y plane. When the PDMS is aligned with the coverslip microarray, the PDMS can be lowered onto the coverslip until contact binding occurs between the PDMS and coverslip. If the PDMS and coverslip are sufficiently clean, the contact binding process is sufficient to maintain the integrity of the device when running a typical MAC chip single cell experiment. The added advantage of using contact binding means that the PDMS architecture can be recovered after the experiment, properly cleaned and reused for future experiments.

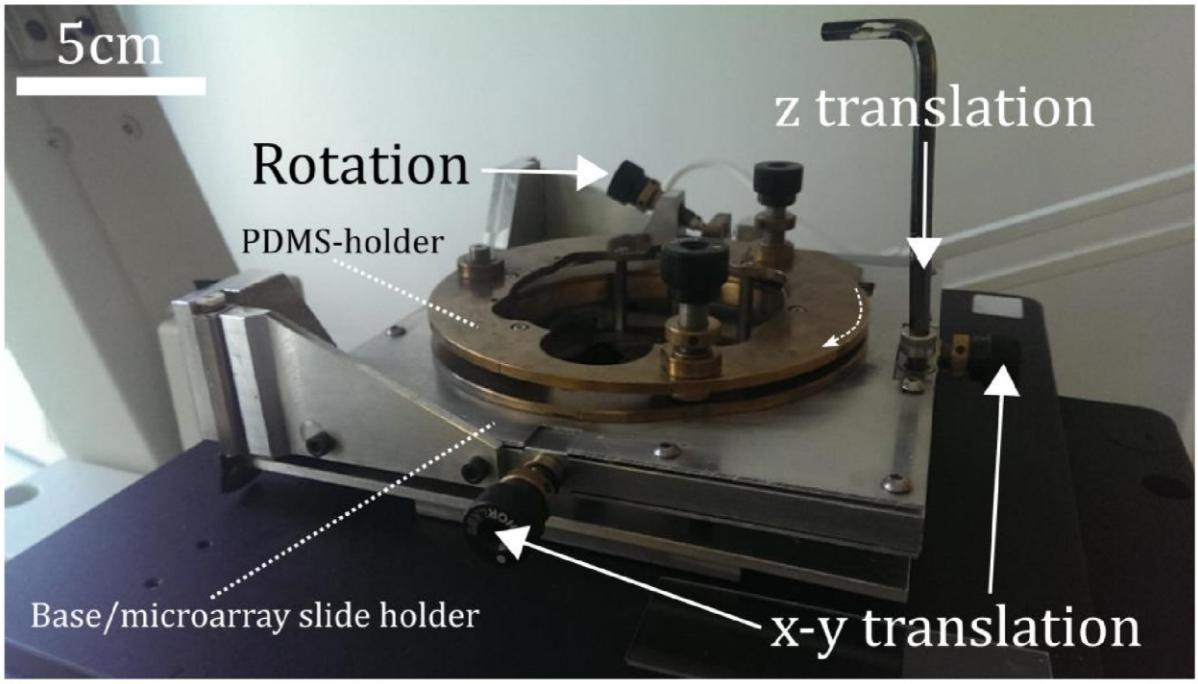


Figure 3.3 The MAC chip bespoke alignment rig. The adjustment micro-screws labelled allow precise movement of the PDMS architecture relative to the microarrayed slide prior to assembly. Picture courtesy of Alastair Magness.

3.2.5 Device Filling and Cell Loading

Once the MAC chip is fully fabricated, the next step was to fill the chip with a solution of 4% BSA [BSA, Sigma, UK] in Dulbecco's phosphate buffered saline, supplemented with the fluorescent secondary antibody at the stated concentration (typically 250.0 or 500.0 ng/mL). The filling was achieved by placing this 4% BSA + secondary antibody solution at the inlet and outlet of the fabricated MAC device and placing this in a vacuum desiccator for 10–20 min.[118] The cells used in this thesis were grown in several conditions, though all were isolated and resuspended (typically requiring trypsinisation treatment) in phenol red free RPMI media with the concentration of secondary antibody. This cell solution was drawn in to the main channel of the device by pulling the cell solution through from a small reservoir over the device inlet using a microfluidic syringe pump [SPS01, Labsmith Inc, UK]. Once the main channel was filled with cells, the optical trapping methods (detailed in Section 2.1) followed by the optical lysis methods were used to isolate and lyse the cells to allow the final single cell analysis of protein copy number. As many cells as possible were trapped and isolated within 1 h, which was usually enough time to capture a full amount of 50. Once the cells were successfully isolated into individual analysis chambers and lysed, the chip was imaged typically every 30 min for 2 h using the TIRF microscopy techniques.

3.2.5.1 Loading of Cells into the MAC Chip

A microfluidic pump [SPS01, Labsmith Inc, UK] was attached to one end of the main channel and on the other end a solution of cell suspension in phenol red free RPMI was loaded.[118] The pump allows the user to draw the cell suspension through the main channel for subsequent optical trapping to isolate 45–50 cells into the individual analysis chambers.

3.2.5.2 Optical Trapping for Single Cell Isolation

The 45–50 cells that were loaded are then isolated from the main channel and loaded into individual analysis chambers via an optical trap.[142] The optical trapping technique can create forces upon the cells of an ideal energy to safely manipulate the cells without disrupting the subcellular compartments or cell integrity. The principal behind the optical trap is to use a tightly focussed laser beam which goes through an objective lens creating a steep spatial light gradient. This light gradient interacts with dielectric particles to impose a force onto the particles (or cells in this scenario) to pull them in the direction of the greatest intensity, thus drawing the cells to the focal point of the laser light. The laser also propagates a scattering force which shifts the cell in the direction of the beam that results in transfer of momentum from the laser photons to the cell in the beam path. The equilibrium of both the scattering and beam gradient force causes the trapping of the cell and then by moving the position of the trap with respect to the cell's environment, the cell can be moved to any desired location in the x and y axis. The main requirement for successful trapping was that the cell solution must not be too viscous as this might exceed the trapping force of the laser and thus impeding the movement of the cell.[143] The optical trap allows for specific cells to be chosen, which can be achieved by surface marker expression or even by simple identification of characteristic cell morphology.

The laser to provide the single cell trapping was formed of a single-beam produced by an ytterbium fibre laser [YLM-5; IPG Photonics, UK] at a wavelength of 1070.0 nM, with the objective focal and trapping planes being coincident. This laser traps the cell that then can be readily moved in the microfluidic chip by moving the motorised stage. In reality, it is the MAC chip itself that is moved, and the cell held static.

3.2.5.3 Optical Single Cell Lysis

Once the cells are loaded into their individual analysis chambers, the final handling step was cell lysis.[144] The lysis was achieved by a high energy laser pulse (E=14μJ; 6ns pulse; λ=1064nm) into the medium near the cell. The laser pulse creates a cavitation bubble that ruptures the cell membrane

and releases the cellular contents into the analysis chamber. This method was the method utilised for the cell lysis of all cells within this project. The cell lysis pulse energy is set to 14.1 ± 0.3 μJ which corresponds to a 100% probability of plasma formation and thus cavitation bubble formation. The laser used was a Q-sw Nd:YAG laser [Surelite SL I-10, Continuum, USA]

3.2.5.4 TIRF Readout

The readout came from total internal reflection fluorescence [TIRF] microscopy based on single molecule imaging of fluorescence at the printed Capture Agent spot.[133] Once the assay reached an equilibrium, the amount of bound protein was imaged using the readout TIRF laser [Vortran, UK, λ=405, 488, 532 or 647 nM] and an Andor iXon DU-897E EMCCD camera [Andor iXon DU-897E EMCCD camera, Andor Technologies, Ireland]. As mentioned previously, all the steps to the cellular manipulation through to lysis and analysis were achieved using optically-based methods and setup on a standard inverted microscope [Nikon TE2000U microscope, Nikon, Japan.

3.2.6 Localisation Counting Algorithm

The final stage of the MAC chip experiment was to analyse the TIRF images taken to determine the single molecule count, which is a direct measure of protein copy number.[33,119] There are two methods used: the 'non-congested' method and the 'congested' method. These methods were developed in-house and written in ImageJ.

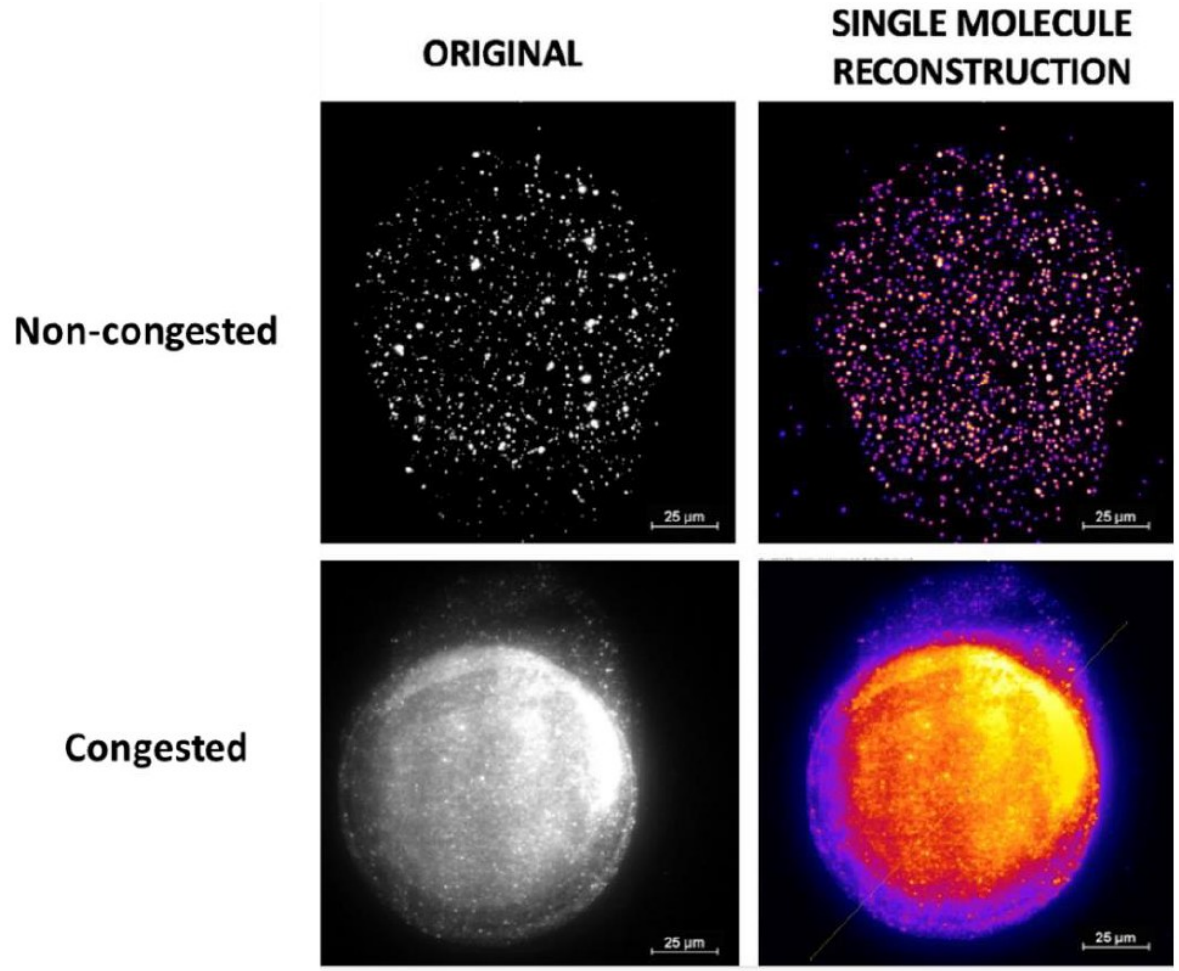


Figure 3.4 Example of non-congested (top) and congested (bottom) images and their reconstructions. The top left shows the captured image of the Capture Agent spot with bound fluorophores which are spatially separate from one another (non-congested). The top right shows the reconstruction of this image using the non-congested algorithm and the assigned single molecule intensity. Bottom left image shows a Capture Agent spot that has a high number of bound fluorophores which cannot be spatially distinguished. The bottom right shows the use of the congested algorithm to assign the single molecule count. Image from Ho et al.[145]

For both non-congested and congested analysis (each example can be seen in Figure 3.4 in the left-hand column) the first stages were background corrections. As the illumination is not consistent across the chip, this was corrected with control images that have no antibody spot but does have the background solution containing the secondary antibody. The control images can be used to correct for the variation in the illumination intensity. Secondly, images were also taken of the antibody spots and their interaction with the secondary antibody, which gives the single molecule background count for each of the analysis chambers. The images are then averaged to give a background subtraction, which is subtracted from the obtained single molecule count from the image taken 2 h after cell lysis to give a more accurate measure of the single molecule count. It was also possible to subtract the background in a chamber by chamber manner, depending on the experiment.

The counting methods are broken down into full methodical detail in the following sections.

3.2.7 Non-congested Counting

The non-congested counting method was a key step for both non-congested single molecule counting and for accurate congested image counting also. The method utilised was a gaussian localisation process that is broken down into the following flowchart:

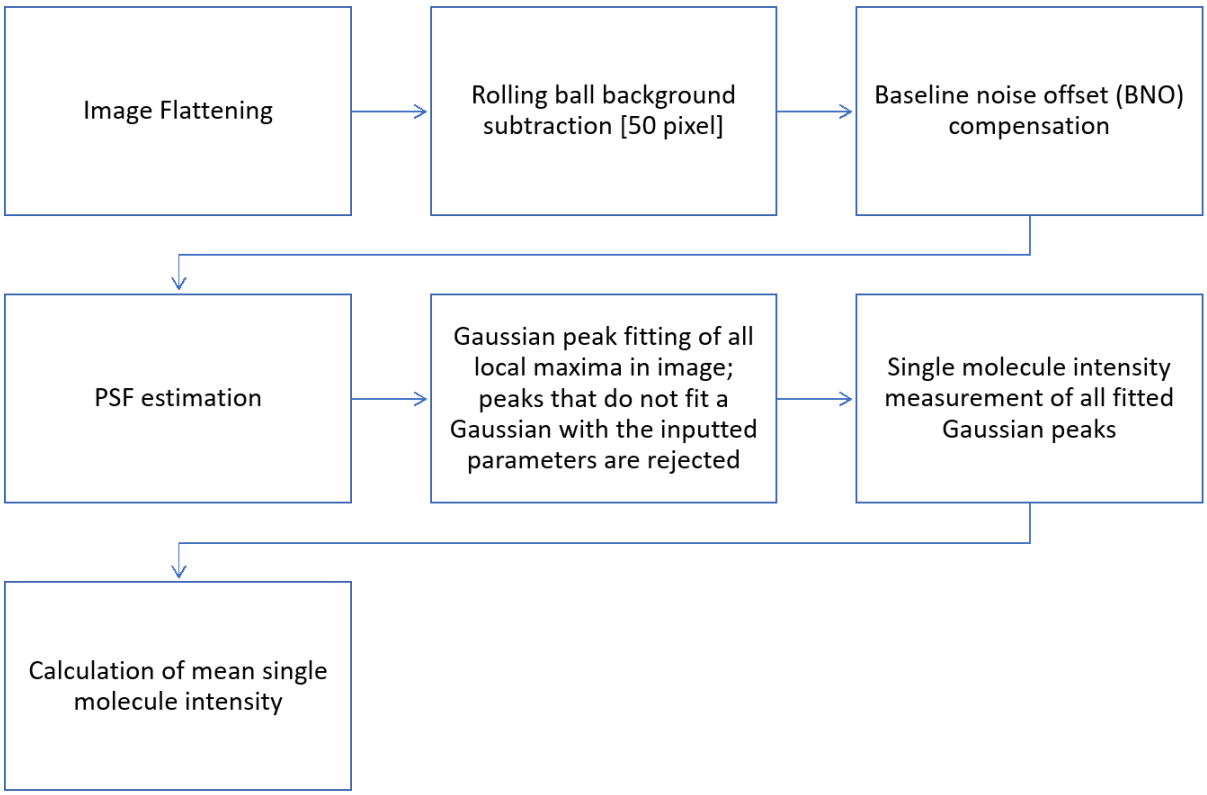


Figure 3.5 Flowchart of the image processing steps for the single molecule counting algorithm.

The non-congested counting program was the most widely used counting method in this thesis. In the presence of a low amount of antigen, the image of the fluorescence accumulated from the sandwich assay was populated with single molecules that are spatially resolved. Being spatially resolved means the pixels of the observed single molecules do not overlap each other.

This non-congested analytical method used a relatively sophisticated technique that can determine whether a single molecule was considered a 'real' molecule, rather than simply noise in the image. This determination was based on analysing the Gaussian distribution profile of the pixel intensities. The used algorithm utilised the 'GDSC Single Molecule Light Microscopy' plug-ins from the University of Sussex.[146] This plug-in attempts to assign a Gaussian profile to each detected molecule by taking parameters which are set by the user to provide an accurate fit (it can be tuned to accommodate for if the program is over-counting or under-counting molecules). If a molecule meets the inputted criteria, then it is highlighted as a single molecule and its intensity is calculated. One benefit of this

algorithm is that it can assign multiple overlapping Gaussians to accurately measure neighbouring single molecules. This is detailed stepwise in the following subsections.

3.2.7.1 Image Flattening and Background Subtraction

This subsection details the image flattening, background subtraction, and baseline noise offset compensation steps of the analysis software. As the TIRF laser had a Gaussian intensity profile it means the periphery of the image was often less illuminated compared to the image centre. Thus, it was important to normalise the image so the that a fluorophore excited at the image periphery and an identical fluorophore excited in the centre have the same apparent brightness. This is done by dividing the raw single molecule image by an image of the laser profile from a series of single molecule images from the experimental run that is being analysed. These images should be from the same experimental run (each MAC chip experiment has its own background measurements taken). In practise this was achieved by leaving 5 MAC chip analyte chambers blank; 5 chambers were sufficient to accurately analyse the laser profile and still maintain a good number of cells to be analysed (45 cells per MAC chip). The algorithm generated a suitable approximation of the laser profile by creating an image stack from the sparsely populated images. The algorithm then performed a median intensity projection through the stack, followed by a Gaussian blur [default r = 50 pixel], to smooth out discontinuities in the resultant image. A final step subtracted the camera bias from the profile [100 analogue-digital units [ADU] for the Andor iXon 897].

The flattening process can be disturbed by intensity variations that do not arise from single molecules. The two main sources of these disruptions come from scattered laser light of the TIRF interaction with the PDMS architecture or from intrinsic autofluorescence in either the sample or antibody spot itself. These variations were removed using a rolling ball background subtraction with the ball itself having a correct radius. The rolling ball algorithm was designed to remove image features that have a space larger than the radius of the ball itself. The rolling ball works as follows: any 2-dimensional image can be thought of as a 3-dimensional surface, where a third height dimension is defined by the pixel intensities at each point in the image. A virtual ball is rolled across the underside of this surface, and the whole volume that is reachable by the ball defines parameters which constitute the background. Areas smaller than the ball itself are inaccessible to it and so these do not form part of the background volume and are not subtracted. The key to highly accurate background subtraction was to accurately define the correct rolling ball radius to ensure large unwanted features are removed without effecting the single molecule data.

The final stage was the baseline noise offset compensation, or BNO. This was used because even the pixels which have ‘nothing’ (i.e. a single molecule etc.) still have inherent noise within them. Measuring the intensity profile across a flat, background subtracted image, it was still observed that the profile was noisy, and varies randomly around an arbitrary level – close to but not exactly zero. Without BNO compensation, the counting programs – mostly the congested counting program – will overcount the number of single molecules. This was because even if the intensity of a pixel with ‘nothing’ was low, when this was multiplied across many pixels in a whole image [512x512 in this project] the overall net contribution was large and would bias the data. The BNO was calculated from taking 4 line profiles in the bottom left edge of an image, the bottom left was an arbitrarily chosen periphery as it was most likely to not encounter any single molecules, thus it will not incorporate single molecule information into the measurement. The mean and standard deviations of the pixels intensities along the single line profiles were measured. If a high standard deviation was observed in these measurements, it was highly likely that a fluorescent single molecule had been captured in the measurement.

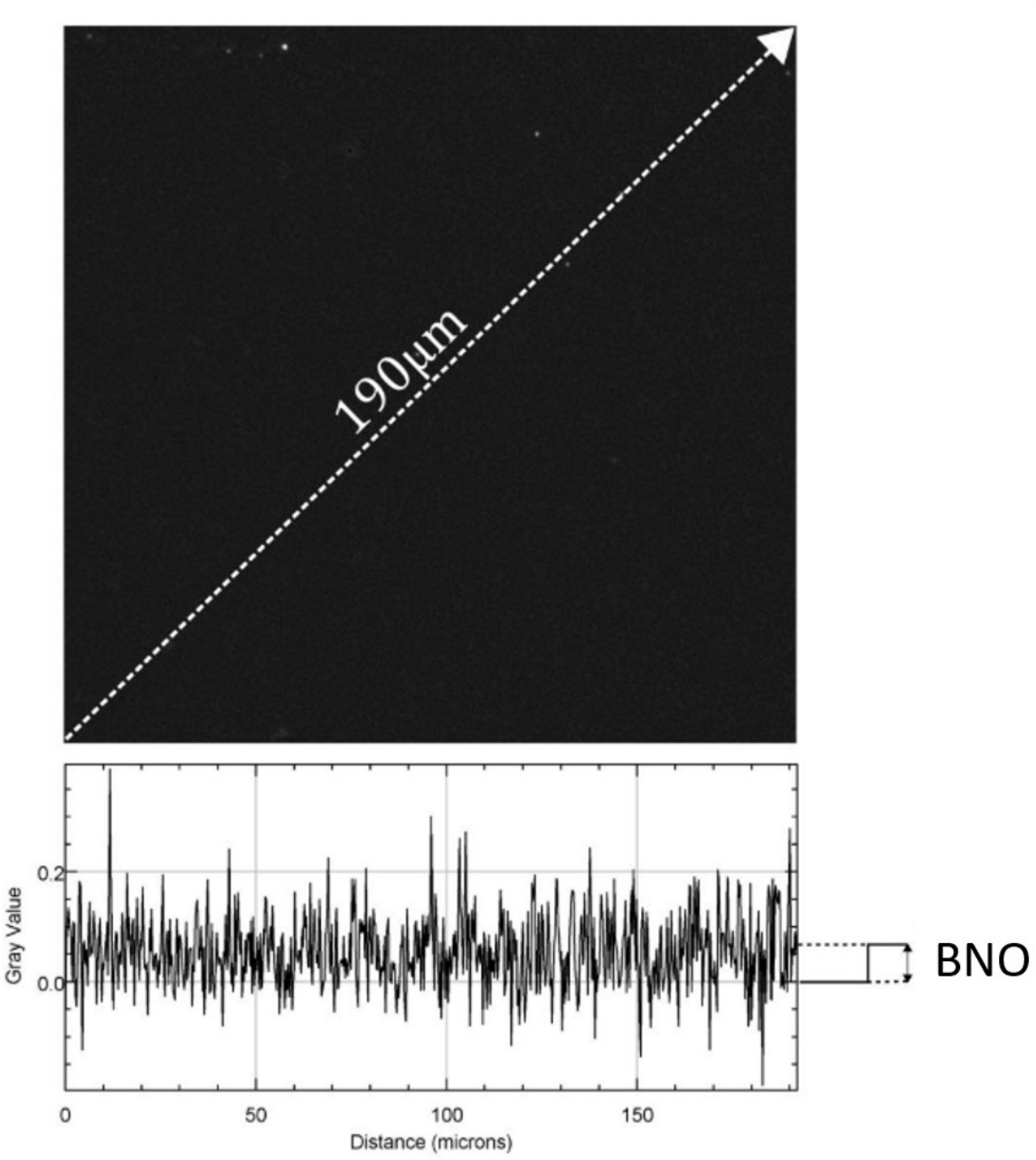


Figure 3.6 Illustration of the Baseline noise offset. Profile is taken from bottom left to top right. Usually the noise floor of the image has a finite value which is observed in all images and experiments. Subtracting the BNO from every pixel produces images where the noise floor is on average at 0. This means the only contribution to the total integrated intensity now comes from single molecules.

3.2.7.2 PSF Estimation and Single Molecule Counting by Gaussian Fitting

After the flattening and background subtraction stages, the only contributor to the total image intensity was the single molecules. The next stage was to estimate the point spread function (PSF) of the microscope, so that the subsequent least-squares Gaussian fitting routine has an appropriate reference as to what a true single molecule should look like. This was achieved by the PSF Estimator plugin of the GDSC SMLM toolset.[146] This plug-in makes a best guess as to the true profile of a single

molecule by randomly selecting N peaks, typically 1000, in the image and using least-squares fitting for the intensity of the surrounding pixels and then calculating the average of the Gaussian parameters of each peak. The estimator uses the starting configuration to fit N peaks taken from randomly selected frames in the image stack. The average of the fitted parameters was then used as the starting parameters to perform fitting again. This iterates until the Gaussian parameters does not significantly change.

Once the Gaussian profile parameters were obtained, the Peakfit algorithm within the GDSC SMLM package can test every intensity peak in an image and identify each as to whether it was a single molecule. The two contributing factors were signal and width and these define the degree of flexibility for the fit. This toolset will output the number of single molecules identified in each image along with the average single molecule intensity.

This concludes the use of the algorithm to accurately determine the number of single molecules found within a non-congested image. This process was also run initially for a congested analysis by analysing the background images, prior to loading the chip with analyte. This process was necessary to acquire the average single molecule intensity (ASMI) for analysis of congested images.

3.2.8 Congested Counting

Once the images single molecules can no longer be spatially resolved from each other and the profiles overlap, the image was considered ‘congested’ and the single molecule counting algorithm could no longer be used. A key calculation that the single molecule counting algorithm gives – used for non-congested images – is the averaged single molecule intensity (ASMI) for the fluorescent antibody. The calculated ASMI will vary from several factors, such as the fluorophore used, the number of fluorophores tagged to each antibody and the illumination intensity (laser power) used in the experiment. As the individual molecules vary in intensity, the ASMI is calculated over several thousand molecules taken from several images in the same experiment and provides a surprisingly consistent intensity for experiments using the same fluorescent antibody. The determination of the ASMI was very important to help detect the number of molecules in a congested image.

3.2.8.1 Congested Counting Method

The congested count works differently from the non-congested algorithm and was a simpler technique. In this case, the total intensity for each image was taken and then divided by the previously calculated ASMI giving the single molecule count for the image. This was a valid method,

although it was imperative that the TIRF EMCCD camera was not saturated during image capture, because this would lose the intensity information for the image and thus no intensity-based calculation could be made. While this was typically not an issue, the acquisition settings were still monitored to ensure the camera was not saturated and the optimal dynamic range was utilised.

This section has detailed the whole process for the fabrication and experimental design of the MAC chip methodology. It has detailed the experimental theory behind the MAC chip – through all the optical methods for the isolation, lysis and analysis of single cells and the use of microfluidics to bring the assay down to a single cell sensitivity. Nearly all the experiments detailed in this thesis utilised this workflow.

3.2.9 Data presentation

The data in this thesis is typically presented as a histogram format. This is because a histogram is a suitably accurate representation of the distribution of individual data points within a population. Histograms give a simple-to-digest view of the density and distribution of the data to make it easy to interpret statistics found in the population.[147]

For the work presented in this thesis, the x-axis bins represent the observed single molecule count that is obtained from the algorithm detailed in Section 2.4. These bins are normalised with respect to the number of cells analysed and the spread of the data. The y-axis shows the cell count, which is the number of cells that gave the single molecule count within the given bin range.

3.3 Cell Culture Techniques

3.3.1 Toledo Cell Line

Toledo (ATCC® CRL-2631™) B Lymphocyte cells [ATCC® CRL-2631™, ATCC, UK] were cultured in RPMI-1640 [RPMI-1640, Invitrogen, UK] supplemented with 10% (v/v) foetal bovine serum [FBS, Sigma, UK] at 37.0 °C and 5.0% CO_2 atmosphere. To harvest, the cells were spun down at 1000 rpm for 10 min and the pellet washed twice with 10.0 mL PBS and the pellets collected again after centrifugation at 300 rpm for 5 min. The pellet was resuspended in phenol red free RPMI and concentrated to 500,000 cells/mL, which was measured by a cell counter haemocytometer. The viability was measured by a trypan blue stain that was added 1:1 to a 10.0 µL sample of the cell suspension.

3.3.2 MCF7 Cell Line

The MCF7 human breast carcinoma cell line was cultured using Dulbecco's Modified Eagle Medium [DMEM, Corning, UK] supplemented with 10% foetal bovine serum [FBS, Corning] at 37 °C and 5.0% CO_2 atmosphere. To harvest, cells were washed with PBS and then detached from the culture flask using Accutase [Accutase, Thermo Fisher, UK], re-suspended in DMEM, pelleted at 200 RCF and re-suspended at a concentration of ~5 x 10^5 cells/mL in phenol red free RPMI.

3.3.3 Beas-2b Cell Line

BEAS-2B cells were cultured using Keratinocyte Media [ATCC, UK] supplemented with 5% (v/v) Bovine Pituitary Extract [BPE; ThermoFisher, UK] at 37 °C and 5.0% CO_2 atmosphere. They were cultured on PureCol® Collagen Coated flasks [PureCol®, Advance BioMatrix, US] to enhance adhesion. To harvest, cells were washed with PBS and then detached from the culture flask using Accutase (Thermo Fisher), re-suspended in DMEM, pelleted at 200 RCF and re-suspended at a concentration of ~5 x 10^5 cells/mL in phenol red free RPMI.

3.3.4 Lung Resection Culture

Resected lung cells were cultured from lung resection surgical tissue in LHC-9 media [Invitrogen, Paisley, UK] in collagen (1% w/v) coated 24-well plates [Advance BioMatrix, US] at 37 °C and 5.0% CO_2 atmosphere. To harvest, cells were washed with PBS and then detached from the culture flask using Accutase [Thermo Fisher], re-suspended in DMEM [DMEM, Sigma, UK], pelleted at 200 RCF and re-suspended at a concentration of ~5 x 10^5 cells/mL in phenol red free RPMI.

Collection and processing methods are described in more detail in Section 3.5.1.

3.3.5 Sputum Freezing

Collected sputum samples are discussed in detail in 3.5.2 for their collection and processing. The freezing media used was 10.0% DMSO in Hanks' Balanced Salt solution [HBSS, Sigma, UK]. Cells were stored at -150 °C and resuscitated immediately prior to their analysis.

3.4 Other Methods

3.4.1 Western Blot

Gels were transferred to a MeOH pre-treated PVDF membrane [Gibco BRL] using a MeOH/tris-glycine transfer buffer and a current of 400 mA for 90 minutes. The membrane was blocked using a 5% milk protein in TBS/tween buffer for 1 h at rt. The membrane was then treated with the primary antibody in 5% milk protein in TBS/tween buffer for 1 h at rt. The membrane was then rinsed 3 times for 10 min each with TBS/tween buffer. The membrane was then treated with secondary-HRP antibody in 5% milk protein in TBS/tween buffer for 1 h at rt. The membrane was then rinsed 3 times for 10 min each with TBS/tween buffer.

3.4.2 Western Blot Imaging

Western blot membranes were imaged using HRP-substrate [Bio-Rad] in a 639 FujiFilm Image Reader LAS-3000 Pro [Fujifilm LAS-3000, Fujifilm, Japan].

3.4.3 Bulk Cell Lysis for Western Blots

Cells were lysed at 90% confluence by rinsing with ice-cold PBS and treating with 300.0 µL lysis buffer (1% Triton X-100, 0.1% SDS and 150 mM sodium chloride in PBS containing protease 87 inhibitors [Complete Mini EDTA-Free, Sigma Aldrich] and incubating on ice for 30 min. The membrane fraction was removed by centrifugation and the lysate stored at -20 °C or -80 °C.

3.4.4 Fluorescent Labelling of Antibodies

Antibodies were conjugated where necessary with Alexa Fluor 488 using either an APEX Antibody Labelling Kit (Life Technologies) or a Monoclonal Antibody Labelling Kit [Life Technologies, UK]. Samples were further filtered using either a dye removal column or a molecular weight cut-off filter as required.

3.4.5 DNA Hybridisation

The single stranded oligomers were hybridised by heating to 95 °C and allowing to cool over several hours. This DNA oligomer contained a terminal biotin group which allows it to bind to the functionalised glass coverslip.

3.5 Patient Sample Specific Methods

3.5.1 Lung Resection Tissues

All subjects gave informed written consent and the study was approved by the NRES London-Chelsea Research Ethics committee. All methods were performed in accordance with the relevant guidelines and regulations.[148] 1 cm^3 section of lung tissue was flushed with 40 mL Hanks' Balanced Salt solution, using a needle and syringe to remove blood and macrophages. The tissue was cut into 2 mm sections and digested using DNASE1 50.0 U/mL and Collagenase 75 U/mL in 10 mL Hanks' solution, which was incubated at 37 °C for 35 min on the vortex incubator, set at 150 rpm. The digested tissue was agitated up and down with 10 mL FCS-containing media using a pastette. The mixture was filtered through a 70.0 µM Bal filter and then centrifuged at 1500 rpm for 10 min. The supernatant was removed, and the pellet was resuspended in 3.0 mL of LHC-9 for a T25 or 10 mL for a T75. The cells were then transferred to a collagen-coated flask and placed in a CO_2 incubator for 5–7 days. After 3 days, a further 2.0–3.0 mL of media was added. All media was replaced after 1 week with 5.0 mL of fresh media. The media was continued to be replaced two times a week until the cells reached 80% confluency. The cells were then frozen at a $1x10^6$ cells/mL confluence in LHC-9-supplemented media with 10% DMSO. The cells were resuscitated into LHC-9 media 2 days prior to their use and seeded onto 1% collagen-treated 24 well array plates. The media was changed every 24 h with no passages undertaken to keep consistent comparisons between the two populations.

The cells were detached using Accutase before being resuspended in phenol red free RPMI. To distinguish viable from non-viable cells during MAC chip loading, 10.0 µL of sample was incubated with 10.0 µL 0.04% trypan blue [Life Technologies] in phenol red free RPMI media. This allowed for the analysis of cell viability of the cells using a Countess cell counter [Countess, Invitrogen, UK] to monitor the viability before being loaded onto the MAC chip. The dissociated cells were made up to a concentration of $1x10^6$ total cells/mL to be transported on ice to the analysis laboratory to be

further diluted to $0.5x10^6$ total cells/mL when secondary antibody was added. To sort viable from non-viable cells in the MAC chip, the cells were incubated with 0.0001% Trypan blue.

Once the samples were loaded, the standard MAC chip methods were employed, which includes the optical trapping and lysis steps run in the same fashion as detailed in section 3.2.5.2. As many cells as possible were trapped and lysed within 60 min before TIRF analysis was run for 2 h. The number of cells successfully isolated and lysed varies from 20 cells to a full sample of 45 cells. This variation arose from certain samples being difficult to successfully trap and isolate the cells from, due to the laser power being insufficient to move certain cells and the time constraints associated with these experiments. The maximum allowed total time from cell dissociation to completion of cell lysis was 1.5 h.

3.5.2 Sputum Processing and Cell Isolation

The primary harvesting of the sputum cells was undertaken in the NHLI by the collaborators Peter Barnes et al.[149] The subjects inhaled 200.0 µg of salbutamol using a metered dose inhaler 10 min before the induction process. The subjects mouth washed thoroughly with water before inhaling 3.5% saline nebulised via an ultrasonic nebuliser [DeVilbiss 99, Heston, UK] for an average duration of 15 min. Subjects were asked to cough deeply after 5 min and at every 3 min afterwards. Induction was terminated when 1 mL of sputum was collected, which on average took 25 min. The collected sputum was collected in a polypropylene pot and all saliva was discarded separately.

After recording the samples, they were diluted with 2 mL of Hanks' balanced salt solution (HBSS) that contained 0.05% dithiothreitol (DTT) [Sigma Aldrich] and placed on a rocker at rt for 30–40 min. When the samples were homogenous, they were further diluted in HBSS to a workable sample solution. Traditionally, at this stage, the cells were centrifuged at 300 g for 10 min and the cell pellet resuspended to a desired cellular concentration.[149] This protocol was used with the intention to analyse the cells immediately after induction. The samples were also analysed using a haemocytometer to ensure there was a low level (<40%) of squamous epithelial cells present because this was an indicator that the sample was contaminated with saliva.

The samples were processed at the Royal Brompton Hospital, London and the optical MAC chip set up at Imperial College London, South Kensington Campus, London, which was 10 min away. The closeness of the two locations meant that it was possible to analyse the cells directly after sputum induction, in the traditional method. Sputum samples were infrequently taken, which meant that if samples were directly analysed after being taken, the amount of experiments possible would be

strictly limited. Therefore, as part of this collaboration, it was decided to investigate methods to freeze and store the cells, decoupling the need to directly analyse the sputum sample directly after induction.

To determine the optimal methods for safe storage of samples, the samples were divided at certain stages of the induction process. The freezing media used was 10% DMSO in HBSS. The first condition tested was to take the sputum directly after induction and dilute directly with freezing media – these were termed as 'Raw Samples'. The second condition tested was to take the cells through the DTT treatment and vortexing stages and then dilute into the freezing media – these were termed as 'DTT-Treated Samples'. The final condition tested was to collect the cell pellet at the last centrifugation step and resuspend in the freezing media instead of just HBSS – these were termed as 'Fully-Treated Samples'.

The cells after resuscitation were treated in a similar fashion to any cells being resuscitated; the samples were rapidly warmed to 35.0 °C in a water bath before being centrifuged for 5 min at 300 rcf and the pellet resuspended in phenol red free RPMI. Prior to MAC chip analysis, the cells were tested with trypan blue to determine cell viability, and viability was then monitored on chip using the protocol detailed in Section 8.2.1.

3.5.3 On-Chip Cell Selection and Sorting

As detailed later, a sputum sample is highly heterogenous in terms of output material. There are several cell types present along with dead cells, mucin debris and other unwanted materials. To select only viable cells of interest, three strategies were utilised to isolate said target cells. Using the same trypan blue protocol as used in the lung resection analysis in 8.4.1, only cells which were unstained by trypan blue were selected. Furthermore, a CD3 marker with a fluorescent tag at 536 nm [UCHT1, Thermofisher, UK] was also incorporated. This marker is specifically found on T-cells and provided a method of detection and subsequent isolation of T-cells only.[150] This proved an effective technique for detecting T-cells in a heterogenous sample where many cells shared the same morphology.

The other cell type of interest for analysis were epithelial cells. There are several methods to label epithelial cells and one widely used method is to use an EpCAM marker that will bind to cell surface marker proteins specific to epithelial cells. In these experiments, epithelial cells were easily identified by their unique morphology. The cells found in sputum are classified as ciliated pseudostratified columnar epithelium, which encompasses multiple cell types that are found to

constitute the outer layer of the respiratory epithelium. The majority of ciliated pseudostratified columnar epithelium found in sputum are made up of 3 types: i) ciliated cells, ii) goblet cells and iii) basal cells. All these cells share a distinct morphology of being columnar or cuboidal in shape, and in the case of the goblet cells, a goblet shape. These distinct morphologies mean it is very simple to identify and isolate epithelial cells in a sputum derived heterogenous sample. Studying airway epithelial cells as well as T-cells would provide another suitable COPD marker, as epithelial cells are known to be involved in inflammation also and so should provide a clear distinction with FoxO1 analysis.[151]

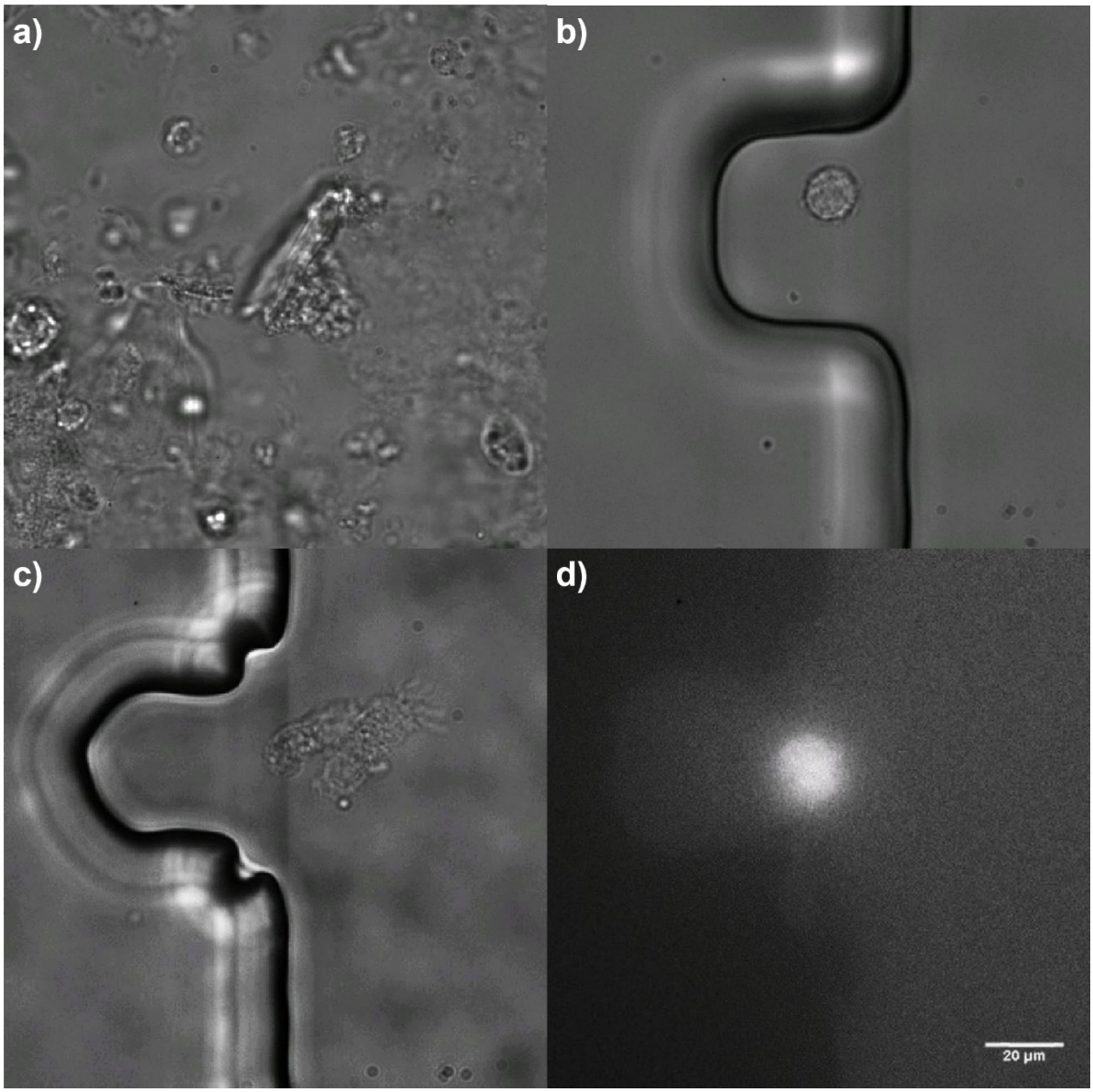


Figure 3.7 – A selection of images showing typical sputum derived cell trapping and identification. A) Shows the heterogeneity of cell types present along with the various cell and sputum debris, b) an isolated T-cell, c) 2 epithelial cells showing their unique cuboidal shape, the left seems basal while the right cell is a terminally differentiated ciliated cell, d) an isolated T-cell identified by the CD3 surface marker with a 536 nm fluorophore tag.

3.6 Equipment and Vendor List

Table 3.1 List of biological reagents used for cell culture and cell perturbation studies.

BIOLOGICAL REAGENTS	VENDOR
DULBECCOS PHOSPHATE BUFFERED SALINE	Sigma-Aldrich
RPMI MEDIA 1640	Thermo Fisher
RPMI 1640 MEDIUM, NO GLUCOSE	Thermo Fisher
BOVINE SERUM ALBUMIN	Sigma-Aldrich
KERATINOCYTE CELL CULTURE	Thermo Fisher
PITUITARY EXTRACT BOVINE	Sigma-Aldrich
TOLEDO CELL LINE	ATCC
MCF7 CELL LINE	ATCC
BEAS-2B CELL LINE	ATCC
GLUCOSE	Sigma-Aldrich
ZSTK474	Selleckchem

Table 3.2 List of all assay reagents tested and their vendors.

ASSAY REAGENTS	VENDOR
DNA CAPTURE AGENTS (PRE-ANNEALED, HPLC PURIFIED)	IDT DNA
FOXO1 (DU 1071)	MRC Pure Reagents
HUMAN FOXO1/FKHR ANTIBODY MAB5939	R&D Systems
ANTI-FOXO1A ANTIBODY (AB111029)	AbCam
ANTI-FOXO1A [EP927Y] ANTIBODY (AB52857)	AbCam
ANTI-FOXO1A ANTIBODY (AB150059)	AbCam
ANTI-FOXO1A ANTIBODY [3B6] (AB126826)	AbCam
ANTI-FOXO1A [EPR12020] ANTIBODY (AB179450)	AbCam
ANTI-FOXO1A ANTIBODY (AB89433)	AbCam
ANTI-FOXO1A ANTIBODY (AB1102)	AbCam
ANTI-FOXO1A ANTIBODY (AB131206)	AbCam
ANTI-FOXO1A ANTIBODY (AB12161)	AbCam
HUMAN FOXO1/FKHR MAB (CLONE 597554)	Novus Bio
FOXO1 (C29H4) RABBIT MAB #2880	Cell Signalling Technologies
FOXO1 (C29H4) RABBIT MAB #2891	Cell Signalling Technologies
FKHR ANTIBODY (C-9): SC-374427	Santa Cruz
SCC	Sigma-Aldrich
BETAINE	Sigma-Aldrich

Table 3.3 Reagents needed for MAC chip fabrication and western blots.

MAC CHIP FABRICATION & BIOLOGICAL EQUIPMENT	VENDOR
GLASS COVERSLIPS NO.1.5	VWR
PDMS + CROSSLINKER	Sylguard
GPTES	Sigma-Aldrich
APTES	Sigma-Aldrich
KOH	Sigma-Aldrich
ETHANOL	Sigma-Aldrich
ACETONE	Sigma-Aldrich
SODIUM BICARBONATE	Sigma-Aldrich
IBRIGHT PRESTAINED PROTEIN LADDER	Thermo Fisher
PRECAST GEL	Bio-Rad
MYCOALERT – MYCOPLASMA TEST KIT	Lonza

Table 3.4 Equipment list for all experiments run in the thesis.

EQUIPMENT	VENDOR
OMNIGRID MICRO ARRAYER	ArrayIt
ANDOR 887 EMCCD	Andor
VORTRAN 4 WAVE LASER	Vortran
YLM-5 YTTERBIUM FIBRE LASER	IPG Photonics, UK
SURELITE SL I-10, Q-SW ND:YAG LASER	Continuum
NIKON TE2000E WIDEFIELD MICROSCOPE	Nikon
PAN APO TIRF 60X 1.49NA OBJECTIVE	Nikon
ND FILTER SET	Nikon
NIKON TE2000U MICROSCOPE	Nikon
SMP2 PIN HEAD	ArrayIt
FIBRE OPTICS	Thor Labs
TYPE A IMMERSION OIL	Nikon
WET TANK BLOTTING SYSTEM	Bio-Rad

4 Identification and characterisation of FoxO1 antibodies and Capture Agents.

4.1 Outline

This chapter describes the workflow utilised to take a range of commercially available antibodies and DNA sequences and test their viability for use in the MAC chip format. Initially, an "open chip" strategy is used to provide a hit-to-lead methodology that investigated which antibody and DNA pairings could successfully bind to recombinant FoxO1 protein. The open chip method showed that several agents were unable to bind FoxO1 at the necessary sensitivity to be utilised in the MAC chip format. After testing, two successful antibody pairings were discovered.

The DNA studies uncovered a need to improve the DNA surface conjugation techniques. Initially, ten different capture agent sequences, adapted from literature sources, were designed to mimic an active consensus sequence. The first open chip format used conjugation techniques utilising GPTES functionalisation to bind the DNA to the glass slide. These experiments showed that the GPTES surface treatment led to a high level of background binding and was unsuitable for the MAC chip format. Following on from this result, it was decided to investigate different conjugation techniques to provide a low background count and successful FoxO1 binding. This resulted in a biotin-neutravidin technique that also allowed future multiplexing with the antibody printing methods for future studies. Further studies using this technique showed that only one potential DNA-antibody pairing was suitable to be taken forward to cell studies.

4.2 Introduction

To achieve sufficient capture of the specific protein of interest, in this case FoxO1, it is necessary to screen a wide range of antibodies and Capture Agents. To date the MAC chip technology has used antibodies to provide both the capture and the detection of the chosen protein of interest.[20,33,118] Antibodies are a traditionally preferred method of capture in many biological analytical systems as they typically provide a high affinity and specificity (around the nanomolar level) for the target protein making them the gold standard in assays, as K_D of the reagents is often the limiting factor to an assays success.[7,152] However, antibodies have their limitations: i) the process of isolation and purification of antibodies is extremely prone to batch to batch variation; ii) their large size can disrupt typical binding interactions in *in vivo* studies; iii) their size can reduce their capture efficiency

due to antibodies coating the surface in the print process; and iv) their specific intrinsic protein folding makes antibodies less stable than smaller molecules, such as DNA oligonucleotides, aptamers, affirmers and drug conjugates.[138,153,154] The limitations associated with antibodies highlights the need for optimisation of alternative reagents for capture or detection.

Transcription factors have an inherent ability to bind specific DNA sequences to initiate their transcriptional activities. This innate DNA binding ability means their specific DNA consensus motifs are well characterised. Utilizing these specific consensus motifs allows for the use of small chain DNA oligonucleotides in the sandwich assay format. DNA based Capture Agents can provide many advantages over the use of antibodies while maintaining the high affinity and specificity required for the assay. DNA oligonucleotides compared to antibodies are; cheaper and do not suffer from batch to batch variations (assuming high purity is achieved for the DNA). They are also easier to functionalise with linkers and tags and have a smaller footprint, which leads to a higher capture efficiency, as they have a higher concentration of unbound Capture Agent which drives the equilibrium to bind more analyte. Finally, they are more stable thus more suited for long term storage. The use of DNA as a Capture Agent in ELISAs is well studied and there are commercially available kits that can be purchased to achieve this goal, even for the recognition of FoxO1.[32,155–159] While these transcription factor DNA binding kits are available from several vendors, they do not divulge the sequences they use for capture and therefore novel sequences must be created.

Both antibodies and specific DNA sequences were screened to investigate which of the two could be optimally utilised for both capture and detection agents in the MAC chip assay. A comprehensive list of FoxO1 antibodies was produced, including the epitope binding sites when available. The key properties that were prioritized during antibody choice were; monoclonality, well defined epitope binding sites, concentration, suspension buffer and cost. Monoclonality is generally preferred for most assays as they typically show less batch to batch variation and often have a better-defined epitope binding site, most importantly they have a single binding site not several. Defined epitope sites are beneficial as they allow for optimal choice of capture and secondary antibody. As the assay designer can ensure the two antibodies bind to distinctly separate regions of the protein, ensuring no issue with capture and detection of the protein of interest. Purchasing antibodies that are already provided at a sufficient concentration (≥1 mg/mL) is beneficial as it requires less handling and preparation of the antibody. Extra handling steps of the stock antibody can denature the antibody and reduce its affinity. The suspension buffer should not include any glycerol if the antibody is to be used for capture, as the glycerol will reduce the printing efficiency and lower the capture efficiency by blocking antibody-antigen interaction.[160] Although there are methods for buffer exchange it adds

extra handling steps to the antibody and thus increases the chance of the antibody denaturing and it is common to lose some antibody in the process.[161]

As mentioned previously, the use of DNA and its known consensus motifs can afford sub nanomolar specificity to the epitope binding sites which tackles many of the issues affecting antibody choice. The key complication with the use of DNA is creating a sequence that shows sufficient affinity to the protein of interest. There are many hurdles to ensure the sequence will only bind the protein of interest and not exhibit cross reactivity whilst also annealing correctly without self-dimerization. To minimize these issues and design optimal sequences, the potential sequences can be monitored using the 'Hamming distance' method. The 'Hamming distance' method is defined by the number of matching places where two base pairs differ between the two strands and also the similarity within the same strand to cause hair pin loops.[162] This method helps to reduce the chance of cross binding or complementary pairing in which the sequences can bind sub optimally to each other or themselves. A traditionally used method which helps avoid this is to keep the percentage GC content at 50%.[163] This can help to achieve perfect matching with the complimentary strand and perfect matching will give optimal binding strength for the two strands and stabilize the annealed strand.[138] Traditionally sequences chosen for microarrays are kept at short lengths ranging from 20 to 150 base pairs (bp) with most falling into the 20-50 base pair region.[164] For this reason the initial sequences were designed at 30 base pairs. This provided a sufficient length to include the necessary consensus motif along with a spacer that would separate the consensus motif from the glass surface to allow for protein binding. It is known that every 10 base pairs typically correspond to a 34Å extension from the origin, which makes a 30 base pair sequence around 102Å long. The reported size of the FoxO1 forkhead region bound to its consensus motifs is at around 10 $Å^3$ according to Brent *et al*[71], although this is speculative and overall the full protein is likely to be significantly larger with its footprint. However, a 30 bp sequence is considered sufficient to reduce steric hindrance.

Initial design of the DNA sequences started by a thorough literature search to find any sequences that have already been utilised for FoxO1 capture. This yielded limited results and only one paper by A. Sidhu *et al.* showed a potential sequence for the capture of FoxO1.[165] Using a SELEX process Sidhu *et al.* refined a set of clones down to 3 potential sequences and demonstrated a binding affinity of 33 ± 4 nM which has been demonstrated to be sufficiently high for the MAC chip format.[20] This exact sequence was taken and labelled 'Capture Agent 1' (CA1) and derivatives were created from CA1 by using it as a skeleton structure. Initially 9 sequences were designed which will be discussed later. The designs consisted primarily of including the known IRE sequence which is documented to have the highest affinity towards FoxO1.[49] Papers have also demonstrated that certain flanking sequences

help to increase binding efficiency that include AT rich 3' regions and also the sequence 5'-ACAACA-3'.[165] The designed sequences looked to include all the factors mentioned above and were labelled CA1-9.

A selection of antibodies were chosen based on the parameters mentioned previously alongside the 9 DNA sequences to bind FoxO1. Of this selection some of the antibodies were also chosen to be used as the secondary detection species. Antibodies can be purchased conjugated with a range of tags, including biotin and a range of fluorophores. If these conjugated antibodies are not available for purchase, there are a multitude of antibody conjugation kits available that attach the fluorophores to the antibody. For the experiments outlined below, Alexafluor-488 was the chosen fluorophore as the optical system used could only use this wavelength.

4.3 Validation Protocol

To rapidly determine which antibodies and DNA Capture Agents are suitable for the assay format, a workflow has been established that uses a "hit to lead" based approach. The initial hit to lead screen is achieved by what is deemed the 'open chip format' which can test a range of parameters and agents simultaneously. In this approach, the sandwich assay is used to capture recombinant protein because the recombinant protein can be easily quantified with respect to capture efficiency. The 'open chip format' allows for the printing of 3 arrays of 8 columns and defined rows, where each column can be a different Capture Agent whilst all utilizing the same solution of secondary antibody and recombinant protein. The 3 blocks are also separated by PDMS walls, meaning that each block can utilise; a different secondary antibody or a different concentration of secondary antibody or a different concentration of recombinant protein or cell lysate or a combination of all these. Therefore, this format can result in a total of 24 possible unique experiments that can be run in tandem.

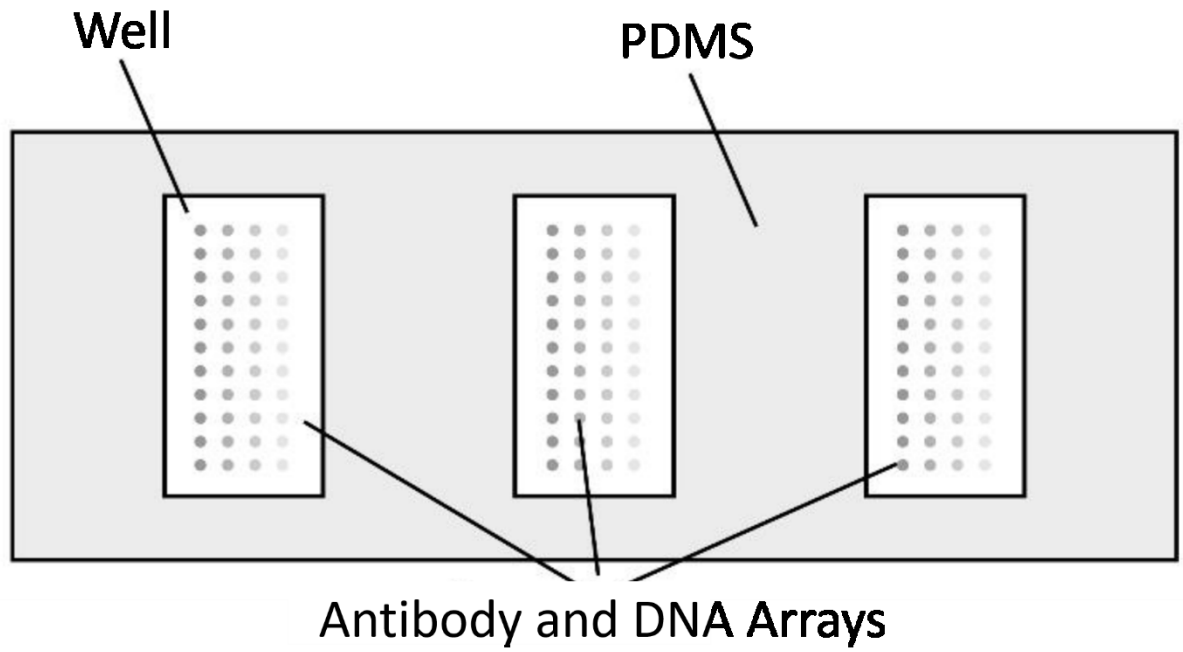


Figure 4.1 Schematic of the 'Open Chip' format. Multiple primary antibodies or printing conditions can be simultaneously tested, and the relative fluorescence at the antibody spot can be analysed to determine strongly performing antibody pairs. 2-8 columns of individual Capture Agents can be printed into 3 identical arrays on a chip.

Whilst the open chip format is a powerful tool for the initial analysis of potential assay agents, it does have limitations, so results from this method do not necessarily align with what will work in the MAC chip format. The main reason for discrepancies is the lack of a confined volume in the open chip. The lack of confined volume means it only provides a 'bulk' measurement and thus a broad, less accurate model of the MAC chip assay. The MAC chip has confined volumes surrounding the individual Capture Agent spots which means that while the concentration of protein and secondary remains the same, if the volume is decreased by orders of magnitude it means the total amounts of secondary antibody and protein molecules is reduced. This reduction will affect the binding equilibria and therefore require the assay to be more sensitive in order to bind the smaller amount of total protein present.[35]

Once the open chip experiments determined the validity of the capture and secondary agents, these were further screened using the MAC chip. Initially the concentration was still varied, typically in orders of magnitude, spacing from $1x10^2$ molecules per nanolitre to $1x10^7$ molecules per nanolitre of recombinant protein. In these experiments, several MAC chips were printed using the chosen Capture Agent and subsequently vacuum filled with FoxO1 recombinant protein and secondary antibody at a fixed concentration. One chip was filled with only the secondary antibody to obtain a pseudo background, which was then used to determine the level of off-spot binding. These

experiments are then compiled to take the average single molecule count observed with respect to known numbers of FoxO1. This data was converted into a calibration curve to show the linear range of detection and the limit of detection. It can also be used to convert the observed single molecule count into total copy number of the protein.

A map of potential antibodies and their binding sites was created to allow for ease of choice as to which should be paired together. This map was utilised to determine which parings were initially placed together.

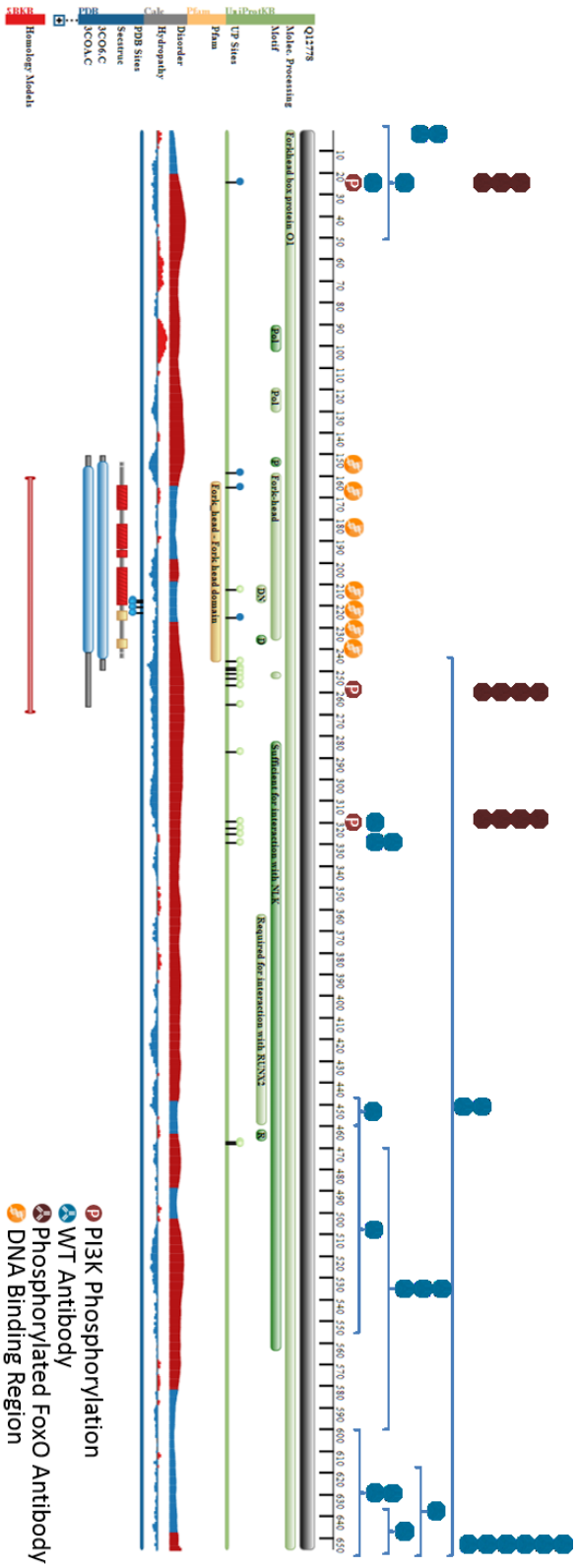


Figure 4.2 A map showing the range of antibodies available for purchase and their documented epitope binding sites. This was produced in 2014 by analysing antibodies from AbCam, Sigma, Origene, Santa Cruz Biotechnology and MRC Pure Reagents. The chosen antibodies were chosen from this infographic by ensuring their epitopes did not overlap and then following the criteria mentioned previously in this section. The FoxO1 protein sequence is adapted from Calnan et al.[49]

The following chapters detail the design and validation of the antibody Capture Agents and the DNA Capture Agents separately to allow a greater discussion of the problems faced with each, even though all studies were performed in tandem.

4.4 Antibody Based Assay Development

This section details the development of an assay which utilises antibodies for both the capture and detection of FoxO1 following the methods detailed in earlier sections. This work initially details the limitations of using in-house fluorescent tagging kits compared to purchasing fluorescently tagged antibodies outright. The section then goes on to detail the work flow from 'open chip' to 'MAC chip calibration' until two viable assays were discovered.

4.4.1 Antibody Conjugation Strategies

For the development of the antibody-based assay, 16 antibodies were purchased [See Appendix 11.1] which exhibited the optimal parameters as discussed in the previous section. A selection of these antibodies were purchased again with a fluorescent label incorporated and some were tagged using a lightning link® conjugation kit. This section details the limitations of these in-house kits and rationalizes why tagged antibodies were purchased wherever possible for these experiments.

There are many antibody conjugation strategies available on the market with a variety of labels and simple use. Most of these strategies share a similar methodology where typically the antibody will be incubated with the label of interest and subsequently purified through a size exclusion column to remove excess dye to provide a purified sample of labelled antibody. Most of these labelling kits all share the similar method of utilizing simple biocompatible techniques. Most will target lysine amine residues using n-hydroxy succinimide (NHS) chemistries or target thiol residues of cysteines using maleimide cross coupling techniques through a 1,2- Michael addition, given their NHS moiety.[166]

Conjugation were investigated to work out the optimal technique to utilise. Most of these kits utilise NHS moieties for lysine binding, though cysteines binding strategies were also employed. Despite these kits being simple to use during the assay development, they were seen to be inconsistent in their labelling capabilities. A nanodrop 5000 was used to measure the given concentration of the antibody pre- and post-labelling as well as the concentration of label present after conjugation. It was common to observe differing concentrations of label present when conjugating several batches of the same antibody between runs. This provided a potential problem as even though the same

concentration of antibody would be used in each experiment, the varying label concentrations would likely alter the perceived binding of FoxO1 in the sandwich assay.

Another problem observed with in-house kits is the varying levels of label bound to individual antibodies in the same sample. The typical bioconjugation technique employed is the use of the NHS ester to selectively label the lysines present on the antibody. Whilst this is an effective reaction due to lysines being highly abundant in proteins, it means the level of labelling is significantly hard to control. This causes many problems as it can cause false counts for the protein of interest because a single antibody binding event may be multiply counted. An additional common issue with these kits is the buffer compatibility, as high concentrations of glycerol can impede the binding. There are methods to make the buffer sufficiently compatible with the labelling strategy such as dialysis or buffer exchange columns, and whilst these have proven effective, they also expose the antibodies to denaturing conditions. Therefore, although the antibody may provide better labelling, the antibody may also lose affinity to the protein via the denaturing conditions. Furthermore, the provided purification columns are usually low quality meaning multiple runs or higher quality columns must be used adding extra costs and time. The use of the in-house labelling without sufficient purification would often show a significantly increased level of non-specific binding going from the averaged 150 single molecules per frame to 300 to 1000 molecules (as determined from the method detailed in Section 3.2.7). This increase was due to the insufficient purification techniques leaving unbound fluorophores present in the antibody stock.

For these reasons discussed, it is likely that the in-house labelled secondary antibodies; FoxO1 (DU 1071), Human FoxO1 mAb5939, Anti-FOXO1A antibody (ab111029) and Anti-FOXO1A antibody (ab150059) were not suitable for use. Considering this, the antibodies were instead purchased pre-conjugated due to these specialised companies having better access to appropriate equipment and more robust labelling techniques.

4.4.2 Open Chip Validation Studies

Initial trialling using the open chip format showed that despite the antibodies claiming a high K_D value, many were unsuitable and showed no apparent binding to FoxO1, as observed in the open chip experiments. Moreover, only in-house labelled antibodies were used in the initial runs and it was clear that the conjugation steps yielded poor labelling of the antibodies. The issues with in-house conjugation strategies are detailed in Section 4.4.1.

Despite issues arising with conjugation steps as detailed in Section 4.4.1, the use of the open chip format did show some candidates for use in the assay. Map 5.1 shows the antibody parings in a heat map style, with a rating of; red meaning unsuitable as no binding observed, yellow meaning some binding was observed (but only with high concentrations of FoxO1 at $1x10^5$ molecules/nL or higher present) and green meaning that binding of FoxO1 was still observed at concentrations as low as $1x10^3$ molecules/nL. Even though the green hits were considered the most promising, the yellow hits were also brought forward for further analysis. This was decided because the open chip format is an insufficient hit to lead strategy and the yellow category pairings could still be suitably sensitive for MAC chip use. As the open chips experiments are only the initial testing stage they were typically not quantified, and only qualitative analysis was used for comparison. This analysis was deemed suitable at this early stage as the aim was to find any antibody pairings that showed any level of binding.

As seen in Map 5.1 many of the pairings were unsuitable for use in the MAC chip assay. Despite the fact they were picked to (as best as possible) not have overlapping epitope binding sites, one issue that may arise is from the actual folding of the protein itself. Typically the C- and N-terminus of a protein are separate but for FoxO1 these termini are actually spatially close due to its folding.[71] As many of the pairs utilised C- or N-terminus epitope sites, the steric hindrances that could potentially arise from these termini could explain why these pairs did not yield optimal binding. The predominant reason for lack of binding is likely due to an insufficient K_D present and these issues are further detailed in Section 4.4.1. As the open chip can only yield a quantitative analysis with respect to a MAC chip validation. For this reason, the results were colour graded according to the level of binding observed. Red being no observable binding up to green being high levels of binding. Examples can be seen in:

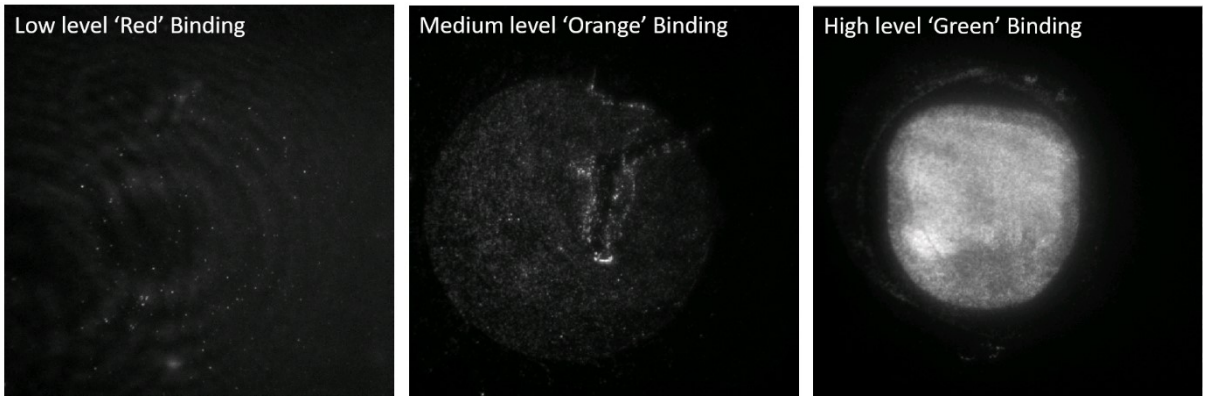
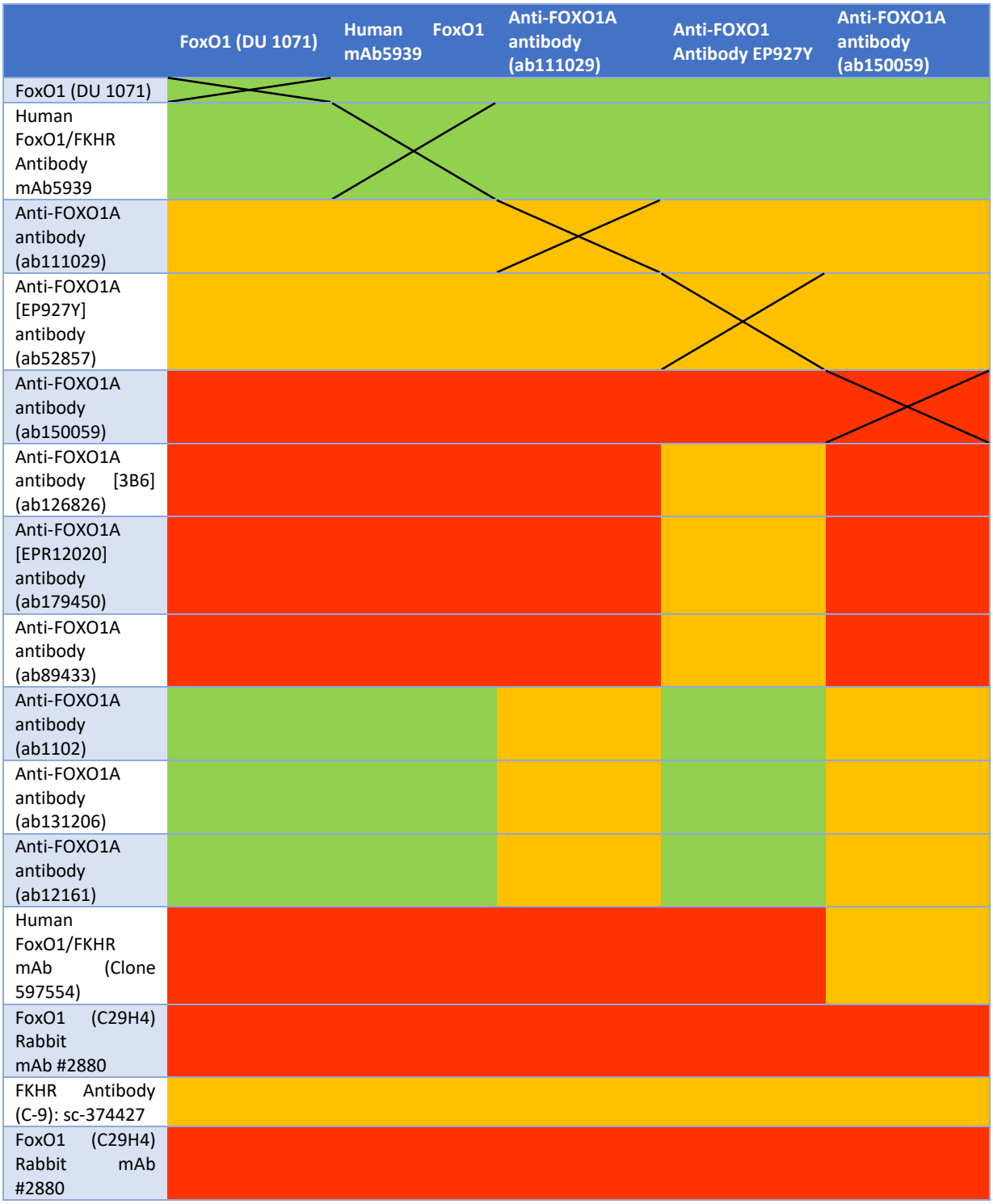


Figure 4.3 Images demonstrating the colour classifications in all subsequent heat maps. Red demonstrates no binding, yellow some binding and green a high degree of binding.

Map 4.1 A heat map detailing antibody pairings trialled for use in the assay, the y-axis shows the capture antibodies and the x-axis the fluorescently tagged secondary antibodies. Red demonstrates no binding, yellow some binding and green a high degree of binding. A cross shows where the detection and secondary antibody were the same therefore untested. The levels of binding were only qualitatively measured at this stage and the analysis was by comparison with the other pairs.



4.4.3 Bimolecular Binding Tests

The initial open chip studies relied on a trimolecular binding process of capture binding to antigen and this complex binding to the secondary antibody, which means there are two variables in binding efficiency; one variable being the Capture Agent and the other the secondary fluorescent antibody. To decouple these variables, FoxO1 recombinant protein was fluorescently tagged using the same methodology used with the antibody labelling. This enabled the testing of individual antibodies without the need to rely on a secondary tagged partner.

The usual limiting factor to be the Capture Agent due to its randomly oriented immobilisation and limited degrees of freedom, which in turn reduces its ability to bind to its epitope.[119,136] To test whether the Capture Agents were the limiting factor in the open chip assays, these were tested again in the open chip system but fluorescently tagged FoxO1 was used as the detection agent instead. Using tagged FoxO1 protein meant that the study was now a bimolecular binding system, instead of trimolecular, and the only agent being tested was the Capture Agents themselves. The two most promising antibody Capture Agents as seen in the open chip format were mAb5939 and DU1071 (refer to Table 3.1) and so both were chosen for testing. These Capture Agents were printed in the open chip format and a range of tagged FoxO1 concentrations were investigated. The results are shown in Figure 4.4.

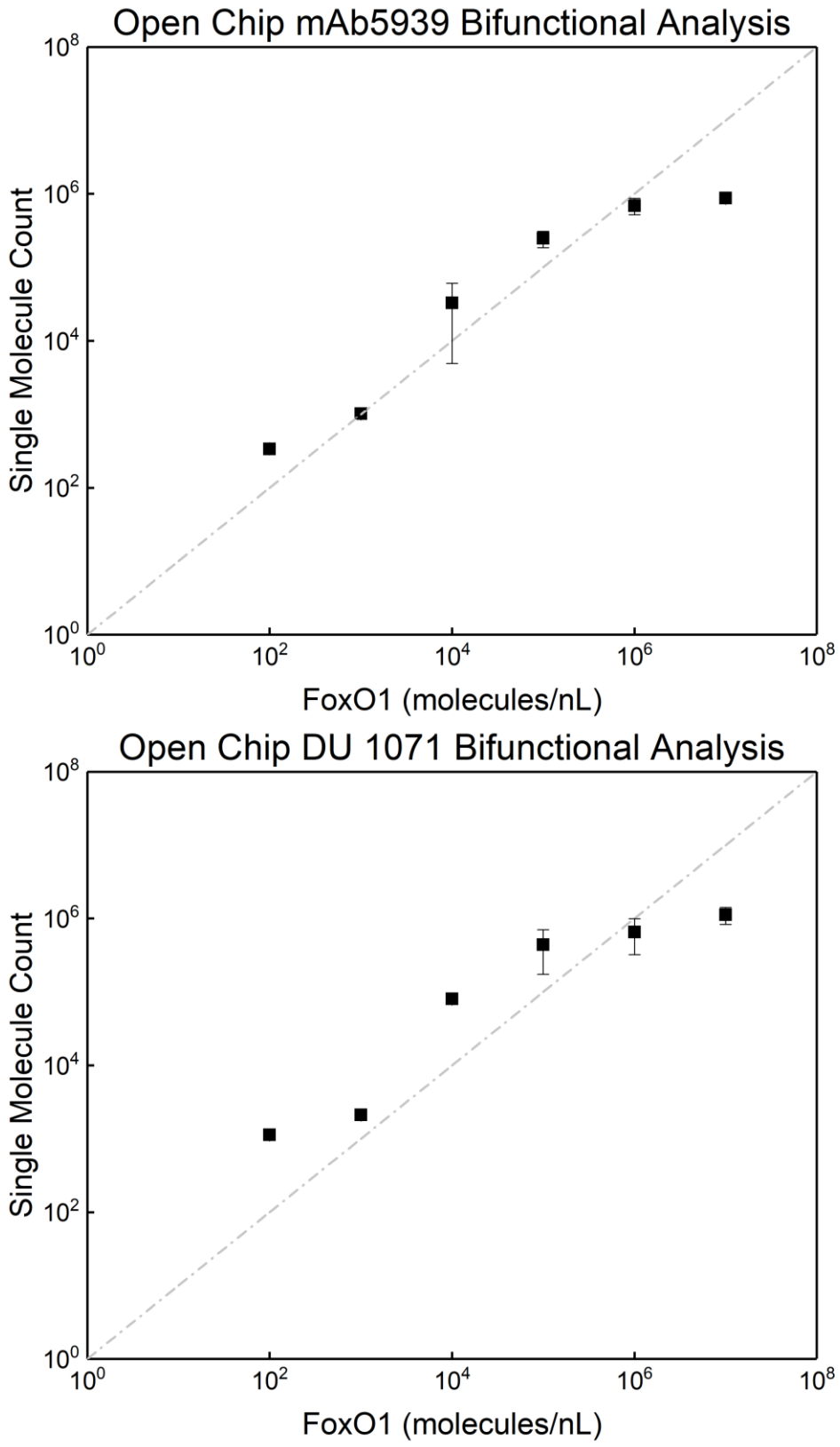


Figure 4.4 Bimolecular analysis of the potential Capture Agents mAb5939 and DU1071 against fluorescently tagged recombinant FoxO1. The error bars are standard deviation, the long tail on them is due to the log scale of the y-axis. The grey dashed line shows perfect 100% binding.

The bimolecular studies detailed in Figure 4.4 show that both Capture Agents tested show a sigmoidal binding with a limit of detection at around $1x10^3$ molecules/nL for both antibodies. Interestingly the observed single molecule count looks to be over 100% binding at certain concentrations of FoxO1 (binding. Figure). This occurs as there is no volume restriction with an open chip. Therefore, when FoxO1 binds, the excess concentration in solution can replenish the now bound FoxO1 via diffusion towards the Capture Agent spots. This also drives the equilibrium towards a bound state. This observation may also arise from the use of in-house labelling of FoxO1 recombinant protein and potentially from the inaccuracies of the open chip format.

4.4.4 MAC Chip Calibration

Following on from the 'bulk' studies that the open chip studies provided, the next step was to test the most viable pairings using a more suitable model. The MAC chip calibration set up was used to further validate the antibody pairings. This Section details the validation of the mAb5939 and DU 1071 antibody Capture Agents both using the secondary antibody EP927Y.

The experiments in Figure 4.5 were performed with the 'traditional' 50 chamber 4.5 nL MAC chips. Several chips were aligned using slides from the same print run to keep consistency and subsequently filled with a concentration series of FoxO1. FoxO1 was introduced in a solution of 4% PBSA and 250 ng/mL fluorescent EP927Y secondary antibody. The solutions were added to the chip using the desiccation method as mentioned in Section 3.2.5. In a typical MAC chip experiment, the vacuum filling step is used to introduce the 4% BSA and secondary antibody solution, to provide a blocking step and a background run respectively. In these calibration runs there is no method to introduce the recombinant protein effectively by flow, so the FoxO1 recombinant analyte is added using the vacuum filling process. This can potentially increase the background counts, so to obtain an accurate background count, one chip is filled in the typical method with only secondary antibody and no recombinant protein. Once the chips are filled, they are imaged using the TIRF set up in the same fashion as a single cell experiment (see methods section). The images are acquired for 120 minutes to ensure thermodynamic equilibrium is reached. The data was quantified using the PALM localisation counting algorithm coupled with the baseline noise offset to stop the loss of data which can occur in the image flattening process. The counting algorithm is described in Section 2.4.

At this point, many of the antibody pairings proved to be ineffective when brought down to the MAC chip confined chambers. After testing the pairs in the MAC chip system, there were only 2 antibody

pairs that showed a sufficient limit of detection and linear range; Capture Agents mAb5939 and DU 1071. Both pairs utilised the same detection antibody, AbCam EP927Y with an Alexafluor 488 tag.

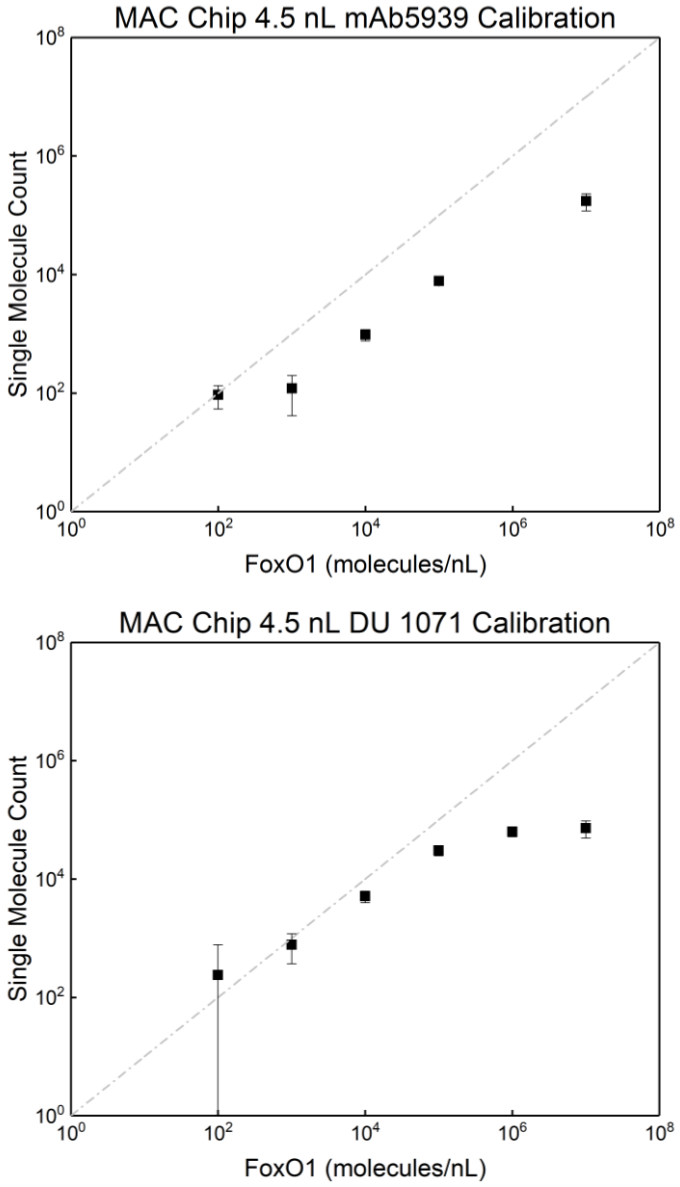


Figure 4.5 4.5nL MAC chip Calibration. The data points show the counts from 6 orders of magnitude. These can be compared to the black line which shows the perfect, 100% binding across a large dynamic range. The top plot details the mAb5939 assay and the bottom the DU 1071 assay.

The plots above also show that the fraction bound differs across the dynamic range. For mAb5939 (the top plot) the majority of the linear region showed around 10% capture efficiency albeit with significant deviations at the lower concentrations of the curve, which effects the accuracy of the lower limit of detection. The lower limit of detection is the key limiting factor to achieving absolute quantification for cells expressing low levels of protein as the lower limits add a significant degree of inaccuracy to the results.

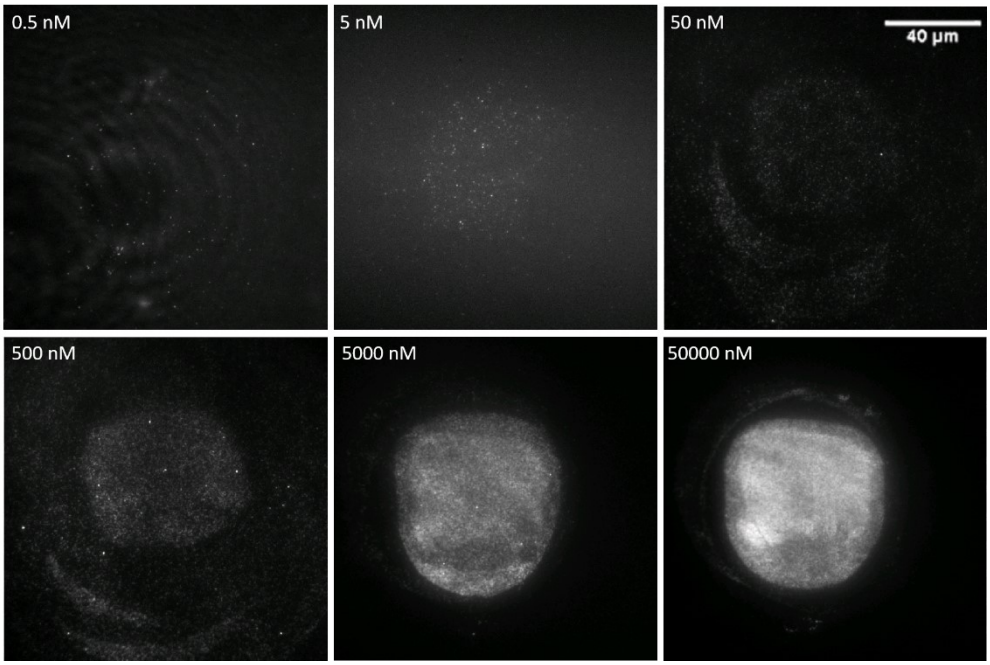
The second antibody tested, DU 1071, shows a higher yet inconsistent capture efficiency. The lower end seems to show an 80% capture efficiency at 10^3 molecules per chamber vs the theoretical 100% capture regime, which drops down to 5% by 10^6 molecules per chamber. The lack of consistency and lack of specificity at the lower limit of detection make this calibration curve questionable. Due to the DU 1071 calibration curve inconsistency and the fact that it was also a polyclonal (a fact found out later from purchase and validation) the later single cell studies utilised mAb5939.

4.5 DNA Based Assay Development

For the development of the DNA based assay, 9 DNA Capture Agents were developed using the literature discovered consensus motifs as detailed in Section 1.7. These agents all shared the same consensus motif but had altered spacer sequences to try optimising the parameters mentioned in Section 3.

One of the main reasons for using DNA was to utilise methods that provide oriented and covalent attachment of the Capture Agent to the slide surface. DNA based arrays are covered in the literature with many examples presented for the use of transcription factor, mRNA and ssDNA capture among other uses.[159,167,168] The traditional methodology used for DNA printing is to add a 5'-terminus amine group, a cheap and simple modification, and use this to react with a surface functionalised with (3-Glycidyloxypropyl)trimethoxysilane (GPTES). Using an acid catalysed nucleophilic addition of the DNA amine tag to the epoxy surface, a covalent attachment of the oligonucleotide to the surface can be achieved. This method reports that up to 10^7 oligos can be attached per spot.[169] This is comparable, if not a higher, printing efficiency than that seen with antibody based studies.

Tests were run to determine the printing efficiency observed with a fluorescein tag attached to the complimentary oligo along with the amine tag on the lead strand. The fluorescein tag provides a method to run a single molecule analysis on the number of oligos conjugated to the surface. This mock DNA strand was printed at concentrations ranging from 0.5 nM up to the traditional printing concentration of 50 µM. This study clearly demonstrated a linear increase in oligo bound against printing concentration as seen in Figure 4.6. However, the results showed that the printing density only increased to 10^6 molecules per spot. The possible issues causing this could be sterics of too compact DNA with respect to spot size, the GPTES hydrolysing and thus stopping binding, or potentially the epoxy group density being too low. Regardless a concentration of 10^6 oligos per spot is sufficient and comparable to Capture Agent densities obtained by antibody-based capture methods.



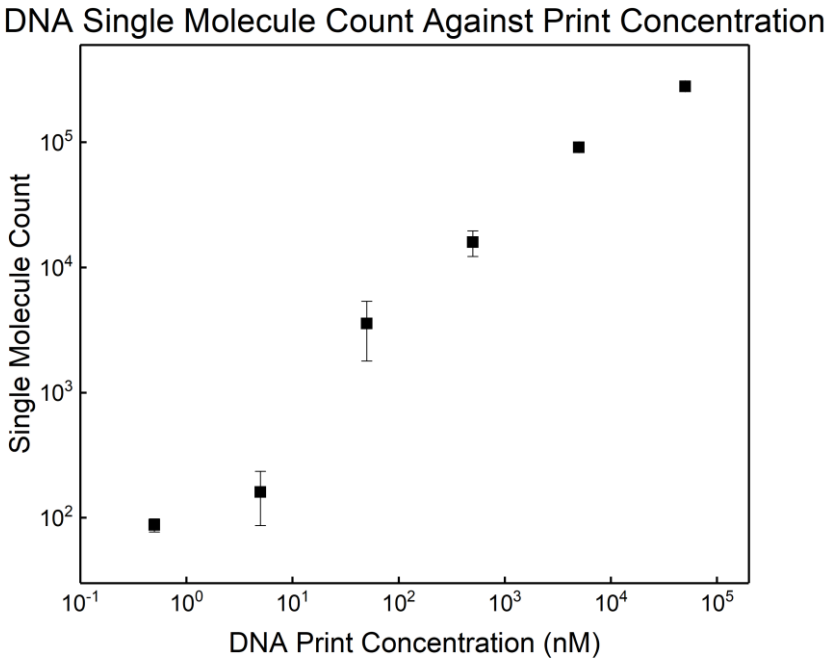


Figure 4.6 Images (above) and calculated SM count (below) showing an increase in relation to the increase in DNA print concentration. This shows an almost magnitude increase in relation to printing density. These were taken without saturation of the camera sensor to ensure accuracy of the single molecule count. These images were translated into the plot using the counting algorithm which is detailed extensively in Section 3.2.6.

In the same fashion as the antibody validation, open chip experiments were initially run using the DNA Capture Agents tagged with a 5'-amine moiety on a GPTES surface. As previously mentioned, the open chip method is a commonly used technique for assay validation[14,118], but it is usually used in bulk studies where the total number of target analyte is higher than what will be present at the

single cell level. These experiments used a 4% BSA blocking solution, consistent with the antibody experiments, to try and reduce the level of non-specific binding, as BSA will block non-specific sites on the antigen. Compared to the PEG-Neutravidin slides used with antibodies, the level of bio passivation is reduced in these DNA experiments, meaning that there was increased of non-specific binding. Non-specific binding comes from several interactions which are; fluorophore to surface, fluorescent secondary to printed Capture Agent spot, endogenous fluorophore to Capture Agent spot. These interactions occur from all types of intermolecular interaction.

Table 4.2 The DNA- Antibody pairings trialled for use in the assay, the y-axis shows the capture antibodies and the x-axis the fluorescently tagged secondary antibodies. Red demonstrates no binding, yellow some binding and green a high degree of binding.

	FoxO1 (DU 1071)	**Human FoxO1 mAb5939**	**Anti-FOXO1A antibody (ab111029)**	**Anti-FOXO1 Antibody EP927Y**	**Anti-FOXO1A antibody (ab150059)**
FoxO Capture Agent 1					
FoxO Capture Agent 2					
FoxO Capture Agent 3					
FoxO Capture Agent 4					
FoxO Capture Agent 5					
FoxO Capture Agent 6					
FoxO Capture Agent 7					
FoxO Capture Agent 8					
FoxO Capture Agent 9					

Consistent with the antibody studies, Table 4.2 shows the tests of the 9 DNA Capture Agents with an amine tag on a GPTES surface, in combination with the same detection antibodies used in the antibody-antibody based assays.

It is clear from Table 4.2 The DNA- Antibody pairings trialled for use in the assay, the y-axis shows the capture antibodies and the x-axis the fluorescently tagged secondary antibodies. Red demonstrates no binding, yellow some binding and green a high degree of binding. that the amine tether was an unsuitable method for the assay because even at the open chip level no clear binding above background levels was observed. For all the Capture Agents, a significant amount of non-specific binding even off spot was observed making it difficult to know what was actual binding and what was non-specific binding. This off-spot binding can be seen in the left-hand image of Figure 4.7. The level of non-specific binding likely comes from the unreacted epoxy surface being prone to reaction and subsequent reactivity with biomolecules.[170] Whilst BSA blocking is used to block this epoxy interaction it may not be sufficient to prevent fluorescent molecules binding.

After repeat experiments it was decided that GPTES functionalisation was unsuitable for use in the MAC chip assay and so other surface chemistries were explored for the immobilisation of the DNA Capture Agents. These immobilisation strategies will be discussed in subsequent sections.

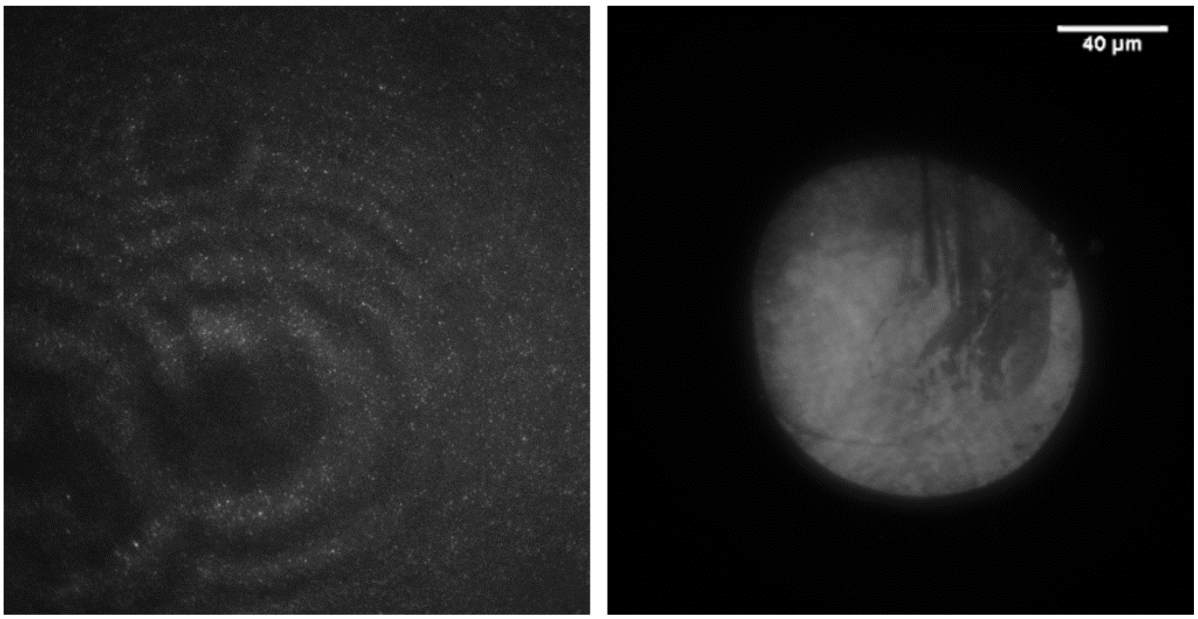


Figure 4.7 Left shows the levels of nonspecific binding seen using GPTES slides, where single molecules are homogenously spread across the image, the right shows a perfect situation with little if no non-specific binding.

4.5.1 DNA Immobilisation Strategies

As GPTES was not a suitable functionalisation strategy a range of other methods were tested for use in these DNA-based assay. Conveniently, there are a plethora of functionalised silane species which are commercially available, as can be seen on the sigma site [https://bit.ly/2LSIXNR]. One species that commonly used (3-Aminopropyl)triethoxysilane (APTES). APTES will functionalise the surface

with a coating of amine groups, which the group currently reacts with a mixture of functionalised PEG species to provide bio passivation. Due to the APTES functionalisation protocol being comparable to that of GPTES, this was utilised here and the DNA Capture Agent was purchased with a 5' NHS ester tag instead of an amine tag. The biocompatible reaction of NHS with amine to form a covalent amide bond is well documented.[132,171,172] This strategy would again provide an oriented and covalent attachment of the DNA Capture Agent to the surface. There would have been methods to optimise the GPTES system, such as ester hydrolysis which were not followed as the use of APTES would allow for multiplexing with the PEG systems.

Much like the use of GPTES, this method does not utilise the PEG-Neutravidin bio passivation and the same issues with GPTES were observed with APTES. No binding was observed over the high level of non-specific binding observed with similar images as seen previously in Figure 4.7.

The GPTES and APTES experiments showed that methods using a pure silane surface did not provide sufficient bio passivation and reduced the signal to noise ratio (SNR) too much to be usable in the MAC chip method. The SNR was defined by the signal seen from the background readings vs the readings taken with the analyte introduced. The next experiments investigated using PEG functionalised surfaces as these are proven to significantly reduced background binding.[173,174] The first tests performed took the 9 Capture Agents with no added modifications. Although this is not traditionally used in DNA based assays, an un-oriented print strategy for the antibodies in the MAC chip was used. These experiments much like the APTES and GPTES experiments showed no use as a Capture Agent.

These experiments revealed that it was not only important to have a sufficient level of bio passivation to have a sufficient SNR, but it was also important to have an oriented print strategy. For this reason, PEG based strategies were investigated to provide the necessary passivation and oriented print. PEG has many different functional groups available to provide a method for passivation as well as linking strategies; one of which is a Cu-free click chemistry reagent. Click chemistry has been heavily reviewed as a method for the selective and rapid method for the covalent linking of an azide to an alkyne.[175] This method is typically used for binding untethered molecules such as fluorophores to modified proteins for simple detection. Typically, these agents rely on a Copper(I)-catalysed azide-alkyne cycloaddition (CuAAC) to make a heterocyclic ring and provide a covalent attachment of reaction partners. Despite these methods being highly robust, the use of the copper catalyst can interfere with *in vivo* studies due to coppers cytotoxic properties. Due to coppers cytoxicity, methods by Bertozzi et al[176] incorporated a strained dibenzocyclooctyne

(DBCO) around the alkyne where the electron-withdrawing fluorine and ring strain destabilizes the alkyne. This destabilization drives the reaction of the alkyne with the azide to relieve the ring strain. This gives the same heterocycle as the copper catalysed reaction and stabilizes the cyclooctyne. This methodology has been successfully incorporated into living systems without the cytotoxicity, although the reaction is somewhat slower that the traditional CuAAC method. Another benefit to this methodology was that the DNA Capture Agent would be free in solution before click reaction with the strained alkyne surface, theoretically increasing the chance of FoxO1 binding. This in theory would increase capture efficiency. The tests run did not include the open chip method but instead run directly with the MAC chip calibration methodology.

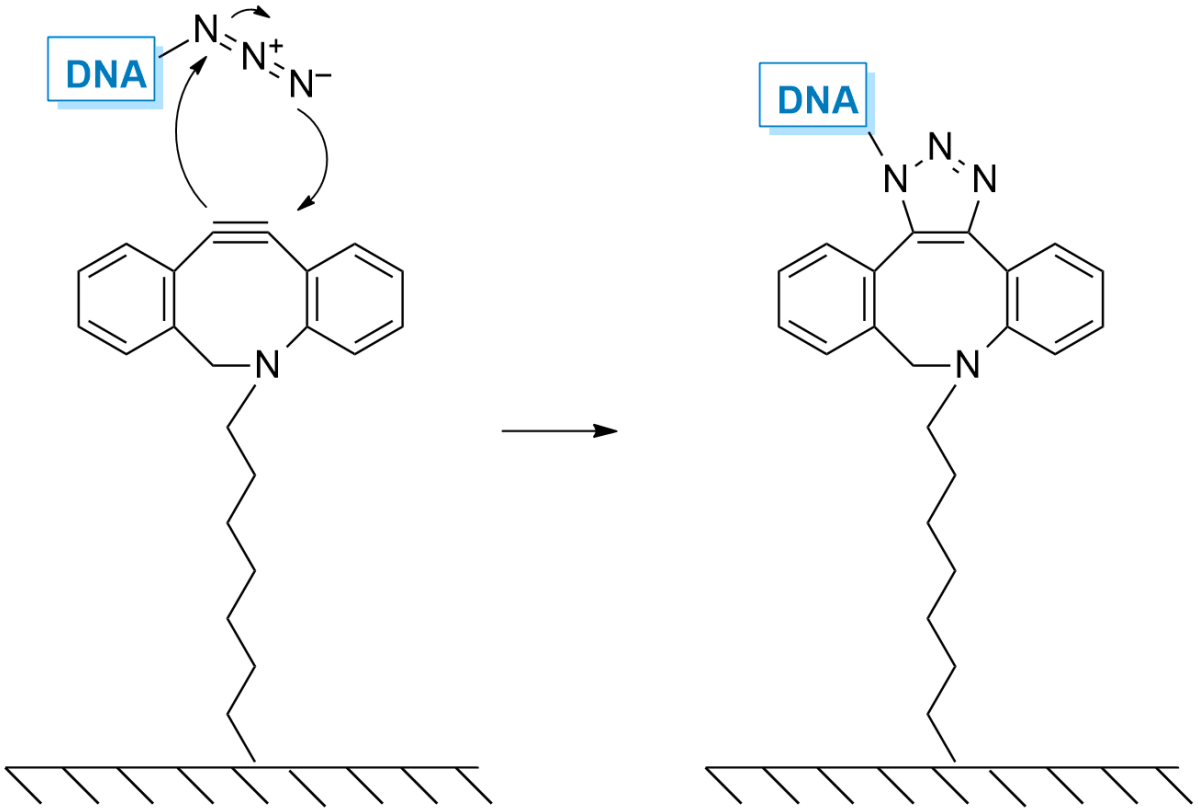


Figure 4.8 Simplified diagram of the strained ring Click chemistry reaction. The DNA was azide tagged with the surface treated with the strain ring system. This would allow the DNA to have greater freedom of movement to bind the FoxO1 before covalent tethering to the treated slide.

Dibenzocyclooctyne-PEG4-N-hydroxysuccinimidyl ester was purchased to be used in conjunction with the described PEG protocol. This would provide a passivated surface with a functional moiety that would specifically react with any present azides. To utilise this functionalisation the Capture Agents 7, 8 and 9 [see Appendix for sequences] were purchased a 5'-azide group incorporated. Only a selection of Capture Agents were purchased as these 3 showed the most promise at the time.

Experiments were run in the same method as detailed in Section 4.4.4 with the MAC chip calibration studies.

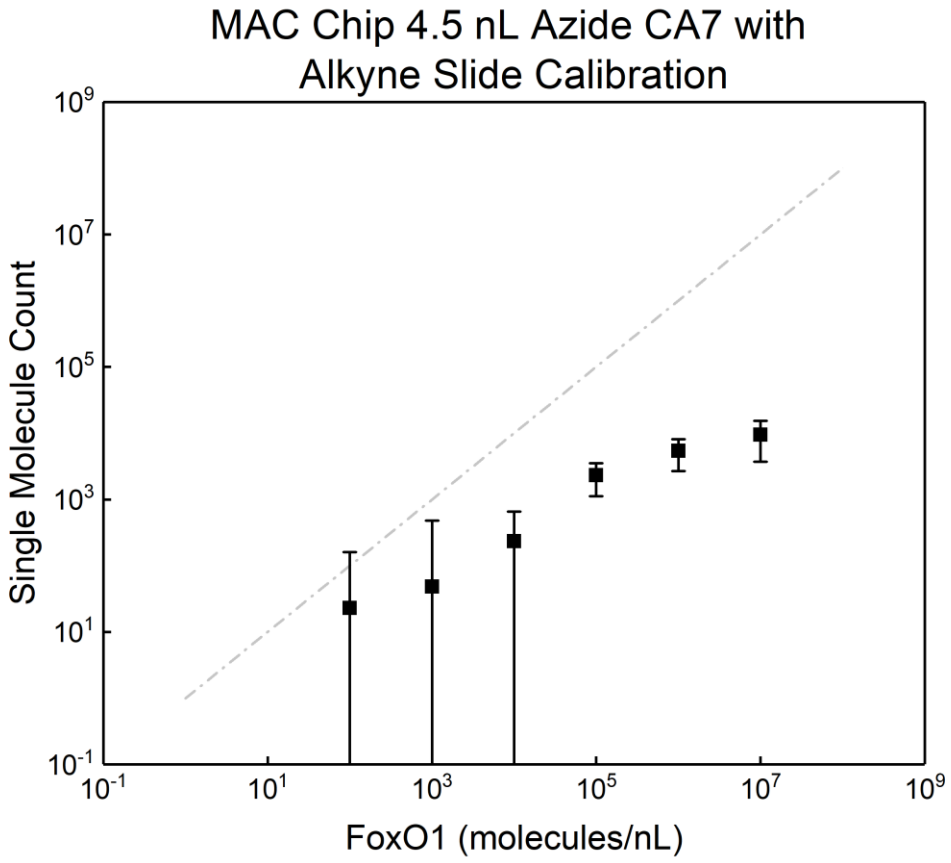


Figure 4.9 Calibration curve of Capture Agent 7 using azide and strained alkyne attachment methodologies. The lower error bars trail given the logarithmic axis.

Out of the three Capture Agents, 7, 8 and 9, the only one to show any potential for use as a Capture Agent in the MAC chip format was CA7 [seen in Table 4.2]. The calibration curve can be seen in Figure 4.9 and whilst the curve seems linear, the standard deviation at the lower concentrations adds a significant degree of inaccuracy. The observed capture efficiency is erratic and averages at under 1%, by comparing the obtained results to the perfect fit seen by the grey dashed line, and therefore this method would not work in the MAC chip assay.

4.5.2 Biotin modified Capture Agent Assay Development

To test DNA in the same format as the antibody studies, the PEG neutravidin format was tested by purchasing the Capture Agents with a 5'-biotin modification. This provides cheap functionalisation and the interaction between biotin and neutravidin is one of the strongest non-covalent interactions

known to date. Thus, this technique should provide a method for providing an oriented print whilst still providing the required passivation. The results for the biotin-neutravidin method are presented in the same way as the antibody open chip testing strategies, with the success and failure of the method shown in Table 4.3. Table 4.3 shows that out of the 9 Capture Agents, 3 showed a small level of binding [which was measured using the same method as all experiments detailed in this thesis, found in Section 2.4) whilst one, Capture Agent 7 showed a high level of binding for potential use in the MAC chip. In light of these results, Capture Agent 7 was taken forward for calibration testing.

Table 4.3 The biotin DNA- Antibody pairings trialled for use in the assay, the y-axis shows the capture antibodies and the x-axis the fluorescently tagged secondary antibodies. Red demonstrates no binding, yellow some binding and green a high degree of binding.

Column1	FoxO1 (DU 1071)	Human FoxO1 mAb5939	Anti-FOXO1A antibody (ab111029)	Anti-FOXO1 Antibody EP927Y	Anti-FOXO1A antibody (ab150059)
FoxO Capture Agent 1					
FoxO Capture Agent 2					
FoxO Capture Agent 3					
FoxO Capture Agent 4					
FoxO Capture Agent 5					
FoxO Capture Agent 6					
FoxO Capture Agent 7					
FoxO Capture Agent 8					
FoxO Capture Agent 9					

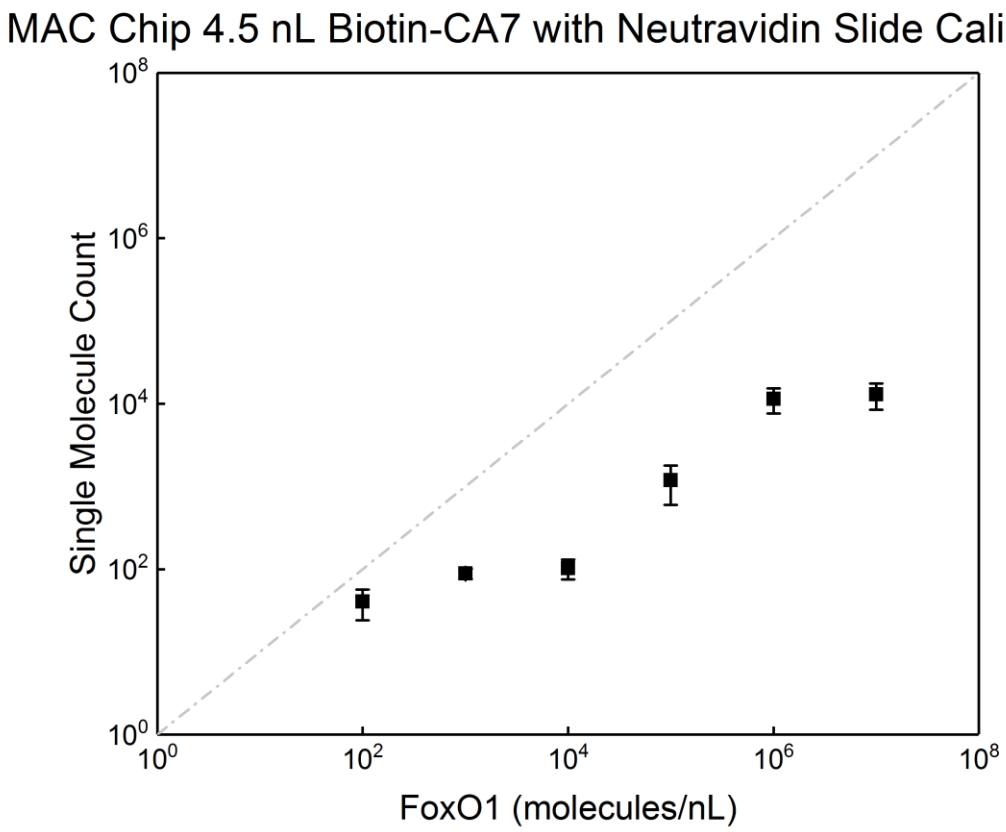


Figure 4.10 Biotinylated Capture Agent 7 4.5 nL MAC chip calibration. The x-axis represents the number of molecules of FoxO1 which is present in the solution loaded into the experiment, the y-axis shows the single molecule count which is calculated using the counting algorithm that is used for all of the experiments in the thesis, The grey dashed line represents the theoretical perfect scenario of 100% binding, where the calculated count is the same as the number of FoxO1 molecule present within the solution.

Figure 4.10 shows that CA7 had a high limit of detection, defined by only seeing binding above background at high FoxO1 concentrations at 10^4 FoxO1 copy number per nL and a compact linear range only starting at 10^4 FoxO1 copy number per nL. However, it also showed a higher level of consistency in FoxO1 capture at the tested concentrations and so CA7 was brought forward to cell studies. Despite the open chip experiments providing evidence that some of the DNA agents would potentially work in the assay, the MAC chip calibration suggested that it would be less accurate than the antibody agents.

The lack of a sufficient linear range and limit of detection for DNA Capture Agent 7 (and also Capture Agent 8 and 9) was hypothesised to come from steric hindrance from a high density of printing, thus inhibiting the optimal amount of binding of FoxO1 to the Capture Agents. To test this theory, a small spacer sequence was developed of CGATCGAT which would create gaps between the capture sequences to potentially increase the binding events due to less steric hindrance.

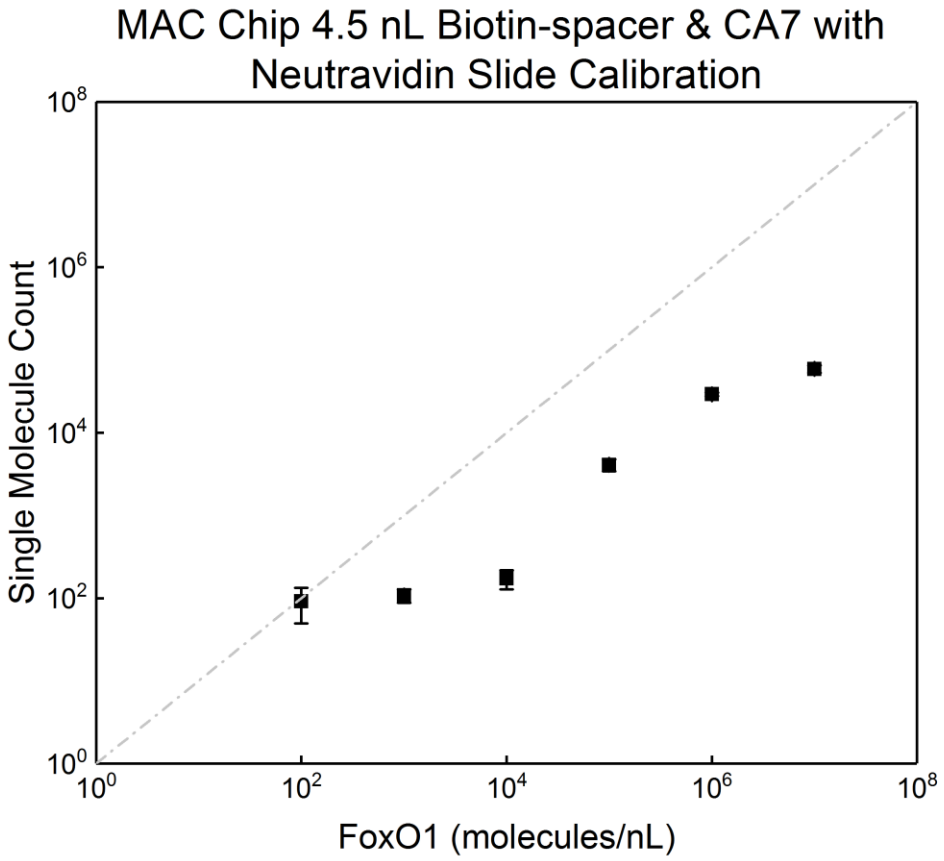


Figure 4.11 Biotinylated Capture Agent 7 with spacer addition in 4.5 nL MAC chip calibration attempt.

The addition of the spacer did not improve binding efficiency but did show comparable results as shown in Figure 4.11. For this reason, its use was not continued as it did not enhance the assay efficiency and added to assay costs. The use of the spacer was also tested with Capture Agents 8 and 9 again showing no improvement in binding efficiency.

A potential reason for the non-binding of recombinant FoxO1 to the DNA Capture Agents lies with the innate biology of FoxO1. FoxO1 relies on its intrinsic folding to bind to its consensus motifs as well as certain PTMs [see Section 1.6 for a in depth discussion of the main PTMs which are implicated with FoxO1 binding] to aid motif binding. As the purchased recombinant FoxO1 protein was raised in a bacterial vector it was hypothesised that the bacteria did not have the natural machinery to appropriately fold and package the FoxO1 recombinant protein, and therefore lowers the recombinants DNA binding ability. To test this theory, CA7 was carried on to the cell line studies. Cell lysate was considered for testing for this purpose but the typical conditions to obtain cell lysate often rely on the use of SDS and other denaturing agents which could again affect the DNA binding

ability of the FoxO1. Thus, it was believed simply carrying CA7 through to single cell studies was deemed the best course of action.

In conclusion, this chapter has detailed the use of a hit-to-lead workflow process which has yielded positive results to find two suitable antibody-antibody assay set ups for the detection of total FoxO1 levels, along with a novel DNA-antibody pair for the detection of active FoxO1. These assays were successfully determined by the use of a relatively inaccurate 'open chip' format which provided initial evidence of binding of FoxO1 from a range of Capture Agents- detection (secondary) antibodies pairings. During the open chip experiments, it became clear that in-house antibody labelling strategies did not provide a suitable secondary antibody for the assays due to their aggregation and multiple labelling issues. This problem was easily solved by only testing antibodies purchased with a label. After the open chip experiments had provided evidence of the optimal pairs, these pairs were taken forward for testing in the MAC chip format. After the MAC chip tests were completed two viable antibody pairs were discovered along with a DNA-antibody pair. In this chapter, a novel method for the MAC chip was designed for the successful covalent and oriented attachment of DNA Capture Agents to the PEG surface which also yielded successful capture of FoxO1 recombinant protein, albeit with seemingly less affinity compared to the antibody-antibody pairs.

5 Validation of Assays Using Single Cell MAC Chip Experiments

5.1 Outline

This chapter details the progression of the optimised pairings of antibody and DNA based assays into cellular studies. Taking in account that the end goal of this project was to successfully look at theoretical changes in FoxO1 copy number in COPD vs healthy patient samples, this was a logical next step to validate the assays abilities to bind observe alterations in FoxO1 copy number.

The initial experiments used the commonly utilised cell line for FoxO1 studies, Toledo B-cells. The MAC chip experiments were performed with untreated Toledo cells using both the antibody-antibody (total copy number) and the DNA-antibody (active copy number) pairings. These experiments resulted in the 'basal measurement' of both total and active FoxO1 copy numbers. In order to validate that the assays were able to observe changes to FoxO1 copy number, the cells were next treated with ZSTK474 and glucose to observe an increase and decrease in FoxO1 copy number respectively. These two studies successfully demonstrated the ability of both assays to observe increases and decreases in FoxO1 in the Toledo cell line. The tests were statistically validated with a student t-test.

The process of basal, ZSTK474 and glucose treatment studies was continued on further cell lines to further validate the assays ability to observe perturbations in FoxO1 copy numbers. The cell lines used to provide further validation were MCF7 and Beas-2b cell lines. The most important validation came from the Beas-2b cell line as they were derived from bronchial epithelial cells, and thus the most comparable cell line to the end goal of COPD patient samples.

5.2 Introduction

This section details the experiments undertaken to validate the designed assays. Using a cell line known to highly express the protein of interest is the best first step to prove an assays viability. Once an optimal cell line is determined, a set of experiments can be designed which should, dysregulate the expression of the protein of interest to either increase or decrease. This section details the choice of initial cell line, the methods to perturb the copy number of FoxO1 and the results of these perturbation experiments. Determining the assays ability to successfully observe changes in the level of FoxO1 expression validates the assay as a tool to monitor altered expressions of FoxO1 in

unknown samples. Validation in cell lines will increase confidence in clinical sample observations where the responses are unknown and it is important to have faith in the results.

The first stage was to determine an optimal cell line for the study of FoxO1. B-cell lymphomas are widely used for the studies of FoxO1 and its effects on B cell differentiation and regulation[177–180]. The Toledo large diffuse B cell lymphoma cell line was initially used for the studies of FoxO1. These cells have dysregulation of PI3K/Akt/mTor signalling pathways which effects their cellular growth and metabolism which is known to effect FoxO1 activation and copy number.[47] Because of this, the cells overexpress FoxO1 to allow for control and regulation of the PI3K pathways. For these reasons, the Toledo cell line makes the perfect model for testing the limits of the MAC chip assay. Furthermore the human protein atlas also shows that this cell type exhibits some of the highest FoxO1 protein expression levels with respect to all cell types.[181]

There are many B cell lymphoma cell lines, but the Toledo cell line posed an important advantage as it is negative for Epstein-Barr virus (EBV). The Epstein-Barr virus infection is usually involved with the development of most B-cell lymphoma cell lines including both Hodgkin's and Burkitt's lymphomas. Infection with EBV is typically used to establish immortalised cell lines of lymphoblastoid cells (LCLs), which occurs from the virus altering a diverse range of cellular molecules leading to immortalisation and B-cell growth. Whilst infection with EBV is a beneficial as a procedure to immortalise a cell line, the EBV disrupts innate FoxO1 biology.[152] Reports show that EBV infection leads to downregulation of FoxO1 by PI3K mediated nuclear export, inhibition of FoxO1 mRNA expression and even by altering the pattern of posttranslational modifications of FoxO1[182]. As the EBV immortalisation procedure is known to interact with FoxO1, the cell line (Toledo) chosen for analysis in the MAC chip assay was negative for Epstein-Barr virus. Additionally, the Toledo cells (and all B-cell lymphoma lines) are a suspension cell line, which means they are extremely easy to handle.

5.3 Toledo Cell Line Antibody Studies

5.3.1 DU1071 Basal FoxO1 Distributions

The first step in validating the assay was to take a basal reading of Toledo cells. This reading was measured by simply culturing the cells in optimal conditions before loading them into the MAC chip for analysis. This results from this reading would yield a basal expression and distribution of FoxO1 for which to compare the perturbation studies that follow. This methodology is followed for all subsequent cell lines and assay pairs detailed in this chapter.

As discussed in Chapter 3, the most promising assay development came from the antibody pairings DU 1071 and mAb5939 which were both paired with the detection agent EP927Y. Therefore, these pairings were utilised in the first single cell assays. The first experiments run were Toledo cells suspended into clear serum free RPMI media and flowed in using the protocol found in Section 3.2.5. In every experiment, the maximum number of cells were trapped and lysed within 1 hour of harvest. This protocol keeps all cell assays as consistent as possible but does provide limitations to the number of cells that could potentially be analysed in one experiment.

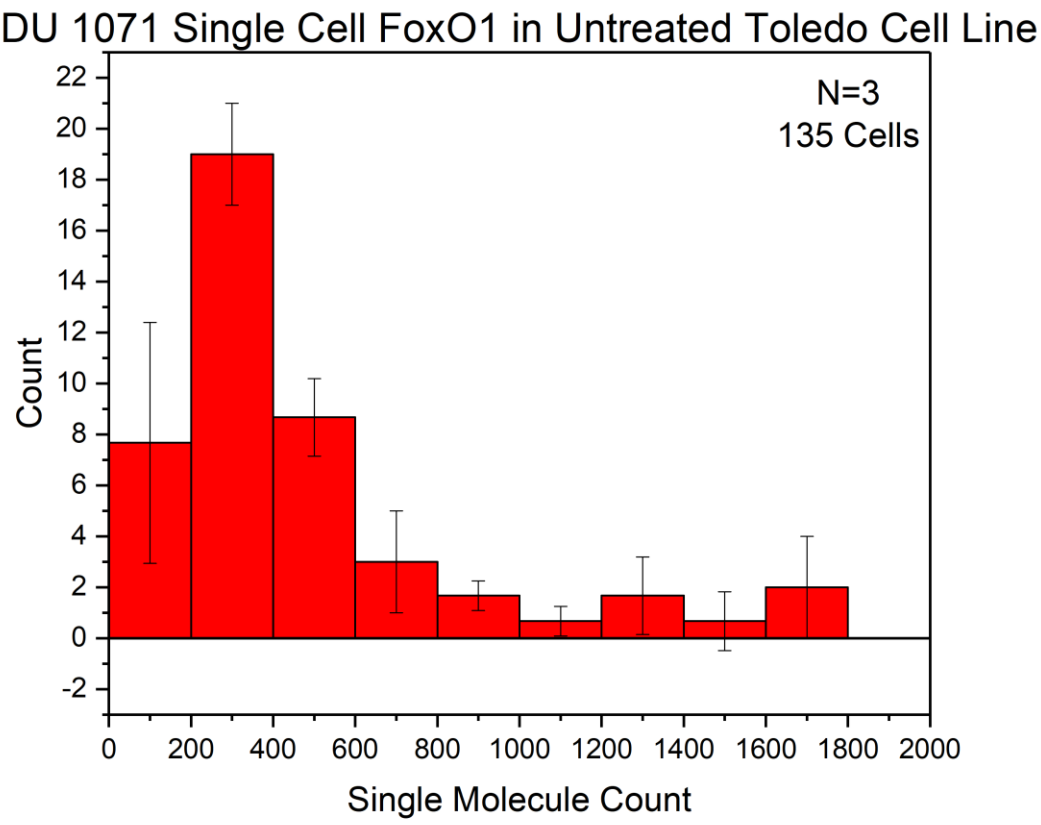


Figure 5.1 Histogram showing the single molecule distributions of FoxO1 in 135 untreated Toledo cells, compiled of 3 separate experiments.

Figure 5.1 shows the 'basal level' of expression with a right leading tail of higher expressing outlier cells which highlights the heterogeneity of the cell line [see Figure 2.2 for the process of how all MAC chip results were obtained]. The heterogeneity of cellular expression has been documented in all previous assays.[33,183] These high expressing cells likely arise from gene expression noise amongst other environmental factors.[20,33,183] These results provided a typical basal level of expression with a mean of 474 ± 35 single molecule counts per cell, which allows a comparison to cells that are treated with different factors.

The single molecule count observed was lower than what was seen in the MAC chip p53 assay.[20,33,35,118] At the time, the p53 assay was the only other fully working MAC chip assay to draw comparisons to. Work by Michael Barclay showed the typical level of p53 single molecule binding, in the high p53 expressing BE cell line, was in the orders of tens of thousands single molecule counts. Even the wild-type p53 expressing cell line MCF7 showed average binding in the thousands.[183] This implied one of two things; either the designed FoxO1 assay using DU 1071 had a lower affinity for FoxO1 compared to the K_d seen with the p53 assay or there is a lower copy number of FoxO1 present compared to p53. Despite there being some ambiguity as to why the FoxO1 assay count was lower compared to the p53 assay, there was still sufficient binding and the experiments show the assays ability to work in the single cell regime.

To conclude, this work demonstrated the assay was able to detect a measurable level of FoxO1 expression in a basal, or 'untreated' Toledo cell line. Therefore, the next experiments performed involved perturbing the cells in an attempt to show altered expressions of FoxO1. This will validate if the assay can resolve the expected changes in FoxO1 copy number.

5.3.2 ZSTK474 Treated Experiments with DU1071

The first tests were to determine whether expected increases in FoxO1 copy number could be observed. To achieve this, the pan selective PI3K inhibitor ZSTK474 was employed. As detailed in Section 1.6.1, inhibition of the PI3K pathway has several effects on both the copy number and activity of FoxO1. Firstly, PI3K via activation of the Akt pathway will directly phosphorylate FoxO1 at Thr-24, Ser-256, and Ser-319 which sequesters FoxO1 from the nucleus and subsequently FoxO1 is ubiquitinated and degraded by the proteasome[116,179]. By inhibiting this interaction, the levels of total FoxO1 and its activity should increase. ZSTK474 was chosen as the PI3K inhibitor as it is pan selective. ZSTK474 being pan-selective means that despite there being many PI3K subunits with varying expressions in different cell lines, ZSTK474 should show the most comparable inhibition across all cell lines tested. ZSTK474 was initially thought to be selective to the PI3Kγ subunit but competitive inhibition studies to classify the drug showed that it was a competitive ATP inhibitor, binding in the ATP-binding pocket of each PI3K isoform. The competitive inhibition studies by Kong *et al.* determined ZSTK474 had Ki values for PI3Kα, -β, -δ and -γ of 6.7, 10.4, 1.8 and 11.7 nM, respectively.[184] Kong also showed that ZSTK474s IC50 value was 30-fold more potent than that of LY294002, which is another commonly used PI3K inhibitor with a similar mechanism of action.[55] Furthermore, studies were undertaken to observe ZSTK474 cross reactivity and showed that tested

against 139 protein kinases it only showed specificity to PI3K.[185] Therefore, ZSTK474 makes an ideal candidate for looking at downstream targets such as FoxO1 due to its high specificity.

The Toledo cells and all subsequent cell lines were treated with 10 µM of ZSTK474 overnight before analysis in the MAC chip format. The reported K_i of ZSTK474 is lower than the used concentration, in the nanomolar ranges, but due to no reported secondary effects of ZSTK474 at this dosage it was tested at 10 µM.

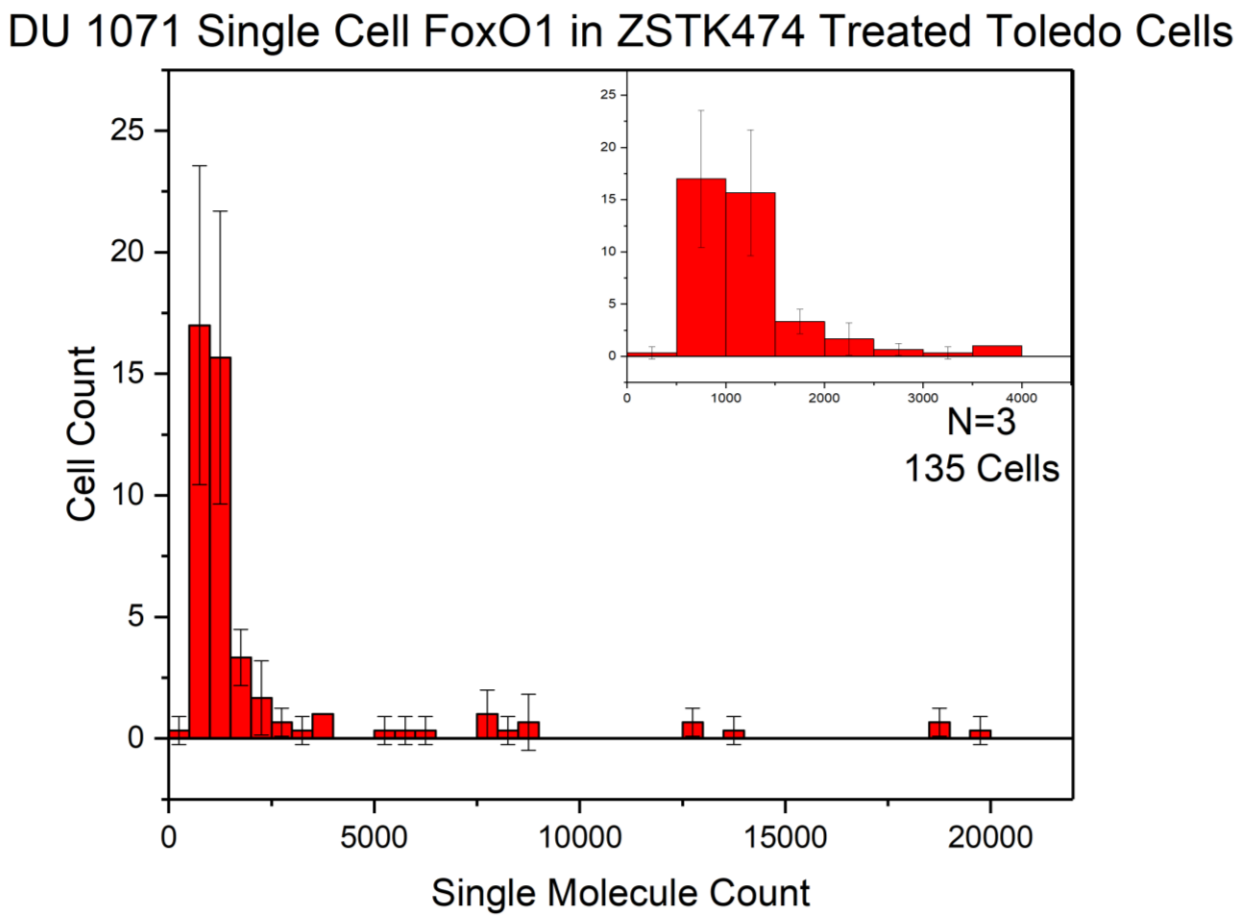


Figure 5.2 Assay validation test of DU1071 using Toledo cells treated with ZSTK474 showing the expected increase in total FoxO1 copy number. Compiled of 135 cells collected over 3 experiments. The inset graph shows the lower expressing region which is still over 2 times higher than the basal level.

The significant increase in total FoxO1 molecules with treatment of ZSTK474 can be seen in Figure 5.2, with the calculated mean alone showing an increase over 4 times from the basal level at 2291 ± 301 FoxO1 single molecules per cell. Over 12% of the cells measured >10 times the basal mean counts showing an increase in heterogeneity. These histograms were made from 3 repeat single cell experiments to generate the compiled histogram seen in Figure 5.2, the same as with the basal experiments. These results clearly showed that the assay can observe increases in total FoxO1.

In previous studies and validations utilising drug treatments, such as those run to validate the MAC chip p53 assay[33], the treatments showed a bimodal distribution where there was a significant non-responsive population present. This ZSTK474 experiment did not yield the expected bimodal distribution. The p53 studies utilised MCF7 cells which are a commonly used cell line for the studies of p53, so this non-responsive population may have been a trend only observed in this cell line. The average single molecule count in the FoxO1 assay vs the p53 assay is significantly lowered. The average single molecule count for untreated MCF7 cells in the p53 assay was found to be at 5000 single molecules per cell, which is an order of magnitude higher than that seen with the FoxO1 assay. This suggests the lack of the expected bimodal distribution is likely due to the lowered sensitivity of the FoxO1 assay with this antibody pairing compared to the p53 assay. The lowered sensitivity for FoxO1 means the assay has a weaker resolving power compared to the previous p53 assay.

These initial results showed that the DU1071 assay was able to successfully distinguish increases to the basal level of FoxO1 in Toledo cells even if it has lower sensitivity to previous p53 assays. These experiments were run at the same time as the other assays and thus its lower limits of detection were not tested at this time.

5.3.3 mAb5939 Basal FoxO1 Distributions

The following sections detail the experiments undertaken to validate the mAb5939 + EP927Y assay pairing, the same method as used for the DU1071 is used here.

The use of DU1071 as a Capture Agent along with fluorescently tagged EP927Y did show binding and the ability to see expected increases in FoxO1 copy number and activity, although it had a disadvantage. DU1071 is a polyclonal antibody, which are known to have issues with batch to batch variability and thus will affect DU1071's reproducibility. Despite DU1071 showing a greater affinity to recombinant FoxO1, it was decided to test mAb5939 because it is monoclonal and should show less batch to batch variability compared to DU1071.

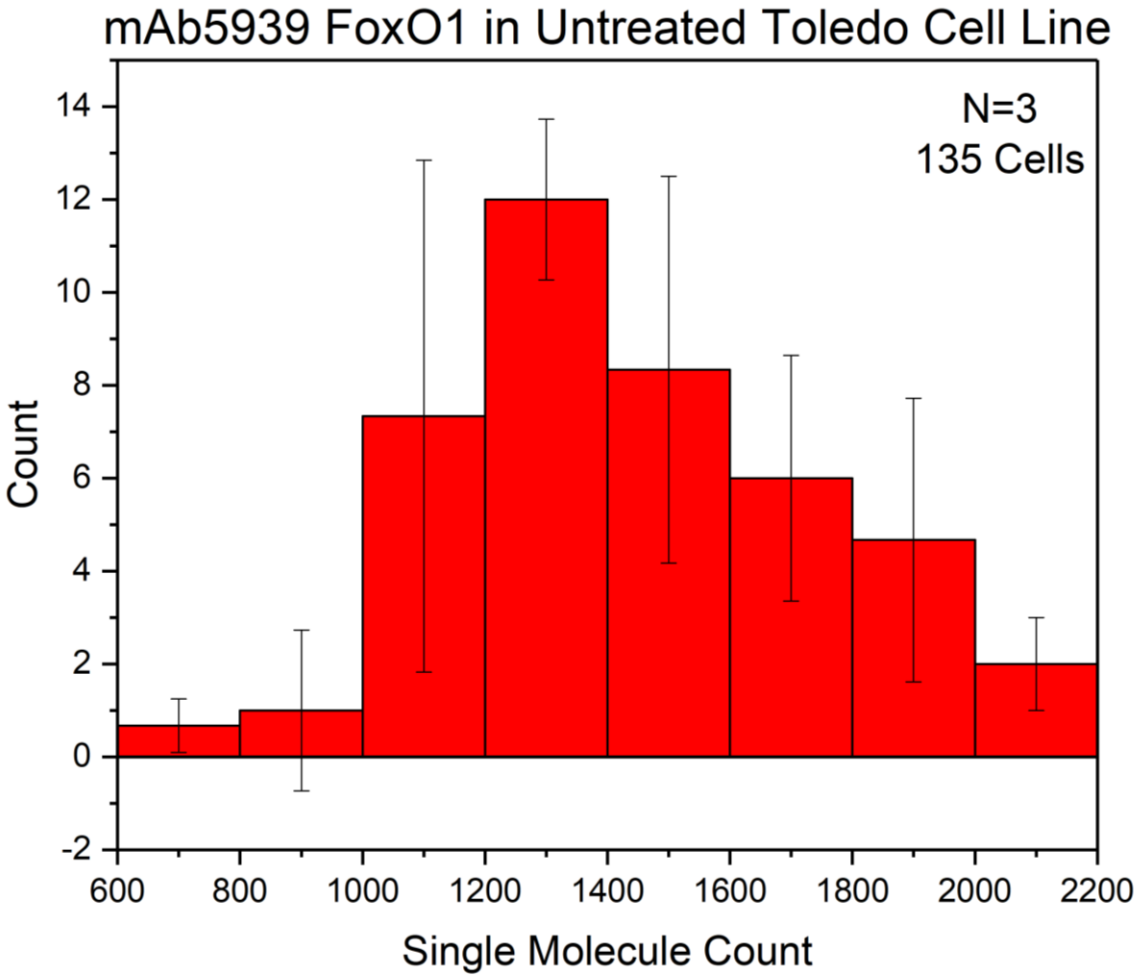


Figure 5.3 Histogram showing the single molecule distributions of FoxO1 in 135 untreated Toledo cells with the mAb5939 + EP927Y antibody assay pairing. Collected over 3 experiments.

The same single cell tests used for DU1071 were repeated for mAb5939 to initially determine the basal FoxO1 distribution. The results from these experiments are shown in Figure 5.3. The mAb5939 experiments provided a higher mean count compared to DU1071 at 1515 ± 33 single molecule counts per cell; making the average basal count over three times higher than that seen in the DU1071 based assay. The reason for the enhanced count is likely due to the mAb5939 assay having an enhanced $K_{D,}$ making it more suitable for analysing perturbations in FoxO1 total copy number changes. Both DU1071 and mAb5939 assays showed basal level FoxO1 bindings that were at the lower limit of their respective calibration curves. This would make it difficult to truly resolve the absolute copy number of FoxO1. However, if the assays show a sufficient shift in single molecule count the assays would still be suited for differentiating patient derived cells from different disease states (i.e. healthy from COPD). The basal count still exhibited a right-hand tail which is thought to

be from protein burst and gene expression noise, as cells as they divide will show bursts of high expression to drive certain pathways and also to be ready to divide.[186,187]

5.3.4 ZSTK474 Treated Experiments with mAb5939

The ZSTK474 experiments were then repeated for mAb5939 utilising Toledo cells and treating them with 10 µM ZSTK474 to observe if the FoxO1 increase is observable.

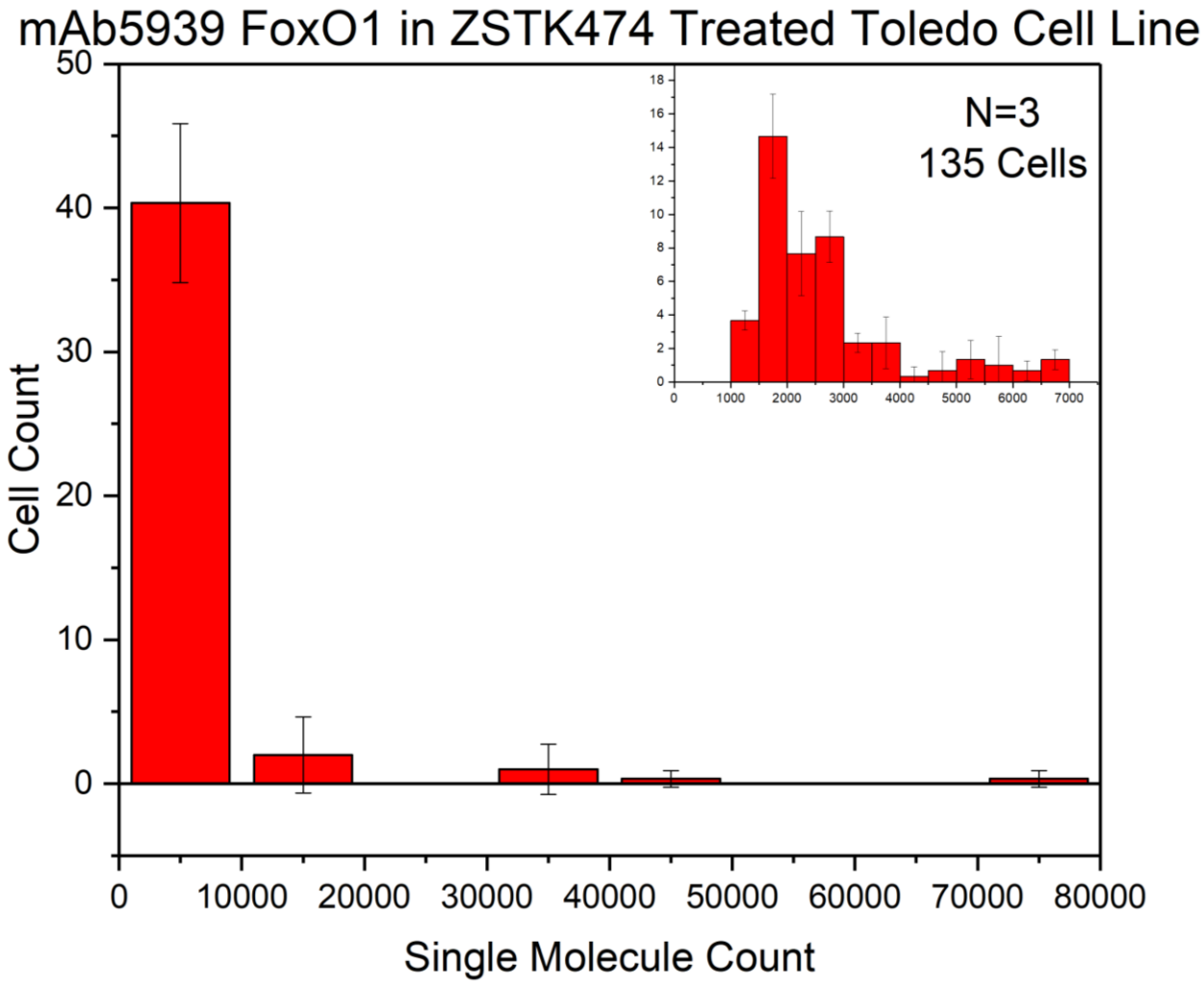


Figure 5.4 Assay validation test of mAb5939 using Toledo cells treated with 10 µM ZSTK474 showing the expected increase in total FoxO1 copy number. 135 cells were analysed over 3 experimental repeats. The inset graph shows the lower expressing region which is still over 3 times higher than the basal level.

The observed counts of FoxO1 under ZSTK474 treatment showed a distinct increase from basal at 4955 ± 763 counts per cell, which is over three times higher than the basal mean, by comparing the mean count of this experiment to the mean count of the basal experiment [Figure 5.3]. There were some observed counts that were drastically over the mean plus standard deviation. These high

expressing outliers may arise from the use of cells at a certain time in the cell cycle which causes gene expression noise or a protein burst event as mentioned previously.[183] This assay showed that the use of mAb5939 gave a better resolution compared to DU1071 when comparing ZSTK474 perturbations in the Toledo cell line. This antibody pairing was also unable to resolve an expected bimodal distribution.

5.3.5 Glucose Treated Experiments with mAb5939 + EP927Y Pair

To further test the assays ability to observe perturbations to FoxO1 levels, the experiments listed in this subsection were designed to decrease the level of FoxO1 copy number.

An increase in the concentration of glucose can lead to higher rates of glucose metabolism, which in turn leads to hyperactivation of the Akt pathway.[188–190] This is expected because the Akt path is known to regulate certain metabolic paths such as GLUT1[191–193] and mitochondrial interactions.[194] Furthermore, increased levels of glycolysis, which can be activated by increased glucose metabolism rates, plays a role in hydroperoxide detoxification that is known to control and lower FoxO1 activity and total copy numbers.[75] High glucose is also known to induce Akt signalling, which subsequently attenuates the inactivation and subsequent degradation of FoxO1, thus leading to a drop in copy number. This drop in copy number is indeed observable in the FoxO1 total and active assays.[194,195]

Toledo cells were tested using the same MAC chip methodology as previously described with the media being supplemented with 20 mM of glucose. This is a concentration which mimics a high glucose environment which is typically at 5 mM, which will consequently induce the expression of Akt pathway.[194] This process could have been achieved by the direct use of insulin or a PI3K activator such as 740 Y-P, but by utilising endogenous homeostatic pathways it will further validate the ability of the assay to identify and resolve changes to biological effects on the FoxO1 pathway.[196]

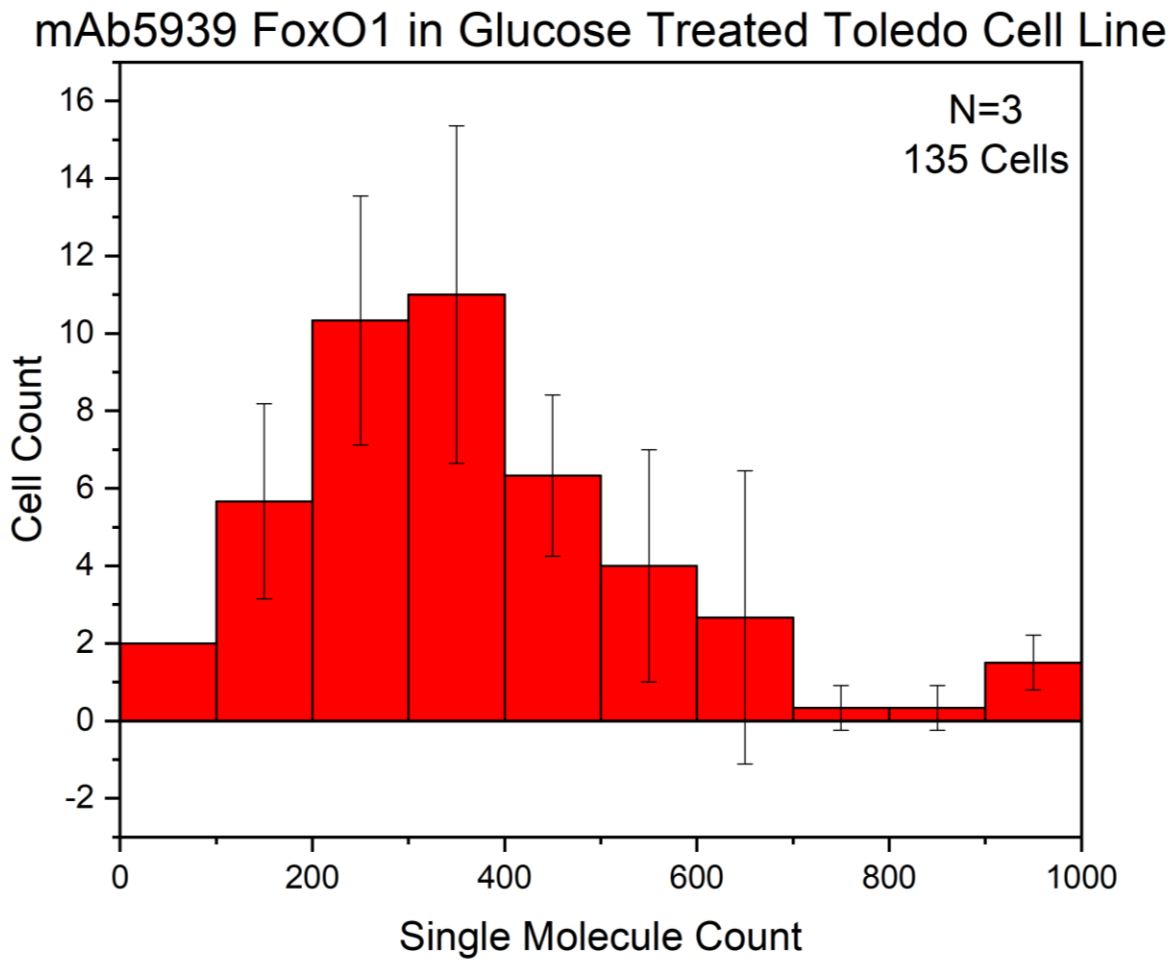


Figure 5.5 Assay validation test of mAb5939 using 135 Toledo cells, across 3 experimental repeats, treated with 20 mM glucose showing the expected decrease in total FoxO1 copy number. The mean single molecule count has decreased almost 6 times the basal expression level.

The compiled experiments used 135 cells over 3 chips and show nearly a six-fold decrease in the average single molecule count at 262 ± 23 counts per cell (results shown in Figure 5.5). This decrease was expected from the extended glucose treatment. This is a significant decrease and validated that the assay could see both increases and decreases in alterations of total copy numbers of FoxO1. While the decrease in total copy number is detectable, the log normal distribution seen in the previous basal and ZSTK474 treated results is lost. This is likely due to the FoxO1 copy number present in the cells being at the lower limits of detection of the assay, rather than an alteration in the expected distribution. This experiment could have been optimised to determine the exact limit of detection to provide an accurate distribution of FoxO1. However, it was decided that the validation was sufficient to show the mAb5939 capture assay was suitable for detecting both increased and decreased levels of total FoxO1.

It is possible to use the calibration curve for the antibody assay which was determined in Section 4.4.4 it was decided that the ability to accurately quantify phenotypic shifts from biological pathways at the single cell level was sufficiently accurate to bring forward to other cell lines and subsequently patient samples.

5.4 Toledo Cell Line DNA Capture Agent 7 Studies

The set of experiments described in this section were run using the MAC chip method to validate the Capture Agent 7 (CA7) + EP927Y assay. The ability to resolve alterations in total FoxO1 copy numbers is a novel assay, which has not existed previously in the field of single cell proteomics, however the ability to distinguish the ratio of total protein vs an active form or including a post translational modification of interest is a sought-after commodity. There was a lack of a sensitive Capture Agent 7 calibration curve during the assay design detailed in Section 4.5 but it was decided to bring the DNA Capture Agent 7 to the single cell experiments. The unsuccessful production of a calibration curve was thought to be from the recombinant protein being at an insufficient quality.

It is widely known that the methods used for bacterial based protein expression are robust, with many different; vectors, bacterial species, commercially available plasmids and purification kits available. Despite bacterial protein expression robustness, there are still caveats and issues with it.[197] One key issue with bacterial expression is poor protein activity, through incomplete or incorrect folding of the protein. The protein may form a stable and soluble conformation but the architecture of the active site could fold incorrectly compared to the endogenous protein.[198] There are reported methods to address protein folding issues, such as including certain small molecules or prosthetic groups in the media to aid the correct the final folded conformation. Incorrect folding can only be tackled whilst performing in-house bacterial expression and when the issue is known to the final user. It cannot be tackled after the protein is brought from a supplier. Purchasing recombinant protein without expressly asking for the manufacturing technique means there is no way to know the protein folding quality and whether optimal growth conditions were used.[199]

Incorrect protein folding is also known to occur from erroneous disulphide bond formation, which can cause significant alterations to the active domains and thus protein inactivity.[200] The FoxO family are extensively studied as redox sensitive proteins that have acquired cysteines in certain unstructured regions during their evolution from DAF-16 into vertebrate evolution. These FoxO1 cystines have been shown to cause differential redox-dependent interactions between the several FoxO species.[201] This process of redox sensitivity relies on reversible Cys oxidation to initiate

interactions with CBP and p300 which are key regulators of FoxO1 transcriptional output and activity.[79] The Cys oxidation path shows that endogenous folding of the FoxO1 recombinant protein is necessary to allow binding to the consensus motif. Without this folding, it is not a sufficient *in vitro* model for FoxO1 DNA capture. Therefore, the DNA Capture Agent 7 was analysed in the same fashion as the antibody assay. This was to test the theory that the lack of a sensitive calibration curve arises from the lack of endogenous folding of the active site of FoxO1.

5.4.1 CA7 Basal FoxO1 Distributions

Utilising the same MAC chip methodology as detailed in Section 2.1, the first CA7 tests investigated whether a basal level of FoxO1 could be observed in Toledo cells. The MAC chip lysis method releases endogenously folded FoxO1 from the cell and so the released FoxO1 should be able to bind Capture Agent 7.

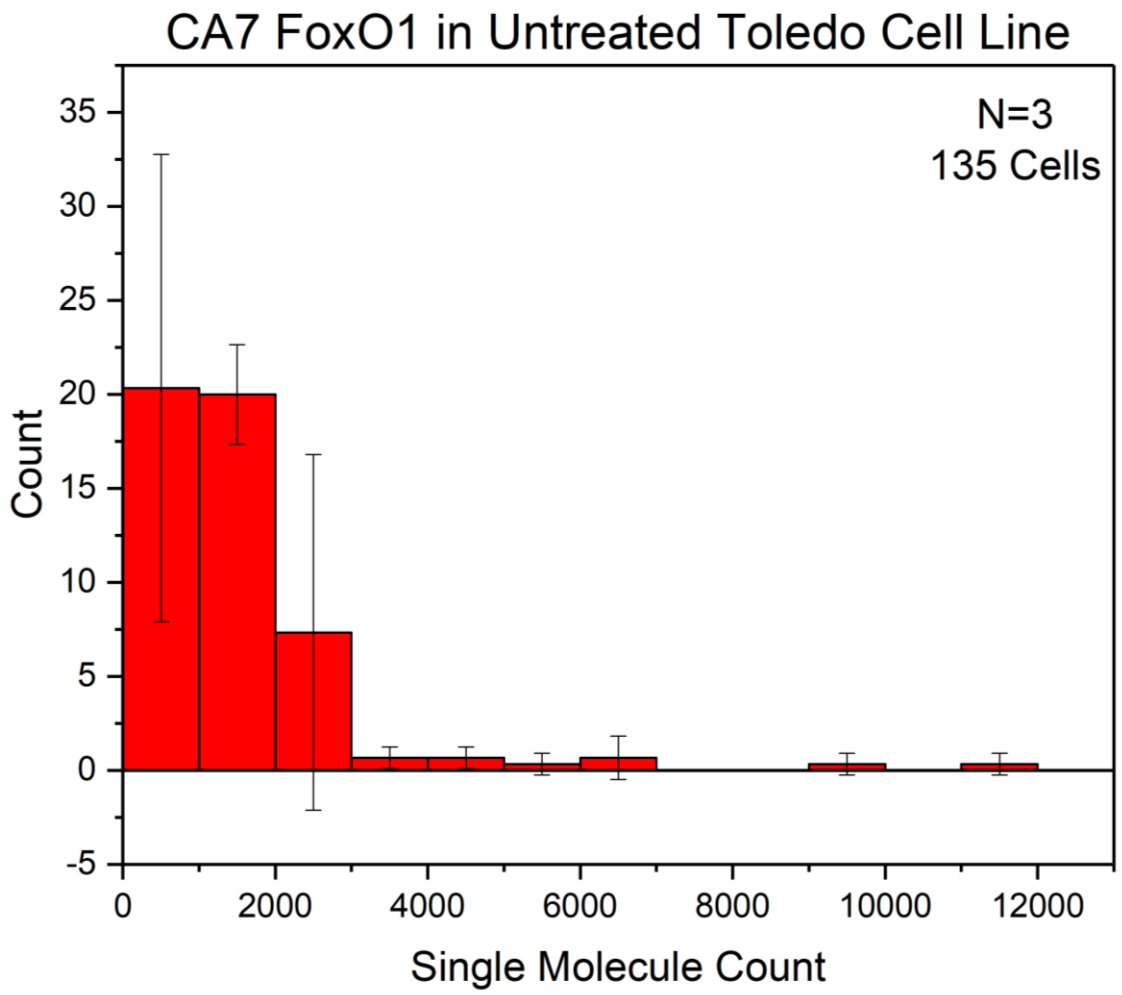


Figure 5.6 Histogram showing the single molecule distributions of FoxO1 in 135 untreated Toledo cells over 3 experimental repeats, with DNA Capture Agent 7 + EP927Y assay in 4.5 nL volume chambers, data is combined over 3 MAC chips.

The DNA based capture assay was printed with SSC: Betaine print buffer at 50 µM and the secondary antibody (EP927Y) at a concentration of 0.25 µg/mL; which is the same concentration used in the antibody-based capture assays. After lysis and background subtraction an observable level of binding was present. Furthermore, there were even outliers seen with each repeat showing binding significantly over the mean of 1528 ± 120 single molecules per cell. This level of binding was a great success for the development of the project. As the use of DNA capture to bind subpopulations of an analyte of interest had not been achieved previously in MAC chip experiments. This novel DNA capture proposed a method to analyse and understand the biology of a protein system at a higher resolution. The distinct count outliers that were observed also correlated with the known biology of FoxO1. One of FoxO1s major pathways is to control and regulate growth cycle checks and promote both senescence and apoptosis.[38] The use of DNA capture was a step forward for probing the FoxO1 system in untreated Toledo cells, with the basal level found the next experiments were to test the assays with ZSTK474 and glucose perturbations.

5.4.2 ZSTK474 Treated Experiments with Capture Agent 7 + EP927Y Pair

This section, much like the previous validation section, investigates whether Capture Agent 7 could be utilised to observe increases in active FoxO1 copy number. ZSTK474 was expected to indirectly increase the copy number of active FoxO1, as shown previously, by inhibiting the inactivation pathway of FoxO1 by PI3K. ZSTK474 would not necessarily directly increase the activity but rather the total copy number. Regardless, the response should still be observable by this DNA capture assay as in theory the level of active FoxO1 would increase with the total pool of FoxO1.

The automatic binning provided by Origin 2017 does not resolve the trend in ZSTK474 experiments with Capture Agent 7 (Figure 5.7) and so the inset plot was added to better resolve the trend seen in the data. As seen previously, the use of ZSTK474 has caused the expected increase in single molecule count, with the average mean count increasing by around 3 times to 5078 ± 960 single molecules per cell. Another interesting point of this plot is that there is a sizeable portion, around 33%, of the cells that now show FoxO1 levels to be like that of the basal population (aka a non-responsive population), if not slightly lower. This lower population shows a non-responsive population of the Toledo cells to the treatment of ZSTK474. The ability to observe drug resistance is an incredibly important factor to distinguish when designing new therapeutic agents.[202] This observation of a non-responsive population is a similar trend to the p53 assay and is likely due to the DNA capture assay

having the necessary sensitivity to resolve the alteration of FoxO1 activation at the lower limit of detection. Observing this non-responsive population further validates the theory that the lack of a sensitive calibration curve produced in Section 4.5.2 is due to the of a quality and incorrect folding of the recombinant FoxO1 protein.

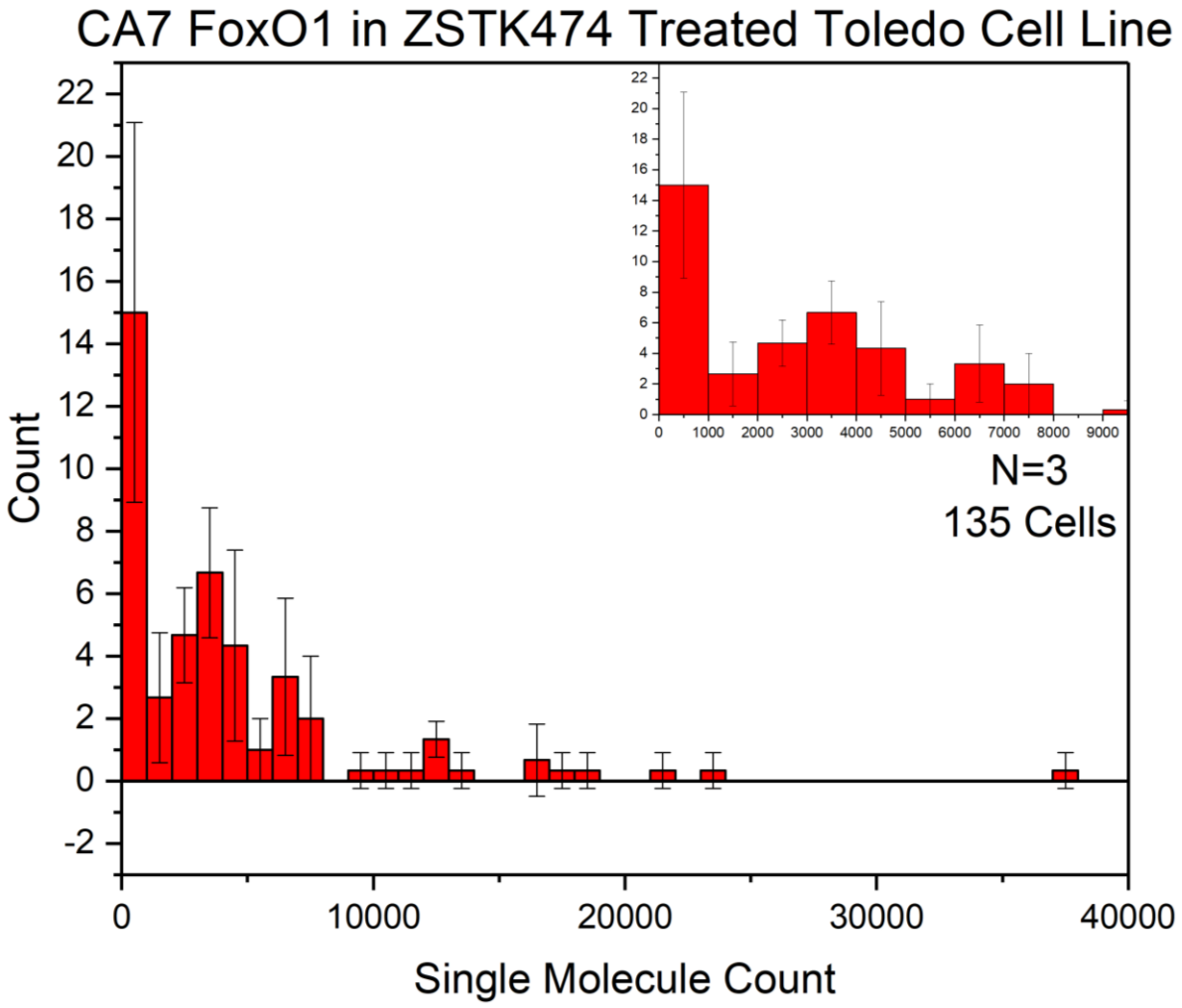


Figure 5.7 Assay validation test of CA7 using 135 Toledo cells over 3 experimental repeats, treated with 10 µM ZSTK474 showing the expected increase in total FoxO1 copy number. The inset graph shows the lower expressing region which is still over 3 times higher than the basal level. The main plot is generated with the automatic binning with Origin 2017, this lost much of the detail in the plot, hence the insert was added to show the 2 populations which had formed.

As mentioned previously, the DNA assay is a measurement of the level of FoxO1 activity not total copy number. By targeting an upstream mediator of FoxO1, rather than FoxO1 directly, it further validates the assays ability to distinguish and observe biological pathways rather than direct effects on FoxO1 itself.

The viability of the cells is tested in every experiment using a trypan blue exclusion assay with the cell sample having to be over 90% viable for use in MAC chip experiments. Since viable cells are

being utilised, the non-responsive population is likely a result of drug resistance in the cell population, highlighting the value of working at the single cell level and the type of issues seen with traditional ensemble techniques. To determine whether the non-responsive populations could be reduced, the concentration of drug was doubled to see if the non-responsive population would decrease. This experiment did result in a decrease, but it only showed a decrease of 9% with a 24% non-responsive population observed. Even though this result shows a potential for decreasing the non-responsive population, it was deemed unnecessary for further optimisation of the therapeutic response.

5.4.3 Glucose Treated Experiments with Capture Agent 7 + EP927Y pair

The next stage was to determine the Capture Agent 7 assays ability to observe reduced levels of FoxO1. The glucose treatment was predicted to illicit the same, if not a more significant response to FoxO1 binding as previously seen in the antibody assays. As the antibody assay studies showed a clear drop in total copy number of FoxO1, which occurs from the inactivating phosphorylation from Akt, the DNA based capture of active FoxO1 should also be significantly lowered.

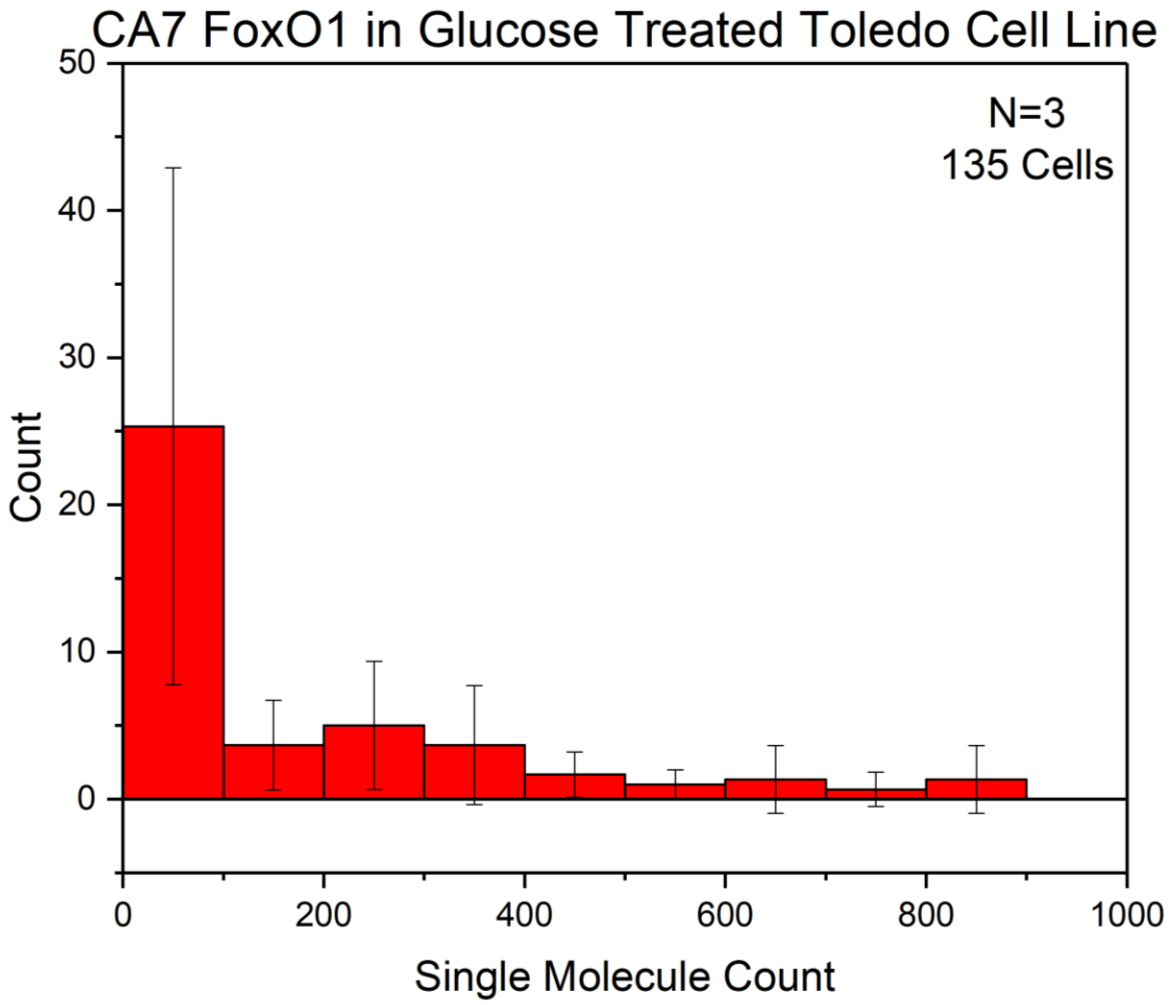


Figure 5.8 Assay validation test of Capture Agent 7 using 135 Toledo cells, over 3 experimental repeats, treated with 20 mM glucose showing the expected decrease in active FoxO1 copy number. The mean single molecule count has decreased almost 10 times the basal expression level.

The results from these experiments are shown in Figure 5.8 which showed a significant drop in the of active FoxO1 levels. The mean single molecule count was 178 ± 19 single molecules per cell, which is close to 10 times lower than the basal level, the mean and standard deviation is calculated from the single molecule counts of the individual cells using Origin 2017. This drop in single molecule count is larger than that seen with the antibody based assays. The drop is expected due to the inactivation of FoxO1 being a direct effect of the Akt axis, which is what is being targeted in these glucose studies. This experiment corroborated well with the biological theory and the expected significant drop in activity compared to total copy number was observed.

This assay was operating at its limit of detection with a significant majority of the counts below 50 single molecules after background subtraction. Being able to resolve down to such low binding levels shows the capability of the TIRF system and counting algorithm.

Table 5.1 Summary of the mean and standard deviation of the Toledo experiments using the DU1071, mAb5939 and CA7 Capture Agents. The table shows there is clear separation between the different perturbation experiments.

	DU1071			MAB5939			CA7		
BASAL	474	±	35	1515	±	33	1528	±	120
ZSTK474	2291	±	301	4955	±	763	5078	±	960
Glucose	-		-	262	±	23	178	±	19

This concludes the initial validation studies of both the mAb5939 and CA7 + EP927Y assays for studying the total and active copy number of FoxO1 respectively in the Toledo cell line. These experiments demonstrated the ability of both the mAb5939 and CA7 to readily monitor the alterations of FoxO copy number from biologically relevant perturbations. The next stage was to further validate the assay in other cell types to prove the versatility of the assays.

5.5 MCF7 Cell Line Validation Studies

This section details the experiments performed to validate the mAb5939 and Capture Agent 7 assays on the MCF7 breast cancer cell line. The same MAC chip experiments with the various perturbation studies are employed here to validate that the assay is robust enough to work on several cell lines.

One of the most widely studied cancer cell lines is MCF7 and so it was decided to attempt and validate the FoxO1 assays using MCF7 cells. If successful, it could be used for future multiplexing with the MAC chips other assay, p53. The MCF7 cell line was the first mammary cell line that was stable and able to remain in culture over several months, along with T-47D and MDA-MB-231. MCF7 cells account for more than 67% of all studies on breast cancer.[203] FoxO1 is ubiquitously expressed in MCF7 cells, albeit with lowered expression levels compared to B cell lines. This lower expression is explained by the innate biology of MCF7 cells and their enhanced expression of insulin-like growth factor-1 (IGF-1), which is a key upstream mediator of the PI3K signalling cascades. This chronic activation of the PI3K pathway is further exacerbated by a key mutation of the p110 subunit of PI3K, which is the catalytic subunit. Furthermore, there is the loss of PTEN signalling within MCF7 cells.[204] These combined factors show that FoxO1 levels are expected to be depleted and activity to be lowered compared to B-cell or T-cell lines. The level of FoxO1 within breast tissues is lowered compared to that found in immune system cells.[181]

Only the mAb5939 + EP927Y antibody pairing was tested with the MCF7 cell lines as this showed the greater separation between the different perturbations. mAb5939 is also monoclonal, so restocking this antibody should have less batch to batch variability with respect to DU1071. These tests were

performed in rapid succession as they were only for proof of concept to show the robustness of the assay.

5.5.1 mAb5939 + EP927Y Basal FoxO1 Distributions

The studies discussed here were performed to obtain the basal level of total FoxO1 present in MCF7 cells utilising the mAb5939 + EP927Y assay pair. All assay conditions (antibody printed in SCC:Betaine and the secondary EP927Y concentration kept at 0.25 µg/mL) were kept constant with the Toledo cell line studies. Cells were collected and trapped in a maximum 1 hr window before their lysis.

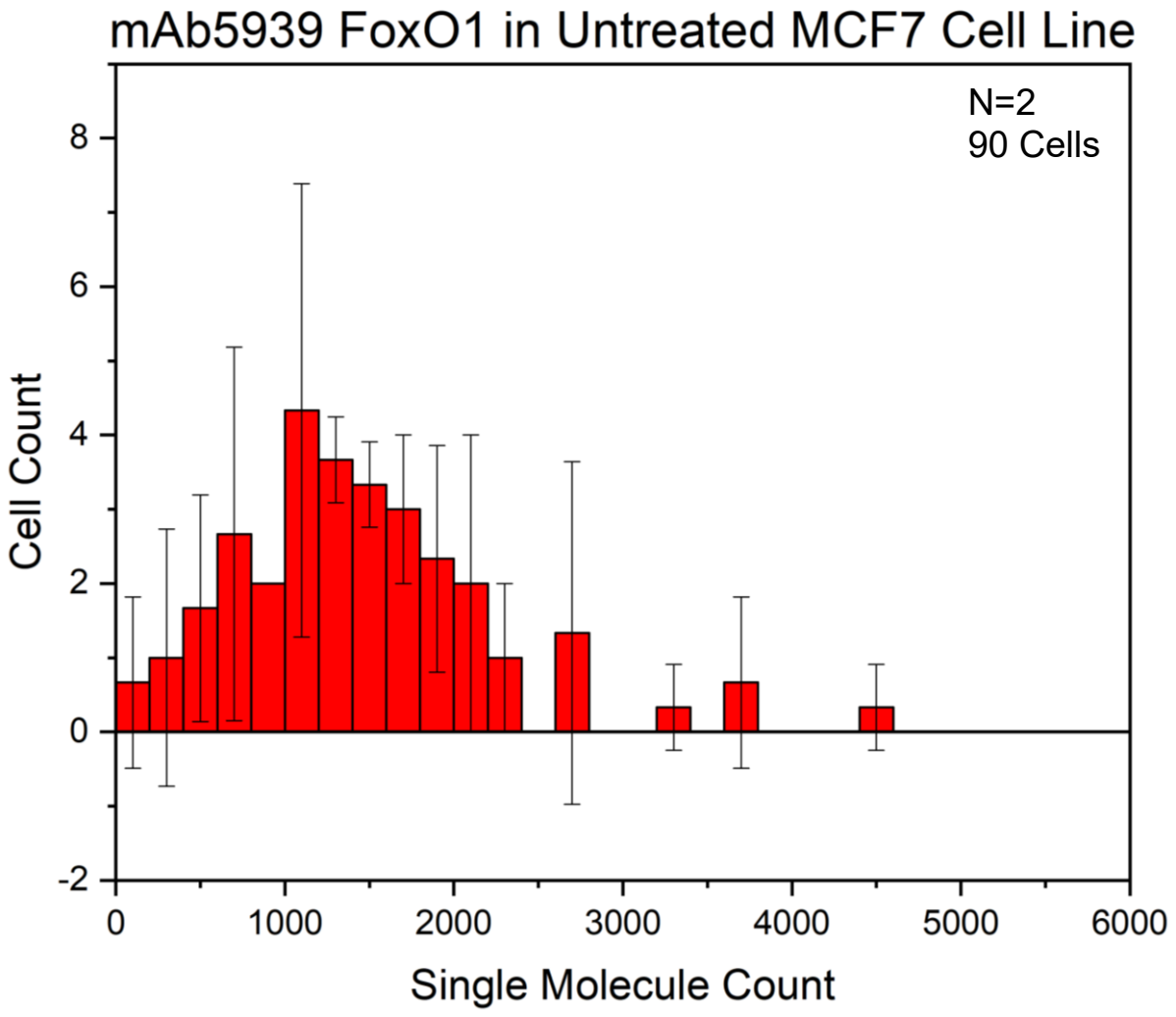
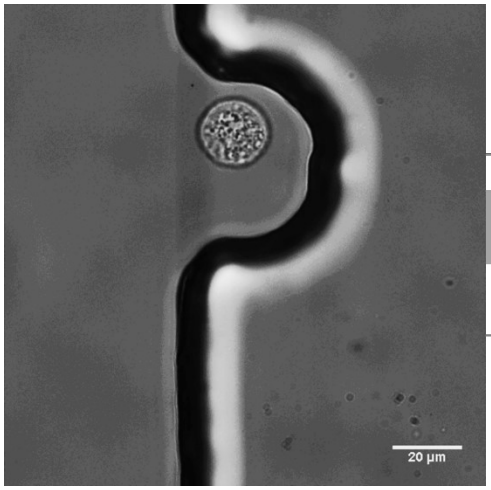


Figure 5.9 Histogram showing the single molecule distributions of FoxO1 in 90 untreated MCF7 cells with the mAb5939 + EP927Y antibody assay pairing. Compiled from 2 experiments and 90 cells.

The diagram in Figure 5.9 shows the basal distributions of 90 MCF7 single cells that exhibits the expected long tail and gamma distribution linked to gene noise. The theory going into these tests was MCF7 would show lowered activity and potential expression due to the dysregulation of the

PI3K pathway. Within these 3 basal MCF7 experiment repeats, only 85 cells were isolated across the 3 chips. This relatively small sample size was due to the larger size of MCF7 cells making them difficult to trap using optical methods. The results gave a mean single molecule count per cell calculated at 1491 ± 100, which interestingly was comparable to that seen with the Toledo cell line.



Cell Line	MCF7	Toledo
Cell Radius (µm)	9.5	5.5
Cell Volume (μm^3)	3591	697

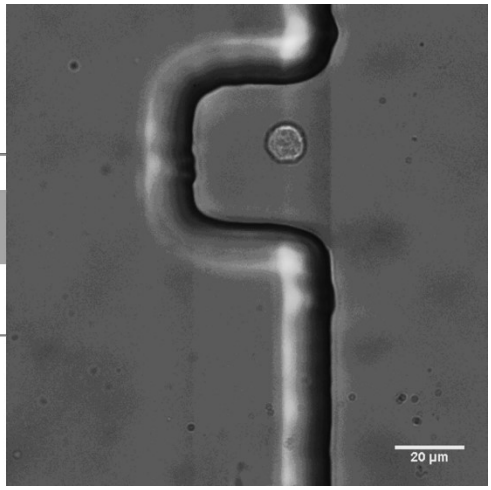


Figure 5.10 Images of MCF7 (left) and Toledo cells (right) in MAC chip chambers with a calibrated scale bar to show the differences in cell radius and diameter. The centred table shows the comparison of cell radius and the subsequent calculated volume, with MCF7 being over seven times higher in cell volume compared to the Toledo cell.

The diagrams in Figure 5.10 show that the radius and cellular volume differences of Toledo versus MCF7 cells are significant. MCF7s are about 7 times larger than Toledo cells and the fact the average copy number of FoxO1 is similar in both lines suggests that MCF7 cells have a lowered expression of FoxO1 with respect to cell size. Protein expression varies with cell size and therefore affects the cellular concentration of the protein of interest. Interestingly, one variable that is constant across all cell lines is the concentration of DNA (at least comparing all diploid cells) so it is important for transcription factor concentration to scale with cell volume to maintain their function.[205]

This explains that whilst the levels of FoxO1 look similar by mean count, if this was scaled by the cell volume, we would expect a higher FoxO1 copy number in the MCF7 cells. Therefore, the observed copy number seemed to corroborate well with the theory and gave an averaged basal level of FoxO1 to compare to subsequent manipulation tests.

5.5.2 ZSTK474 Treated Experiments with mAb5939 + EP927Y pair

The experiments described here, analysed MCF7 cells treated with ZSTK474 to observe if an increase in FoxO1 expression could be detected, utilising the mAb5939 assay. The experiments were run as described previously for the Toledo experiments, but instead analysing MCF7 cells. Despite the

mutation at the p110α subunit in MCF7 cells, ZSTK474 is a pan selective PI3K inhibitor and therefore should show a therapeutic response across all the PI3K subunits and show inactivation of the PI3K path .[204]

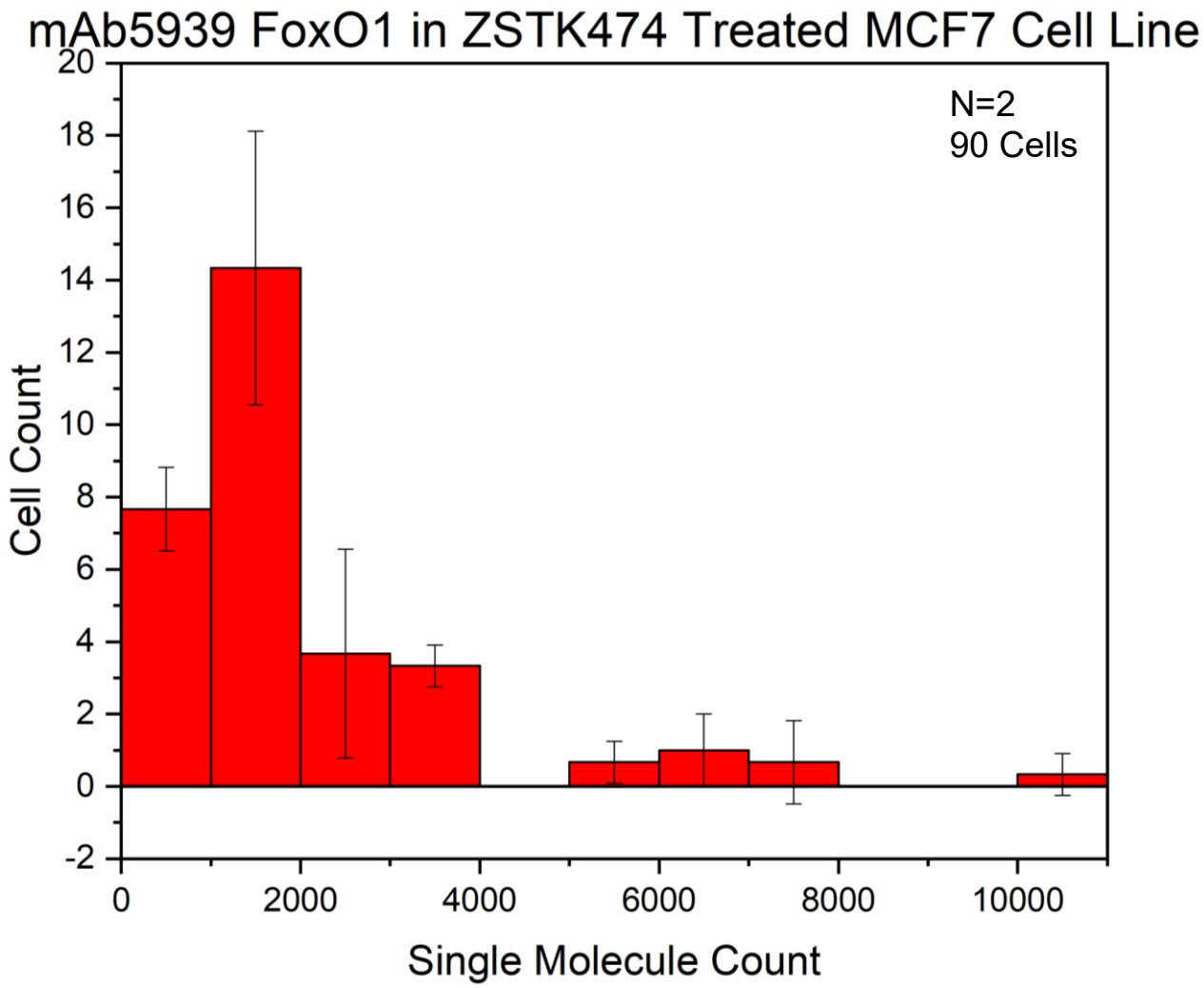


Figure 5.11 Assay validation test of mAb5939 using 95 MCF7 cells treated with 10 µM ZSTK474 showing the expected increase in total FoxO1 copy number. Compiled of 2 experiments and 90 single cells.

Interestingly, the results shown in Figure 5.11 show that ZSK474 treatment gave little increase in the levels of FoxO1. Also, Figure 5.11 shows an increase in the tail of the plot with a larger number of cells with high FoxO1 expression levels. This increase suggests that the treatment had less of an effect on the PI3K pathway in MCF7 cells compared to Toledo cells. The average single molecule count per cell was calculated to be 2030 ± 179, which was not a significant increase over the basal calculations. With more repeats, the results could potentially show a mean count closer to basal levels instead of showing an increase. However, due to time constraints and reagent constraints, it

was decided to run the glucose measurements instead of further ZSTK474 repeats to determine if a drop in FoxO1 could still be observed.

5.5.3 Glucose Treated Experiments with mAb5939 + EP927Y Pair

This section details the mAb5939 pairing tested on MCF7 cells that were treated with glucose. The same measures as used in the Toledo experiments were used to maintain consistency. A printing issue meant only 2 repeats were undertaken for both the ZSTK474 experiments and the glucose experiments.

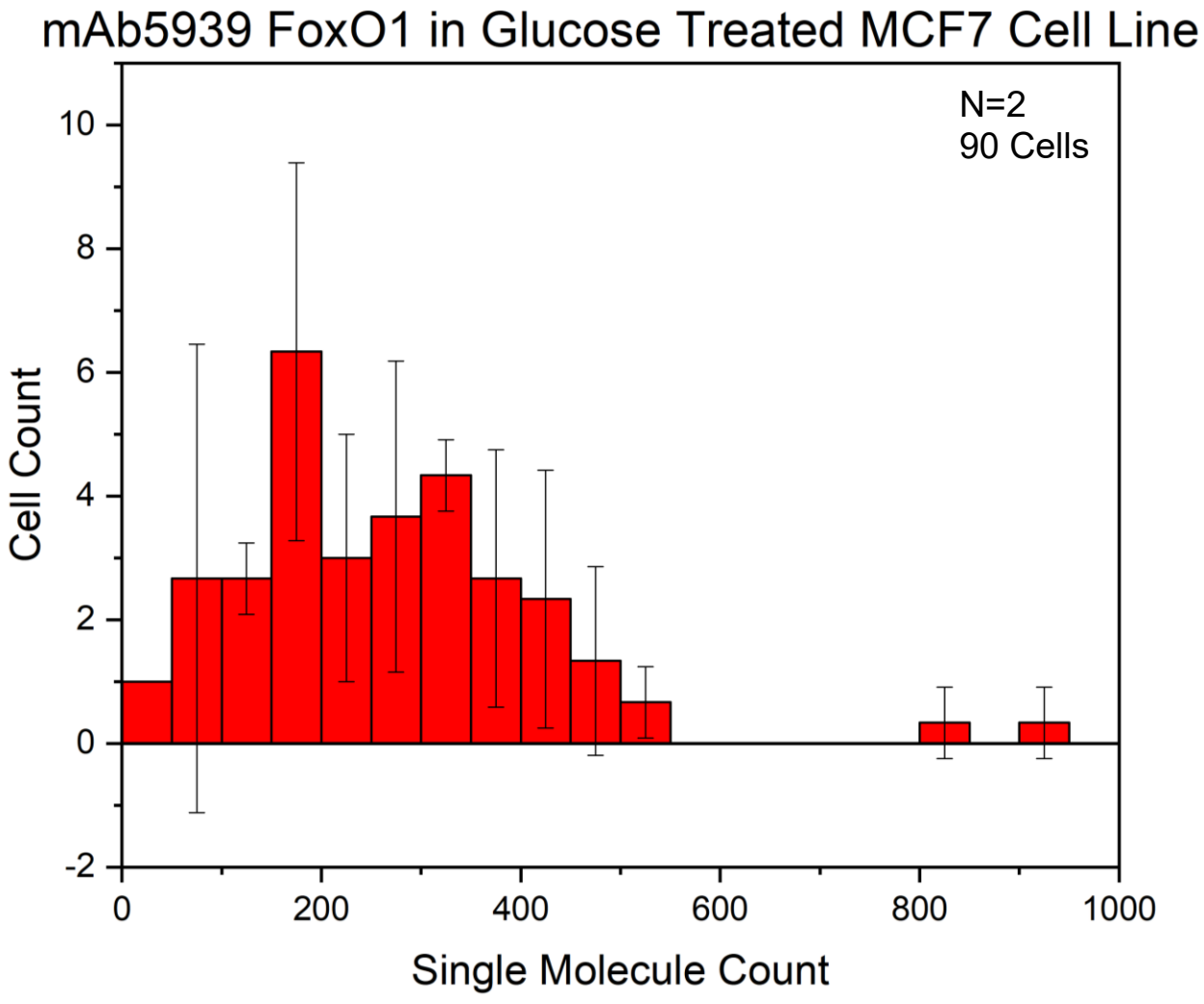


Figure 5.12 Assay validation test of Capture Agent 7 using 90 MCF7 cells treated with 20 mM glucose showing the expected decrease in total FoxO1 copy number. The mean single molecule count has still decreased under 3 times the basal expression level. Compiled of 2 experiments and 90 single cells.

As the PI3K pathway is overactivated in MCF7 cells, which in turn activates the Akt pathway, it was unclear whether it was possible to further inactivate FoxO1 expression through glucose treatment.

The final test to validate the antibody based total copy number FoxO1 was a success, showing a significant drop in the copy number of FoxO1. The average count per cell was calculated to be 230 ± 18, which was over 3 times lower than the basal expression. This drop was not as pronounced as the change observed with the Toledo cell line. Despite a less prominent drop, this experiment still showed the assay was in a functionally sensitive range. Even in an Akt dysregulated MCF7 cells which directly effects the levels of total FoxO1.

Given the dysregulation of the PI3K pathway in MCF7 cells, it is likely that the levels of active FoxO1 will be less effected by PI3K perturbations compared to other cell lines. Furthermore, given the secondary effects of the PI3K on FoxO1 activity it is likely the DNA based activity studies will show a less pronounced effect on copy number.

5.6 MCF7 Cell Line DNA Capture Agent 7 + EP927Y Studies

This section again uses the same MAC chip method to validate the Capture Agent 7 + EP927Y assay on MCF7 cells with the previously described perturbations. The PI3K pathway will affect the activity of FoxO1 via its downstream phosphorylation through Akt, thus the basal level of FoxO1 would likely be significantly lowered and consequently difficult to resolve. Despite the dynamic range of the DNA based assay being problematic to determine in the calibration attempts, it was hypothesised there would be a resolvable expression due to the importance of FoxO1 transcription

5.6.1 Capture Agent 7 + EP927Y pair Basal FoxO1 Distributions

The experiments described here, determined the basal distribution of active FoxO1 in MCF7 cells using the Capture Agent 7 assay. This was run using the MAC chip methods, with the DNA Capture Agent 7 printed in SCC:Betaine and the secondary EP927Y kept at a constant concentration of 0.25 µg/ml.

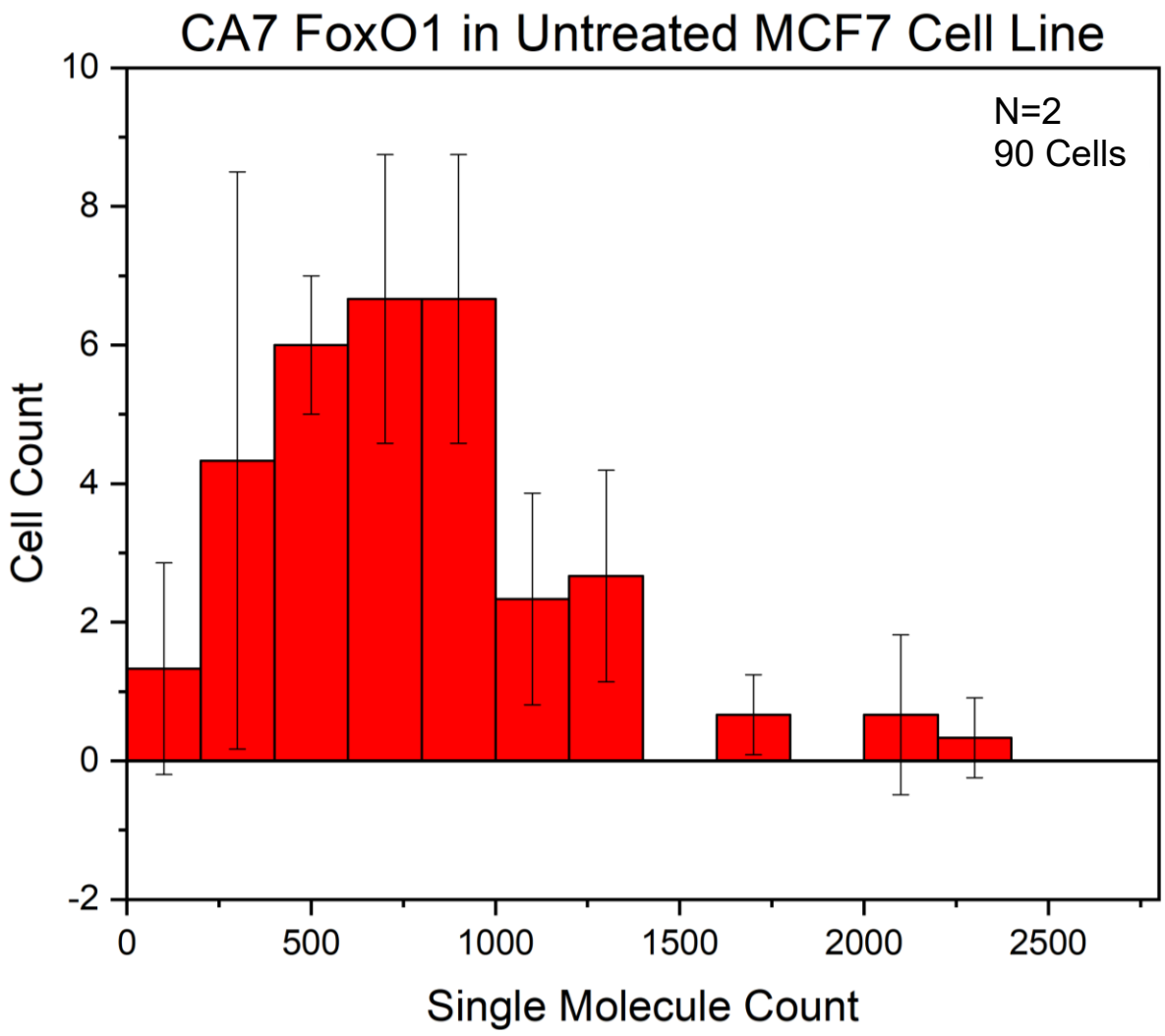


Figure 5.13 Assay validation test of CA7 using 90 untreated MCF7 cells showing the basal level of active FoxO1. Collected over 2 repeats and 90 single cells.

The results in Figure 5.13 show less of a right hand extending tail, although the plot still had a gamma distribution that suggests FoxO1 activity was still distinguishable in MCF7 cells. The average single molecule count was calculated to be 781 ± 43, which was close to half that was observed in the basal Toledo experiments. This drop in count was expected from the overactivation of the PI3K/Akt axis causing the phosphorylation and inactivation of FoxO1. This successful set of experiments promised that the assay could distinguish FoxO1 even at lower expression levels and the validation tests were continued.

5.6.2 PI3K Inhibitor ZSTK474 Treated Experiments with Capture Agent 7 + EP927Y pair

This section details the experiments run to test the ability of the Capture Agent 7 assay to distinguish increases in FoxO1 activity. Despite there being only a slight and potentially negligible increase in total FoxO1 in MCF7 cells, since the phosphorylation and inactivation is directly from the PI3K/Akt axis, treatment was likely to show a more significant increase in active FoxO1.

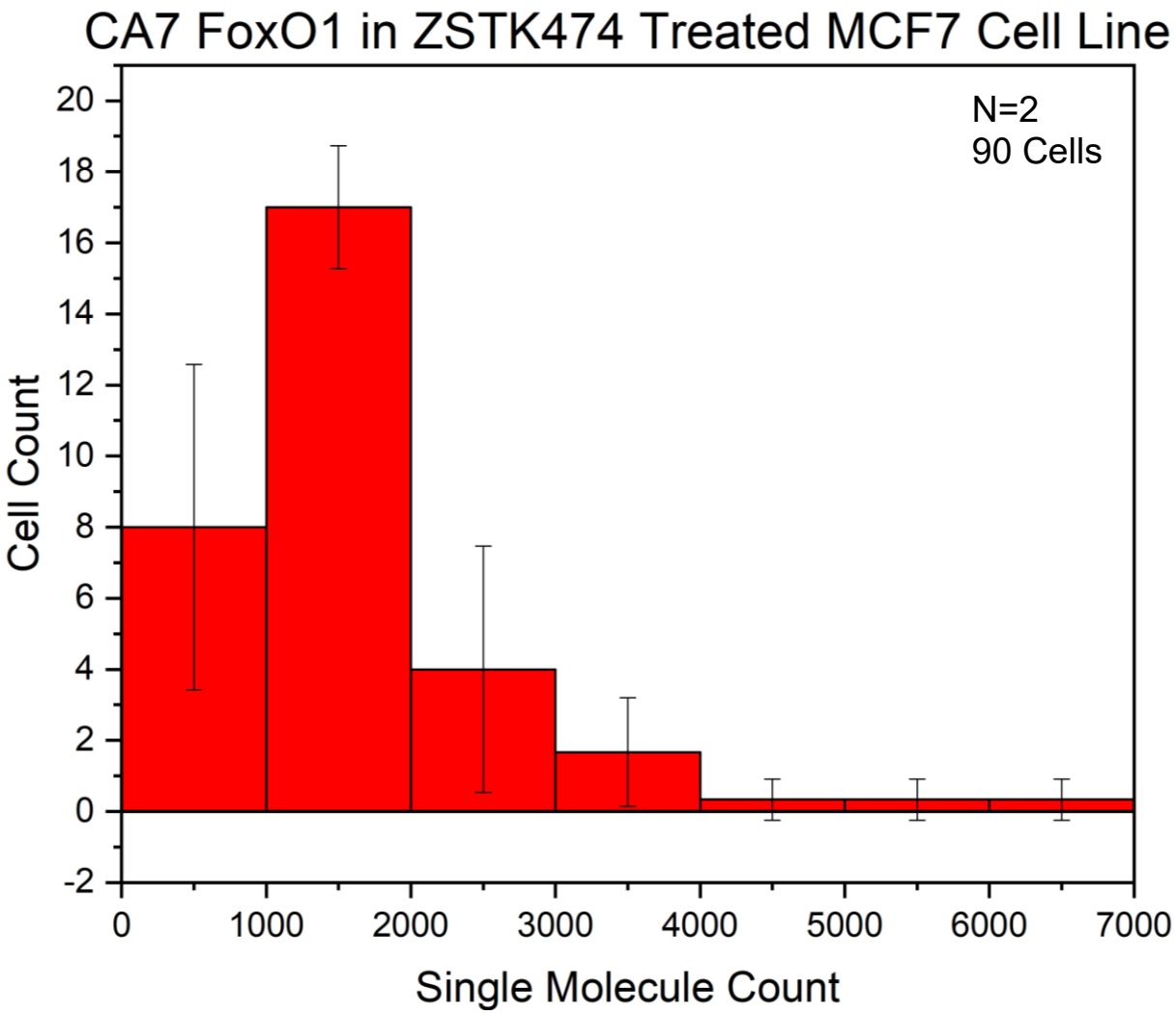


Figure 5.14 Assay validation test of CA7 using 90 MCF7 cells treated with 10 μM ZSTK474 showing the expected increase in total FoxO1 copy number. Collected over 2 repeats and 90 single cells.

The use of ZSTK474 has again seen the expected increase in FoxO1 where the mean has more than doubled from 781 to 2001 ± 161 showing the wanted increase in activity as seen in Figure 5.14. This result confirmed that Capture Agent 7 could detect increases in active FoxO1 copy number in the PI3K dysregulated MCF7 cell line.

5.6.3 Glucose Treated Experiments with Capture Agent 7 + EP927Y pair

This section details the experiments to validate the Capture Agent 7 assays ability to detect decreased levels of active FoxO1 in MCF7 cells. The use of glucose treatment was debated as to whether it would show an observable response on the Akt pathway in MCF7 cells, given the cell lines dysregulations. The reduction in total FoxO1 that was observed in Section 5.5.3, suggested that the response could still be observable, albeit less pronounced compared to the Toledo cell line.

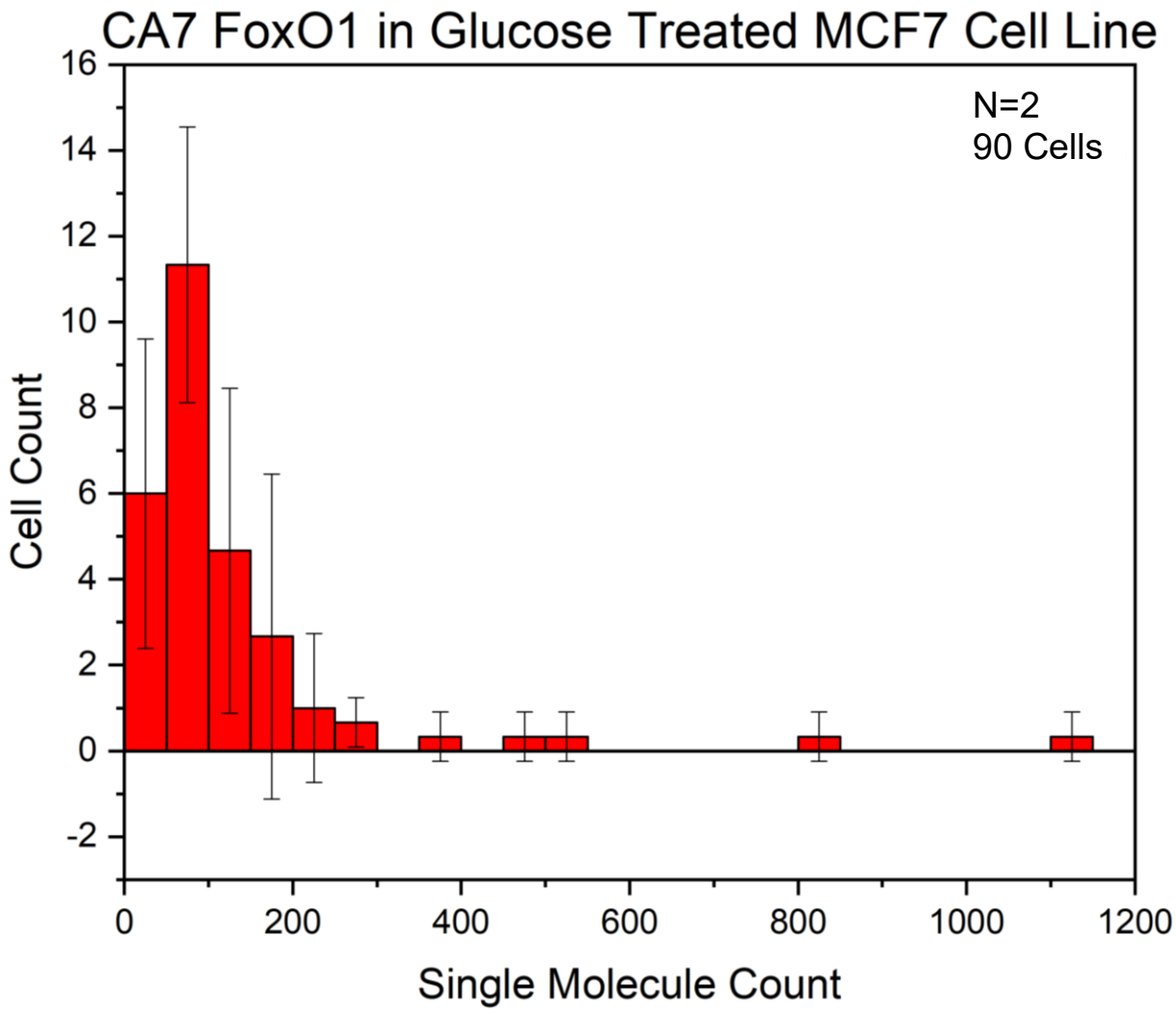


Figure 5.15 Assay validation test of Capture Agent 7 using 90 MCF7 cells treated with 20 mM glucose showing the expected decrease in total FoxO1 copy number. The mean single molecule count has still decreased under 3 times the basal expression level. Collected over 2 repeats and 90 single cells.

Interestingly, the observed FoxO1 reduction was pronounced, with a mean single molecule count of 112 ± 17, showing a 7 fold drop in copy number. This reduction suggests that even with Akt hyperactivation, the pathway is still responsive to external stimuli. Papers have demonstrated the increased proliferation of MCF7 cells in high glucose media (they used 25 mM rather than 20 mM).[206]

This corroborates well with the reduction in the cell-cycle inhibition and apoptotic responses that FoxO1 regulates.

Table 5.2 Summary of the mean and standard deviation of the MCF7 experiments using the mAb5939 and CA7 Capture Agents. The table shows there is clear separation between the different perturbation experiments.

	MAB5939			CA7		
BASAL	1491	±	100	781	±	43
ZSTK474	2030	±	179	2001	±	161
Glucose	230	±	18	112	±	17

This concludes the MCF7 validation experiments. Despite a lowered copy number observed for all assays, this was expected because of the mutations of PI3K. This observable FoxO1 count was a promising result for assay validation as it shows that even in dysregulated FoxO1 pathways there is: i) a detectable copy number, and ii) the ability to still observe changes in copy number. Even though in this project there was no scope to analyse cancer primary cells, the validation of the assay does open the door to later projects to analyse dysregulation of FoxO1 in a variety of cancers if desired.

5.7 Beas-2b Cell Line Validation Studies

The following sections deal with the validation of both assays (mAb5939 and CA7) on the Beas-2b cell line, which is arguably the most important line to validate. The overall objective of this project is to analyse and diagnose lung and respiratory samples for FoxO1 aberrations. Thus, an important cell type to validate is one derived from the lung.

Beas-2B is a human lung epithelial cell line that was SV40 T0-antigen immortalised. This immortalisation is preferred over Epstein-Barr Virus immortalization, as SV40 methods do not interact with FoxO1. This cell line is one of the most widely studied lung derived cell lines and is used widely for *in vitro* modelling of respiratory injury through to toxicology testing, with over 1200 publications referring to the use of Beas-2b cell studies.[207] Originally, Beas-2b cells were harvested from a cancer free human and isolated from their bronchial epithelium.[208] It is important to mention that the Beas-2B cell line is not terminally differentiated, meaning that under certain culture conditions, or if kept at confluence for extended periods, it can malignantly transform *in vitro* under different stress environments. To ensure the Beas-2bs did not terminally differentiate, their confluency was closely monitored. From measurements reported in the human protein atlas studies, the protein expression, aka copy number in bronchial tissues is one of the highest in comparison to other tissues.[181]

Beas-2b cells are not often used to study of FoxO1, there is extensive study of pathways known to interact with FoxO1, such as the JNK and Sirtuin1 (SIRT1) pathways.[74,112] Since Beas-2bs are isolated from a healthy human, it was assumed that Beas-2bs would make an optimal model for assay validation. This is the final cell line that was used for validating the assay, before conducting patient sample studies.

5.7.1 Initial Basal Beas-2b mAb5939 + EP927Y Experiments

As described previously, the first Beas-2b experiments were to analyse whether a sufficient signal could be detected by the assay in a sample of untreated Beas-2b cells. The Beas-2b cells were donated by Peter Barnes *et al*. The cells were cultured in Keratinocyte media supplemented with bovine pituitary extract. This is atypical from the suggested culture methods described by ATCC, where it is recommended to use Bronchial Epithelial Cell Growth Medium (BEGM). The collaborators work with Barnes et al. suggested the use of Keratinocyte media with bovine pituitary extract growth factors, because this has been shown to stimulate cell line proliferation *in vitro* and *in vivo*.[209] This stimulation is beneficial since the cell line is well reported to undergo squamous differentiation in response to different serums. Furthermore, the cells show enhanced glycolytic properties and enhanced respiration, all of which can negatively affect FoxO1 activity and copy number. Active FoxO1 is well reported to decrease the transcription of genes important for glycolysis.[58] Thus, the use of supplemented Keratinocyte media was expected to allow the continued proliferation of the cell line with minimal negative effects on FoxO1 expression.

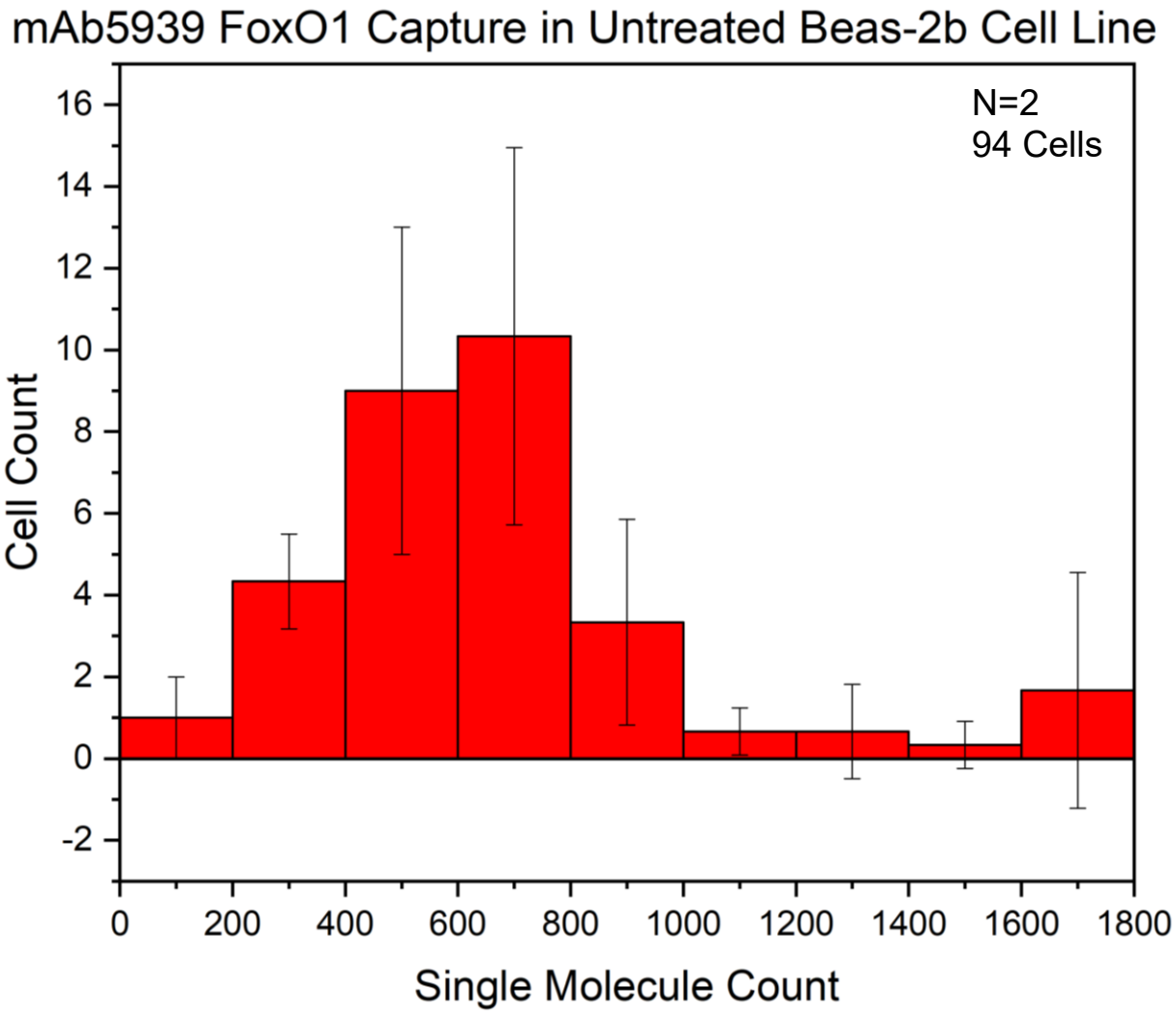


Figure 5.16 94 Untreated Beas-2b cells analysed in the standard MAC chip format with the mAb5939 + EP927Y showing a questionably lowered single molecule count for total FoxO1 compared to what was expected. Compiled over 3 repeats and 94 single cells.

The initial experiments using Beas-2b cells proved extremely challenging because of the extra steps for the cell culture. These steps included not just the use of a specific media but also the cells required a collagen coated flask for sufficient attachment. However, the attachment proved to be challenging with the cells still exhibiting a low level of attachment and multiple times the cells would show a significantly reduced growth rate. The general theory at this time was that there was a potential mycoplasma infection in the cell culture facilities which would explain all these issues. The cells did maintain their expected morphologies which is typically altered with mycoplasma infections. Cells were tested for mycoplasma using a Lonza Mycoalert test and came back negative for infection. This suggested that the issue with the cells was with their handling.

Eventually it was possible to obtain a 'viable' sample, which was when the cells seeded and reached 80% confluency. The cells were harvested before confluency to avoid their terminal squamous

differentiation. The results from these cell studies are shown in Figure 5.16. The calculated mean single molecule count per cell for these untreated cells was 677 ± 35. which compared to previous cell lines was a considerably weaker signal. The reported biology of Beas-2b cells does not have any characteristics to expect a lowered count of FoxO1 and therefore, this was a lower than expected count to obtain. It was at this time that the quality of the reagent pairs were questioned and placed under scrutiny, as like any bioreagent, these reagents can degrade and thus exhibit reduced affinity for their target analyte. In conclusion, the studies of untreated Beas-2b cells has given an unexpectedly lower single molecule count than expected. To further investigate this reduction in single molecule count, the glucose perturbation experiments were performed to observe if the reduction in FoxO1 could still be observed.

5.7.2 Glucose Treated Experiments with mAb5939 + EP927Y pair

Before any strong conclusions were made, it was decided to run the glucose treatment assay on the Beas-2b cell line to check if an expected decrease above background could be observed. Whilst Beas-2b cells can terminally differentiate under certain stimuli, there was no evidence at this time that high glucose concentrations would cause a terminal differentiation. In fact, some papers report the use of high glucose media for Beas-2b culturing. This should still be a suitable method for the inactivation and subsequent downregulation of FoxO1 in Beas-2b cells.

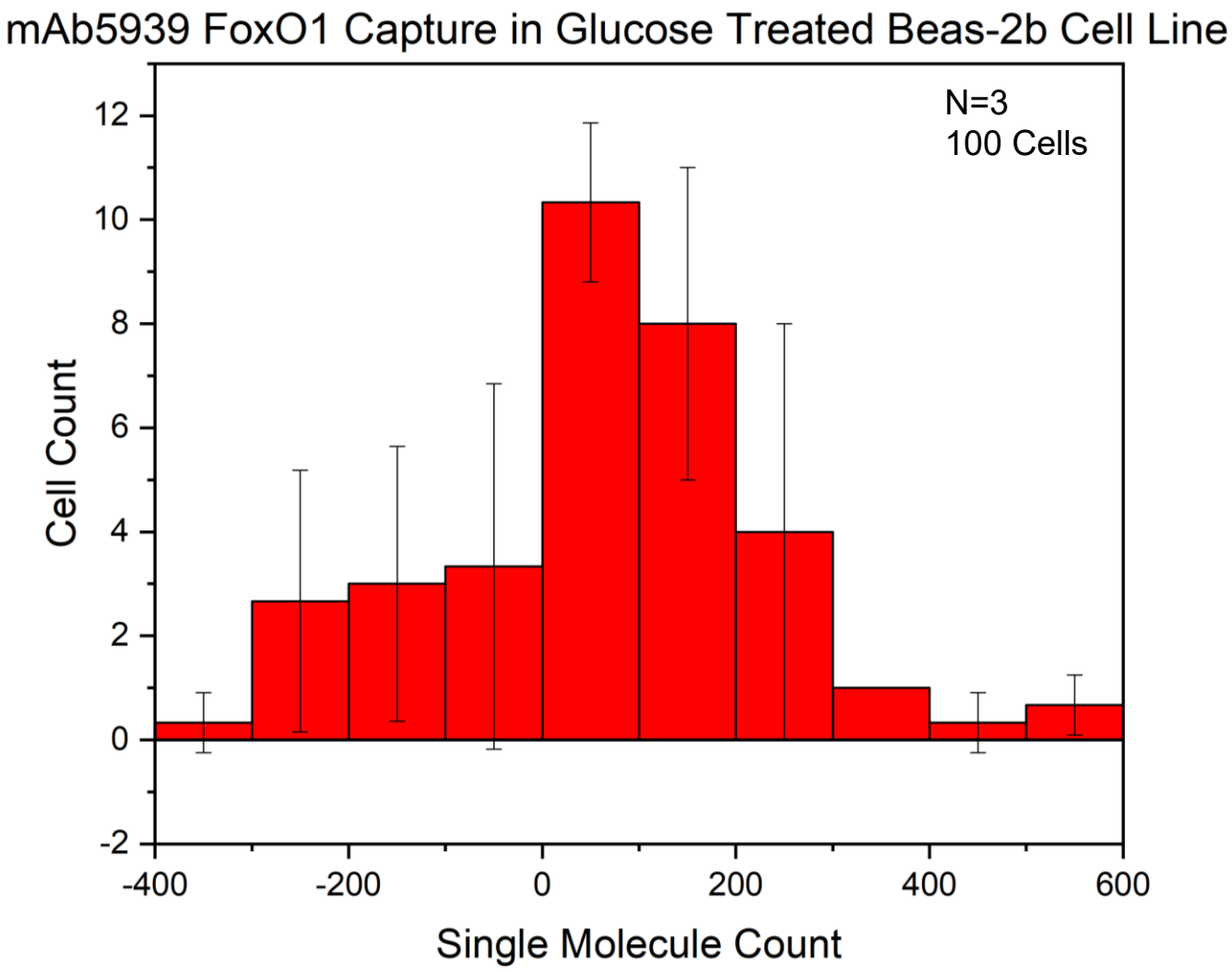


Figure 5.17 100 Beas-2b cells treated with 20 mM glucose over 3 MAC chip experiments, the results showed negligible, if any FoxO1 capture.

Under the same regime as used for the Toledo and MCF7 validation tests, the glucose MAC chip experiments proved to be irreproducible as it was typical to see several cells express FoxO1 at copy numbers below background. The graph in Figure 5.17 shows that over 3 repeats there were clear negative results, providing evidence that one reagent or component of the assay was no longer optimally working. The negative results show there was no binding above the background single molecule count. At this point it was decided to stop any further progress with mAb5939, since the assay reagents had spoiled and needed repurchasing.

5.7.3 Initial Basal Capture Agent 7 + EP927Y Pair Experiments

The following section details the experiments performed in order to test the DNA Capture Agent 7 assay on the Beas-2b cell line. Since the dual antibody assay needed new reagents, the DNA assay was tested in the meantime to check if FoxO1 binding could be observed.

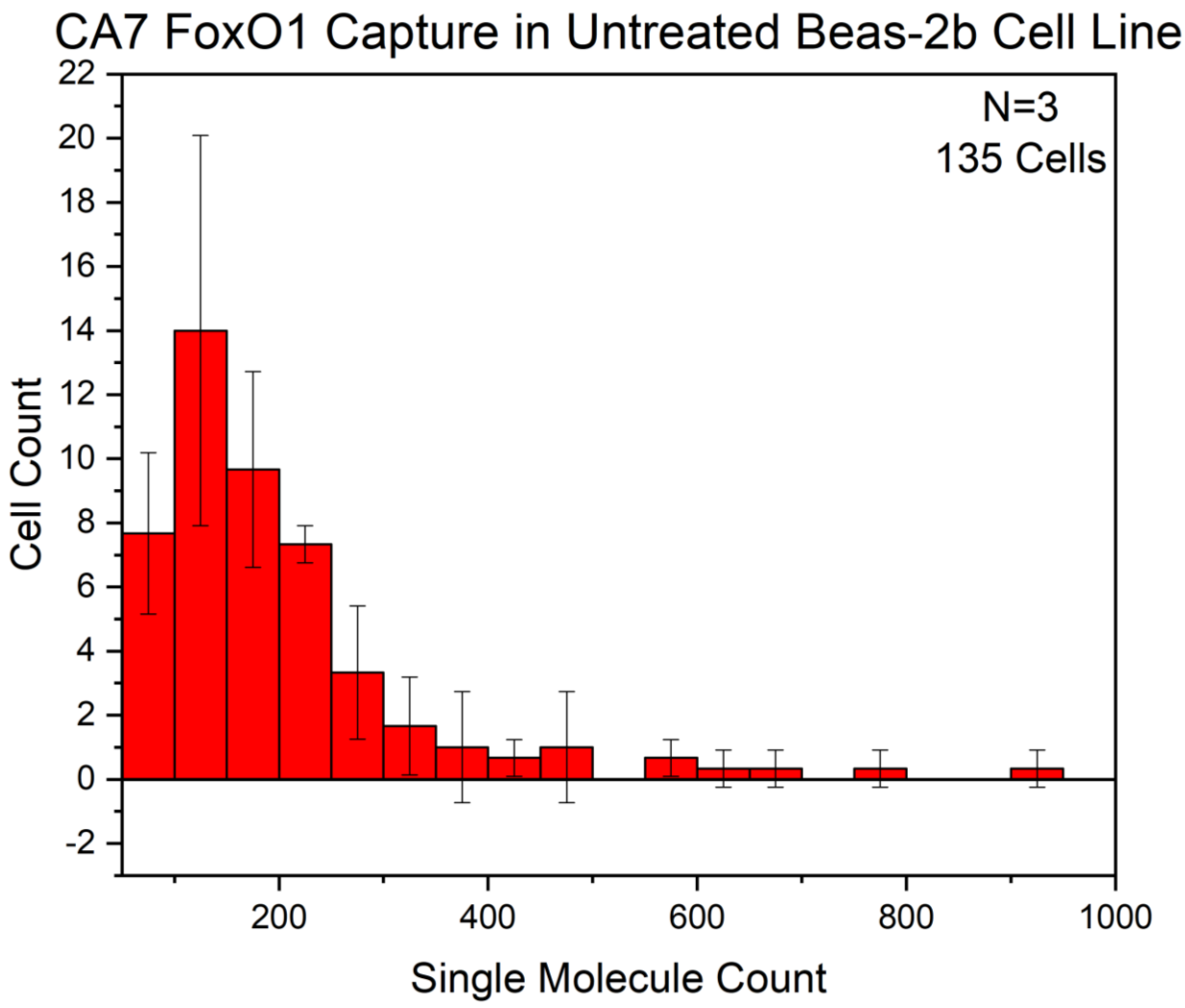


Figure 5.18 135 Untreated Beas-2b cells analysed in the standard MAC chip format over 3 experiments with the Capture Agent 7 + EP927Y showing a questionably lowered single molecule count for active FoxO1 compared to what was expected.

As seen in the previous cell validation studies, the apparent K_D of the DNA assay is higher than that of the antibody assay. A similar single molecule count is observed in these experiments compared to the antibody measurements despite the DNA assay studying a subpopulation, showing that there is a drop in mAb5939 affinity. The average single molecule count of this assay calculated at 194 ± 11 counts per cell which is near three times lower than the total FoxO1 assay. This lowered count again suggested that both the antibody and DNA assays were both not working optimally. To further test this theory, the glucose experiment was run as described in the next section.

5.7.4 Glucose Treated Experiments with Capture Agent 7 + EP927Y pair

The experiment detailed here was performed to investigate where the DNA assay was still able to detect a reduced level of FoxO1 in the Beas-2b cell line. Despite the assay being unlikely to successfully detect active FoxO1 given the low basal level observed, it was still necessary to run the glucose experiment to test the theory. The experiments were run in the same fashion as the mAb5939 experiments.

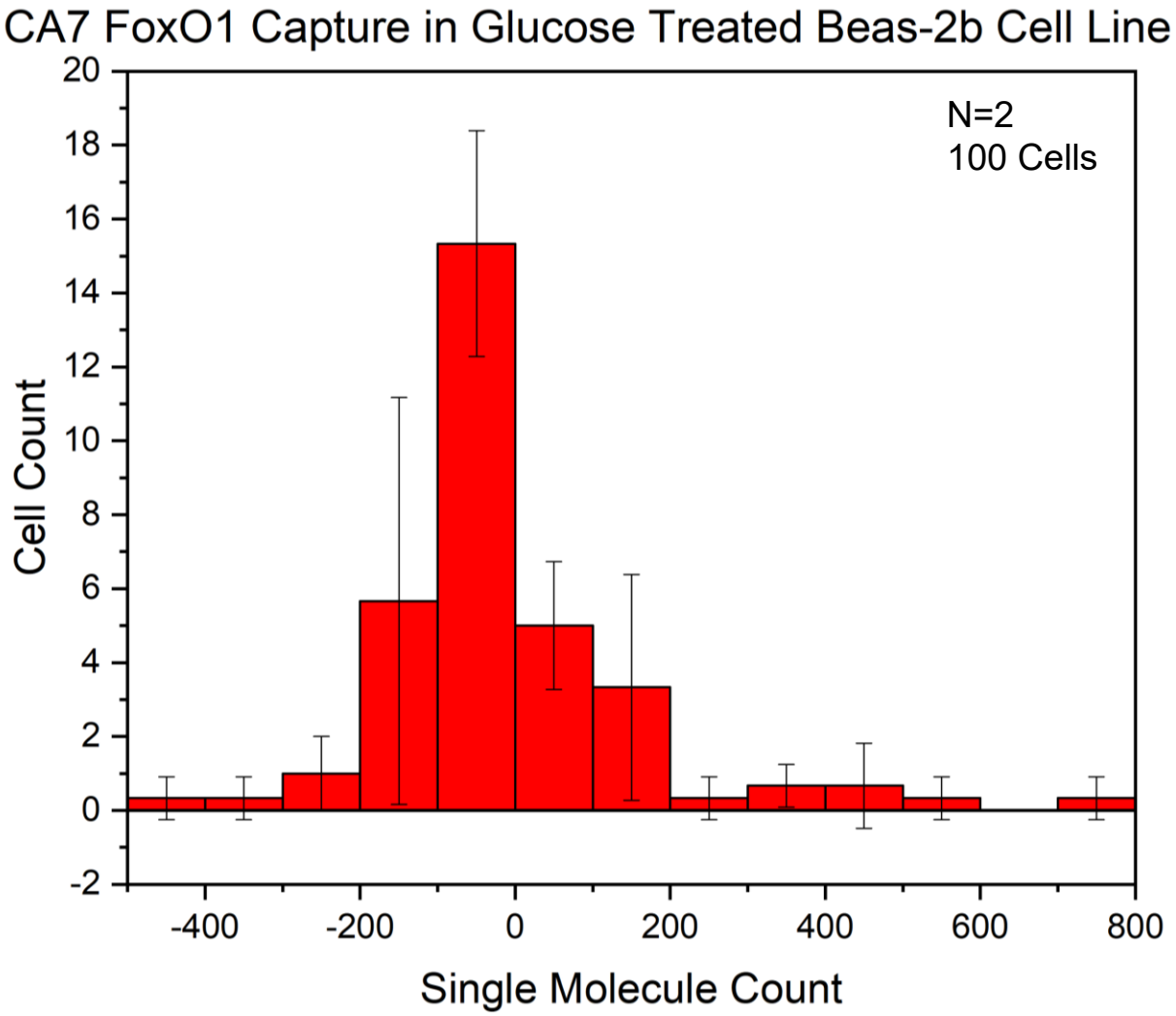


Figure 5.19 100 Beas-2b cells treated with 20 mM glucose over 2 MAC chip experiments and 100 cells, the results showed negligible, if any FoxO1 capture.

Similar to the mAb5939 Beas-2b validation experiments, the glucose treatment has caused a shift in active FoxO1 to below the limit of detection of the assay. Figure 5.19 shows that after background subtractions, the assay has obtained a negative result which shows that the assay was unable to detect active FoxO1 in this cell line.

The reason for this negative result was that the assay simply lacks the resolution to observe the low FoxO1 copy number in the Beas-2b cell line. This is evidenced with the reduced copy number seen from basal counts. The biology of Beas-2b cells does not suggest they should have lower levels of FoxO1 and because the experiments showed a reduced level of both total and active FoxO1, it suggested the assays themselves likely have issues. Both assays showed lowered FoxO1 which shows the same trend. This correlation could be interpreted to mean that the assays are both functional, but they lack the affinity required to accurately detect the apparently lowered copy numbers of FoxO1 in Beas-2b cells.

Table 5.3 Summary of the mean and standard deviation of the Beas-2b experiments using the mAb5939 and CA7 Capture Agents. The table shows the assay was unable to distinguish between an untreated and glucose treated state and even gave negative readings in the CA7 glucose experiments.

	MAB5939			**CA7**		
BASAL	677	±	35	194	±	11
Glucose	97	±	82	-13	±	56

In conclusion, Section 5.7 shows that validation was not achieved for the Beas-2b cell line with both assays. Both the antibody and DNA based assays did not have a sufficient limit of detection to observe changes in FoxO1 copy number when it was lowered with glucose treatment. To understand whether this lack of detection was from the assay or the Beas-2b cell line, the assays were investigated further. This investigation is discussed in the next section.

5.8 Discussion of Total and Active FoxO1 Cell Assay Validations

The previous sections of this chapter describe developing two distinct MAC chip single cell assays for both active and total FoxO1 levels. The chapter details the use of two methods to perturb the levels of FoxO1. The first method was glucose treatment, which upregulates Akt activity that subsequently inactivates and degrades FoxO1 downstream. The second validation method was the use of ZSTK474, which inactivates PI3K and subsequently inhibits the downregulation of FoxO1 to increase FoxO1 activity and copy number. These perturbation methods were then compared to untreated, basal levels of FoxO1 in the cell lines to show the assays abilities to observe phenotypic shifts of FoxO1. While both assays use the same fluorescent secondary antibody, EP927Y, each assay uses different capture methods for monitoring total and active FoxO1. The antibody mAb5939 is able to capture total FoxO1 levels by binding to an unperturbed epitope of FoxO1. This total FoxO1 assay was successfully developed and validated against the Toledo and MCF7 cell lines before the assay lost binding efficiency for FoxO1 in the lung epithelial derived Beas-2b cell line. The assay was then tested again with the Toledo cell line, where it was concluded the assays had degraded and could no

longer reliably observe phenotypic shifts in FoxO1. This process was then continued with the CA7 active FoxO1 assay.

The most likely reasons for the drop in efficiency in the biological assays at this time was from the reagents degrading, as antibodies and other biological reagents are well known to have short shelf lives.[210,211] This chapter and the previous chapter detail the importance of reagent quality, not only in affinity (K_D) but also in the proper handling of said reagents. While this chapter ends with the complications of the assay to detect both total and active FoxO1 in Beas-2b cells, it also shows that it could observe, with high reproducibility and accuracy, alterations in the copy numbers of FoxO1. As there has been no attempt to optimise the assay conditions and reagents before the loss of detection, the next plan of action was to list the potential reagents that have degraded and replace and optimise their concentrations and formulations.

6 Assay Optimisation and Troubleshooting

6.1 Outline

This chapter details the troubleshooting undertaken to try and rectify the loss of binding and sensitivity observed previously in Chapter 5. The work involved analysis of several reagents and pieces of equipment being replaced or tested one by one to observe whether replacing or refining them would bring the assays back to a functional level that was able to observe perturbations in FoxO1 total and active copy number.

Table 6.2 details the list of tested reagents and processes and shows that most had no observable effect on repairing the assay. This process required a step by step analysis of each factor and covered replacing the antibodies and DNA capture agents through to using a different printing pin head to try and isolate the problematic factor. While there were slight improvements to the assay, it was still not sufficient to fully repair the assays.

The final sections in this chapter detail altering the concentrations of the antibodies and DNA reagents, which showed that increasing the concentrations of the secondary antibody, EP927Y, was successful in bringing the assay back to a functional state. The work did also show there was an increase in the level of background binding though this was not an issue as the background subtraction still provided a positive copy number for the basal, glucose and ZSTK474 treatments.

6.2 Introduction

The following chapter will outline the optimisation and troubleshooting strategies of the mAb5939 and Capture Agent 7 + EP927Y assays. This chapter looks at the assays principle components, details their necessity within the MAC chip system and whether the replacement and optimisation of these components helped to improve the assays limits of detection.

Both assays could not detect FoxO1 copy number in the glucose treated Beas-2b cell line, the most relevant cell line for the end goal of analysing patient respiratory samples. These assays were investigated further to determine if the assays had degraded, or if it was simply that the assays had an insufficient limit of detection for the Beas-2b cell line. It was reasoned that reanalysing the Toledo cell line would be a conclusive method to determine if the assays were working at less than optimal conditions. The Toledo cell line was used as it was the easiest to handle and culture and gave the most robust data sets and best resolutions seen for both the mAb5939 and CA7 assays. The first step

was to repeat the experiments with the Toledo cell line in the MAC chip format using the same conditions as previously described (Section 5.3) These experiments will allow us to determine if there was a deterioration in assay reliability or whether Beas-2b cells had a reduced level of FoxO1 than expected.

The results from the repeat experiments on the Toledo cell line are shown in the histograms in Figure 6.1. It is apparent from the histograms that the basal distribution of total FoxO1 and active FoxO1 in Toledo cells are lower compared to the Section 5.3 experiments. For the mAb5939 + EP927Y assay in Figure 6.1, the observed mean single molecule count is 286, which is over a 5-fold drop from the single molecule count of 1515 observed from the previous validation studies (Figure 5.3). This result highlights a significant reduction in the efficiency of the total FoxO1 assay. The same reduction in efficiency was seen with the Capture Agent 7 + EP927Y assay, with a calculated mean of 555 single molecule counts, which is almost a 3-fold drop from the initial validation studies of 1528 single molecule counts seen in Figure 5.6. Both of these results provide evidence that the lower level of binding observed in the Beas-2b experiments is likely to have occurred from the degradation of the reagents used.

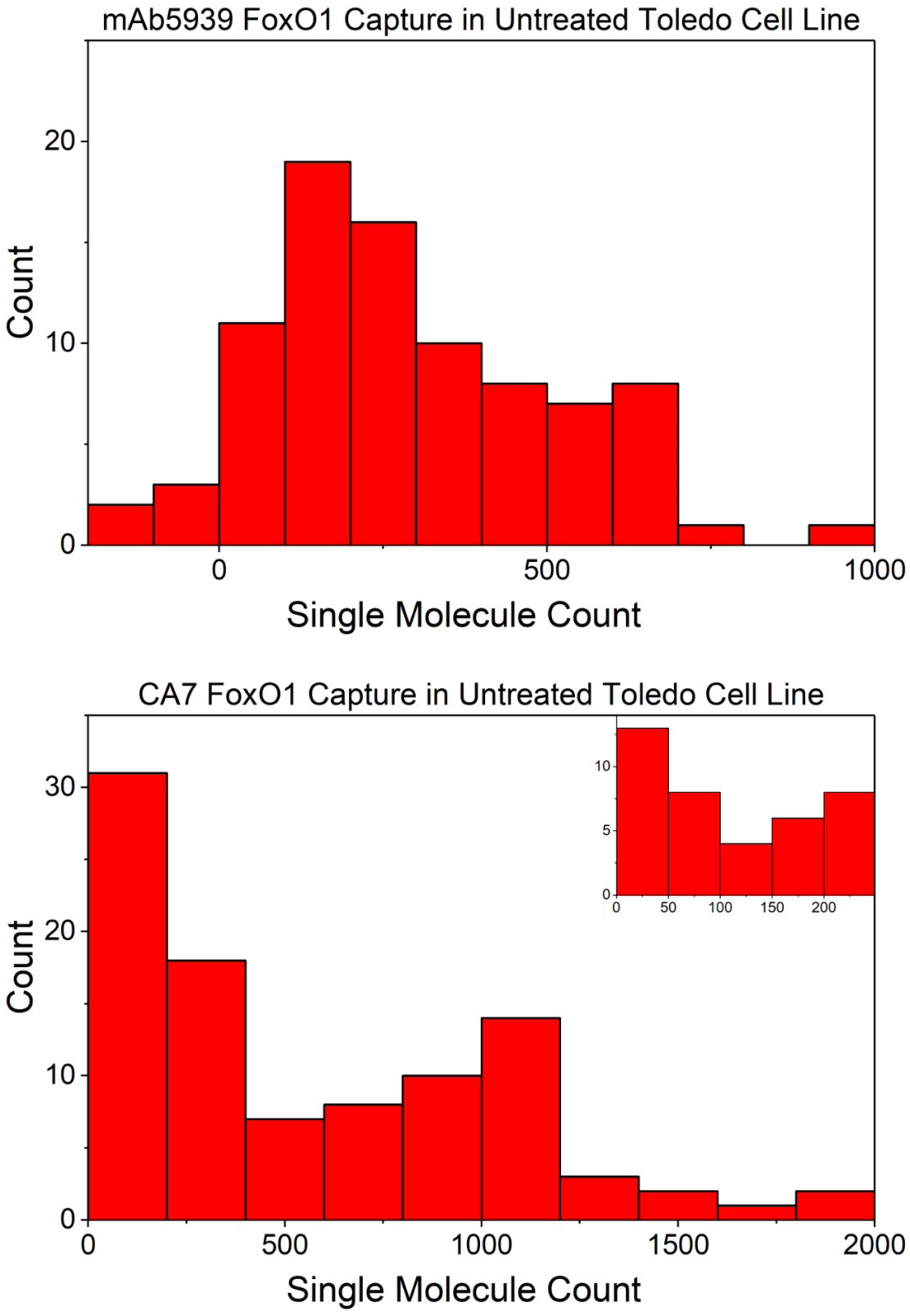


Figure 6.1 Combined histogram plots showing the distribution of total and active FoxO1 shown in each plot respectively. The top plot shows 86 Toledo cells with a significantly lowered basal total FoxO1 single molecule distribution compared to that observed in previous experiments using mAb5939 capture. The bottom shows 95 Toledo cells with a lowered basal active FoxO1 distribution with respect to previous Toledo experiments using Capture Agent 7 (CA7) DNA capture.

A major issue faced with many biological reagents is their stability and their propensity to degrade. As previously mentioned, antibodies are a protein, and thus heavily rely on complex folding mechanisms and a plethora of non-covalent interactions to maintain optimal function. Most companies will recommend a shelf life of 6–12 months for any antibody and the shelf life will vary whether the antibody is in a dry format, what buffering agents are used and what temperature it is stored at. As mentioned in previous sections, every antibody used is kept in aliquots to avoid repeat freeze thaw cycles and are stored at -20 °C unless otherwise specified. This ensures that the reagents last as long as possible. Along with optimal storage of the antibodies the same level of attention is kept with the oligonucleotides. As previously mentioned, upon delivery the oligos are annealed and subsequently aliquoted at 100 µM to ensure they are immediately ready for printing when necessary. Oligonucleotides are well understood to have an improved stability compared to that of antibodies, although they still have a shelf life which typically lies in the range of 12-24 months.

From the experiments seen in Figure 6.1, it appeared that a reagent or several reagents had degraded, thus leading to the observed reduction in FoxO1 affinity. Interestingly, in these experiments it is shown that the dual antibody assay resulted in a more significant drop in efficiency compared to the DNA + Antibody assay. This suggests that the use of DNA as a Capture Agent is seemingly more stable than its antibody counterparts. Since the reduction in efficiency is seen in both assays, the most likely degraded reagent was the secondary detection antibody EP927Y because this is present in both assays. Furthermore, this reagent was the most handled.

To test whether the issue was with the secondary antibody, the stock of EP927Y was repurchased from the same batch number. The same batch number is important because it will remove as much variation as possible. The new batch was handled in the same way as before with the hope the assay would show a similar level of sensitivity as seen previously.

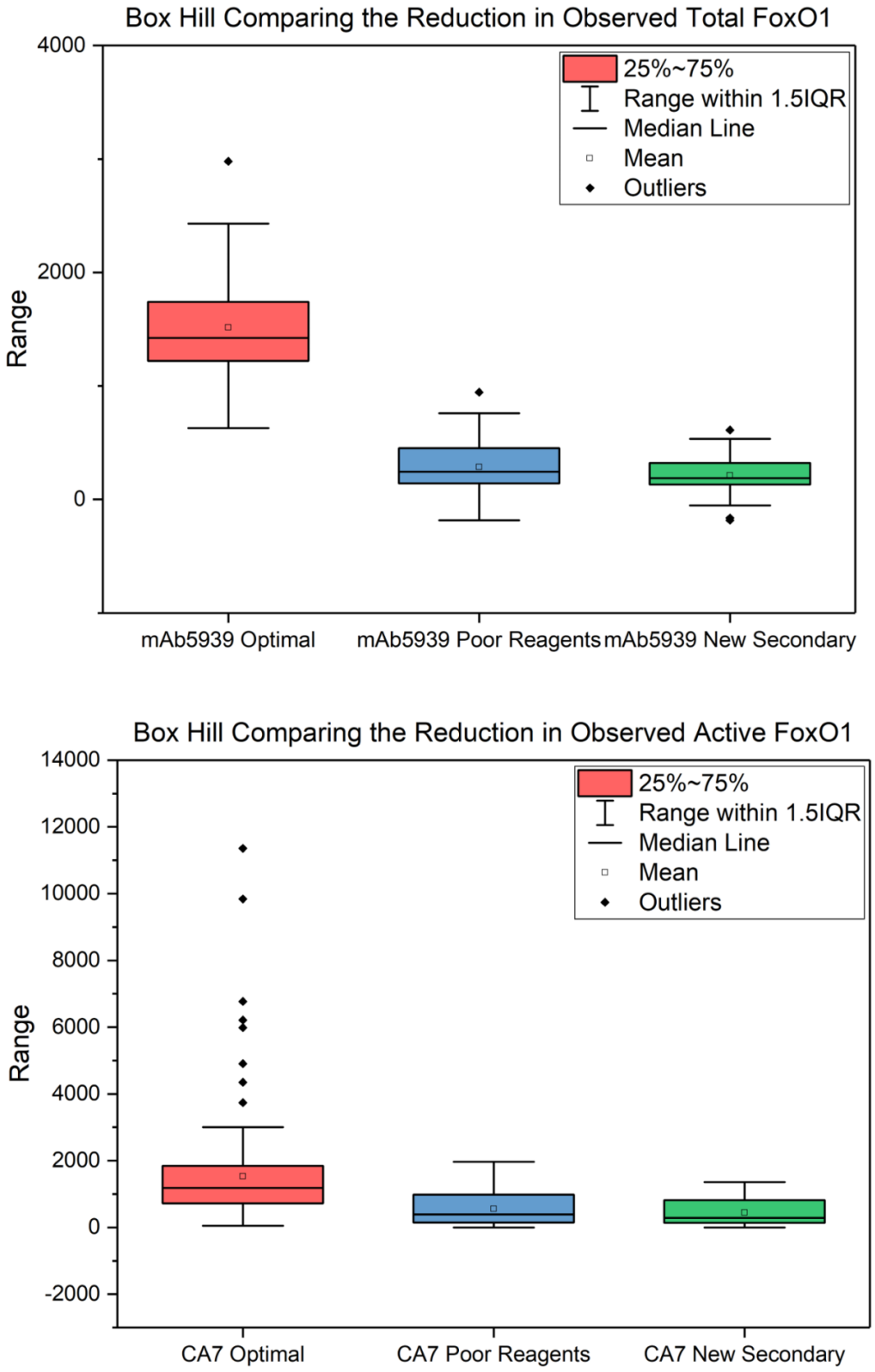


Figure 6.2 Box Hill plots demonstrating that the restock of EP927Y was unsuccessful in recovering the optimal single molecule distribution of FoxO1 in both assays using Toledo cells, the top shows the drop in the mAb5939 antibody total FoxO1 with the bottom showing the drop in the CA7 active FoxO1 assay.

The box hill plots shown in Figure 6.2 demonstrate the drop in the assay efficiencies from the validation experiments in red, the Section 1 testing of the same reagents on Toledo cell lines in blue and the testing of the new EP927Y secondary antibody in green. While the initial tests of the new secondary included only two repeats, testing 90 and 95 Toledo cells (mAb5939 and CA7 respectively), it was sufficient to confirm that the assays had degraded. The results showed no level of improvement and both the total and active assays showed a mean which more closely overlapped with the plots seen in Section 1. This was a significant set-back to the project since it meant that there were underlying issues with the robustness of the assays. The next stage was to conduct a further investigation to the reason for this reduction in the assay affinity.

Repurchasing new 'fresh' secondary EP927Y antibody did not improve the assay, therefore the other reagents were tested to bring the assay back to its optimal functionality. The most distinct decrease in binding was present in the mAb5939 + EP927Y pair, suggesting that it was possible both antibodies had degraded over time. For DNA capture, there was no marked improvement, but the observed decrease was less pronounced than that of the dual antibody assay. Therefore, to bring the assay back to full working order it was determined that all the reagents used in both assays should be repurchased.

The new reagents were then tested in the MAC method with no alterations to the concentrations or methodology. These experiments were repeated in duplicate for both the mAb5939 and Capture Agent 7 + EP927Y assays, but neither showed any improvement in the assays sensitivity. The means of both assays were like those observed in the assays referred to in Figure 6.2. This posed a potential issue for the future of the assay as it showed there was a significant problem with the robustness of the assay. However, before this point, the reproducibility of the assay was highly consistent providing results that were readily comparable.

6.3 Analysis of Assay Reagents

This section details the analysis and replacement of most reagents used in the fabrication and running of the MAC chip experiments. The end goal of these experiments was to bring the assay back to a fully working and reproducible level so that experiments on patient-derived samples could commence.

The method to fix the assay seemingly proved not to be as simple as restocking the capture and detection reagents. Therefore, there was a clear need to understand and review the other possibilities of why both the assays had reduced in affinity. The full methodology for the fabrication

through to the method for the MAC chip system is detailed in Section 0. It is apparent from this that there are many reagents which could have perished. Several key reagents are briefly analysed and a qualitative detail on their results is mentioned in this section. The quantified results are not detailed in this section, because it is deemed unnecessary to show multiple plots of unsuccessful experiments.

In the PEGylation steps, there are no biological agents used until the final step of the process which involves the treating of the slides with Neutravidin®. Neutravidin® is used for the biopassivation of the slides[153], and allows the biotinylated DNA to bind to the surface for an oriented immobilisation. If the neutravidin that was used had degraded, it is reasonable to predict that the experiments would show a higher level of nonspecific background binding. However, this predicted increase in background binding was not observed in the previous experiments. Despite this lack of extra background binding, the neutravidin reagents were replaced anyway. A more detailed look into the background binding is described later in Section 6.4. The replacement of Neutravidin alone did not improve the assays affinity in Toledo experiments, thus the next reagents were explored.

The next process in chronological order of the experiments, was the printing steps for depositing the antibody or DNA Capture Agents to the functionalised slides. Printing involves the use of printing buffer (3 x SCC with 1.5 M betaine), which is made up in large quantities (1 mL to 5 mL) and is typically used over multiple experiments. Traditionally, 5 µL is used per 4 experiments and so this buffer reagent is rarely replenished. The use of printing buffers is important for a variety of reasons; one of the most important being the production of consistent spots with a desirable morphology.[141] Buffer degradation affects the reproducibility and efficiency of the assays. The replacement of the buffer made no noticeable improvement on the assay. Nevertheless, the new batch was used in future assay optimisation processes.

The next potential issue considered was the use of the contact pin for the deposition of the Capture Agent. The 946MP2 pin, which is widely used with the OmniGrid Micro microarrayer system, provides a constant volume of 0.5 nL per spot and an optimal spot morphology and diameter for the MAC chip chambers. The disadvantage of this method is that the pins are extremely delicate and thus require very delicate handling and careful cleaning processes to ensure they are kept at an optimal quality. Even a small force on the pinhead is enough to deform the pinhead and disrupt the printing morphology. The pinhead quality can be monitored by observation under a 10x objective, and from inspection the pin used for this work was in good condition with no clear deformation present. Despite there being no observable physical deformations, the pin surface chemistry can

also be damaged. Issues with the pin surface chemistry can lead to issues with surface tension properties required for reliable robust printing. Therefore, a colleague's pin was borrowed to ascertain whether the issue was indeed with the pin.

The use of a different pin did not afford any increase in FoxO1 capture for either assay. The only noticeable difference observed was the spot morphology had a slight alteration with the new pin, which likely implied there was a deformation in the new pin rather than the pin previously used. To further validate that the original pin was suitable for use, it was used to print the optimal MAC chip assay for p53.[33] These experiments resulted in a level of p53 binding comparable to that seen in previously published data.[20,33,35,118,183]

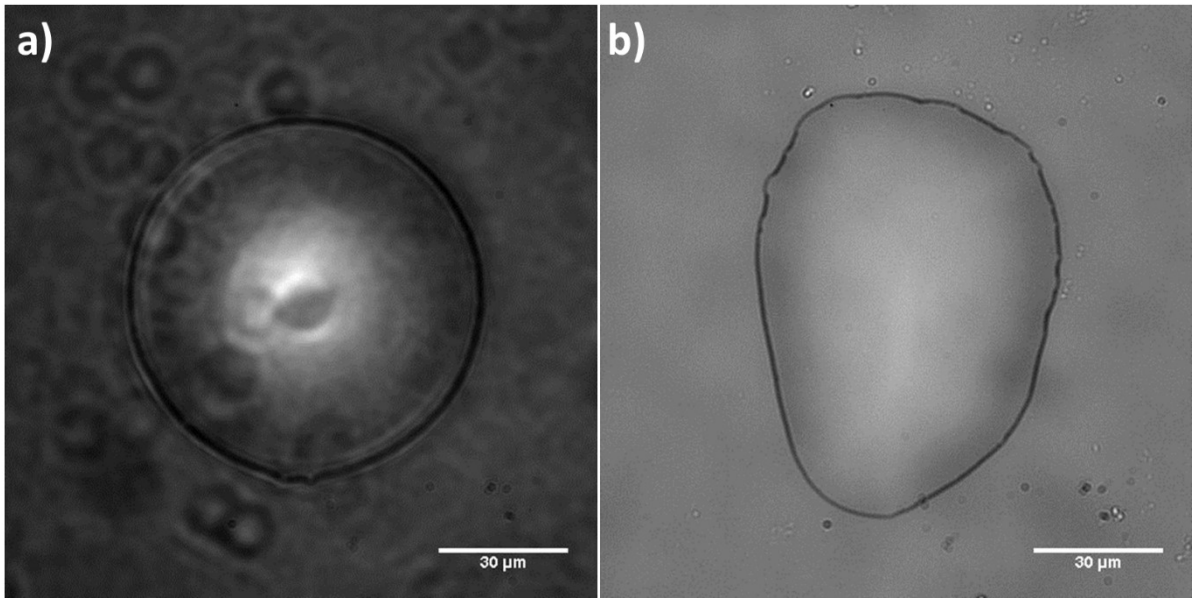


Figure 6.3 A comparison of the printing quality for the different pins used. a) shows the original pin and b) shows the print from a colleague's pin. Both are DNA Capture Agent 7 prints using the same SCC: Betaine printing buffer and the same DNA concentration. Both have a similar print area with spot b) having a slightly more elliptical shape which would slightly increase the total area.

Before use, the secondary antibody was diluted to the desired concentration in a 4% BSA in PBS solution. This solution allows for further surface passivation from the BSA and is incorporated as solution used for adding the secondary antibody to the MAC chip to determine background single molecule count. BSA is widely used in assay protocols as a blocking agent because it will bind to nonspecific binding sites in the sample, and thus increases the chance of the specific antibody-antigen interaction occurring.[212] Consequently, this blocking of non-specific binding will decrease the background noise of the assay and provide a higher signal to noise ratio. BSA is a small, stable and moderately unreactive protein which is stored lyophilized until use, but it is possible that it degraded over time. BSA replacement showed no improvement in the assay affinity.

Dulbecco's phosphate buffered saline (DPBS) is a commonly used solution in biological research as it is isotonic and non-toxic to most cell lines. Even though it was not thought to be the cause of the assays problems, it was also replaced. As expected, the replacement showed no benefit to the assays. A quick experiment was run using a DPBS solution with no calcium or magnesium (previous experiments were run with DPBS supplemented with these ions). This alteration was to test whether the ions were potentially affecting the DNA based assay, as calcium and magnesium are known to affect the physiological environment. Thus these metal ions can be crucial to modulate the catalytic activity of certain proteins and interactions.[213,214] DPBS is supplemented with 4% BSA and is used for the secondary antibody solution. However, it potentially influences the immobilised DNA Capture Agents and could therefore explain the drop in affinity seen in the assays. DPBS replacement did not show any improvements on the capture of FoxO1 in either assay.

One of the most pivotal components of the MAC chip is the microfluidic architecture, which is used to create the individual chambers required to isolate the cells for analysis. A key factor which influences the high dynamic range and high sensitivities required for accurate single cell proteomics is total chamber volume. A small chamber volume helps to create an increased effective concentration of analytes and Capture Agents, which helps to push the equilibrium towards the bound form and thus improves the limit of detection. Another benefit of utilizing microfluidic volumes is the reduction in diffusion time for the binding of the analytes reaching equilibrium.[35] During these experiments, the same architecture was used but the wafer had to be replaced due to typical wear and tear, which is commonplace for any lab utilizing microfluidic techniques. The replaced wafers were all fabricated in the same method as detailed in Section 2.2. The fabrication method provides the exact same architecture in the x and y directions but the z-direction, while still accurate to within several microns. In theory, over time there can be alteration of the z-direction dimensions altering the total chamber volume, which would therefore alter the LOD. This theory was harder to test since the wafers used in older experiments (such as those for the initial Toledo experiments detailed in Section 5.3) were no longer available. Conveniently, there were spare, pre-made MAC chips from the old wafer which had not been used. This meant two more experiments could be run with the previously mentioned replaced to see if the issue was with the current wafer. Similar to the other replacements discussed, the use of the original wafer offered no improvements to the assay.

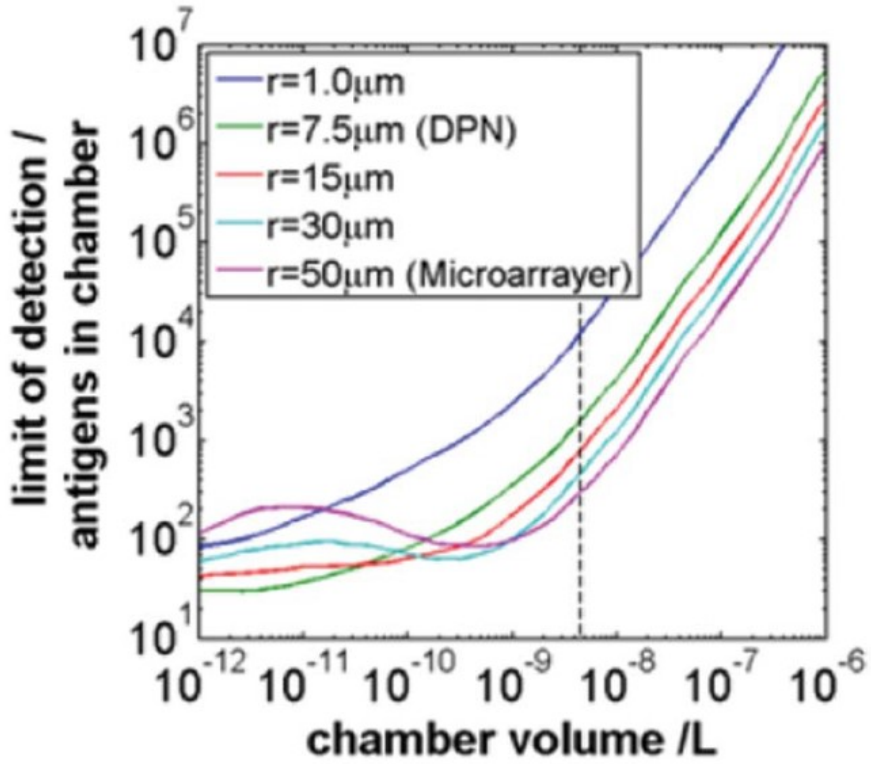


Figure 6.4 Figure taken from Salehi-Reyhani et al.[35] *and shows how the LOD will vary as a function of chamber volume for a range of spot radii. Results are shown for an antibody pair of 1 nM affinity. The vertical dashed line in each figure highlights the 4.5 nL volume of the MAC chamber, which is the same chamber volume as used in these experiments. The data sets for this point are irrelevant but show the alterations in the radius of the printed spot which also has effects on the total capture possible and thus LOD.*

Figure 6.4 used with permission of Salehi-Reyhani et al, shows that with increasing in chamber volume, there is a corresponding decrease in the LOD. This work was performed with the p53 assay which had a documented affinity for the capture and detection agents. As mentioned previously, the actual K_D values for Capture Agent 7 and mAb5939 are unknown. However, the secondary antibody (EP927Y) has a documented K_D of 0.31 nM (from Biacore measurements by Alastair Magness), which is comparable to the p53 assays affinity, and thus a similar trend should be observed.

The experiments detailed in this section, cover a majority of what could have been the cause of the assays failures on the assay side. Since no improvements were made with the replacement of these reagents the next step was to think of factors 'off chip'. This led to the theory that the cells themselves might be under stress. The cells were always kept below high passage numbers, were handled with the utmost care and not allowed to reach confluency. Moreover, the cells were always incubated with the correct media and only when treated with ZSTK474 were they exposed to DMSO, which is known to cause cellular stress. The levels of DMSO were kept at 0.1% v/v with respect to the media, and control studies were run using Toledo cells with pure DMSO at 0.5% which showed

no effect on the FoxO1 copy number, which is also well documented in the wider literature. One uncontrollable factor was that the incubator used was communal and there is a chance that mycoplasma could contaminate the cell line. Due to mycoplasmas small size they are hard to avoid as they are able to pass through many common anti-bacterial filters. These mycoplasma infections have a range of different effects on a cell line. On top of the range of effects, the effects are not constant and will vary depending on; cell line, mycoplasma species, culturing conditions among many other factors.

Mycoplasma tests were performed using the bespoke Lonza MycoAlert™ Mycoplasma Detection Kit [Lonza, Switzerland] with the given methodology to test the media samples of not only the Toledo cells used in these experiments but also the media of the other cultures present in the communal incubator. While the results did test negative for mycoplasma in the Toledo cell line there was an infection present in the media of a colleagues MCF7 culture, suggesting there was a slight chance of cross contamination. As mentioned in the methods, the cells were cultured in vented flasks to prevent contamination as best as possible, however, mycoplasma is so small many strains can potentially pass through the vents.

To test whether mycoplasma was causing the aberrant results in the assays, a frozen stock of Toledo cells was resuscitated that was known to be mycoplasma free. Also, the culture was resuscitated in a different cell culture facility known to have had no recent mycoplasma infections. Furthermore, new media was purchased so there was no chance of passing on potentially mycoplasma contaminated media to the new cells. The same MAC experiments were run as before and no increase in binding events was observed. This section has detailed the replacement of the majority of reagents and conditions in the system. Extensive work had gone into trying to find the culprit reagent or tool which was causing this sudden and inexplicable loss in the assays functionality. While reagent quality is well documented to play a pivotal role in an assays quality, it was not expected to cause such a significant drop in the assays sensitivity to decommission it. The next section details the analysis of the concentrations of the reagents to try and repair the assay issues.

6.4 Effects of the Reagent Concentrations on Assay Sensitivity

The experiments detailed in Section 6.3, shows an extensive review of the replenishment of most, if not all the assay reagents. None of the replacements were sufficient to bring the assay back to a working condition, and so further alteration experiments were designed to try and bring the assay back to its original working order. This section details the alterations in concentrations of the assay

reagents in an attempt to improve the assays LOD. The main goal was to bring the assay back to its original working order, though as detailed here it did not get back to full working order but restored to a functional condition. The key factor to restoring the assay was discovered to be increasing the concentration of secondary antibody. The experiments in this section were run using the typical MAC chip conditions with alterations to the detailed reagent.

6.4.1 Increasing the Concentration of Printed Capture Agent 7

Firstly, experiments were performed with higher concentrations of printed DNA CA7 to try and increase the capture efficiency of FoxO1. CA7 is usually printed at a final concentration of 50 μM, which is a commonly used concentration in many microarray assays. The literature states that DNA assays can be printed at a range of concentrations, from 20 μM to the highest concentration reported to be at 100 μM.[7] From this literature, no higher than double the original concentration of CA7 was printed, because increasing the concentration any further than this would likely show no improvement in capture efficiency.

The first experiments run used 0.1 to 100 μM fluorescein annealed CA7 printed in an open chip format. The fluorescein tag provides a way to measure the total spot intensity that can be subsequently correlated to a single molecule count. This method allows us to observe if there was an increased concentration of CA7 attached to the slide. The range of concentrations was chosen because even though a high concentration should help improve the binding kinetics, too high of a concentration might cause steric hinderances by blocking the capture agent to FoxO1 interaction and consequently hinder and reduce binding events. These experiments consisted of loading open chips with 4% BSA in PBS (pH 7.4) and then the total fluorescent intensity was measured. The observed fluorescent intensity corresponded to the amount of DNA Capture Agent that was printed to the slide.

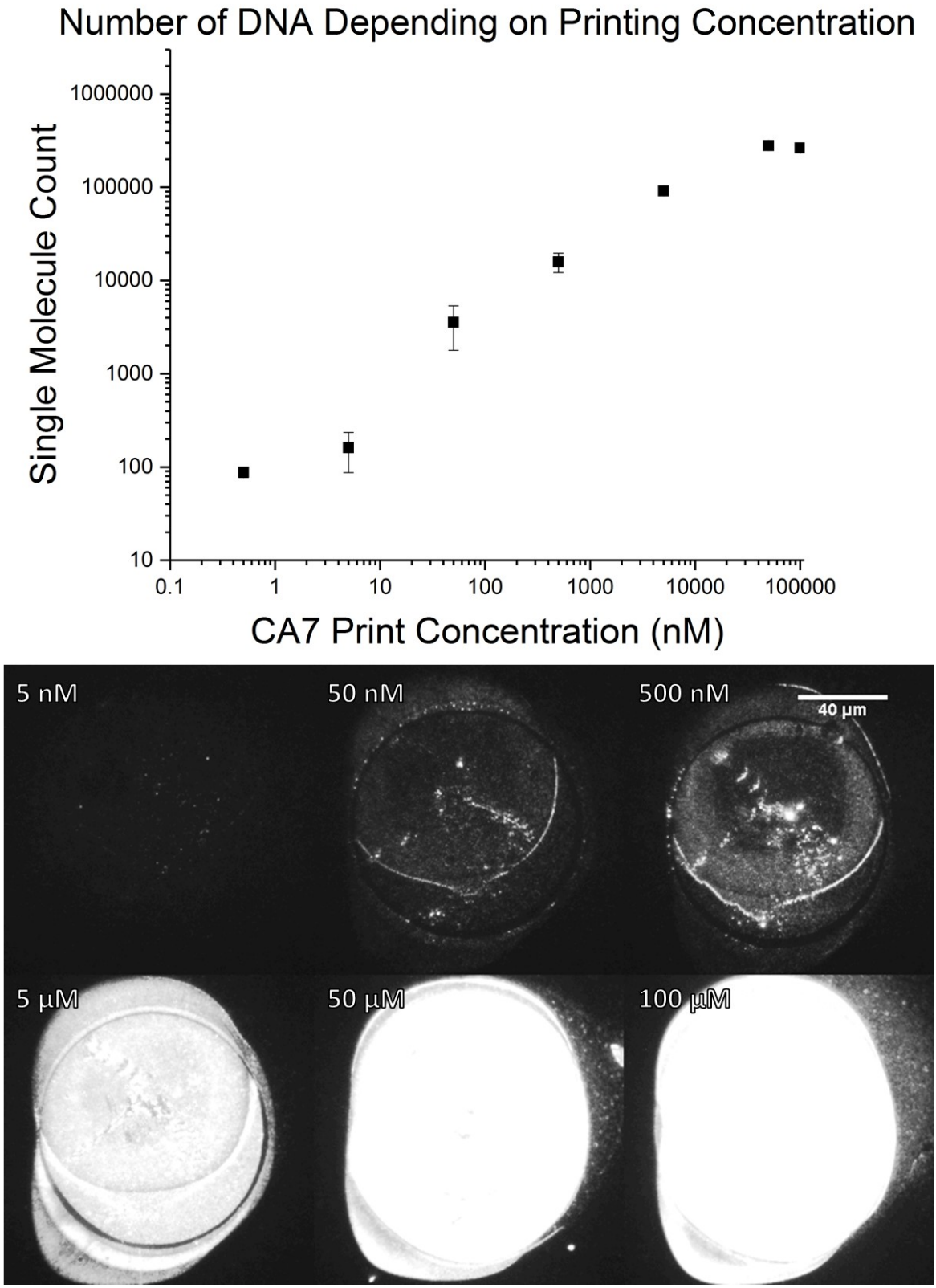


Figure 6.5 A plot showing the effect of DNA printing concentration on the single molecule count of DNA tethered to the surface. The bottom figure shows the images of the spots at the varying concentrations showing that between 50 µM and 100 µM the spot seems to be saturated.

The results of the experiments are shown in Figure 6.5, which shows that the increase in CA7 printing concentration shows a near linear increase in the amount of fluorescent CA7 present on the spot. This near linear increase continues until 50 µM and at 100 µM it plateaus. This plateau shows that the spot is at saturation and therefore increasing the print concentration to 100 µM is unnecessary as it does not provide a marked increase in the level of CA7 present on the spot. Furthermore, this experiment showed that any print concentration below 0.05 µM (50 nM) was insufficient to coat the spot with Capture Agent.

Standard MAC chip experiments were run with Toledo cells on slides printed with the concentrations ranging from 500 nM through to the 100 µM (despite the belief being 100 µM would show no change in binding). These experiments were performed to test whether steric hindrances from a high concentration DNA print density was lowering the level of binding. As tightly packed DNA might block the successful interactions between the consensus sequence and the active domain of FoxO1. Each of these experiments did not show any repair to the assay.

In conclusion, it was found that a linear response was observed until 50 µM, at which point the spot appeared to saturate with DNA. This printing concentration series tested in the MAC chip assay against Toledo cells, which proved unsuccessful in reinstating the assays previous success.

6.4.2 Increasing the Concentration of Printed mAb5939

The next step was to alter the concentration of printed mAb5939 in an attempt to repair the binding efficiency within the antibody based assay. The usual printing concentration used was 0.5mg/mL and was purchased at 1 mg/mL which is the highest concentration it can be purchased at. As the antibody needs to be mixed 1:1 with the 1.5x SCC: 3M Betaine printing buffer the assay already utilises the maximum concentration available.

Unlike the experiments on CA7 detailed in Section 6.4.2, the antibody needed to be fluorescently tagged in house. As detailed in Section 4.4.1, the use of conjugation kits are not suitable for MAC chip experiments. Since conjugation techniques were inaccurate, mAb5939 studies detailed here started with printing various concentrations of mAb5939 for use as the Capture Agent in experiments measuring Toledo cells. The mAb5939 antibody was sequentially diluted to provide a series of printed concentrations of 0.5, 0.25, 0.125 and 0.0625 mg/mL. No concentrations higher than 0.5 mg/mL were tested as the antibody would have to be concentrated, which is known to affect the stability and quality of the antibody. All other variables in the MAC chip experiments were kept constant. None of the experiments showed any binding improvement (including the originally

used concentration of 0.5 mg/mL). This work found the optimal concentration to be 0.5 mg/mL for total spot saturation via non-specific adsorption. These experiments showed that alterations in the Capture Agent concentrations seemed to have no positive effect on the binding efficiency of the assays. Whilst a larger range of concentrations and potentially higher concentrations of DNA and antibody could have been used, it was deemed unnecessary given the observed trends from these experiments.

6.4.3 Increasing the Concentration of Secondary EP927Y in the Capture Agent 7 Assay

The next step after testing the Capture Agents was to test the effects of secondary antibody concentration. The secondary antibody is a crucial reagent to optimise, because alterations in its concentrations have several effects. At a kinetic level, the increase in free secondary antibody present will drive the equilibrium towards a higher level of binding of the target antigen. However, since the secondary antibody is fluorescently tagged, it is also the major source of background count and therefore is the major factor impeding a suitable SNR. As the secondary is the key contributor to impeding the SNR it is important to optimise the concentration. The secondary antibody is considered a key factor in assay efficiency, because unlike the Capture Agent it is free in solution and thus has larger freedom of movement to enable binding of the target analyte.

To test the effect of secondary antibody concentration on the assay, the first experiments were to observe concentration alterations effects on background counts. The experiments detailed throughout this thesis have all been background subtracted and little information has been provided as to the background counts observed. The background counts for the DNA based (CA7 + EP927Y) and antibody based assays (mAb5939 + EP927Y) do vary from each other due to the antibody-secondary antibody interaction being more prevalent than that of Capture Agent DNA – secondary antibody. Despite there being differences in the background counts for both assays, the increase in secondary EP927Y concertation still provided a reproducible background count.

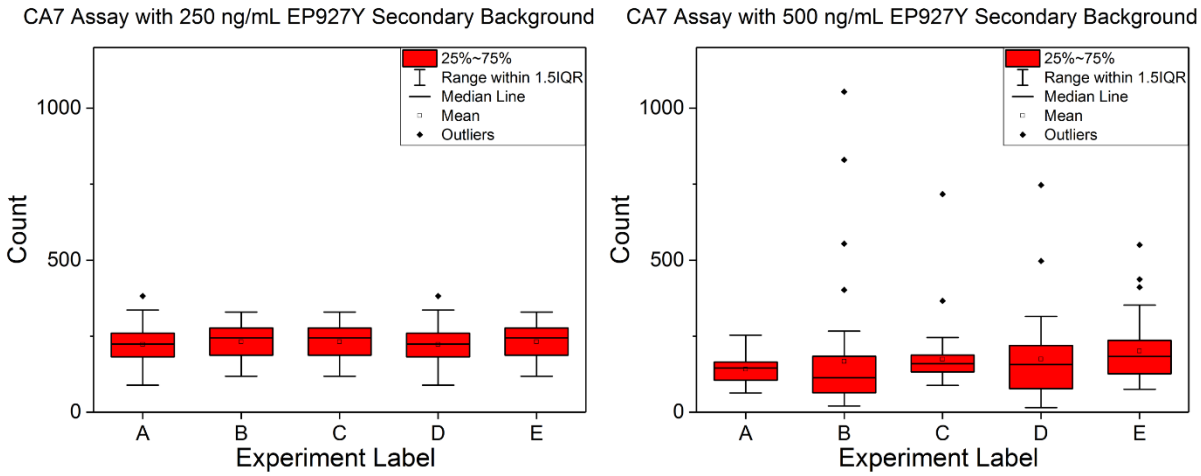


Figure 6.6 A comparison of a random selection of experiments from across the assay validation experiments, the left plot shows the observed background binding seen with a 250 ng/mL concentration of EP927Y secondary antibody and its consistency across multiple experiments. The right plot shows the effect of a twofold increase in the secondary concentration which shows a similar mean but a higher incidence of outliers.

The first analysis undertaken in this section was to analyse the effects on background binding from increased concentration of secondary antibody in the Capture Agent 7 assay. This was a simple comparison to make as background binding counts are taken for every assay run to provide background subtraction in the analysis. The comparison is shown above in Figure 6.6, and shows that there is a high level of consistency in the observed background binding levels with a 250 ng/mL secondary concentration. Also, this consistency is still present when the concentration of secondary is increased to 500 ng/mL. While a manageable background is still obtained with the secondary increase, there is an increase in the frequency of outliers that have a markedly larger background count. The outliers are not considered an issue, as they are easy to distinguish by eye and these high background binding spots can be omitted for single cell analysis. The outliers usually arise from the spot being damaged during handling and chip fabrication steps. The damage might also come from accidental contact of the spot or simply dust embedding onto the spot causing extra binding.

To provide the best comparison to the initial assay conditions, these concentration experiments were then run through the MAC chip protocol to analyse samples of Toledo cells. ZSTK474 and glucose perturbation studies were also performed to determine if the assay was still able to distinguish alterations in FoxO1 activity. The graph shown in Figure 6.7 shows the results from these experiments and shows the successful expected perturbation results. The most striking observation is that the observed single molecule count for all the assays is markedly lower compared to the original assays before they fell into disrepair. The mean basal single molecule count average has gone from 1528 to 340, which is a near 5 times reduction compared to the previously working assay

conditions. This reduction is unwanted, but the assays and repeats still showed consistent results and single molecule counts above the background were obtained.

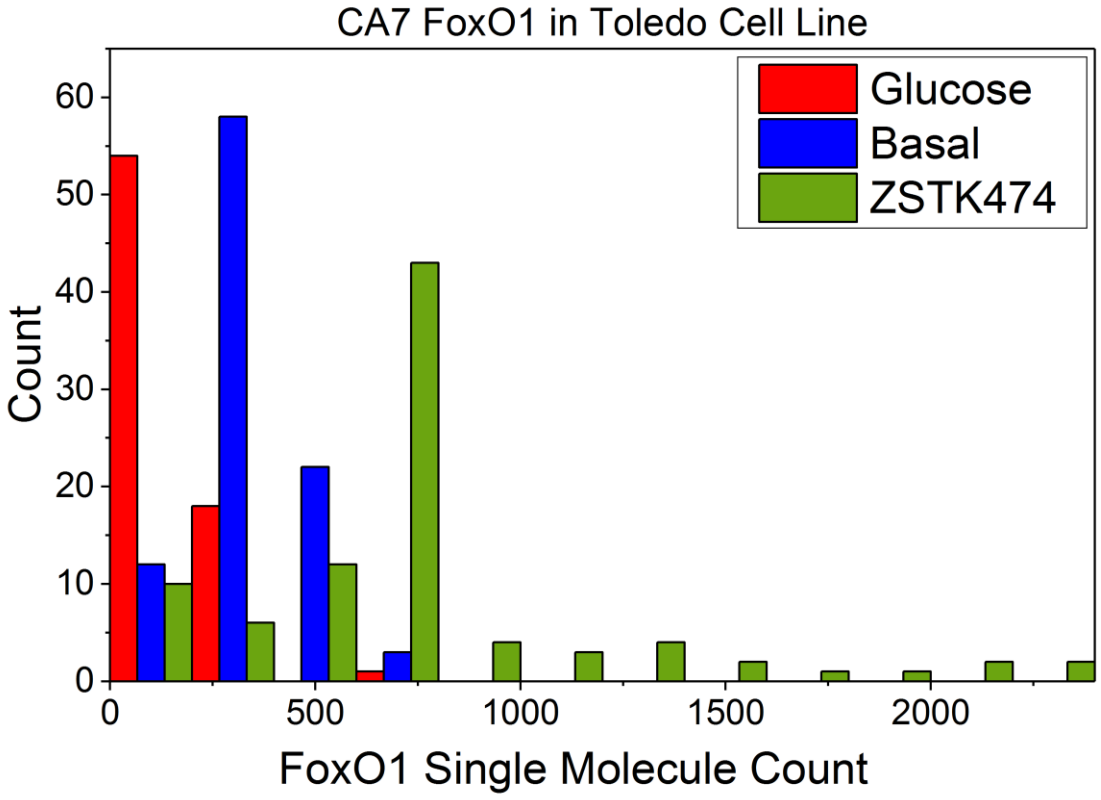


Figure 6.7 Compiled MAC Chip experiments on Toledo cells showing basal level expression (in blue) along with perturbation studies using 20 mM glucose (in red) and 10 µM ZSTk474 (in green) to bring a decrease and increase in active FoxO1 levels respectively. The plot shows the successful detection on the perturbation of active FoxO1 single molecule count.

Figure 6.7 shows that the assays perturbation studies have been successful in detecting phenotypic changes in active FoxO1 levels. The glucose studies have shown over a two-fold reduction from the basal counts in the level of FoxO1 and the ZSTK474 perturbation studies have shown a two-fold increase in the levels of active FoxO1 with respect to the basal counts. These results confirm that while the assay has lost a degree of affinity towards FoxO1, it is still able to detect and resolve changes in active FoxO1 copy number which is the important factor for future work.

In conclusion, this section has shown that by using double the concentration of the EP927Y secondary antibody, it has been possible to bring the assay to a working condition for future work. Furthermore, the increased concentration of secondary antibody has not caused a distinct increase in non-specific background binding, which is an important factor to maintain in the assay. This section utilised the Toledo cell line that is well known to have a high level of FoxO1. To further validate this assay, the next experiments were to run the assay using Beas-2b cells. Previously, the

CA7 assay was unable to detect a level of total FoxO1 in Beas-2b cells even when the cells were treated with ZSTK474. Since the Beas-2b cell line is the most relevant cell line in relation to future patient samples, it was important to make sure the assay was now capable to observe active FoxO1 molecules in this cell line.

6.4.4 Beas-2b Cell Validation Studies using 500 ng/mL EP927Y + CA7 Assay

Now that the CA7 assay was brought back to a functional level, the next step was to ensure that it is functional with the Beas-2b cell line. To provide validation of the CA7 assay the same MAC chip validation experiments were run in duplicate for basal, glucose treatment and ZSTK474 treatment. The results are presented in Figure 6.8 and show that the CA7 based assay is now able to successfully measure active FoxO1 copy number in the Beas-2b cell line. These results, when compared to those found in Section 5.7, show that by doubling the concentration of secondary antibody the CA7 based assay can successfully detect FoxO1 in Beas-2b cells and can now be brought forward to patient sample studies.

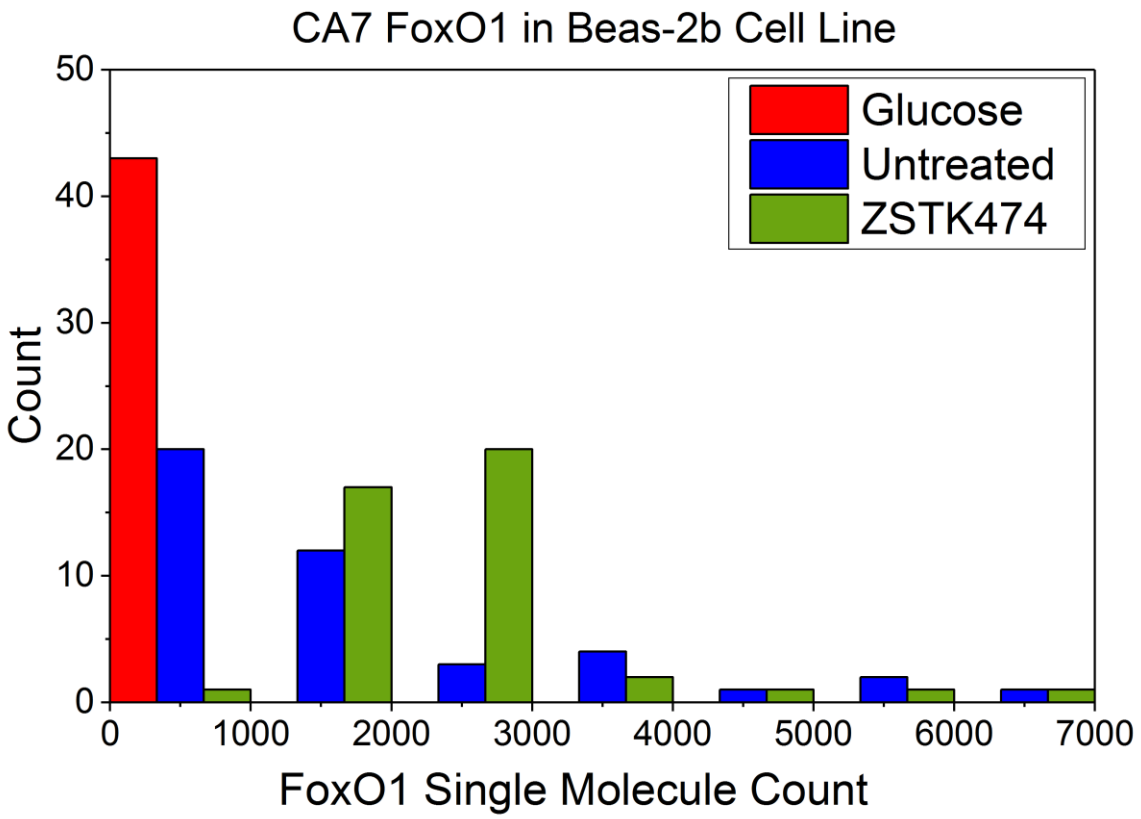


Figure 6.8 Compiled MAC Chip experiments on Beas-2b cells showing basal level expression (blue) along with perturbation studies using 20 mM glucose (red) and 10 µM ZSTk474 (green) to bring a decrease and increase in active FoxO1 levels respectively. The plot shows the successful detection on the perturbation of active FoxO1 single molecule count.

The basal mean average was calculated to be 1714 ± 1536, which is a near ten-fold improvement compared to the studies in Section 5.7. The glucose and ZSTK474 studies show single molecule counts of 323 ± 142 and 2312 ± 1065 respectively, which shows the assay can detect a decreased and increased level of active FoxO1 within the Beas-2b cell line. However, the assay does show a reduced ability to observe increases in the level of active FoxO1 when compared to validations with the Toledo cell line. Nevertheless, the assay was sufficient to bring forward to use with patient samples.

In conclusion, this set of MAC chip experiments which are shown in Figure 6.8 show the success of the CA7 assay to observe perturbations in the level of active FoxO1 in Beas-2b cells. Validation in Beas-2b cells is the best proof of concept assay study to translate across to the patient sample studies. The assay was only repeated in duplicate for each condition due to time constraints, but this is sufficient to carry on to patient samples. Next, it was assessed if doubling the EP927Y concentration in the mAb5939 assay would be able to restore its ability to monitor total FoxO1 levels.

6.4.5 Increasing the Concentration of Secondary EP927Y in the mAb5939 Assay

This section describes the use of the same workflow used in 6.4.3 to reinstate the mAb5939s assay functionality. As described previously, the first analysis undertaken was to observe if doubling the concentration of EP927Y would have a detrimental effect on the level of non-specific binding.

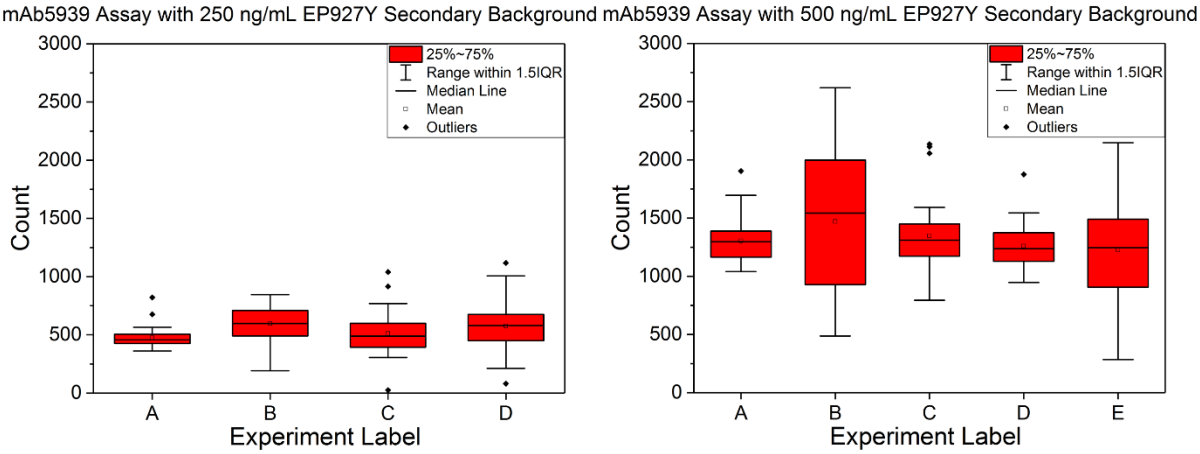


Figure 6.9 A comparison of a random selection of experiments from across the assay validation experiments, the left plot shows the observed background binding seen with a 250 ng/mL concentration of EP927Y secondary antibody and its consistency across multiple experiments. The right plot shows the effect of a twofold increase in the secondary concertation which shows over a two-fold increase in the mean and a similar incidence of outliers.

The diagrams in Figure 6.9 show that the average non-specific background has increased with the increase in secondary antibody concentration. The average background single molecule count in the 250 ng/mL EP927Y concentration experiments was 530 ± 145 and in the 500 ng/mL EP927Y concentration experiments was 1320 ± 400. This result shows a near three-fold increase in the mean average of background binding. However, with the counting algorithms used this was not detrimental to the assay so long as the capture efficiency of FoxO1 was also restored. The observed background is more variable with the increase in secondary antibody concentration. Despite this variability, the assay was considered suitable to bring forward to patient sample experiments, as there is an observable single molecule count with Toledo and Beas-2b cell lines was achieved.

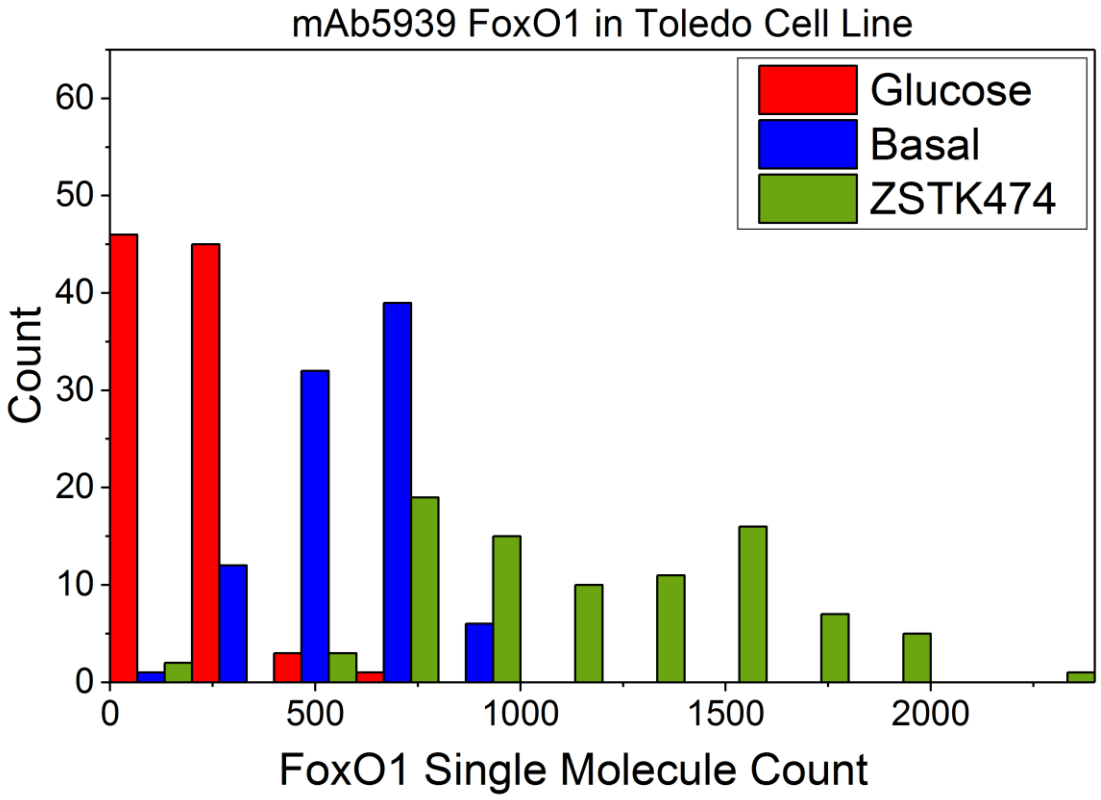


Figure 6.10 Compiled MAC Chip experiments on Toledo cells showing basal level expression (blue) along with perturbation studies using 20 mM glucose (red) and 10 µM ZSTk474 (green) to bring a decrease and increase in total FoxO1 levels respectively. The plot shows the successful detection on the perturbation of total FoxO1 single molecule count.

The diagram in Figure 6.10 shows that in the Toledo cell line, the expected perturbations of total copy number have been observed, with glucose causing a decrease and ZSTK474 an increase in the total copy numbers of FoxO1. The basal mean single molecule count was now calculated to be 593 ± 161, which was three times lower compared to the original assay (1515 ± 33) and had a higher standard deviation. The higher standard deviation shows a larger variability within the individual measurements and is likely because of the increase in secondary antibody causing a higher level of

non-specific binding in the assay. Despite the increase in variability, the assay could successfully distinguish perturbations in total FoxO1 single molecule count.

This section details the use of the same conditions and tests undertaken in Section 6.4.3 to show the successful repair of the mAb5939 based FoxO1 assay. By doubling the concentration of EP927Y, the assay (as also seen with the CA7 assay) was able to observe perturbations in the total copy number of FoxO1 albeit with a lower binding efficiency. The next step was to observe whether the assay was restored to a sufficient level to total FoxO1 copy number in the Beas-2b cell line.

6.4.6 Beas-2b Cell Validation Studies using 500 ng/mL EP927Y + mAb5939 Assay

This section describes the use of the modified mAb5939 based assay, with the doubled concentration (500 ng/mL) of EP927Y, on Beas-2b cell line to validate the assay in the most clinically relevant cell line. The same use of the MAC chip validation experiments were undertaken to determine the ability of the mAb5939 assay to measure phenotypic responses of the Beas-2b cells on total FoxO1 levels.

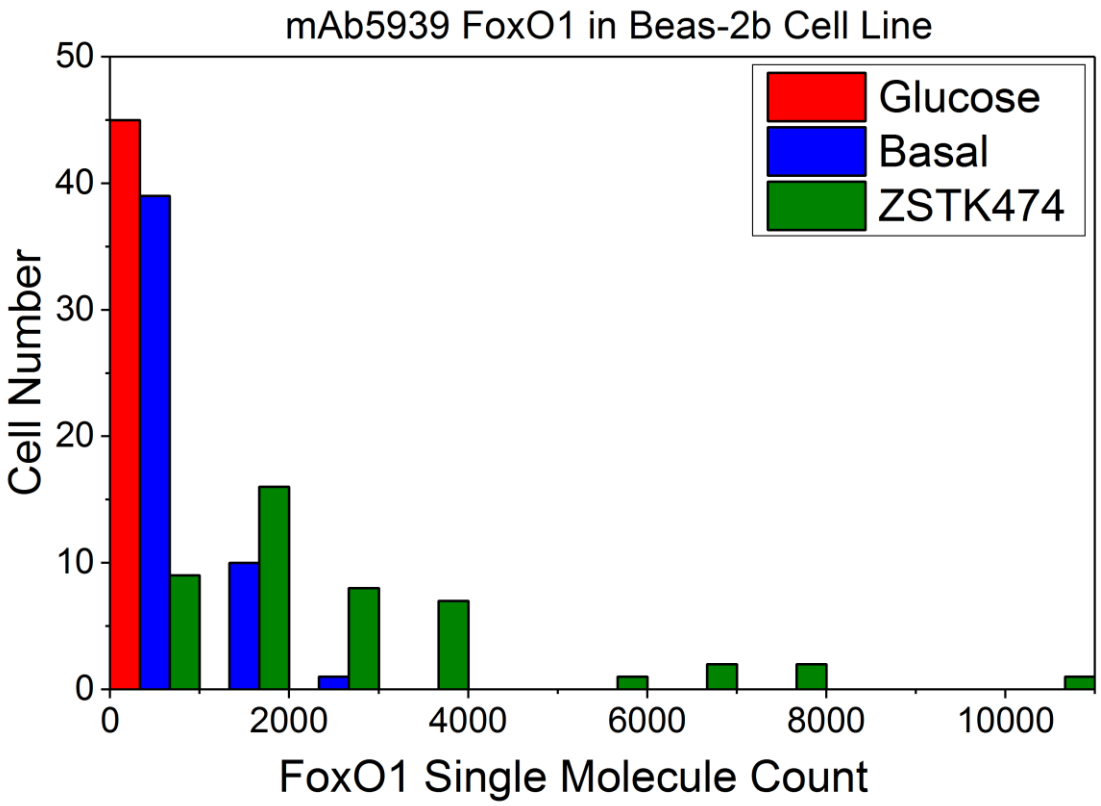


Figure 6.11 Compiled MAC Chip experiments on Beas-2b cells showing basal level expression (blue) along with perturbation studies using 20 mM glucose (red) and 10 µM ZSTk474 (green) to bring a decrease and increase in total FoxO1 levels respectively. The plot shows the successful detection on the perturbation of total FoxO1 single molecule count.

The validation studies were run in duplicate for each of the perturbation studies on the Beas-2b cells and the results are shown in Figure 6.11. The basal total FoxO1 count was calculated to be 775 ± 488. Similar to the Toledo experiments with mAb5939. This standard deviation has increased with the use of the increased concentration of secondary. Despite the increased variability, the assay was able to sufficiently resolve FoxO1 single molecules in basal Beas-2b cells above background. The ZSTK474 tests had a sufficiently increased mean at 2489 ± 2108 and clearly showed the ZSTK474 treatment gave the expected increase in FoxO1 levels, although it did have a large variation. This variation has been observed previously and usually shows the cell to cell heterogeneity towards drug treatment. The glucose experiments also showed large variability and less distinction from basal levels compared to previous experiments with a mean single molecule count of 401 ± 207. This observed count has a less than two-fold decrease in total FoxO1 levels, which is less accurate than studies in other cell lines. However, the assay was functioning at a sufficient enough level take forward to patient sample studies.

This section details how increasing the secondary antibody concentration from 250 ng/mL to 500 ng/mL has successfully reinstated the assay to a working condition. The mAb5939 based capture assay can now observe perturbations to the levels of total FoxO1 using the same validation studies as have been detailed in the previous two chapters. The assay has shown to have less distinction between lowered levels of FoxO1, but as the assay was able to observe any level of FoxO1 in reduced copy number studies it was deemed suitable for use with patient samples. This assay can now be brought forward, along with the CA7 active FoxO1 assay for use with patient derived samples.

6.4.7 T-Test Validation of 50ng/mL EP927Y Assays

This section will briefly detail the use of the student t-test method used to ensure that the populations of the healthy vs. COPD samples were significantly different from each other. This removes analytical biases and given the log normal distributions seen by the data sets, it also removes the bias the tail can create which will skew the standard deviations and mean values.

The Student's t-test provides a method to test a null hypothesis, which usually assumes both means of the two populations are equal or statistically similar and overlap distinctly. This hypothesis assumes the data sets cannot be separately defined, or that any separation is purely due to chance. The t-test aims to reject the null hypothesis and prove that the two sample populations are significantly statistically removed and the levels of overlap are not detrimental. The t-test can be

one-sided or two sided (also termed two-tailed), a one-sided can only specify whether the observed mean is smaller or larger than the hypothesised mean. In this analysis a two-tailed test was run as this simply states whether the means are not equivalent and therefore statistically separate. The t-test will calculate the test statistic *p*, if this t-statistic is more extreme than the reference distributions critical value then the null hypothesis can be rejected. This critical value is dependent on the inputted significance level of the test.

Furthermore, the t-test can be paired or unpaired. In this analysis the paired sample analysis is used as the two populations share the same units and are testing the same sample type. Paired sample measurements are the most common testing methods for patient sample analysis where the two samples are believed to show a difference in mean and distribution. Although this test is usually used for therapeutic intervention. The main issue with this method is that with the increase in statistical power there is also a need for an increased level of tests, as the degrees of freedom are reduced. This means the samples have to be at least doubled to achieve the same degrees of freedom offered by other methodologies. Given the MAC chip regime, each cell analysed can be considered an independent and isolated measurement. These independent measurements are one of the MAC chip methodologies strengths, as one patient sample can give multiple unique readings. For this reason, it was determined this would be a sufficient statistical model to ensure the two populations were separated and analysis could be undertaken on these samples.

The perturbation assays had less distinction with respect to the basal counts. In order to ensure the assays could distinguish between basal and perturbed cells a t-test is the optimal statistical validation. The t-tests were run comparing the glucose and ZSTK474 against the basal results. The tests showed that there is significant separation of the observed single molecule counts between the ZSTK474 and glucose experiments against the basal experiments. This significant separation was seen in both the Toledo and Beas-2b experiments.

Table 11 Mean and 2.Standard Deviations along with T-Test analysis of the basal experiments compared to the ZSTK474 and Glucose perturbation experiments. The results show that the assays ability to resolve copy number changes from known perturbations is still achieved by the mAb5939 and CA7 assays.

Toledo Validation mAb5939

Treatment	Mean	2xSD	p-Value wrt Basal	T-Test Result
Untreated	593	161	-	-
ZSTK474	1154	455	8.61E-18	Significant
Glucose	214	116	1.65E-32	Significant

Toledo Validation CA7

Treatment	Mean	2xSD	p-Value wrt Basal	T-Test Result

Untreated	352	112	-	-
ZSTK474	733	468	1.39E-11	Significant
Glucose	138	99	3.67E-20	Significant

Beas-2b Validation mAb5939

Treatment	Mean	2xSD	p-Value wrt Basal	T-Test Result
Untreated	713	410	-	-
ZSTK474	2489	218	5.99E-07	Significant
Glucose	401	207	3.28E-05	Significant

Beas-2b Validation CA7

Treatment	Mean	2xSD	p-Value wrt Basal	T-Test Result
Untreated	1714	536	-	-
ZSTK474	2312	1065	5.57E-03	Significant
Glucose	323	142	4.95E-07	Significant

6.5 Discussions on Optimisation and Repair of the Total and Active FoxO1 Assays

This chapter discusses the various reagents and strategies used to optimise and restore both the mAb5939 and CA7 based FoxO1 MAC chip assays. By detailed analysis of the process taken to fabricate and run a MAC chip experiment, the reagents and processes used have been optimised to bring both assays into a functional state. This work was a surprisingly challenging process which required a lot of effort and still did not bring the assays into the same level of efficiency that was seen in initial validations seen in Chapter 1.

Table 6.2 Table of replaced reagents and the reasoning. The table shows that almost all reagents were replaced in the assay to try and restore assay function.

REAGENT REPLACED	REASONING	EFFECT
Replacement of Capture Agents (mAb5939 and CA7)	If these reagents had degraded, they would be unable to successfully bind FoxO1	No observable improvement
Replacement of detection agent, EP927Y	If this reagent had degraded it would be unable to successfully bind FoxO1	No observable improvement
Neutravidin	Used for biopassivation and reducing non-specific binding	No observable improvement
Printing buffer	Ensures the Capture Agent is printed uniformly in the printed spot, ensuring optimal capture efficiency	No observable improvement
Printing pin	The pin must produce highly uniform spots to ensure chips are reproducible	No observable improvement
BSA	Used as a blocking agent to reduce non-specific binding, if expired might lead to larger background	No observable improvement
DPBS	Commonly contains ions which might affect DNA and thus hinder DNA capture	No observable improvement
Mac chip architecture	Small changes in chamber volume can negatively affect diffusion times and thus kinetics	No observable improvement
Mycoplasma infection	Infection can have a range of effects on a cell line and could have caused aberrant protein expression	No observable improvement
Increased concentration of Capture Agents (mAb5939 and CA7)	The larger concentration of unbound Capture Agent should shift the equilibria to increased binding of the protein	No observable improvement for DNA capture and antibody capture
Increased concentration of detection antibody, EP927Y	The larger concentration of unbound detection agent should shift the equilibria to increased binding of the protein	Both assays showed significant improvement and brought the assays back to a sufficient sensitivity and reproducibility

There was no single reason as to why the assays could not work at the same efficiency as previously seen. Instead it seems that it was a plethora of different factors compounded to reduce the assays efficiency. The largest factor is most likely from the degradation of crucial reagents; the most prevalent being the secondary antibody EP927Y. By replacing EP927Y and doubling the

concentration, the assay was again able to observe FoxO1 single molecule distributions and perturbations in the copy number arising from different cell treatments. This optimisation demonstrates the potential issues associated with the MAC chip technology and the importance of reagent quality in the use of the system. The work in this chapter shows that even with antibodies that have a high K_D, even slight alterations or drops in reagent quality can alter the reproducibility of the system.

Even though the two FoxO1 assays were functional again, their reproducibility was closely monitored. The inability to maintain the same single molecule count of FoxO1 when reagents were replaced shows the need to run a consistent validation experiment after each replacement of reagent. This allows comparisons to be made to the previous reagents experiments. For future experiments, if a large set of experiments had to be run, the reagents were all replaced and validation of the assays were run with Toledo cells to ensure the assays were working efficiently.

In summary, this chapter presents the need to keep constant vigilance on reagent quality to ensure the ability of the assays to observe changes to FoxO1 levels. Nevertheless, this chapter shows that the assay was restored to a sufficient standard to observe FoxO1 single copy numbers under a range of environmental factors. This work resulted in two assays that could be used to monitor FoxO1 copy numbers in clinical samples.

7 Multiplexed Single Cell Total and Active FoxO1 Protein Expression Analysis in Lung Resection Tissues Using the MAC Chip

7.1 Overview

This chapter details the successful analysis of primary patient lung resection samples in the MAC chip. Both healthy and COPD diagnosed patient samples were successfully analysed utilising a multiplexed MAC chip. Four healthy patient and four COPD patient samples were processed and the population data combined. The results showed alteration in FoxO1 active and total copy number and importantly showed statistical resolution between the two sample sets. The statistical analysis used was a t-test that showed 95% accuracy the populations were statistically resolved showing the potential analytical power of the MAC chip for patient diagnosis.

The initial sections detail the experimental set-up and the processing of the resection tissues and the challenges overcome to obtain the single molecule data. The latter chapters detail the MAC chips ability to measure the total and active populations of FoxO1, and its ability to discern alterations in the copy number the two patient populations. An analysis of the level of overlap and the t-test analysis successfully showed the ability of the assays to observe alterations in copy number between the healthy and COPD samples. The final section details the healthy and active sample data being directly correlated that showed how further detailed analysis can be used to derived even greater sensitivity and resolution in the multiplexed assays.

7.2 Introduction

The aim of this project has been to develop a MAC chip-based assay that is able to study rare clinical samples. The chosen patient cell type was lung-derived tissues for the analysis of COPD patients. COPD was determined as the disease of interest due to its inflammatory symptoms and other pathways with which FoxO1 is also involved. A collaboration was set up with Prof. Peter Barnes and his group at the National Heart and Lung Institute (NHLI), London, to study both healthy and COPD diagnosed lung tissue resections. These lung resection samples were processed with the single cell FoxO1 active and total copy number assays to elucidate FoxO1 alterations between the two sample populations.

Both FoxO1 assays had been optimised, the reagents were also freshly purchased so that all the tests undertaken were kept in consistent conditions. This would allow the assay to provide multiplexed analysis of protein expression and heterogeneity both within and between the healthy and COPD populations.

This chapter shows the successful analysis of lung resection tissue in both COPD and healthy samples and the workflow involved for their analysis. The chapter constitutes a proof-of-principle for the use of single cell proteomics for analysis of clinically-derived samples, and the hope is to develop this into a diagnostic tool for COPD/ inflammatory disorders of the lungs. This work shows that it is possible to take a disaggregated sample of cells, use the optical tweezers for isolating only live cells and then lysing said cells and detecting the multiplexed single FoxO1 molecule binding events.

7.3 Experimental Setup

Single cell experiments were performed as described in Section 3.1. All experiments in this chapter were performed in 4.5 nL standard MAC chips, as this is the geometry used in all previously detailed experiments. The internal volume of the main reservoir channel on this device is approximately 3.3 µL and hence this is the approximate lowest volume that may be processed by the chip and still efficiently isolate cells using the optical trap. Each MAC chip was filled with 50 µL of collected patient cells at a 500,000 cells/mL concentration as the cell samples contained sufficient cell numbers to achieve this concentration consistently.

The MAC chips were printed in a multiplexed regime, meaning each analysis chamber had a printed mAb5939 (total FoxO1) and CA7 (active FoxO1) present in the same chamber, allowing for tandem measurement of total and active FoxO1 in the same cell.

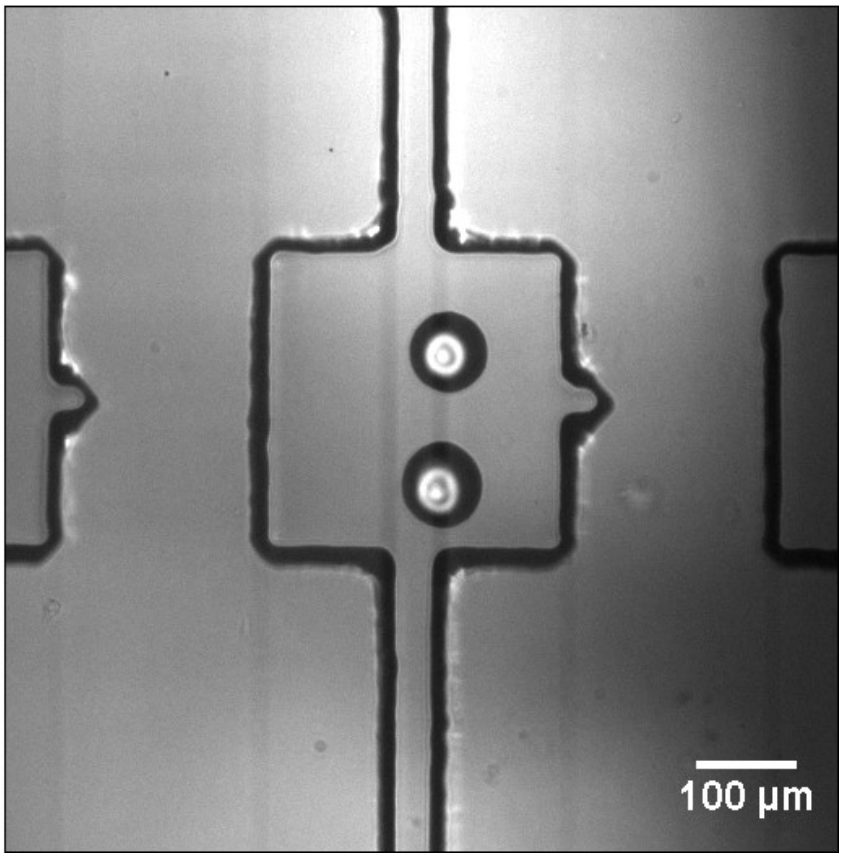


Figure 7.1 Image of a multiplexed chamber. The printing regime used in the patient sample studies allowed for both assays to be printed within the same chamber, allowing simultaneous measurements of both total and active FoxO1.

The trypan blue concentration (detailed in Section 3.5.1) was a sufficient concentration to stain the non-viable cells blue to allow the isolation of only viable cells by visual confirmation. The use of trypan blue can cause cytotoxicity in some cells when using the typical methods provided in the documentation. Although by dropping the concentration by 400x the trypan blue could sufficiently stain non-viable cells while causing the least cytotoxic effects on the cells.

7.3.1 Lung Tissue Resection and Processing

Patient-derived lung tissues were extracted from patients undergoing lung resection surgery at the Royal Brompton Hospital. Lung resected tissues are the most popular primary tissue samples for analysis in the respiratory field, with most primary sample respiratory studies using this technique. While these are the gold standard of lung derived cells, they are extremely precious, as the methods for obtaining the resected tissue is highly invasive and dangerous. These surgeries require careful preparation, with in-hospital mortality rates as high as 11% for pneumonectomies' being cited.[215] Furthermore the use of resected tissues is limited currently, as most studies take bulk measurements and little analysis has been reported at the single cell level. The use of resected

tissues in single cell analytical methods would greatly increase the data economy per sample. At this time a typical resected sample is used on average for 6- 8 tests (as quoted from NHLI collaborators). Given that the smallest number of cells needed for a MAC chip experiment is 50, the use of such a method would increase the testing economy by many orders of magnitude. Generating more data per excised tissue sample allows for an increased range of tests per sample, utilising single cell assays more frequently would allow for the more widespread use of human primary samples in drug discovery and aid personalised treatment regimes.

7.4 Results

8 individual lung resection tissue samples were subjected to the MAC chip analysis: 4 from healthy patients and 4 from patients previously diagnosed with COPD. All the samples were at the same passage and were analysed within one week of resuscitation with the majority within 3 days of resuscitation.

Multiple samples from the same patient were examined as the loading and lysis of these cells was at times challenging, with the optical trap unable to rapidly isolate 50 cells within the hour window. Cell viability would vary sample to sample ranging from 50% to 95%, as determined by trypan blue. The viability was monitored constantly on chip to ensure only live cells were isolated for analysis.

7.4.1 mAb5939 Total FoxO1 Measurements

Single cell total FoxO1 varied markedly between healthy and COPD derived patient samples. All samples run showed a detectable level of FoxO1 although the counts detected were lower compared to cell lines, such as the Toledo cell line. Like the cell line samples several of the tested cells showed expression markedly above the calculated mean. These data show the robustness of the assay to observe the heterogeneity of expression between cells.

All the experiments were run with the patient samples at the same passage number. This was an important factor to keep consistent as it is known primary samples are delicate. Without immortalisation each passage leads to less and less viable cells and increasing inconsistency in the data. An interesting experiment that was beyond the scope of this project would be to observe the effects of increasing passage number on patient sample FoxO1 copy number.

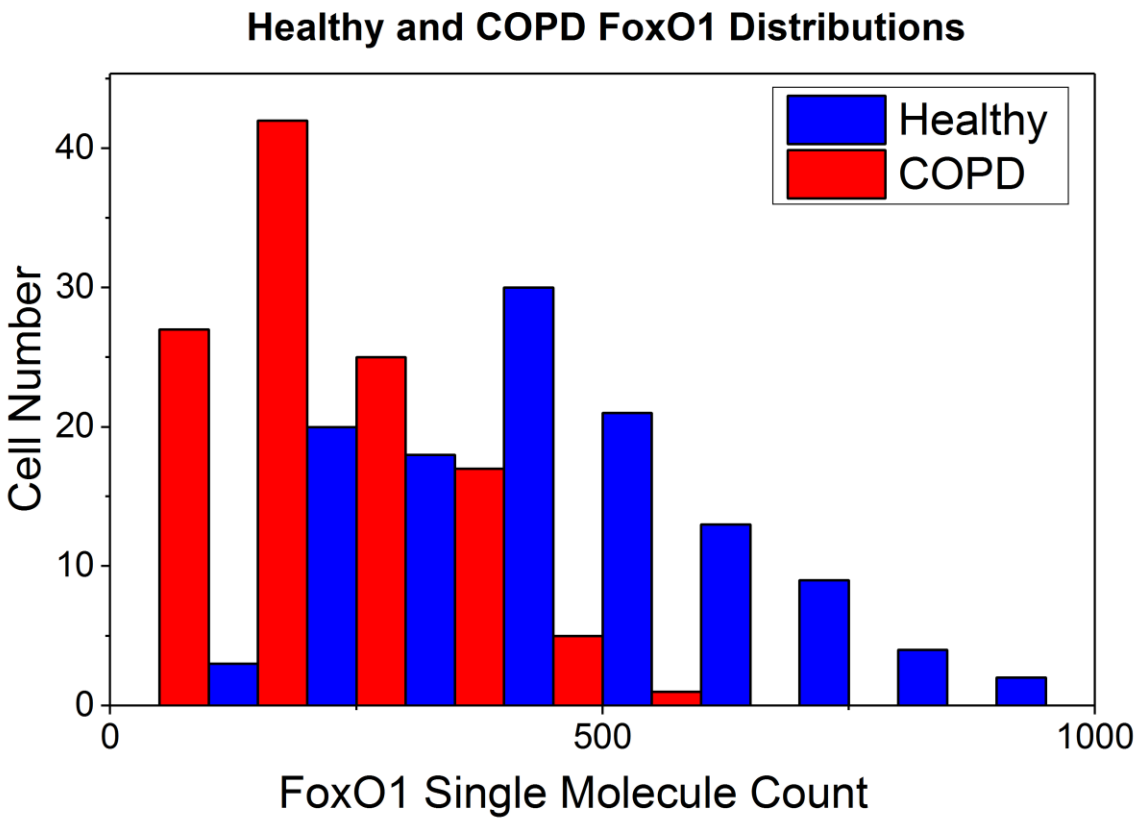


Figure 7.2 Total FoxO1 expression in 4 healthy (n = 120) and 4 COPD (n= 115) samples compiled and compared. The expression levels observed are comparatively low expressing compared to those observed in cell line analyses.

This experiment provided 120 healthy derived cells and 115 COPD derived cells. While it would have been better to have equal numbers of cells analysed for both populations, the total amount analysed for both samples was sufficiently close to allow direct comparison.

Direct comparison of the COPD and healthy patient populations showed two overlapping distributions in Figure 7.2. COPD patient cells show a net decrease in copy number, though there are regions of partial or no overlap. To quantify the levels of overlap the plots were processed in the graphing software Origin 2017, as this offers a plugin which can calculate the overlap between the two populations. This Origin app is detailed in the Appendix 11.3. The calculated overlap from the Origin software was 26% for the total FoxO1 mAb5939 assay. This overlap meant that, in theory, to be 95% confident in assigning an unknown sample of primary cells to the healthy or COPD population should only require 4 cells. This is because each measurement is unique and independent so the percentage error compounds to be more and more accurate with each single cell measurement i.e. the assay is 25% inaccurate with one cell, with two cells it is 6.25% inaccurate and with 3 cells it is 1.6% inaccurate, or 75% accurate with one cell, 94.75% accurate with two cells and 98.4% accurate with three cells.

While this is a widely used method for analysing the overlap between two samples, it is relatively crude. This method shows the overlap across the whole distributions, though in reality there are sections of total overlap. In this assay, if a cell were to show a FoxO1 single molecule count of between 250 to 400 single molecules there would be total overlap between the healthy and COPD populations making it near impossible to designate that single cell into either population. Conversely to this, at counts over 550 there is no overlap between the two populations. This region of zero overlap means that any cell which shows this level of FoxO1 expression can be unequivocally assigned as a COPD patient sample.

While these statements are true for the given plot, before this methodology could be used reliably in a clinical setting a significantly larger and robust dataset would be required. This data provides only the first steps to the use of the MAC chip method as a diagnostic tool for inflammatory disorders within the lung tissue. Typically novel medical devices will undergo thorough research, with many tools, even in their infancy requiring at least 200 unique patient tests.[216,217] Despite the need for significant validation steps, this initial data is a promising first step for the use of clinically derived tissues in a MAC chip based diagnostic tool. The analysis of the biology is discussed later in this chapter to better explain the interplay between this assay and the multiplexed CA7 active FoxO1 assay.

This section has detailed the use of the mAb5939 total FoxO1 MAC chip assay on clinically derived patient lung resection samples. The assay was successful in the capture, lysis and analysis of 120 healthy, and 115 COPD derived cells and provided a direct comparison of total FoxO1 copy number between the two populations. These promising results are only preliminary and to use single cell FoxO1 measurements as a diagnostic technique for COPD (or related diseases) there will have to be a significantly larger number of patients and cells analysed.

7.4.2 CA7 Active FoxO1 Measurements

Similar to total FoxO1 quantification, the samples varied in the quantity of active FoxO1 molecules between sample populations for the CA7 active FoxO1 assay. All the cells tested showed a detectable level of active FoxO1 which was lower compared to levels seen in the cell line models used.

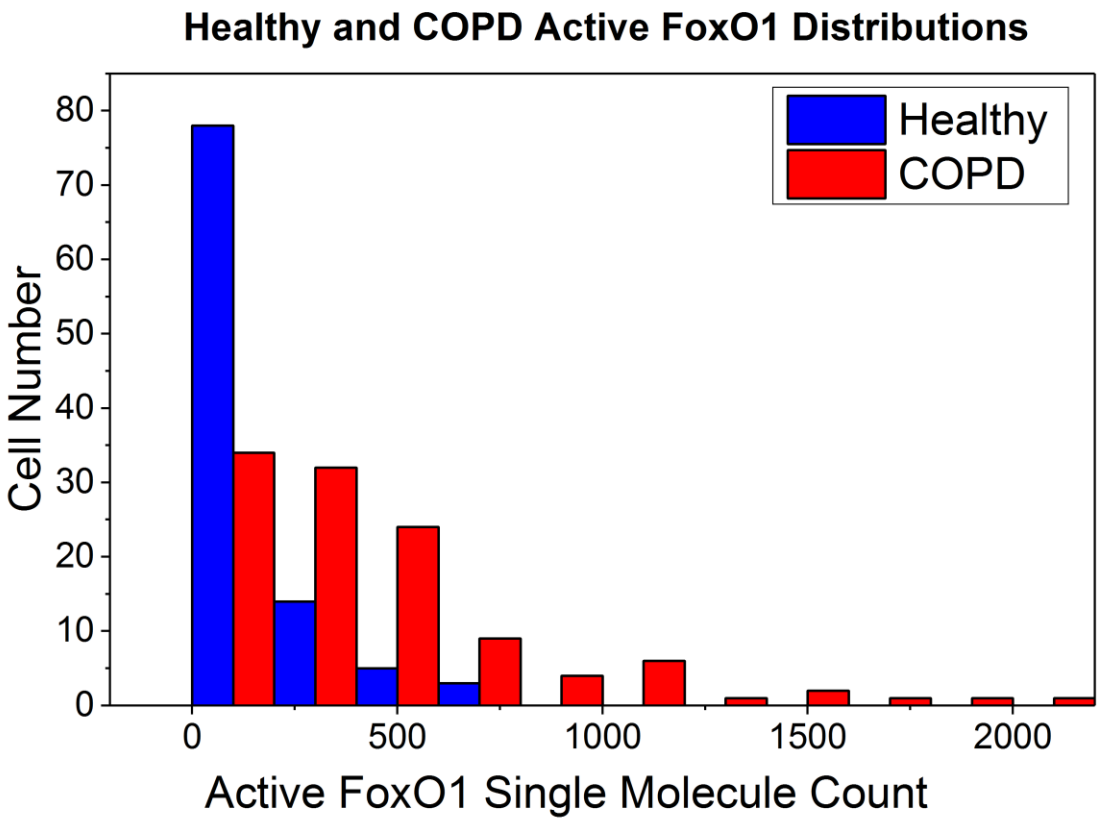


Figure 7.3 Active FoxO1 expression in 4 healthy (n=120) and 4 COPD (n=115) samples compiled and compared. The expression levels observed are comparatively low expressing compared to those observed in cell line analyses.

Interestingly the healthy samples showed a very low level of active FoxO1 compared to the COPD samples. The significance of this lowered level of FoxO1 activity will be detailed later in the discussion. Using the same Origin 2017 [See Appendix 11.3] plugin to analyse the overlap areas shows it is more distinct than the total FoxO1 measurements, with the overlap calculated as 34%, compared to the 24% seen in the total FoxO1 assay. This would imply that to have a >95% accuracy to diagnose a patient with either assay it would require a minimum of 4 cells, and with both assays bimultiplexed this further increases the accuracy of diagnosis.

Despite there being a large section of overlap, there are also initial signs that acquiring a single molecule count of over 750 active FoxO1 single molecules can be assigned with high confidence as a COPD derived cell. This observation is at an early stage and would require a more robust sample size to properly define the regions of overlap and areas without overlap.

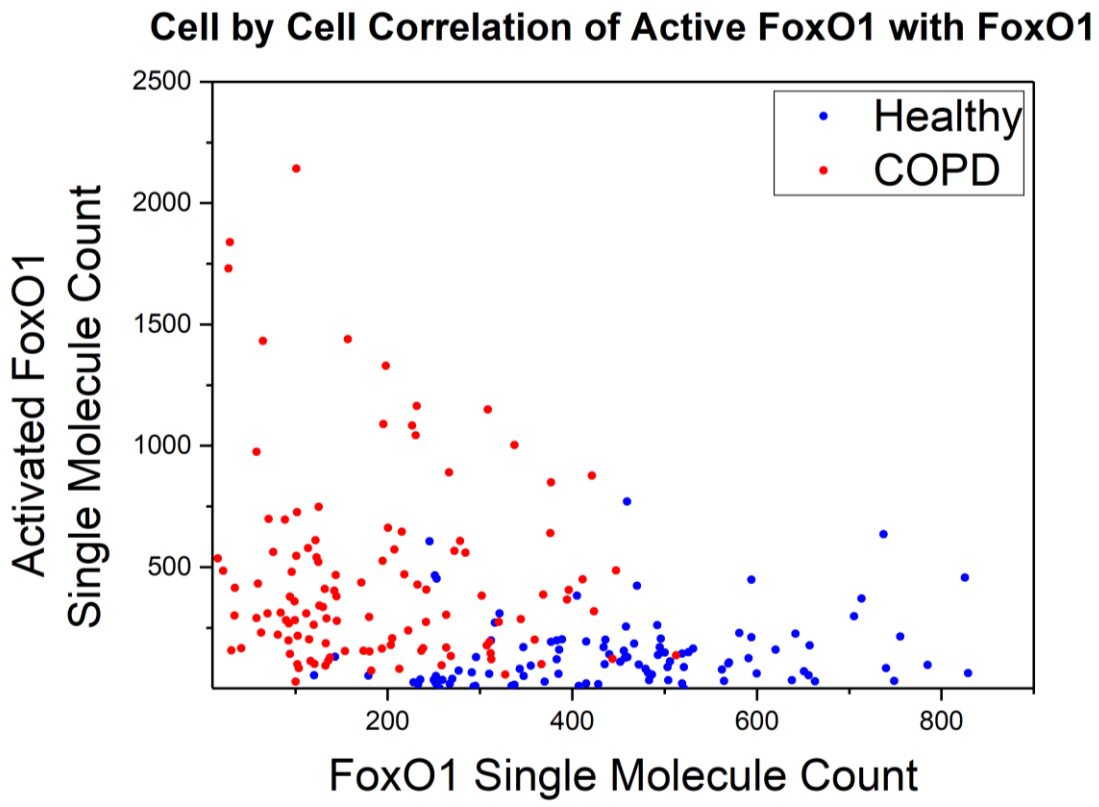


Figure 7.4 A scatter plot comparing the two assays of FoxO1 direct comparison to show the ability of the bimultiplexed assay to distinguish healthy from COPD patient samples. Each point is a single cell with total and active FoxO1 single molecule count on the x and y axis respectively. This plot better demonstrates the separation of the two sample populations if both measurements are considered simultaneously.

Figure 7.4 shows the both multiplexed measurements within the same figure. This method of interpretation shows that by taking tandem measurements of FoxO1 total and active measurements simultaneously, the assay's ability to define single cells as either healthy or COPD is greatly increased. This plot format would greatly increase the assay's ability to accurately assign an unknown sample to a healthy or diseased state. In future, applying the appropriate statistical techniques the 2D overlap between the Healthy and COPD can be calculated. Another option would be to find a method where a barrier line can be imposed over the plot with a 95% confidence of a given unknown cell being either healthy or COPD derived. This analytical design could form a heat map, where there would be regions of different levels of certainty in diagnosis and a region of total overlap where a single cell could not be accurately diagnosed.

Table 7.1 Comparison of the mean, standard deviation (STDDEV) and standard error (STDER) of the two assays for the healthy and COPD populations, also including the calculated overlaps.

	TOTAL FOXO1 (MAB5939)			ACTIVE FOXO1 (CA7)		
	Healthy	COPD	% Overlap	Healthy	COPD	% Overlap
MEAN	480	188	26	144	441	34
STDDEV	177	112		145	391	
STDER	16	10		14	39	

Comparisons of the mean single molecule counts for both assays in both healthy and COPD samples show a clear separation in FoxO1 levels. Observing the mean with standard deviations it is clear there is significant overlap between the healthy and COPD populations in the active FoxO1 assay, this is also observed with the percentage overlap calculations. This observed scatter calculated by the standard deviation is more prevalent in the active FoxO1 readings than the total FoxO1 measurements, this large intracellular scatter could point towards rapid dynamics and heterogeneity of FoxO1 activity. Furthermore, the standard deviations show a higher scatter in the sample for the COPD samples. This increase in scatter could arise from the dysregulation observed from the COPD disease state.[218]

Analysis of the standard deviations shows a significant level of overlap, if these were normal distributions then 95% of the cells would like within 2 standard deviations of the mean.[147] If this were the case then these experimental measurements would significantly overlap. A better model to calculate the uncertainty around the estimated mean is to analyse the standard error. The standard error is a widely accepted method to calculate the confidence intervals of a large sample measurement. To obtain a 95% confidence interval one can take 1.96xStandard Error (STDER), either side of the mean.[219] The principle behind this sampling is to provide contrast between the two sample populations and to better quantify the significance of overlap or the lack thereof.

Table 7.2 A table showing the mean ± 1.96xSE, providing a 95% confidence interval in the obtained values. This analysis shows that none of the samples overlap and could potentially be readily assigned by these criteria.

	TOTAL FOXO1 (ANTIBODY)			ACTIVE FOXO1 (DNA)		
HEALTHY	480	±	31	144	±	27
COPD	188	±	20	441	±	76

Table 7.2 shows that the mean ± 1.96xSE of each of the assays shows no distinct overlap with 95% confidence limits. This further proves the validity of the data and the assay's ability to distinguish

between healthy and diseased samples. One important detail of this analysis is that calculation of the standard deviation and standard error typically are used for data with a normal distribution. Whilst this data does not fit a normal distribution, this only means that the remaining 5% is not equally scattered above and below the confidence limits but is instead more likely to lie above. While this is considered a limitation, it does not overly affect the validity of the conclusions drawn. Further statistical analyses are undertaken in later sections.

In conclusion, this section has demonstrated the ability of the multiplexed total and active FoxO1 assays ability to detect measurable levels of active FoxO1 in both healthy and COPD derived samples. The overlap observed within the active FoxO1 measurements is more pronounced than that observed in the total FoxO1 measurements. There is also an analysis of the statistics to determine the extent of the overlap and the 95% confidence intervals of the two assays. Although assuming the same trend is maintained in future resection measurements this section details the first steps to using the MAC chip as a diagnostic tool for patient samples.

7.4.3 Student T-test Analysis of the Multiplexed Assays

Student T-tests were undertaken to further validate the significance of the results. The breakdown of T-tests can be found in Section 6.4.7. For FoxO1 in both cases for the antibody and the DNA assay studies the data had a p-value where $p < 0.00001$ with a two-tailed hypothesis model. This confirms that the assays can distinguish to some degree whether a patient exhibits signs of COPD from their FoxO1 copy numbers. The exact results are for the total FoxO1 assay: t-value is 15.25216. The p-value is < 0.00001. The result was set to be significant at $p < .01$. Then for the active FoxO1 assay: t-value is -7.3579. The p-value is < 0.00001. The result was set to be significant at $p < .01$. These were calculated using Origin 2017 Statistical Analysis tool set. This is clear evidence that the healthy and COPD samples were distinguishable to a significant degree, and the analysis of the biological relevance of this data was therefore possible.

It is important to mention again, much like the use of mean and standard deviation and error, the t-test also assumes a normal distribution of the data. This is due to the p and t values associated with the t-test are derived from standard deviation values. Although as mentioned previously this does not impair the results greatly, instead it just means that the confidence limits are not able to assume the extra 1% is evenly distributed above and below the confidence limits.

In conclusion, this section details the use of a paired student t-test to confirm the validity of the data collected from the patient sample multiplexed assays. The analysis confirms the ability to resolve the

alterations in total and active FoxO1 copy numbers between previously diagnosed healthy and COPD derived samples.

7.4.4 Discussion

The bimultiplexed detection of FoxO1 activity and total copy number has discovered an interesting change in activation against total pool. The role of FoxO1 under inflammatory responses has been debated over the years. The modulation of FoxO1 levels is controlled by several upstream mediators, with one of the most prevalent widely accepted as the PI3K axis.[110] Under typical conditions the PI3K axis will keep FoxO1 phosphorylated at specific sites causing its shuttling out of the nucleus to the cytoplasm thus stopping its transcriptional activity.[39,57,220] This suggests that FoxO1 levels within patients with COPD would have a lower level of FoxO1 copy number and activity. Though interestingly it is observed that while the total copy number is decreased, the levels of active FoxO1 have increased. This increase in activity is likely because in the presence of oxidative stress, the MST1/JNK pathways are also hyperactivated[221], which has several effects on the FoxO1 pathway. Firstly these pathways have key phosphorylation sites on FoxO1 to cause its nuclear localisation and activation and secondly it is also involved in the phosphorylation of 14-3-3 proteins inhibiting key interactions with FoxO1 and inhibiting its cytoplasmic shuttling.[63] From these measurements, it seems the activation of the JNK pathway has a pronounced effect on the activation of FoxO1 in cells under oxidative stress typically seen with the COPD patient samples. JNKs phosphorylation of 14-3-3 proteins antagonises the role of the PI3K-Akt axis to sequester FoxO1 from the nucleus and inhibit its inactivation of FoxO1, which helps to decouple the role of FoxO1 in inflammatory responses and longevity.[70,72,84]

The use of MAC chip multiplex analysis has provided a key insight into the interplay between activation and balance of FoxO1. Traditionally a typical patient sample analysis could only observe either the total copy number or the active copy number of a protein of interest. Taking in tandem measurements of FoxO1 and its activated form better shows the cellular pathways controlling and balancing the activation of FoxO1 responses. The results in this section show in greater resolution the importance of what many describe as the 'FoxO Code'. The results show the specific and biologically separate responses that the FoxO1 transcription factor can achieve. Interestingly the standard deviations found in Section 7.4.2 show a significantly higher variability within the COPD samples. This higher variability likely arises from the disease state causing aberrant perturbations within the cells, which leads to the higher heterogeneity within the cells. It is well documented that

copy number variation and diseases are linked, and from the COPD assay results the MAC chip assay has been able to observe this biological behaviour.[222,223]

As FoxO1 is not a routine biomarker of COPD, the results here should be viewed more as a proof-of-principle in translational single cell proteomics. It is important to mention that this work does not necessarily diagnose between healthy and COPD. Instead it shows healthy against known inflammatory responses. More work would have to be taken to determine what other disease states the FoxO1 assay detects. There is a high chance that other inflammatory disorders such as asthma would also elicit a response within these assays.

The work here is on lung resection samples, but this protocol can be applied to any disaggregated clinical material from any source. The scarcity of primary materials and the ability to work with low viability samples makes the MAC chip a clear candidate for the proteomic profiling of any primary samples that can be collected. The low number of cells needed for a MAC chip experiment also means that the analysis of clinical material can be readily extended, be it by further MAC chip analysis with different analyte detection or by running other assay formats in parallel without restriction from the quantity of sample available. The MAC chip format can be developed to analyse any protein of interest, provided there are Capture Agents with sufficient affinity available for the target. The ability to see the interplay between several clinically relevant markers could open the door to guided drug therapies. If a physician was able to notice that perturbations in a disease state were affecting only one protein path and not another then the most potent therapeutic interventions can be used. This would find great application in other therapeutic areas, e.g. oncology, where the anti-cancer agents are known to have serious detrimental effects to the patients' quality of life. Being able to tailor therapeutics would improve treatment potency and reduce the negative side effects which are commonplace with chemotherapy.

This chapter has detailed the first successful use of purely patient derived samples in the MAC chip assay. The MAC chip was multiplexed so that it was able to observe both active and total FoxO1 copy numbers by using the CA7 and mAb5939 assays respectively. The use of the multiplexed assay has successfully observed the FoxO1 expression levels in both healthy and COPD derived samples, and more crucially, a difference in expression levels between the two populations. This alteration in FoxO1 total and active levels has shown that patients with COPD express a lowered level of total FoxO1, while showing an increase in activity. This result was interesting as it would commonly be expected that with a decrease in total copy number there would also be a decrease in the observed activity. Whereas a non-linear relationship has been observed. This separation of total vs active

FoxO1 has been corroborated with the wider literature with respect to the various known pathways that are impacted in COPD as well as FoxO1 regulation.

8 Use of Clinically Derived Sputum in FoxO1 Multiplexed MAC Chip Analysis

8.1 Overview

This final results chapter details the MAC chips potential ability to utilise non-invasive sampling methods that can still acquire clinically relevant data. This section demonstrates the optimisation of the sputum freezing and handling procedure in order to process and analyse both T-cells and epithelial cells found in sputum samples. The isolation of these specific cell types showed that, currently, the MAC chip has lowered sensitivity. This might arise from the processing times or might suggest further assay optimisation is needed to obtain resolution between healthy and COPD derived samples.

The initial section of this chapter details the analysis of current sputum handling protocols and the aims to better improve the methods in order to allow freezing and later analysis of the samples; these methods have currently been a roadblock for sputum testing methods. This section also analyses the current processes and determines the best opportunity to allow freezing of the sputum samples for later processing and analysis. The latter sections detail the active and total FoxO1 measurements taken from T-cells and epithelial sputum derived cells respectively. For both cell types, as well as for healthy and COPD patients, the copy numbers of FoxO1 were, for the majority of the tests, lower compared to previous studies in this thesis. The reduced capture of FoxO1, both active and total, likely shows that the assay might need increased sensitivity for greater resolution in the analysis of sputum samples. Alternatively, the sputum processing techniques may need to be improved in order to yield a higher level of viable cells that can be analysed in the MAC chip. Despite this lowered level of FoxO1 total and active copy number capture, the same trends seen in Chapter 7 were observed with respect to the non-linear relationship of total vs active copy numbers.

8.2 Introduction

Chapter 7 presented the first use of the MAC chip assay with clinically derived patient samples. This chapter will detail taking the same experimental set up and analysing sputum derived epithelial and T-cells. Here we detail the next step in utilising the MAC chip method for the analysis of patient derived cells and demonstrate the versatility of the method in a clinical setting. The work presented here was again in collaboration with Peter Barnes and his group at the National Heart and Lung Institute, London. The material was obtained using a typical sputum induction procedure for sample collection of both healthy and COPD diagnosed patients.

Both assays, mAb5939 (total) and CA7 (active) FoxO1 assays were again multiplexed and experiments were run in the same method as the lung resection samples. The lung resection chapter has detailed the first analysis of patient derived samples in the MAC chip format. While this work detailed a successful proof-of-concept result for the use of patient samples, the method to obtain cells is highly invasive and requires extensive training to run the procedure. To bring the MAC chip to a more clinically relevant setting, the utilization of easily obtained cells is a key priority. For this reason, it was decided to use sputum derived cells. Sputum is the mucus specifically produced in the airways which plays a critical role in lung innate immunity. Mucus hypersecretion is a primary symptom of COPD and its exacerbation. The major component of sputum is mucins, and in chronic lung diseases such as COPD; DNA, filamentous actin, proteoglycans, and microbes are also present.[224] Though most importantly the secretion contains a variety of immune and bronchial epithelial cells which makes sputum a safe and non-invasive source of cells.[225]

Induced sputum methods are standardised and have been shown to offer a reliable and valid approach to obtain relatively viable cells. The viability of the cells has been examined in the literature and shows a viability of around 62-65% which can be validated using trypan blue.[226] A key advantage of induced sputum is that it can be carried out at any major hospital with a pulmonary function test (PFT) laboratory equipment and the appropriately trained staff. The training for sputum induction is simple, requiring only a week for staff who have previous experience in respiratory practices and the theory of sputum induction.[227] This technique has been used for several years as a method for investigating lower airway inflammation by analysis of cellular markers and cell count correlations.[227] Studies on the levels of sputum eosinophil cells and concentrations of eosinophil cationic protein (ECP) are known to correlate with increasing levels of severity of asthma. This correlation is also linked to the viability of the eosinophils.[228]

While a clear differentiation between COPD and asthma is sometimes difficult, giving their overlap with physiological and inflammatory profiles, a more common change in COPD is an increase in products associated with neutrophil activation and an increase in neutrophil cell count.[229] The ability to take highly accurate protein copy number measurements of sputum derived cells would greatly benefit the analysis and treatment management of COPD and asthma disorders.

While work has gone into the use of sputum for the diagnosis and analysis of airway inflammation, the typical procedures involve study of either the cell count and cell type distribution, or the analysis of cell surface markers in flow cytometry.[230] A paper by Vethanayagam et al.[229] states that 'sputum analysis gives the opportunity to gauge the degree of inflammatory cell activation in airway diseases… It is proposed as a clinical measurement for asthma and COPD patients to determine the inflammatory processes and assist in diagnosis and management of disease.' The use of the MAC chip and the same multiplex analysis hopes to provide the same proof-of-concept diagnostic tool as seen with the lung resection tissues.

The work detailed in this section will show the proof-of-concept experiments for the analysis of sputum derived cells for the diagnosis of COPD or inflammatory airway disorders. The work used the same MAC chip methodologies as detailed in previous chapters and shows the successful analysis of healthy and COPD derived sputum.

8.3 Experimental Set Up

Single cell experiments were performed as described in Chapter 2.1. All tests were performed in the 4.5 nL standard MAC chip with a multiplexed printing regime to include both the mAb5939 (total) and CA7 (active) FoxO1 assay Capture Agents in each chamber. As detailed both assays use the same EP927Y 488-labelled secondary antibody.

8.4 Results

This results section details novel methods for the handling and use of sputum samples in the MAC chip FoxO1 active and total multiplexed assays. The first sub section briefly details the validation of the optimal methods to store and resuscitate the samples to ensure optimal results when loaded onto the MAC chip. The latter sections detail the results of the multiplexed MAC chip analysis for both T-cells and epithelial cells.

Multiple samples of healthy and COPD derived cells were collected as frozen aliquots and brought to Imperial College London, these samples were thawed immediately prior to the MAC chip experiment.

Multiple samples were obtained from the same donor, to appropriately determine the optimal methods for freezing and storage of the cells. Different donors make up the sputum analysis of healthy against COPD histograms and scatter plots as detailed later.

8.4.1 Optimising Cell Freezing Protocol

It was possible to take the sputum 'fresh' from the Royal Brompton for rapid analysis, although this imposed limitations. The main limitation being that if only 'fresh' samples could be analysed then the rate of assays is strictly limited to when sputum samples can be tested. This would greatly slow the rate of analysis and hinder progress. Thus, decoupling the collection and analysis would allow for a higher throughput of data and easier sample storage.

During the MAC chip FoxO1 active and total assay measurements, the resuscitated samples under the 3 different freezing conditions (detailed in Section 3.5.2) were carefully monitored for viability and ease of analysis. The end objective here was to determine the optimal methods to freeze the samples after collection to ensure they are optimally preserved to allow rapid and simple analysis. The four sputum conditions analysed were: a) fresh sputum directly analysed, b) frozen sputum with no treatment, c) sputum frozen after 0.05% DTT treatment, d) fully processed sputum subsequently frozen. The test was to compare the sputum cell viability to determine which condition best stored the sputum. The fresh sputum was considered the control, with the want to keep as high of a viability as possible compared to fresh sputum. The same patient sample was used and divided into each of these conditions to allow direct comparison.

Table 8.1 The cellular viability in the sputum samples arising from the effects of the different storage conditions.

SPUTUM CONDITION	PERCENTAGE VIABILITY VIA TRYPAN BLUE STAIN (%)
FRESH	68
FROZEN UNPROCESSED	57
FROZEN DTT ONLY TREATED	62
FROZEN FULL PROCESSING	39

Table 8.1 shows the different viabilities observed in the sputum samples. The highest viability found was at 68% with freshly processed sputum and the lowest viability at 39% seen with the fully processed (DTT treatment and centrifugation into freezing media). A viability of 68% is still low compared to the use of a well maintained immortalised cell lines viability. These observed viabilities demonstrate the importance of monitoring the viability during the cell identification and isolation steps when the cells are loaded on chip. It is interesting to observe that the lowest cellular viability is observed with the full treatment and subsequent freezing, as one would expect removing the DTT would provide a higher cellular viability and be more comparable to the fresh sputum samples. It is likely that the drop in viability seen with the full treatment is due to the sample undergoing an extra round of centrifugation which is documented to be detrimental to cellular viability.[231] It seems that the effect of the small percentage of DTT is less detrimental to the viability than the repeat centrifugation steps, as seen in Table 8.1 showing the DTT only treatment having the greater viability. From this analysis and comparison of viabilities it was decided the best method for storing and analysing the cells was to add freezing media to the sputum samples directly after the DTT treatment and freeze the cells for optimal storage at this stage. While repeated centrifugation is known to cause a drop in viability[232], frozen primary cells viability is known to vary widely sample to sample in general.[233] Further analysis of the effects of the storage method were not undertaken at this time given the scarcity of the samples.

8.4.2 mAb5939 Total FoxO1 Measurements in Sputum Derived T-cells

This section details using the mAb5939-EP927Y assay pair for measurements of total FoxO1 copy number in sputum derived T-cells. The experiments were carried out in a multiplexed study in the same fashion as detailed with the lung resection results chapter. The study compares the total copy number of FoxO1 in healthy and COPD derived samples to observe whether the proposed assay provides a marker for airway inflammatory disorders. All samples tested did show a detectable level of FoxO1 albeit lowered compared to immortalised cell line analysis.

All experiments shown in this section, unless otherwise specified were run directly after resuscitation while using the DTT freezing protocol detailed in Section 3.5.2. This was to keep all cells in a consistent environment. This data was collected over 3 healthy and 3 COPD diagnosed patients and due to the heterogeneity of the samples only 46 healthy T-cells and 40 COPD diagnosed T-cells could be analysed.

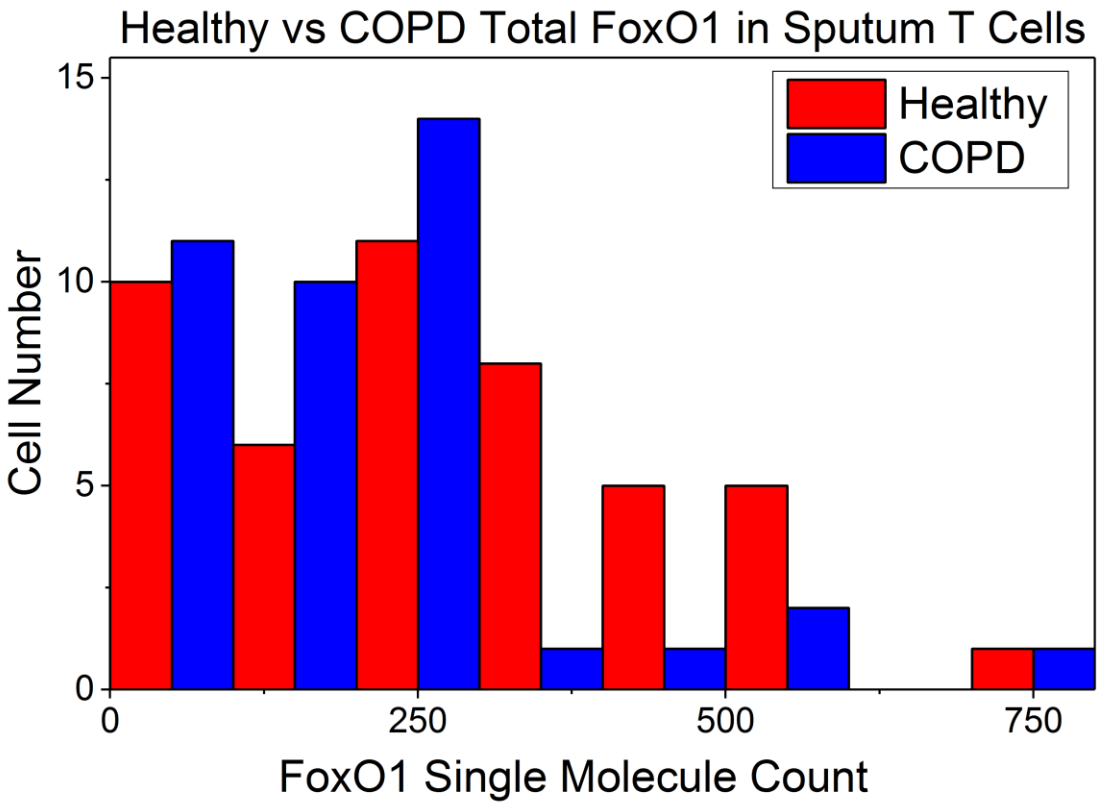


Figure 8.1 Total FoxO1 expression in 3 healthy and 3 COPD sputum derived T-cell samples compiled and compared. The expression levels observed are comparatively low expressing compared to those observed in cell line analyses and in lung resection analysis with most of the single molecule counts falling below 500 per cell.

The isolation of T-cells was simple with the CD3 marker giving efficient labelling of the T-cells, although given their spherical morphology to the other cells present it took longer to find and then isolate cells of interest. Given the added time it took for the detection of the T-cells the data set is less robust than compared to the homogenous lung resection tissues. The need to identify the T-cells also meant that the number of T-cells varied patient to patient. Similar to the lung resection samples the cells viability was monitored using a 400x dilution of trypan blue, this ensured that the cells isolated were viable. Interestingly the trypan blue determination demonstrated the low viability of the cells in the sputum samples. There were several times over the collection of this data where a cell was isolated and when it came to lyse them they were deemed unviable, as judged by their loss of their morphology and clear signs of undergoing apoptosis. Showing that these cells were very sensitive and even within an hour they can show signs of becoming unviable.

By direct observation and statistical analysis, it is clear that the two samples show a high level of overlap. Given a basic analysis it is clear there is no region of absolute certainty for either population, suggesting that this assay is unsuitable for the diagnosis of COPD/ airway inflammation disorders using sputum derived T-cells. Given that the origin plot overlap function only considers the

areas under the curves, running the plot through the overlap function only showed an overlap of 39%. Given more time and a better grasp of programming, it would be possible to edit the function to isolate key single molecule counts where there is a higher percentage certainty of a cell being in either population. Although this would take time to research and implement. The results were also subjected to a student t-test with a p-value of <0.05 being considered statistically significant, with this test the two populations were considered not significantly different from each other. This failing of the t-test was expected given the clear overlap of the datasets.

In conclusion this section shows that the well-established mAb5939 total FoxO1 assay was unable to observe any alterations in total copy numbers of FoxO1 between healthy and COPD diagnosed patients. This shortcoming could show that the assay lacks the sensitivity required to observe the changes in FoxO1 copy number in this cell type. It could also show that currently the data set is too small to give an accurate study of total FoxO1 in T-cells. Time constraints prevented the analysis of more sputum samples but adding further samples to the compiled data would show a greater level of resolution between the two populations, as observed by the overlap function and statistical analysis. Future work will be undertaken to see if the process and inferences can be improved on.

8.4.3 CA7 Active FoxO1 Measurements in Sputum Derived T-cells.

Akin to the lung resection single cell analysis, the mAb5939 assay was multiplexed with the CA7 assay to give in tandem readouts of total and active FoxO1 copy numbers. These experiments again showed a detectable level of active FoxO1 though this copy number was lowered with respect to the cell line validation studies. This does mean the sample population is relatively low and more repeat measurements for this study would be beneficial.

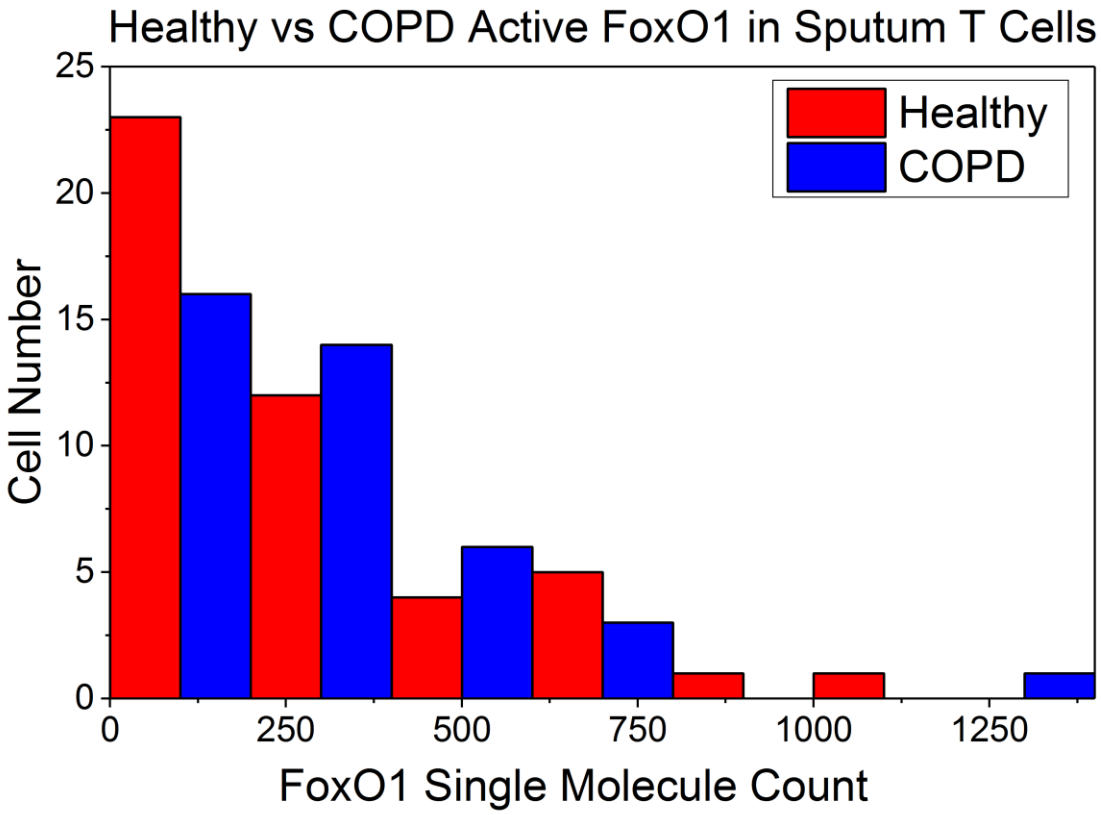


Figure 8.2 Active FoxO1 expression in 3 healthy and 3 COPD sputum derived T-cell samples compiled and compared. The expression levels observed are comparatively low expressing compared to those observed in cell line analyses and in lung resection analysis with most of the single molecule counts falling below 500 molecules per cell.

Figure 8.2 shows that active FoxO1 analysis was unable to resolve any difference in active FoxO1 copy number. This was a disappointing finding as this cell type was easy to isolate and identify in the sputum samples and they are relatively abundant in sputum. It is clear by eye that there is a complete overlap of the two populations and compared to the total FoxO1 T-cell sputum analysis the distributions for each population is distinctly similar. Using the Origin 2017 function to analyse the overlap confirms the significant overlap of this data with the overlap calculated at 78%, this reflects that the distributions and areas under the curve are all very similar. To further test any statistical significance of the data a student t-test with a p values of <0.05 was run and the two populations were found to not be significantly different from each other.

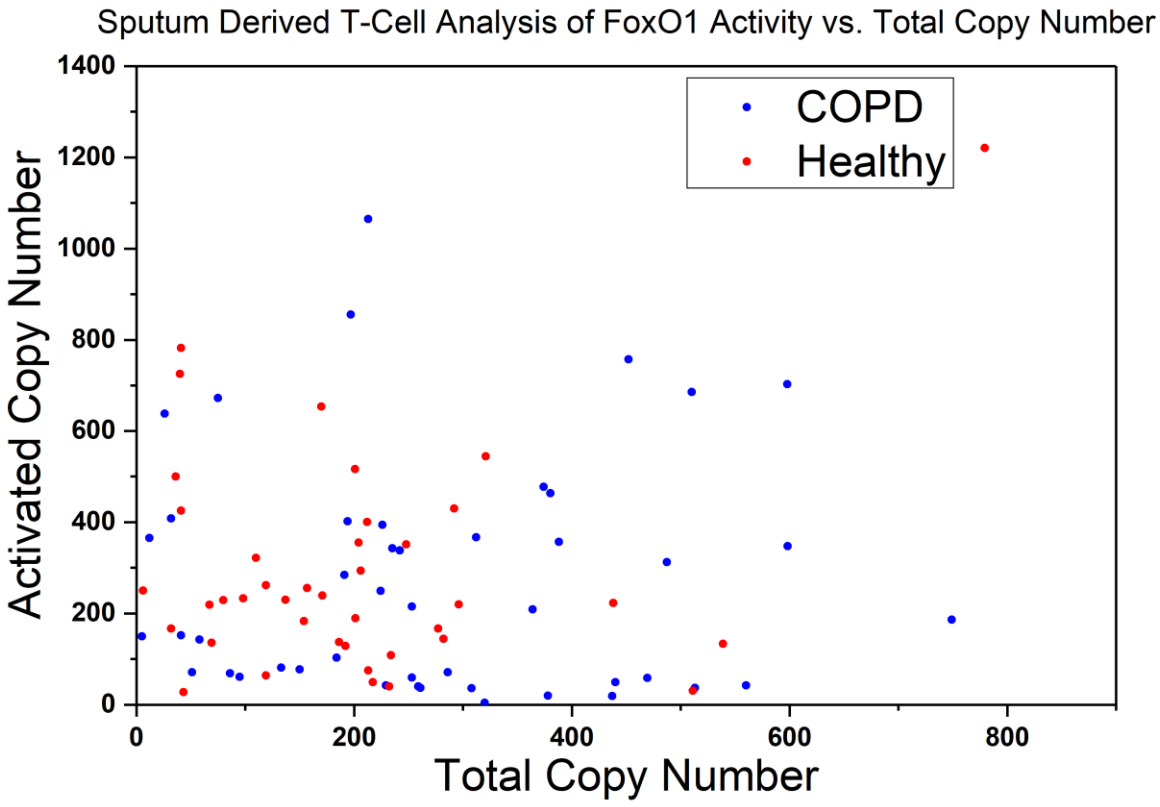


Figure 8.3 A scatter plot comparing the two assays of FoxO1 direct comparison to show the overlap of the bimultiplexed assay with healthy and COPD sputum derived T-cell patient samples. Each point is a single cell with total and active FoxO1 single molecule count on the x and y axis respectively. This plot shows even with both multiplexed measurements combined there is distinct overlap and no real resolution of healthy from COPD samples.

Figure 8.3 shows the multiplexed measurements within the same figure. This method of interpretation still shows that the multiplexed measurements were unable to clearly resolve any changes in FoxO1 total or active copy number in sputum derived T-cells. While it seems that this methodology is unsuitable for primary T-cell analysis, until the data set is significantly more robust it is hard to draw any clear conclusions from the data. Given more cells and analysis for both populations it might be possible to elucidate greater separation with the two populations.

Table 8.2 Comparison of the mean, standard deviation (STDDEV) and standard error (STDER) of the two assays for the healthy and COPD populations, also including the calculated overlaps.

	TOTAL FOXO1 (MAB5939)			**ACTIVE FOXO1 (CA7)**		
	Healthy	COPD	% Overlap	Healthy	COPD	% Overlap
MEAN	279	199	39	272	291	78
STDDEV	180	155		259	239	
STDER	26	25		38	38	

Comparing the mean single molecule counts for both assays and the two populations shows clear overlap in the observed counts. The overlap between the assays is large and the standard deviations and standard errors further show this, the overlap is far more prevalent in the active CA7 assay which may reflect the dynamic role of FoxO1 activity in times of cellular distress. Although the scatter seen by the standard deviation is comparable in both healthy and COPD samples in the CA7 active FoxO1 assay, and so this might show that FoxO1 is highly dynamic in T-cells in general.

Using the previously described confidence intervals method to analyse the overlap and 95% confidence by taking 1.96xSTDER either side of the mean shows overlap for the active FoxO1 measurements and little distinction with the total FoxO1 counts. This further signifies the overlap for both assays with T-cell analysis.

Table 8.3 A table showing the mean ± 1.96xSE, providing a 95% confidence interval in the obtained values. This analysis shows that the active FoxO1 samples overlap and total FoxO1 measurements show little discrepancy.

	TOTAL (ANTIBODY)		**FOXO1**	**ACTIVE FOXO1 (DNA)**		
HEALTHY	279	±	51	272	±	74
COPD	199	±	49	291	±	74

In conclusion, this section has shown a current limitation of the MAC chip FoxO1 total and active multiplexed assay. Taking primary sputum samples and analysing the isolated T-cells has shown that there is no apparent alteration in the copy numbers of total or active FoxO1. The overlap is described using several statistical methods all concluding that there is no clear distinction or diagnostic efficiency with the bimultiplexed assays currently. Despite this, the assays were able to successfully detect a copy number of total and active FoxO1 in both healthy and COPD derived sputum samples. There might be an improvement on the resolution given a higher population of analysed cells to compile into the plots and future work will go towards populating this data set.

8.4.4 Discussion of FoxO1 Measurements in Sputum Derived T-cells

In this section we have shown how the MAC chip can successfully measure FoxO1 levels in sputum derived T-cells, however we were unable to discriminate between healthy and COPD patients via this bimultiplexed measurement. One reason as to the lack of distinction between the healthy and COPD diagnosed samples could lie with the assay itself. The observed single molecule counts for cells analysed in both assays has shown a small copy number with respect to the previously discussed

cellular analyses. It is previously mentioned in Chapter 1 that the assays had to be optimised to be able to observe FoxO1 copy numbers, this T-cell sputum analysis could show that the assays need further optimisation before they can be successfully utilised for T-cell analysis. Although a likely situation is that the current size of the data set is simply too small to be able to draw any definitive conclusions from and a larger population study may still yield the wanted diagnostic ability of the assay with T-cells.

Regardless of the potential assay issues, there is still a likelihood that the issues observed stem from the inherent biology present in T-cells. The literature regularly discusses the role of FoxO transcription factors throughout T-cell biology with FoxO1 and FoxO3 being particularly involved.[234] T-cells are well documented to be increased in patients with COPD, furthermore the perpetual activation of their inflammatory response is also observed in mild through to severe COPD.[235] This increased inflammatory response is seen to function potentially through the inactivation of FoxO3 and it is believed that this can affect T cell function.[236] This is hypothesised to be true also of FoxO1, although less studies on FoxO1 in COPD and inflammation in T-cells is available. Though given the similarity between FoxO1 and FoxO3 activity in T-cell regulation and function it is a grounded hypothesis. On top of this, due to the range of predisposing factors in COPD, such as oxidative stress, inflammation and FoxO1s innate regulation of T-cells, there is a large possibility that the FoxO1 responses cannot be decoupled from 'healthy' and 'diseased' T-cells. As T-cells rely heavily on FoxO1 for their typical growth cycles, as well as for inflammatory/ oxidative stress responses, there is a likelihood that the cell to cell heterogeneity is very high given the growth cycle dependence for both healthy and COPD samples, and this cannot be decoupled with the FoxO1 total and active MAC chip assays.

In conclusion, the MAC chip bimultiplexed assay was unable to observe any alterations in FoxO1 total or active copy numbers between healthy and COPD samples. While this might be due to the assays themselves not having a low enough limit of detection, a more likely reason is that the innate biology of T-cells. The role of FoxO1 in T-cell growth cycle makes it hard to resolve whether FoxO1 copy number alterations are due to external factors (COPD) or growth cycle regulation. This theory will be tested in future work as the number of patients and single cells analysed increases.

8.4.5 mAb5939 Total FoxO1 Measurements in Sputum Derived Epithelial Cells

Given the heterogeneity of the sputum samples, it was possible to isolate and analyse T-cells and epithelial cells from the same sample. This section details the isolation and analysis of sputum

derived epithelial cells. The results with respect to the T-cell analysis show greater separation. Although the separation is reduced compared to that of the lung resection tissues. All the cells analysed again showed a detectable level of FoxO1 though like every patient derived sample analysed a relatively low level of total and active FoxO1 was seen. Given the lack of time before the end of this project the same limitations to patient analysis occurred, so only 3 healthy and 3 COPD patients were analysed with no repeats. These epithelial cells were analysed in the same sputum samples as the T-cells and isolated and lysed with the same methodology. In total 46 healthy and 37 COPD cells were analysed, due to the time constraint of 1 hour the amount per patient varied much like in the T-cell analysis. As these cells were isolated from the same sputum samples as the T-cells they were subjected to the same conditions and were resuscitated after freezing at the DTT step detailed in Section 8.4.1.

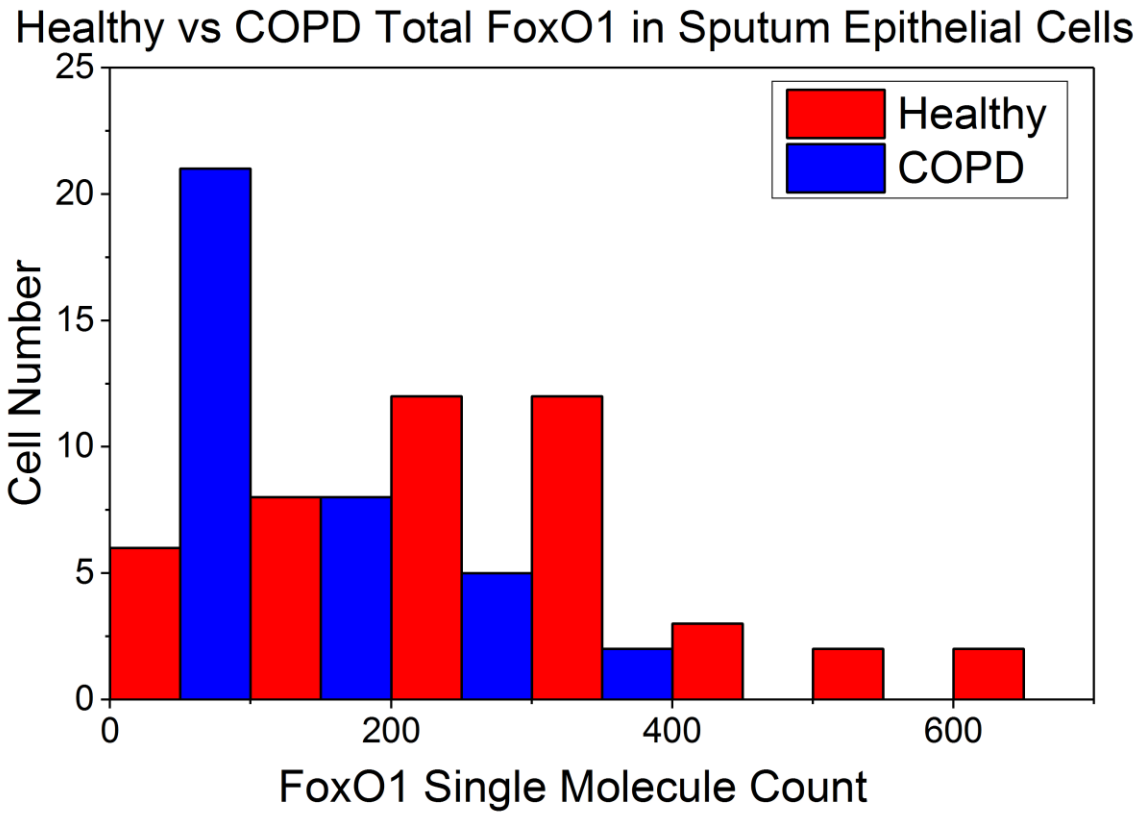


Figure 8.4 Total FoxO1 expression in 3 healthy and 3 COPD sputum derived epithelial samples compiled and compared. The expression levels observed are comparatively low expressing compared to those observed in cell line analyses and in lung resection analysis with most of the single molecule counts falling below 500 per cell.

The isolation of epithelial cells in both healthy and COPD sputum samples was simple given the distinct morphology of these cells. There are several characteristics of bronchial epithelial cells in sputum samples to make direct observation and isolation of them simple, such as their simple columnar or cuboidal shape and their elongated nuclei in a sample of otherwise spherical cells.[237,238]

Despite the simplicity in identifying these cells a large issue was the abundance of cells present, the literature is conflicted as to how many epithelial cells percentage wise should be expected in a typical sputum sample ranging from 0.1-10%.[227,239] This meant that it was hard to obtain a high frequency of cells in the given hour, although if the time for isolation and lysis was increased it would increase the cell count analysed, although it might also have a detriment on the viability and quality of analysis. As all other experiments up to this stage of the project kept to an hour time frame for isolation and lysis this was kept for the sputum measurements also. The trypan blue 400x dilution present was sufficient to detect viability of the cells, although at times the stain was faint. Though it was also clear by eye if a cell is undergoing stress states or apoptosis.

The results shown in Figure 8.4 show a degree of overlap which is higher than that observed by the lung resection tissues, yet lower than that of the sputum derived T-cells. Using the Origin 2017 overlap function the overlap was calculated to be 37%. This overlap is relatively pronounced. Though it also shows total FoxO1 single molecule counts that would give 100% certainty of a healthy cell with any count over 400 theoretically being healthy. Currently the dataset for both healthy and COPD is sparse, and more cells and patients would need to be analysed before any firm conclusions are drawn. Running a student t-test at a $p < 0.05$ level shows that the data sets are significantly different from each other, showing that the assay is capable to distinguish between the healthy and COPD populations.

This section has shown the use of the total multiplexed assay to successfully observe FoxO1 single molecule counts in healthy and COPD sputum derived samples. Not only did the mAb5939 capture assay observe total FoxO1 it also shows separation between the healthy and COPD observed single molecule counts which were validated with a paired student t-test. Though given the small population of cells for the healthy and COPD states, before stronger conclusions can be made more cells and patients need to be tested.

8.4.6 CA7 Active FoxO1 Measurements in Sputum Derived Epithelial Cells

Similar to total FoxO1 quantification, the multiplexed active FoxO1 measurements showed a difference between the healthy and COPD populations. All the isolated epithelial cells showed a detectable level of FoxO1 albeit again lowered with respect to cell line studies.

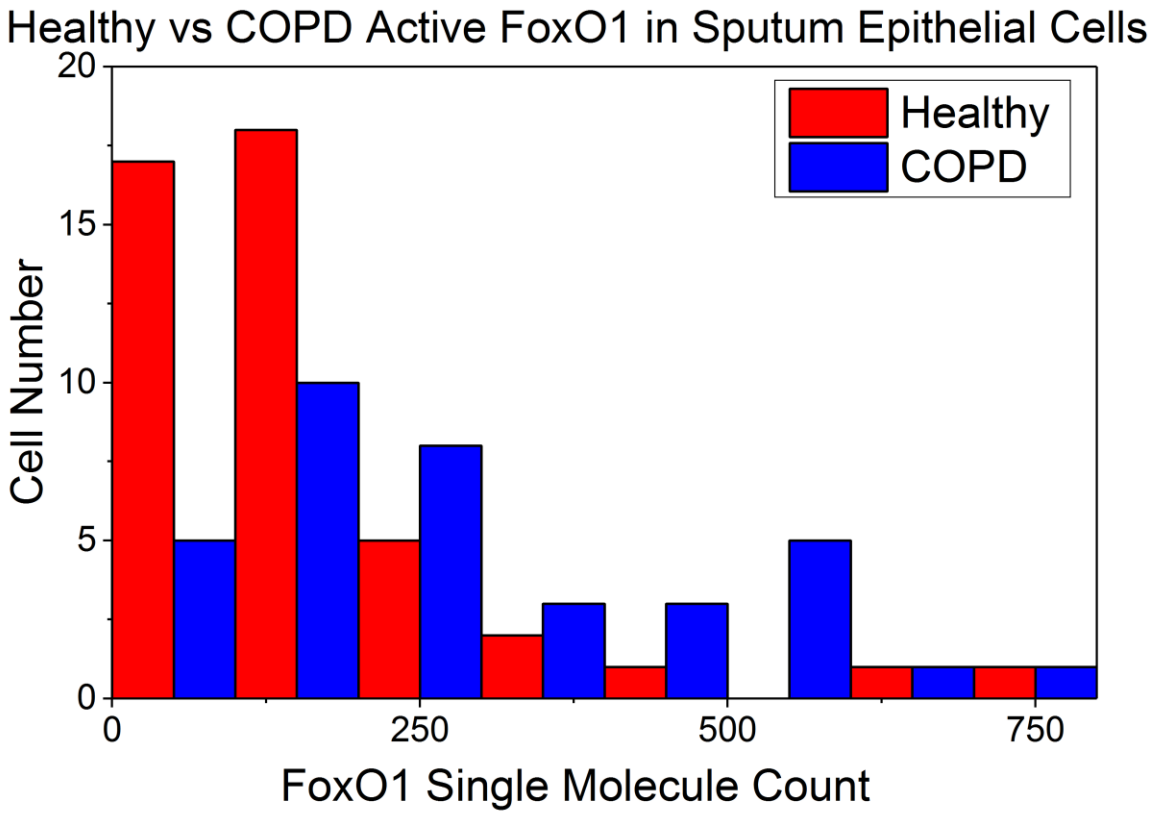


Figure 8.5 Active FoxO1 expression in 3 healthy and 3 COPD sputum derived epithelial samples compiled and compared. The expression levels observed are comparatively low expressing compared to those observed in cell line analyses and in lung resection analysis with most of the single molecule counts falling below 500 per cell.

Active FoxO1 analysis has shown again a distinct overlap, with the observed single molecule counts falling within one another. The overlap found using the Origin 2017 function was calculated to be 33%. Although given the function of the Origin overlap analysis where it takes the areas under the curve and given the distribution of these populations, the function does not consider the spread of the single molecule counts seen with both the COPD and healthy distributions. Despite this there is a trend for COPD diagnosed cells to express a higher single molecule counts of active FoxO1. This is the same trend that was observed with the lung resection epithelial sample data. Thus, this data corroborates well with the previous inferences. Given the small population analysed for both populations, there is good reason to hypothesise that with further experiments with more patients and more cells analysed that this plot will show a reduced overlap of these two populations. This data was again processed with a paired student t-test which at a of $p < 0.05$ level shows that the data sets are significantly different from each other which further bolsters the theory that increasing the data set will yield better separation of these populations.

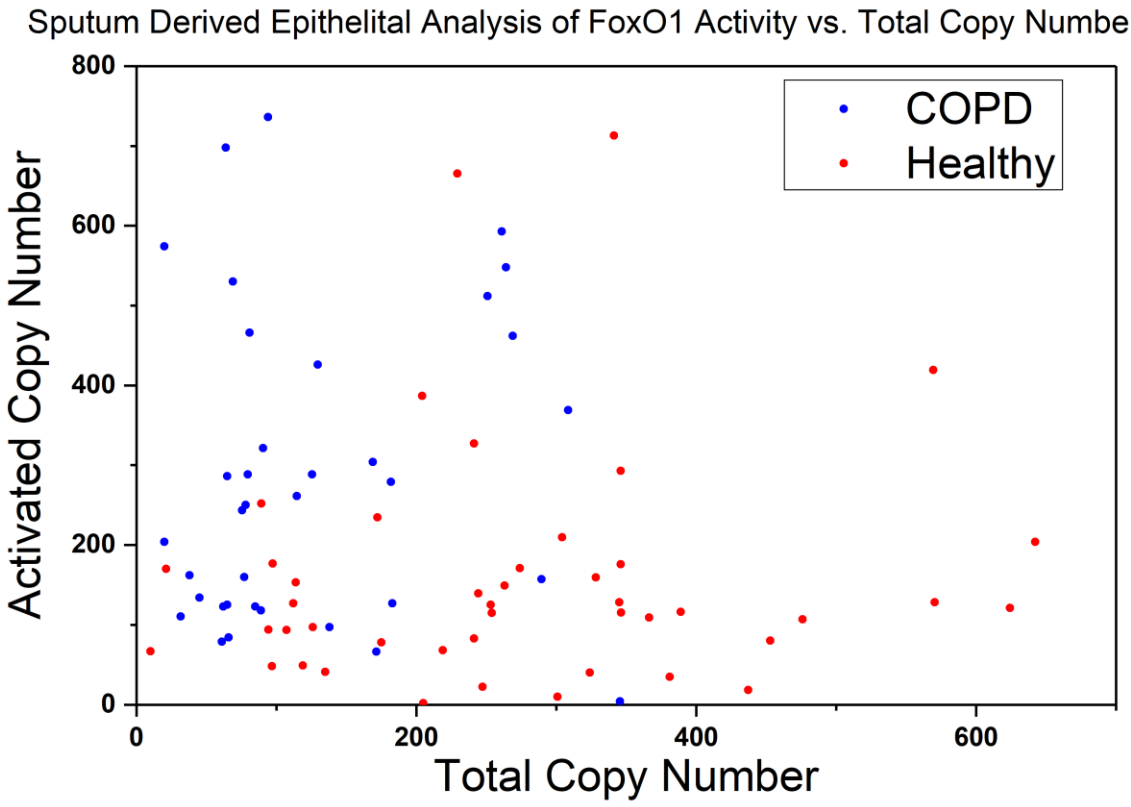


Figure 8.6 A scatter plot comparing the two assays of FoxO1 direct comparison to show the overlap of the bimultiplexed assay with healthy and COPD sputum derived epithelial cell patient samples. Each point is a single cell with total and active FoxO1 single molecule count on the x and y axis respectively. This plot shows even with both multiplexed measurements combined there is a relative overlap which might show further separation given further sample analysis.

Figure 8.6 shows the bimultiplexed analysis for sputum derived epithelial cells. Similar to the lung resection samples in Section 7.4 there is still further separation of the healthy and COPD populations by utilizing both measurements simultaneously. This scatter better demonstrates the same interesting biology that was observed with the lung resection samples, where there is a lower total copy number, yet increased FoxO1 activity observed in the COPD patient derived cells. This is the same trend as observed in Section 7.4.4 which provides greater detail as to the potential biology at play in this sample. In brief, given some key pathways involved in COPD which are; PI3K, JNK and MST1, (where PI3K has an inverse effect on FoxO1 compared to the latter proteins) it seems the dynamic interplay of these proteins has elicited a unique response of FoxO1 in COPD patients.

Table 8.4 Comparison of the mean, standard deviation (STDDEV) and standard error (STDER) of the two assays for the healthy and COPD populations, also including the calculated overlaps.

	TOTAL FOXO1 (MAB5939)			**ACTIVE FOXO1 (CA7)**		
	Healthy	COPD	% Overlap	Healthy	COPD	% Overlap

MEAN	271	126	37	158	286	33
STDDEV	154	90		148	193	
STDER	22	15		22	32	

The observed mean and standard deviation shows clear overlap which is again due to the variation seen in both the healthy and COPD derived samples, which is common place when analysing cell to cell heterogeneity. Similar to the previous patient samples the standard deviations present show a clear overlap at 2σ between the two samples. Using the described 1.96xSTDER for a 95% confidence interval, there is definition between the two populations. Although this analysis isn't particularly accurate due to the small sample sizes and because the data is not normally distributed. Although as a best fit estimate it does show no overlap between the healthy and COPD samples with a 95% confidence interval.

Table 8.5 A table showing the mean ± 1.96xSE, providing a 95% confidence interval in the obtained values. This analysis shows that the active FoxO1 samples are close to overlap and total FoxO1 measurements are well defined.

	TOTAL (ANTIBODY)			**ACTIVE FOXO1 (DNA)**		
HEALTHY	271	±	43	158	±	43
COPD	126	±	29	286	±	63

In conclusion this section has detailed the use of the MAC chip multiplexed assay on sputum derived epithelial samples in both healthy and COPD diagnosed clinical samples. The analysis has shown that both the total (mAb5939 assay) and active (CA7 assay) single molecule counts of FoxO1 show separation between the two sample populations. While this work is still in its infancy, it does show a promising start to a translatable methodology to analyse a protein of interest in patient samples derived using non-invasive methodologies.

8.4.7 Discussion of FoxO1 Measurements in Sputum Derived Epithelial Cells

The results of this assay is highly comparable to the discussion in Section 7.4.4. The same non-linear correlation is observed when comparing the total to active pools of FoxO1, where despite there being a smaller observed total copy number of FoxO1 present there is an apparent increase in the active copy number in patients diagnosed with COPD. This is the same pattern which was observed in the lung resection analysis, which is expected as both assays used epithelial derived samples.

The sputum derived epithelial cells and the lung resection tissue epithelial cells share very similar biology. Whereas sputum derived epithelial cells only come from the bronchial tract and the larger airways, lung resection tissues can be obtained from various locations in the lung (though still typically the bronchial tubes).[237] However it is sputum samples which display a far greater degree of heterogeneity in cellular composition within each sample. As the sputum samples have a far higher heterogeneity, with different terminally differentiated cells such as ciliated and secretory cells it can be challenging to obtain only one lung epithelial cell type of choice.[237] This issue compounds with the scarcity of epithelial cells present in sputum samples. Despite the challenges faced with obtaining sputum epithelial cells this work has demonstrated the feasibility of the identification and isolation of said cell type. Another important point to mention is that the increased occurrence of epithelial cells in the sputum is indicative of COPD. Epithelial cells present in the sputum are already likely in a state of stress and could already be showing cellular markers of said stress, this would also be true of cells found in healthy sputum patients also.[240] This could pose a limitation on the assays that look at FoxO1, as it is a stress induced transcription factor. Though given the current small data set there is promise that this is not an issue, but it is important to keep in mind going forward with using sputum derived cells.

In conclusion, this chapter has demonstrated the use of the two MAC chip assays to observe both total and active FoxO1 copy numbers in sputum derived epithelial cells. The healthy and COPD populations both show the same trend as seen in the lung resection data, which was to be expected as both sets of cells share an epithelial profile. Given there was the same trend observed as there was for the lung resection samples it was acceptable to draw positive conclusions as to the outcome and results seen in this section. This work is an early stage proof of concept to show the potential use of the MAC chip assay for the analysis of patient samples for a particular biomarker of interest. While there are several single cell analysis platforms which are capable of higher degrees of multiplexed analysis, the majority are incapable of efficient sorting of heterogeneous samples to a high efficiency.[6] This demonstrates the MAC chip assay's unique advantage within the ever growing field of single cell science and proteomics.

9 Conclusions and Future Work

9.1 General Conclusions

This thesis has detailed the development of two single cell sensitive assays for the detection of FoxO1. The first is comprised of an antibody-antibody pairing which can analyse the total copy number of FoxO1, the second utilised a DNA-antibody pairing which would specifically capture active FoxO1. The work presented shows the workflow to determine these capture and detection assay pairs of reagents. This is followed by validation of the assays and analysing the expression in two sources of patient derived samples. The initial workflow showed an 'open chip' method which could quickly measure several different reagents and environments to rapidly find the best performing pairs of capture and detection reagents. The assays were then successfully validated in the Toledo, MCF7 and Beas-2b cell lines under 3 conditions (basal, glucose and ZSTK474 treatment) to demonstrate the successful ability of the assays to observe phenotypic changes in both total and active FoxO1 copy number. During studies in Beas-2b cell lines, issues arose about the stability of the assays and the work pivoted to bring the assays back to a reproducible and sensitive state. Once the issues of reproducibility were repaired, the assays were taken forward for use with patient derived samples.

9.2 Assay Design and Optimisation

Previous work has seen several assays attempted, although the majority did not show the required sensitivity for single cell analysis. By developing the previously used methods, we successfully determined the optimal capture and detection reagents for both the total and active FoxO1 assays. This project also documents the first successful use of a DNA Capture Agent within the MAC chip format, which shows the potential for the use of DNA reagents in future projects to probe more specific protein isoforms.

Some of the previous assays were able to generate calibration curves, allowing the raw single molecule data to be translated to absolute copy numbers. In this project, as it was not possible to generate a calibration curve for the DNA based active FoxO1 assay, which was likely due to the recombinant protein not having the correct PTMs in order to be active. The work presented instead monitored changes in the single molecule count alone to observe phenotypic responses of FoxO1 copy number.

9.3 Assay Validation

The assays were successful in monitoring the phenotypic changes of FoxO1s total and active copy number in the 3 cell lines. The experiments placed the cells in conditions demonstrated to either increase or decrease the levels of FoxO1, with respect to the basal levels found in unperturbed cells. This work was successful in the Toledo and MCF7 cell lines until the testing of the Beas-2b cell line, which showed no binding over the background, suggesting the limit of detection was insufficient for this cell line. At this point efforts were made to replace the reagents and optimise the assay so that it had the necessary sensitivity for use with patient samples.

The optimisation studies were a success and further validation showed the assays could detect FoxO1 total and active copy numbers in the 3 cell lines. This work did however show the limitations of the assays and the importance of choosing the best capture and detection reagents. As well as determining the optimal concentrations to ensure the assays are as robust and reproducible as possible for all studies.

The development of two successful assays was an achievement and opened the doors to new studies and the opportunity to multiplex with other developed assays for a deeper and more accurate analysis of biological events at the single cell level.

9.4 Lung Resection Studies

The two validated and optimised assays were printed adjacent to each other to allow multiplexed analysis for each captured single cell. This section detailed the first use of pure patient derived samples and showed the successful analysis of said cells. The results showed an interesting pattern of total vs active copy number within the COPD derived samples when compared to the healthy samples. The data for healthy samples was directly compared with the COPD samples and showed relative separation for the copy number of FoxO1. The separation of the copy numbers suggests that, with refinement, these studies may provide a diagnostic tool for the analysis of disease states such as COPD and other respiratory inflammation diseases. The work suggested that in theory only a small number of cells would be required for the accurate diagnosis of COPD.

This work is in its infancy and before any decisive conclusions can be made the number of cells and number of patients would have to be greatly increased. The increase of experiments will show how distinct the separation of copy number is between the healthy and COPD populations. There are other limitations, such as environmental factors (smoking etc), which would affect the results and

this needs to be addressed. As smoking will exacerbate inflammatory processes and so it is important to ensure that the donor has not smoked prior to the sample donation.

9.5 Sputum Sample Studies

The lung resection studies showed that it was possible to analyse patient derived epithelial cells using the assays. This was a proof of concept analysis, to further test the ability of the assay other patient samples had to be utilised. Sputum was chosen as a source of cells for several reasons, firstly these samples are highly heterogeneous. The heterogeneity of the sample provided the opportunity to demonstrate the ability of the MAC chip to separate and collect cells of interest with 100% accuracy. Secondly collection of sputum samples is much less invasive compared to lung resection samples, which means the successful use of sputum samples demonstrates the assays ability to use non-invasive methods and still achieve single cell accuracy as a diagnostic tool.

At this time, the work only managed to show that T-cells and epithelial cells could be successfully isolated and analysed with both the total and active FoxO1 assays. The number of cells collected and analysed is too small to be able to draw firm conclusions, though it did show that there was some degree of separation of the observed single molecule counts between healthy and COPD samples in the epithelial derived cells. A larger number of patient samples would have to be collected before any suitable analysis of the diagnostic ability can be concluded. The work has however clearly demonstrated the potential of the MAC chip to analyse sputum samples effectively and reproducibly.

9.6 Future Work

This project has demonstrated the creation of two novel assays for the analysis of total and active FoxO1 with single cell sensitivity which can be utilised in not only cell lines but also patient derived samples. The use of these assays will provide new insights into the pathways of the FoxO1 network and the implications this protein has in several disease states. While it was not possible to obtain accurate calibration curves for the active FoxO1 assay, this does not mean future work cannot look to find a better recombinant protein source, or potentially a recombinant FoxO1 protein with the necessary PTMs for DNA binding. This would allow both assays to provide details on the exact copy number of FoxO1. Although the work demonstrated in this project has shown that relative single molecule count is still an extremely helpful tool. The addition of two new assays for use in the MAC

chip also expands the library of multiplexing potentials. This allows a greater level of biological detail to be disclosed, thus a greater level of understanding of disease states.

A promising avenue to explore is the idea of a four-coloured assay, which could increase the level of multiplexing by having a mixture of Capture Agents present in each spot. This combined with secondary detection antibodies tagged with different fluorophores opens the potential to increase the maximum level of multiplexing possible within the MAC chip. This would make it much easier to multiplex with other proteins of interest along with the sub populations of different PTMs or in an active state. This multiplexing would help determine the dynamics of protein expression in a single cell. There are several proteins which could be analysed upstream of FoxO1, such as PI3K, Akt, JNK or MST1 which would provide an interesting insight into the dysregulation of these paths in diseased states.

The main challenge faced for future MAC chip work is being able to develop assays with the required single cell sensitivities. Even if the capture and detection agents are very specific, they still need to have a sufficiently high affinity to allow the detection of analyte at a single cell level. There are several options to improve the sensitivity of the assays. It has been previously mentioned that a reduction in chamber volume will improve the capture efficiency, though it comes with disadvantages such as issues with cell isolation and chip alignment. Despite these current issues, other researchers have shown microfluidic systems that are able to utilise smaller volume chambers and still isolate single cells. Thus, considering the advances in microfluidics could help to improve future assay sensitivity.

A second way of expanding the library of assays by enhancing the assays sensitivity is to utilise more novel bioreagents such as aptamers and affimers. Aptamers and affimers are small peptide and nucleotide chains respectively, which are designed using novel protocols and evolved to have extremely high sensitivity towards a protein or molecule of interest. These biomolecules have similar specificity and affinity to that of antibodies but offer several advantages. Aptamers and affimers are; highly stable with respect to antibodies, they are small molecules, meaning that more can be present in a single spot which should enhance the binding kinetics, and they can be synthetically manufactured which will stop batch to batch variation. They can also be easily bio conjugated to allow covalent binding to the surface. This would help improve the stability of the assay and thus improve the reproducibility. Utilizing these methods would help to expand the number of assays developed for use with the MAC chip.

Once the MAC chip has a wide library of assays and can probe the proteome extensively, there are opportunities for it to be used in the clinic. Currently our method of administering chemotherapeutics is mostly a 'trial and error' model. This model when applied to cancer leads to a poor quality of life for the patient given the toxicity of the chemotherapies. If the MAC chip projects were to focus on designing assays for proteins targeted by these therapeutics, it would provide a novel method to better tailor drug regimens for chemotherapeutics. This project has shown that even with a small sample of cells a lot of biological information can be found. By monitoring which proteins are the largest effectors in an individual's disease state, it allows clinicians to better tailor personalised therapies to ensure the highest efficacy from the treatments and maintain a greater quality of life for the patients. The example here is cancer, although this idea is readily applicable to any disease state of interest.

To better utilise the data generated from the MAC chip, it would be a good next step to bring in a data scientist. As more data is generated which can populate the healthy vs diseased comparative plots, this can be used as training data. Once sufficient data is generated an accurate program can be created which will automatically take in any MAC data and be able to accurately diagnose whether the sample has COPD. As more assays are generated and there are higher degrees of multiplexing available, there is opportunity to design analytical tools which can look for key markers and help clinicians better infer the severity of a disease and look for early stage disease markers. Thus, better informing the optimal course of treatment for the patient.

10 References

1 E. F. Petricoin, K. C. Zoon, E. C. Kohn, J. C. Barrett and L. a Liotta, *Nat. Rev. Drug Discov.*, 2002, **1**, 683–95.

2 G. MacBeath, *Nat. Genet.*, 2002, **32 Suppl**, 526–32.

3 P. Liang and A. B. Pardee, *Nat. Rev. Cancer*, 2003, **3**, 869–76.

4 J. P. Le Quesne, K. A. Spriggs, M. Bushell and A. E. Willis, *J. Pathol.*, 2010, 220, 140–151.

5 J. L. Freeman, *Genome Res.*, 2006, **16**, 949–961.

6 M. Mondal, R. Liao and J. Guo, *Chem. - A Eur. J.*, 2018, 1–10.

7 Q. Xu and K. S. Lam, *J. Biomed. Biotechnol.*, 2003, **2003**, 257–266.

8 a F. M. Altelaar and A. J. R. Heck, *Curr. Opin. Chem. Biol.*, 2012, **16**, 206–13.

9 M. Stoneley and A. E. Willis, *Curr Mol Med*, 2003, **3**, 597–603.

10 T. N. Seyfried and L. C. Huysentruyt, *Crit. Rev. Oncog.*, 2013, **18**, 43–73.

11 E. L. Burnham, W. R. Taylor, A. A. Quyyumi, M. Rojas, K. L. Brigham and M. Moss, *Am. J. Respir. Crit. Care Med.*, 2005, **172**, 854–860.

12 S. Nagrath, L. V Sequist, S. Maheswaran, D. W. Bell, P. Ryan, U. J. Balis, R. G. Tompkins and D. A. Haber, *Nature*, 2007, **450**, 1235–1239.

13 M. Cristofanilli, G. T. Budd, M. J. Ellis, A. Stopeck, J. Matera, M. C. Miller, J. M. Reuben, G. V. Doyle, W. J. Allard, L. W. M. M. Terstappen and D. F. Hayes, *N. Engl. J. Med.*, 2004, **351**, 781–791.

14 M. Barclay and Michael, Imperial College London, 2017.

15 D. Di Carlo, K.-H. Jeong and L. P. Lee, *Lab Chip*, 2003, **3**, 287.

16 R. H. Templer and O. Ces, *J. R. Soc. Interface*, 2008, **5 Suppl 2**, S111-2.

17 O. Rinner, L. N. Mueller, M. Hubálek, M. Müller, M. Gstaiger and R. Aebersold, *Nat. Biotechnol.*, 2007, **25**, 345–352.

18 R. Fan, O. Vermesh, A. Srivastava, B. K. H. Yen, L. Qin, H. Ahmad, G. a Kwong, C.-C. Liu, J. Gould, L. Hood and J. R. Heath, *Nat. Biotechnol.*, 2008, **26**, 1373–8.

19 Q. Shi, L. Qin, W. Wei, F. Geng, R. Fan, Y. Shik Shin, D. Guo, L. Hood, P. S. Mischel and J. R. Heath, *Proc. Natl. Acad. Sci.*, 2012, **109**, 419–424.

20 E. Burgin, A. Salehi-Reyhani, M. Barclay, A. Brown, J. Kaplinsky, M. Novakova, M. a a Neil, O. Ces, K. R. Willison and D. R. Klug, *Analyst*, 2014, **139**, 3235–44.

21 A. J. Hughes, D. P. Spelke, Z. Xu, C.-C. Kang, D. V Schaffer and A. E. Herr, *Nat. Methods*, 2014, **11**, 749–55.

22 S. C. Bendall, E. F. Simonds, P. Qiu, E. A. D. Amir, P. O. Krutzik, R. Finck, R. V Bruggner, R. Melamed, A. Trejo, O. I. Ornatsky, R. S. Balderas, S. K. Plevritis, K. Sachs, D. Pe'er, S. D. Tanner and G. P. Nolan, *Science (80-.).*, 2011, **332**, 687–696.

23 K. J. Meaburn, P. R. Gudla, S. Khan, S. J. Lockett and T. Misteli, *J. Cell Biol.*, 2009, **187**, 801–12.

24 P. Rompolas, K. R. Mesa and V. Greco, *Nature*, 2013, **502**, 513–518.

25 C. Giesen, H. A. O. Wang, D. Schapiro, N. Zivanovic, A. Jacobs, B. Hattendorf, P. J. Schüffler, D. Grolimund, J. M. Buhmann, S. Brandt, Z. Varga, P. J. Wild, D. Günther and B. Bodenmiller, *Nat. Methods*, 2014, **11**, 417–422.

26 W. Schubert, B. Bonnekoh, A. J. Pommer, L. Philipsen, R. Böckelmann, Y. Malykh, H. Gollnick, M. Friedenberger, M. Bode and A. W. M. Dress, *Nat. Biotechnol.*, 2006, **24**, 1270–1278.

27 J.-R. Lin, M. Fallahi-Sichani and P. K. Sorger, *Nat. Commun.*, 2015, **6**, 8390.

28 P. Zrazhevskiy and X. Gao, *Nat. Commun.*, 2013, **4**, 1619.

29 R. von Wasielewski, M. Mengel, S. Gignac, L. Wilkens, M. Werner and A. Georgii, *J. Histochem. Cytochem.*, 1997, **45**, 1455–1459.

30 S. L. Stott, C.-H. C.-H. Hsu, D. I. Tsukrov, M. Yu, D. T. Miyamoto, B. a. Waltman, S. M. Rothenberg, A. M. Shah, M. E. Smas, G. K. Korir, F. P. Floyd, A. J. Gilman, J. B. Lord, D. Winokur, S. Springer, D. Irimia, S. Nagrath, L. V. Sequist, R. J. Lee, K. J. Isselbacher, S. Maheswaran, D. a. Haber and M. Toner, *October*, 2010, **107**, 18392–7.

31 A. Palmieri, S. V. Ley, K. Hammond, A. Polyzos and I. R. Baxendale, *Tetrahedron Lett.*, 2009, **50**, 3287–3289.

32 Y. S. Shin, H. Ahmad, Q. Shi, H. Kim, T. a Pascal, R. Fan, W. A. Goddard and J. R. Heath, *Chemphyschem*, 2010, **11**, 3063–9.

33 A. J. Magness, J. Squires, B. Griffiths, K. Khan, A. Swain, K. Willison, D. Cunningham, M. Gerlinger and D. Klug, *Converg. Sci. Phys. Oncol.*, 2017.

34 N. Li Jeon, S. K. W Dertinger, D. T. Chiu, I. S. Choi, A. D. Stroock and G. M. Whitesides, 2000.

35 A. Salehi-Reyhani, S. Sharma, E. Burgin, M. Barclay, A. Cass, M. a a Neil, O. Ces, K. R. Willison and D. R. Klug, *Lab Chip*, 2013, **13**, 2066–74.

36 E. A. Ottesen, J. W. Hong, S. R. Quake and J. R. Leadbetter, *Science (80-.).*, 2006, **314**, 1464–1467.

37 V. Chaitankar, G. Karakülah, R. Ratnapriya, F. O. Giuste, M. J. Brooks and A. Swaroop, *Prog. Retin. Eye Res.*, 2016, 55, 1–31.

38 R. Martins, G. J. Lithgow and W. Link, *Aging Cell*, 2015, 1–12.

39 A. Eijkelenboom and B. M. T. Burgering, *Nat. Rev. Mol. Cell Biol.*, 2013, **14**, 83–97.

40 K. Hannenhalli, Sridhar ; H. Kaestner, *Nat. Rev. Genet.*, 2009, **10**, 233–240.

41 E. Lai, V. R. Prezioso, E. Smith, O. Litvin, R. Costa and J. Darnell J. E., *Genes Dev.*, 1990, **4**, 1427–1436.

42 D. Weigel and H. Jäckle, *Cell*, 1990, **63**, 455–456.

43 S. Kousteni, *Bone*, 2012, 50, 437–443.

44 D. N. Gross, M. Wan and M. J. Birnbaum, *Curr. Diab. Rep.*, 2009, 9, 208–214.

45 J. Zhao, J. J. Brault, A. Schild, P. Cao, M. Sandri, S. Schiaffino, S. H. Lecker and A. L. Goldberg, *Cell Metab.*, 2007, **6**, 472–483.

46 T. Becker, G. Loch, M. Beyer, I. Zinke, A. C. Aschenbrenner, P. Carrera, T. Inhester, J. L. Schultze and M. Hoch, *Nature*, 2010, **463**, 369–73.

47 Z. Li, H. Zhang, Y. Chen, L. Fan and J. Fang, *J. Biol. Chem.*, 2012, **287**, 17737–45.

48 A. K. Brown and A. E. Webb, *Curr. Top. Dev. Biol.*, 2018, **127**, 165–192.

49 D. Calnan and A. Brunet, *Oncogene*, 2008, 2276–2288.

50 K. Siddle, *J. Mol. Endocrinol.*, 2011, **47**, R1-10.

51 K. Okkenhaug, *Annu. Rev. Immunol.*, 2013, **31**, 675–704.

52 R. Fritsch and J. Downward, *Cell*, 2013, **154**, 940-940.e1.

53 T. Yamamori, O. Inanami, H. Nagahata and M. Kuwabara, *Biochem. Biophys. Res. Commun.*, 2004, **316**, 720–30.

54 S. Guo, *J. Endocrinol.*, 2014, **220**, T1–T23.

55 C. J. Vlahos, W. F. Matter, K. Y. Hui and R. F. Brown, *J. Biol. Chem.*, 1994, **269**, 5241–8.

56 X. Zhang, N. Tang, T. J. Hadden and A. K. Rishi, *Biochim. Biophys. Acta - Mol. Cell Res.*, 2011, **1813**, 1978–86.

57 H. Daitoku, J.-I. Sakamaki and A. Fukamizu, *Biochim. Biophys. Acta*, 2011, **1813**, 1954–60.

58 W. Zhang, S. Patil, B. Chauhan, S. Guo, D. R. Powell, J. Le, A. Klotsas, R. Matika, X. Xiao, R. Franks, K. a Heidenreich, M. P. Sajan, R. V Farese, D. B. Stolz, P. Tso, S.-H. Koo, M. Montminy and T. G. Unterman, *J. Biol. Chem.*, 2006, **281**, 10105–17.

59 H. Tran, A. Brunet, J. M. Grenier, S. R. Datta, A. J. Fornace, P. S. DiStefano, L. W. Chiang, M. E. Greenberg, K. Lin, J. B. Dorman, A. Rodan, C. Kenyon, A. J. Fornace, P. S. DiStefano, L. W. Chiang and M. E. Greenberg, *Science*, 2002, **296**, 530–4.

60 S. Guo, G. Rena, S. Cichy, X. He, P. Cohen and T. Unterman, *J. Biol. Chem.*, 1999, **274**, 17184–92.

61 X. Zhang, L. Gan, H. Pan, S. Guo, X. He, S. T. Olson, A. Mesecar, S. Adam and T. G. Unterman, *J. Biol. Chem.*, 2002, **277**, 45276–84.

62 L. Qiang, A. S. Banks and D. Accili, *J. Biol. Chem.*, 2010, **285**, 27396–401.

63 H. Huang and D. J. Tindall, *J. Cell Sci.*, 2007, **120**, 2479–87.

64 H. Matsuzaki and H. Daitoku, *Proc. Natl. Acad. Sci.*, 2003, **100**, 11285–11290.

65 G. Rena, Y. L. Woods, A. R. Prescott, M. Peggie, T. G. Unterman, M. R. Williams and P. Cohen, *EMBO J.*, 2002, **21**, 2263–71.

66 X. Zhao, L. Gan, H. Pan, D. Kan, M. Majeski, S. A. Adam and T. G. Unterman, *Biochem. J.*, 2004, **378**, 839–49.

67 H. Lu, P. Liu, Y. Pan and H. Huang, *Neoplasia*, 2011, **13**, 854–863.

68 A. Brunet, L. Sweeney, J. Fitzhugh Sturgill, K. Chua, P. Greer, Y. Lin, H. Tran, S. Ross, R. Mostoslavsky, H. Cohen, L. Hu, H. Cheng, M. Jedrychowski, S. Gygi, D. Sinclair, F. Alt and M. Greenberg, *Science (80-.).*, 2004, **303**, 2011–2015.

69 Y. I. Kitamura, T. Kitamura, J.-P. Kruse, J. C. Raum, R. Stein, W. Gu and D. Accili, *Cell Metab.*, 2005, **2**, 153–63.

70 M. A. G. Essers, S. Weijzen, A. M. M. De Vries-smits, N. D. De Ruiter and L. Johannes, *EMBO J.*, 2004, **23**, 4802–4812.

71 M. M. Brent, R. Anand and R. Marmorstein, *Structure*, 2008, **16**, 1407–16.

72 J. Sunayama, F. Tsuruta, N. Masuyama and Y. Gotoh, *J. Cell Biol.*, 2005, **170**, 295–304.

73 J. D. Graves, Y. Gotoh, K. E. Draves, D. Ambrose, D. K. M. Han, M. Wright, J. Chernoff, E. A.

Clark and E. G. Krebs, *EMBO J.*, 1998, **17**, 2224–34.

74 B. Shen, L. Chao and J. Chao, *Am. J. Physiol. Heart Circ. Physiol.*, 2010, **298**, H1048-54.

75 L.-O. O. Klotz, C. Sánchez-Ramos, I. Prieto-Arroyo, P. Urbánek, H. Steinbrenner and M. Monsalve, *Redox regulation of FoxO transcription factors*, Elsevier, 2015, vol. 6.

76 T. N. Schachter, T. Shen, Y. Liu and M. F. Schneider, *Am. J. Physiol. Cell Physiol.*, 2012, **303**, C977-90.

77 A. Brunet, L. B. Sweeney, J. F. Sturgill, K. F. Chua, P. L. Greer, Y. Lin, H. Tran, S. E. Ross, R. Mostoslavsky, H. Y. Cohen, L. S. Hu, H.-L. Cheng, M. P. Jedrychowski, S. P. Gygi, D. A. Sinclair, F. W. Alt and M. E. Greenberg, *Science*, 2004, **303**, 2011–5.

78 Y. S. Hori, A. Kuno, R. Hosoda and Y. Horio, *PLoS One*, 2013, **8**, e73875.

79 T. B. Dansen, L. M. M. Smits, M. H. van Triest, P. L. J. de Keizer, D. van Leenen, M. G. Koerkamp, A. Szypowska, A. Meppelink, A. B. Brenkman, J. Yodoi, F. C. P. Holstege and B. M. T. Burgering, *Nat. Chem. Biol.*, 2009, **5**, 664–672.

80 H. Daitoku, M. Hatta, H. Matsuzaki, S. Aratani, T. Ohshima, M. Miyagishi, T. Nakajima and A. Fukamizu, *Proc. Natl. Acad. Sci. U. S. A.*, 2004, **101**, 10042–7.

81 Y. S. Mao, B. Zhang and D. L. Spector, *Trends Genet.*, 2011, **27**, 295–306.

82 H. Matsuzaki, H. Daitoku, M. Hatta, H. Aoyama, K. Yoshimochi, A. Fukamizu and P. K. Vogt, .

83 T. Furuyama, H. Yamashita, K. Kitayama, Y. Higami, I. Shimokawa and N. Mori, *Microsc. Res. Tech.*, 2002, **59**, 331–334.

84 A. van der Horst, B. M. T. Burgering, F. Baluška, A. Hlavacka, D. Volkmann, D. Menzel, Y. S. Hori, A. Kuno, R. Hosoda, Y. Horio, J. W. Hwang, H. Yao, S. Caito, I. K. Sundar, I. Rahman, H. Matsuzaki, H. Daitoku, M. Hatta, K. Tanaka, A. Fukamizu, A. van der Horst, A. M. M. de Vries-Smits, A. B. Brenkman, M. H. van Triest, N. van den Broek, F. Colland, M. M. Maurice, B. M. T. Burgering, F. Seiler, J. Hellberg, P. M. Lepper, A. Kamyschnikow, C. Herr, M. Bischoff, F. Langer, H.-J. Schafers, F. Lammert, M. D. Menger, R. Bals, C. Beisswenger, E. L. Greer, A. Brunet, H. Huang, K. M. Regan, Z. Lou, J. Chen, D. J. Tindall, X. Zhang, N. Tang, T. J. Hadden and A. K. Rishi, *Nat. Cell Biol.*, 2013, **8**, 1064–1073.

85 M. E. Giannakou and L. Partridge, *Trends Cell Biol.*, 2004, **14**, 404–8.

86 E. L. Greer and A. Brunet, *Oncogene*, 2005, **24**, 7410–25.

87 M. C. Motta, N. Divecha, M. Lemieux, C. Kamel, D. Chen, W. Gu, Y. Bultsma, M. McBurney and L. Guarente, *Cell*, 2004, **116**, 551–563.

88 T. F. Liu and C. E. McCall, *Genes Cancer*, 2013, **4**, 135–47.

89 H. Matsuzaki, H. Daitoku, M. Hatta, K. Tanaka and A. Fukamizu, *Insulin*, 2003, **100**, 11285–11290.

90 M. Aoki, H. Jiang and P. K. Vogt, 2004.

91 A. van der Horst, A. M. M. M. de Vries-Smits, A. B. Brenkman, M. H. van Triest, N. van den Broek, F. Colland, M. M. Maurice and B. M. T. T. Burgering, *Nat. Cell Biol.*, 2006, **8**, 1064–73.

92 T. Obsil and V. Obsilova, *Oncogene*, 2008, 27, 2263–2275.

93 Y. Furukawa-Hibi, Y. Kobayashi, C. Chen and N. Motoyama, *Antioxid. Redox Signal.*, 2005, **7**, 752–760.

94 K.-L. Tsai, Y.-J. Sun, C.-Y. Huang, J.-Y. Yang, M.-C. Hung and C.-D. Hsiao, *Nucleic Acids Res.*,

2007, **35**, 6984–94.

95 J. Weigelt, I. Climent, K. Dahlman-Wright and M. Wikström, *Biochemistry*, 2001, **40**, 5861–9.

96 S. C. Martinez, C. Cras-Méneur, E. Bernal-Mizrachi and M. A. Permutt, *Diabetes*, 2006, **55**, 1581–1591.

97 R. S. Streeper, C. A. Svitek, S. Chapman, L. E. Greenbaum, R. Taub and R. M. O'Brien, *J. Biol. Chem.*, 1997, **272**, 11698–701.

98 T. Obsil and V. Obsilova, *Biochim. Biophys. Acta*, 2011, **1813**, 1946–53.

99 E. Boura, J. Silhan, P. Herman, J. Vecer, M. Sulc, J. Teisinger, V. Obsilova and T. Obsil, *J. Biol. Chem.*, 2007, **282**, 8265–75.

100 M. Doucet, A. Dubé, D. R. Joanisse, R. Debigaré, A. Michaud, M.-È. Paré, R. Vaillancourt, E. Fréchette and F. Maltais, *Thorax*, 2010, **65**, 963–70.

101 A. S. Gershon, L. Warner, P. Cascagnette, J. C. Victor and T. To, *Lancet*, 2011, **378**, 991–996.

102 J. Vestbo, S. S. Hurd, A. G. Agustí, P. W. Jones, C. Vogelmeier, A. Anzueto, P. J. Barnes, L. M. Fabbri, F. J. Martinez, M. Nishimura, R. A. Stockley, D. D. Sin and R. Rodriguez-Roisin, *Am. J. Respir. Crit. Care Med.*, 2013, **187**, 347–365.

103 B. Yawn, D. Mannino, T. Littlejohn, G. Ruoff, A. Emmett, I. Raphiou and G. Crater, *Curr. Med. Res. Opin.*, 2009, **25**, 2671–2677.

104 Y. R. Chen, J. M. Leung and D. D. Sin, *PLoS One*, 2016, **11**, e0158843.

105 P. J. Barnes, P. G. J. Burney, E. K. Silverman, B. R. Celli, J. Vestbo, J. A. Wedzicha and E. F. M. Wouters, *Nat. Rev. Dis. Prim.*, 2015, **1**, 15076.

106

107 T. Ingebrigtsen, S. F. Thomsen, J. Vestbo, S. van der Sluis, K. O. Kyvik, E. K. Silverman, M. Svartengren and V. Backer, *Respir. Med.*, 2010, **104**, 1890–5.

108 A. Agusti, M. Decramer, B. Celli, R. Chen, G. Criner, P. Frith, D. Halpin, M. Nishimura, R. Rodriguez-Roisin and C. Vogelmeier, *POCKET GUIDE TO COPD DIAGNOSIS, MANAGEMENT, AND PREVENTION - A Guide for Health Care Professionals*, 2017.

109 D. H. Kim, J. Y. Kim, B. P. Yu and H. Y. Chung, *Biogerontology*, 2008, **9**, 33–47.

110 D. Lee and A. L. Goldberg, *J. Biol. Chem.*, 2013, **288**, 30515–26.

111 S. F. Van Eeden and D. D. Sin, *Can. Respir. J.*, 2013, **20**, 27–29.

112 Y. Nakamaru, C. Vuppusetty, H. Wada, J. C. Milne, M. Ito, C. Rossios, M. Elliot, J. Hogg, S. Kharitonov, H. Goto, J. E. Bemis, P. Elliott, P. J. Barnes and K. Ito, *FASEB J.*, 2009, **23**, 2810–2819.

113 et al. Griffiths AJF, Miller JH, Suzuki DT, *An Introduction to Genetic Analysis. Bacterial conjugation.*, W.H. Freeman, 2000.

114 A. Alimonti, C. Nardella, Z. Chen, J. G. Clohessy, A. Carracedo, L. C. Trotman, K. Cheng, S. Varmeh, S. C. Kozma, G. Thomas, E. Rosivatz, R. Woscholski, F. Cognetti, H. I. Scher and P. P. Pandolfi, *J. Clin. Invest.*, 2010, **120**, 681–93.

115 N. Huang, I. Lee, E. M. Marcotte and M. E. Hurles, *PLoS Genet.*, 2010, **6**, 1–11.

116 J. Nakae, T. Kitamura, Y. Kitamura, W. H. Biggs, K. C. Arden and D. Accili, *Dev. Cell*, 2003, **4**, 119–29.

117 J. Nakae, W. H. Biggs, T. Kitamura, W. K. Cavenee, C. V. E. Wright, K. C. Arden and D. Accili, *Nat. Genet.*, 2002, **32**, 245–253.

118 A. Salehi-Reyhani, J. Kaplinsky, E. Burgin, M. Novakova, A. J. deMello, R. H. Templer, P. Parker, M. a a Neil, O. Ces, P. French, K. R. Willison and D. Klug, *Lab Chip*, 2011, **11**, 1256–61.

119 A. J. Magness, Imperial College London.

120 G. M. Whitesides, *Nature*, 2006, **442**, 368–73.

121 Y. Xia and G. Whitesides, *Annu. Rev. Mater. Sci.*, 1998, **28**, 153–184.

122 B. Huang, H. Wu, D. Bhaya, A. Grossman, S. Granier, B. K. Kobilka and R. N. Zare, *Science*, 2007, **315**, 81–4.

123 A. Khademhosseini, R. Langer, J. Borenstein and J. P. Vacanti, *Proc. Natl. Acad. Sci. U. S. A.*, 2006, **103**, 2480–7.

124 K. Ren, J. Zhou and H. Wu, *Acc. Chem. Res.*, 2013, **46**, 2396–2406.

125 Y. Zheng, W. Dai, D. Ryan and H. Wu, *Biomicrofluidics*, 2010, **4**, 36504.

126 C.-W. Tsao and D. L. DeVoe, *Microfluid. Nanofluidics*, 2008, **6**, 1–16.

127 K. N. Ren, Y. Z. Zheng, W. Dai, D. Ryan, C. Y. Fung and H. K. Wu, 2010, 554–556.

128 M. W. Tibbitt and K. S. Anseth, *Biotechnol. Bioeng.*, 2009, **103**, 655–63.

129 A. W. Martinez, S. T. Phillips, M. J. Butte and G. M. Whitesides, *Angew. Chem. Int. Ed. Engl.*, 2007, **46**, 1318–20.

130 M. Goebel-Stengel, A. Stengel, Y. Taché, J. R. Reeve and Jr., *Anal. Biochem.*, 2011, **414**, 38–46.

131 R. Lamichhane, A. Solem, W. Black and D. Rueda, *Methods*, 2010, **52**, 192–200.

132 X. Zhu and A. Guo, *Funct. Protein Microarrays Drug Discov.*, 2006, 53–72.

133 A. L. Mattheyses, S. M. Simon and J. Z. Rappoport, *J. Cell Sci.*, 2010, **123**, 3621–8.

134 S. Shashkova and M. C. Leake, *Biosci. Rep.*, 2017, **37**.

135 G. V. Casquillas, *Elveflow*.

136 J. A. Squires, 2017.

137 U. Sauer, *Methods Mol. Biol.*, 2011, **785**.

138 R. Wacker, H. Schröder and C. M. Niemeyer, *Anal. Biochem.*, 2004, **330**, 281–7.

139 M. Fuentes, B. C. C. Pessela, J. V Maquiese, C. Ortiz, R. L. Segura, J. M. Palomo, O. Abian, R. Torres, C. Mateo, R. Fernández-Lafuente and J. M. Guisán, *Biotechnol. Prog.*, 2004, **20**, 1134–9.

140 E. Michelini, L. Cevenini, L. Mezzanotte, A. Coppa and A. Roda, *Anal. Bioanal. Chem.*, 2010, **398**, 227–38.

141 F. Diehl, S. Grahlmann, M. Beier and J. D. Hoheisel, *Nucleic Acids Res.*, 2001, **29**, E38.

142 P. R. T. Jess, V. Garcés-Chávez, D. Smith, M. Mazilu, L. Paterson, a Riches, C. S. Herrington, W. Sibbett and K. Dholakia, *Opt. Express*, 2006, **14**, 5779–91.

143 A. Ashkin and J. Dziedzic, *Science (80-.).*, 1987, **235**, 1517–1520.

144 K. R. Rau, P. a Quinto-Su, A. N. Hellman and V. Venugopalan, *Biophys. J.*, 2006, **91**, 317–29.

145 V. Ho, *Making cell microscopy quantitative by creating a secondary standard BSc Chemistry*,

London, 2016.

146 A. Herbert, .

147 D. G. Altman, M. Altman and J. M. Bland, *BMJ Br. Med. J. Br. Med. J. BMJ*, 1995, **310**, 29828–3317.

148 P. J. Barnes, *J. Allergy Clin. Immunol.*, 2016, **138**, 16–27.

149 V. M. Keatings, D. J. Evans, B. J. O'Connor and P. J. Barnes, *Thorax*, 1997, **52**, 372–374.

150 S. D. H. Chan, G. Luedke, M. Valer, C. Buhlmann and T. Preckel, *Cytometry. A*, 2003, **55**, 119–25.

151 M. J. Holtzman, D. E. Byers, J. Alexander-Brett and X. Wang, *Nat. Rev. Immunol.*, 2014, **14**, 686–698.

152 P. Saviranta, R. Okon, A. Brinker, M. Warashina, J. Eppinger and B. H. Geierstanger, *Clin. Chem.*, 2004, **50**, 1907–20.

153 P. Peluso, D. S. Wilson, D. Do, H. Tran, M. Venkatasubbaiah, D. Quincy, B. Heidecker, K. Poindexter, N. Tolani, M. Phelan, K. Witte, L. S. Jung, P. Wagner and S. Nock, *Anal. Biochem.*, 2003, **312**, 113–24.

154 M. F. Berger and M. L. Bulyk, *Nat. Protoc.*, 2009, **4**, 393–411.

155 R. Wacker and C. M. Niemeyer, *Chembiochem*, 2004, **5**, 453–9.

156 M. Kimoto, R. Yamashige, K. Matsunaga, S. Yokoyama and I. Hirao, *Nat. Biotechnol.*, 2013, **31**, 453–7.

157 R. Bailey and G. Kwong, *J. Am. Chem. Soc.*, 2007, **129**, 1959–1967.

158 M. L. Bulyk, X. Huang, Y. Choo and G. M. Church, *Proc. Natl. Acad. Sci. U. S. A.*, 2001, **98**, 7158–63.

159 Y. Zhao, W. Shao, H. Wei, J. Qiao, Y. Lu, Y. Sun, K. Mitchelson, J. Cheng and Y. Zhou, *J. Proteome Res.*, 2008, **7**, 1315–25.

160 D. Juncker, P.-S. Lo, H. Li, V. Laforte and S. Bergeron, *Anal. Bioanal. Chem.*, 2015, **407**, 8451–8462.

161 H. F. Liu, J. Ma, C. Winter and R. Bayer, *MAbs*, 2010, 2, 480–499.

162 W. Liu, S. Wang, L. Gao, F. Zhang and J. Xu, *J. Chem. Inf. Comput. Sci.*, 2003, **43**, 2014–2018.

163 C. C. Chou, C. H. Chen, T. T. Lee and K. Peck, *Nucleic Acids Res.*, 2004, **32**, e99.

164 R. M. Simon, *Design and analysis of DNA microarray investigations*, Springer, 2003.

165 A. Sidhu, P. Miller, K. Johanson and A. Hollenbach, *Biochemistry*, 2008, 6809–6818.

166 A. M. Sochaj, K. W. Świderska and J. Otlewski, *Biotechnol. Adv.*, 2015, 33, 775–784.

167 D. Di Carlo, L. Y. Wu and L. P. Lee, *Lab Chip*, 2006, **6**, 1445–9.

168 C.-P. Jen, J.-H. Hsiao and N. a Maslov, *Sensors (Basel).*, 2012, **12**, 347–58.

169 M. Berrar, Daniel P., Dubitzky, Werner, Granzow, *A Practical Approach to Microarray Data Analysis*, 2003.

170 E. Berglund, C. Borrebaeck, P. Delfani, A. Gerdtsson, L. Dexlin-Mellby and C. Wingren, *Microarrays*, 2016, **5**, 16.

171 J. E. Lee, J. H. Seo, C. S. Kim, Y. Kwon, J. H. Ha, S. S. Choi and H. J. Cha, *Korean J. Chem. Eng.*,

2013, **30**, 1934–1938.

172 A. Makaraviciute and A. Ramanaviciene, *Biosens. Bioelectron.*, 2013, **50**, 460–71.

173 B. Hua, K. Y. Han, R. Zhou, H. Kim, X. Shi, S. C. Abeysirigunawardena, A. Jain, D. Singh, V. Aggarwal, S. A. Woodson and T. Ha, *Nat. Methods*, 2014, **11**, 1233–1236.

174 P. Pollheimer, B. Taskinen, A. Scherfler, S. Gusenkov, M. Creus, P. Wiesauer, D. Zauner, W. Schöfberger, C. Schwarzinger, A. Ebner, R. Tampé, H. Stutz, V. P. Hytönen and H. J. Gruber, *Bioconjug. Chem.*, 2013, **24**, 1656–68.

175 J. M. Baskin, J. A. Prescher, S. T. Laughlin, N. J. Agard, P. V Chang, I. A. Miller, A. Lo, J. A. Codelli and C. R. Bertozzi, *Proc. Natl. Acad. Sci.*, 2007, **104**, 16793–16797.

176 N. J. Agard, J. M. Baskin, J. A. Prescher, A. Lo and C. R. Bertozzi, *ACS Chem. Biol.*, 2006, 1, 644–648.

177 S. a Omori, M. H. Cato, A. Anzelon-Mills, K. D. Puri, M. Shapiro-Shelef, K. Calame and R. C. Rickert, *Immunity*, 2006, **25**, 545–57.

178 A. Bilancio, K. Okkenhaug, M. Camps, J. L. Emery, T. Ruckle, C. Rommel and B. Vanhaesebroeck, *Blood*, 2006, **107**, 642–50.

179 H. S. Dengler, G. V Baracho, S. A. Omori, S. Bruckner, K. C. Arden, D. H. Castrillon, R. A. DePinho and R. C. Rickert, *Nat. Immunol.*, 2008, **9**, 1388–1398.

180 S. Furukawa, L. Wei, S. M. Krams, C. O. Esquivel and O. M. Martinez, *Am. J. Transplant*, 2013, **13**, 2035–43.

181

182 A. M. Shore, P. C. White, R. C.-Y. Hui, A. Essafi, E. W.-F. Lam, M. Rowe and P. Brennan, *J. Virol.*, 2006, **80**, 11191–11199.

183 E. Lakatos, A. Salehi-Reyhani, M. Barclay, M. P. H. Stumpf and D. R. Klug, *PLoS One*, 2017, **12**.

184 D. Kong and T. Yamori, *Cancer Sci.*, 2007, **98**, 1638–1642.

185 S. I. Yaguchi, Y. Fukui, I. Koshimizu, H. Yoshimi, T. Matsuno, H. Gouda, S. Hirono, K. Yamazaki and T. Yamori, *J. Natl. Cancer Inst.*, 2006, **98**, 545–556.

186 P. S. Swain, M. B. Elowitz and E. D. Siggia, *Proc. Natl. Acad. Sci. U. S. A.*, 2002, **99**, 12795–800.

187 M. Soltani, C. A. Vargas-Garcia, D. Antunes and A. Singh, *PLOS Comput. Biol.*, 2016, **12**, e1004972.

188 A. D. Kohn, S. A. Summers, M. J. Birnbaum and R. A. Roth, *J. Biol. Chem.*, 1996, **271**, 31372–8.

189 R. L. Elstrom, D. E. Bauer, M. Buzzai, R. Karnauskas, M. H. Harris, D. R. Plas, H. Zhuang, R. M. Cinalli, A. Alavi, C. M. Rudin and C. B. Thompson, *Cancer Res.*, 2004, **61**, 7349–7355.

190 R. B. Robey and N. Hay, *Semin. Cancer Biol.*, 2009, **19**, 25–31.

191 D.-I. Kim, S.-K. Lim, M.-J. Park, H.-J. Han, G.-Y. Kim and S. H. Park, *Life Sci.*, 2007, **80**, 626–632.

192 J. F. Clarke, P. W. Young, K. Yonezawa, M. Kasuga and G. D. Holman, *Biochem. J.*, 1994, **300 (Pt 3)**, 631–5.

193 A. Barthel, S. T. Okino, J. Liao, K. Nakatani, J. Li, J. P. Whitlock and R. A. Roth, *J. Biol. Chem.*, 1999, **274**, 20281–6.

194 S. Miyamoto, A. N. Murphy and J. H. Brown, *Cell Death Differ.*, 2008, **15**, 521–529.

195 F. Das, N. Ghosh-Choudhury, N. Dey, A. Bera, M. M. Mariappan, B. S. Kasinath and G. Ghosh Choudhury, *J. Biol. Chem.*, 2014, **289**, 32703–16.

196 E. J. Williams and P. Doherty, *Mol. Cell. Neurosci.*, 1999, **13**, 272–80.

197 G. L. G. L. Rosano and E. A. Ceccarelli, *Recombinant protein expression in Escherichia coli: Advances and challenges*, Frontiers Media SA, 2014, vol. 5.

198 L. A. Palomares, S. Estrada-Mondaca and O. T. Ramírez, in *Recombinant Gene Expression*, Humana Press, New Jersey, 2004, pp. 015–052.

199 A. Vera, N. González-Montalbán, A. Arís and A. Villaverde, *Biotechnol. Bioeng.*, 2007, **96**, 1101–1106.

200 G. L. Rosano and E. A. Ceccarelli, *Front. Microbiol.*, 2014, **5**, 172.

201 M. Putker, H. Vos, K. Van Dorenmalen, H. De Ruiter, A. G. A. G. Duran, B. Snel, B. M. B. M. T. Burgering, M. Vermeulen and T. B. B. Dansen, *Antioxid. Redox Signal.*, 2014, **22**, 15–28.

202 C. Holohan, S. Van Schaeybroeck, D. B. Longley and P. G. Johnston, *Nat. Rev. Cancer*, 2013, **13**, 714–726.

203 H. D. Soule, J. Vazquez, A. Long, S. Albert and M. Brennan, *J. Natl. Cancer Inst.*, 1973, **51**, 1409–1413.

204 R. L. Dillon, D. E. White and W. J. Muller, *Oncogene*, 2007, **26**, 1338–1345.

205 O. Padovan-Merhar, G. P. Nair, A. G. Biaesch, A. Mayer, S. Scarfone, S. W. Foley, A. R. Wu, L. S. Churchman, A. Singh and A. Raj, *Mol. Cell*, 2015, **58**, 339–352.

206 M. Yamamoto, N. A. Patel, J. Taggart, R. Sridhar and D. R. Cooper, *Int. J. Cancer*, 1999, **83**, 98–106.

207 F. Zhao and W. T. Klimecki, *J. Appl. Toxicol.*, 2015, **35**, 945–951.

208 R. R. Reddel, Y. Ke, B. I. Gerwin, M. G. McMenamin, J. F. Lechner, R. T. Su, D. E. Brash, J. B. Park, J. S. Rhim and C. C. Harris, *Cancer Res.*, 1988, **48**, 1904–1909.

209 P. H. Michelson, M. Tigue, R. J. Panos and P. H. Sporn, *Am. J. Physiol.*, 1999, **277**, L737–L742.

210 S. D. Jayasena, *Clin. Chem.*, 1998, **44**, 86–91.

211 A. Chen and S. Yang, *Biosens. Bioelectron.*, 2015, 71, 230–242.

212 Y. L. Jeyachandran, J. A. Mielczarski, E. Mielczarski and B. Rai, *J. Colloid Interface Sci.*, 2010, **341**, 136–142.

213 A. Klug, *Annu. Rev. Biochem*, 2010, **79**, 213–31.

214 C. Sissi and M. Palumbo, *Nucleic Acids Res.*, 2009, **37**, 702–711.

215 G. Gould and A. Pearce, *Contin. Educ. Anaesth. Crit. Care Pain*, 2006, **6**, 97–100.

216 R. G. Tieleman, Y. Plantinga, D. Rinkes, G. L. Bartels, J. L. Posma, R. Cator, C. Hofman and R. P. Houben, *Europace*, 2014, **16**, 1291–5.

217 J. Durán-Cantolla, G. Zamora Almeida, O. Vegas Diaz de Guereñu, L. Saracho Rotaeche, M. Hamdan Alkhraisat, J. Durán Carro, C. Egea Santaolalla and E. Anitua, *Respirology*, 2017, **22**, 378–385.

218 S. Ganesan, B. L. Unger, A. T. Comstock, K. a Angel, P. Mancuso, F. J. Martinez and U. S. Sajjan, *Thorax*, 2013, **68**, 131–41.

219 D. G. Altman and J. M. Bland, *BMJ*, 2005, **331**, 903.

220 S. Bozinovski, R. Vlahos, M. Hansen, K. Liu and G. P. Anderson, *Int. J. COPD*, 2006, **1**, 31–38.

221 F. Seiler, J. Hellberg, P. M. Lepper, A. Kamyschnikow, C. Herr, M. Bischoff, F. Langer, H.-J. Schafers, F. Lammert, M. D. Menger, R. Bals, C. Beisswenger, H.-J. Schäfers, F. Lammert, M. D. Menger, R. Bals and C. Beisswenger, *J. Immunol.*, 2013, **190**, 1603–13.

222 S. A. McCarroll and D. M. Altshuler, *Nat. Genet.*, 2007, **39**, S37–S42.

223 J. S. Beckmann, X. Estivill and S. E. Antonarakis, *Nat. Rev. Genet.*, 2007, **8**, 639–646.

224 L. W. MATTHEWS, S. SPECTOR, J. LEMM and J. L. POTTER, *Am. Rev. Respir. Dis.*, 1963, **88**, 199–204.

225 M. T. Lopez-Vidriero, I. Das and L. Reid, *Thorax*, 1979, **34**, 512–517.

226 A. Bhowmik, T. A. Seemungal, R. J. Sapsford, J. L. Devalia and J. A. Wedzicha, *Thorax*, 1998, **53**, 953–6.

227 I. Pin, P. G. Gibson, R. Kolendowicz, A. Girgis-Gabardo, J. A. Denburg, F. E. Hargreave and J. Dolovich, *Thorax*, 1992, **47**, 25–29.

228 R. LOUIS, L. C. K. LAU, A. O. BRON, A. C. ROLDAAN, M. RADERMECKER and R. DJUKANOVIĆ, *Am. J. Respir. Crit. Care Med.*, 2000, **161**, 9–16.

229 P. Lacy, J. L. Lee and D. Vethanayagam, *Ther. Clin. Risk Manag.*, 2005, **1**, 169–79.

230 A. Bhowmik, T. A. Seemungal, R. J. Sapsford and J. A. Wedzicha, *Thorax*, 2000, **55**, 114–20.

231 I. I. Katkov and P. Mazur, *Cell Biochem. Biophys.*, 1999, **31**, 231–245.

232 I. H. Kim, J. D. Yang, D. G. Lee, H. Y. Chung and B. C. Cho, *Aesthetic Surg. J.*, 2009, **29**, 35–39.

233 K. Tatsutani, B. Rubinsky, G. Onik and R. Dahiya, *Urology*, 1996, **48**, 441–447.

234 S. M. Hedrick, R. H. Michelini, A. L. Doedens, A. W. Goldrath and E. L. Stone, *Nat. Rev. Immunol.*, 2012, **12**, 649–661.

235 P. J. Barnes and M. G. Cosio, *PLoS Med*, 2004, **1**, e20.

236 M. C.-T. Hu, D.-F. Lee, W. Xia, L. S. Golfman, F. Ou-Yang, J.-Y. Yang, Y. Zou, S. Bao, N. Hanada, H. Saso, R. Kobayashi and M.-C. Hung, *Cell*, 2004, **117**, 225–37.

237 R. G. Crystal, S. H. Randell, J. F. Engelhardt, J. Voynow and M. E. Sunday, *Proc. Am. Thorac. Soc.*, 2008, **5**, 772–777.

238 Q. Qiu, N. W. Todd, R. Li, H. Peng, Z. Liu, H. G. Yfantis, R. L. Katz, S. A. Stass and F. Jiang, *Cancer*, 2008, **114**, 275–83.

239 J. BELDA, R. LEIGH, K. PARAMESWARAN, P. M. O'BYRNE, M. R. SEARS and F. E. HARGREAVE, *Am. J. Respir. Crit. Care Med.*, 2000, **161**, 475–478.

240 S. H. Randell, *Proc. Am. Thorac. Soc.*, 2006, **3**, 718–725.

1 E. F. Petricoin, K. C. Zoon, E. C. Kohn, J. C. Barrett and L. a Liotta, *Nat. Rev. Drug Discov.*, 2002, **1**, 683–95.

2 G. MacBeath, *Nat. Genet.*, 2002, **32 Suppl**, 526–32.

3 P. Liang and A. B. Pardee, *Nat. Rev. Cancer*, 2003, **3**, 869–76.

4 J. P. Le Quesne, K. A. Spriggs, M. Bushell and A. E. Willis, *J. Pathol.*, 2010, 220, 140–151.

5 J. L. Freeman, *Genome Res.*, 2006, **16**, 949–961.

6 M. Mondal, R. Liao and J. Guo, *Chem. - A Eur. J.*, 2018, 1–10.

7 Q. Xu and K. S. Lam, *J. Biomed. Biotechnol.*, 2003, **2003**, 257–266.

8 a F. M. Altelaar and A. J. R. Heck, *Curr. Opin. Chem. Biol.*, 2012, **16**, 206–13.

9 M. Stoneley and A. E. Willis, *Curr Mol Med*, 2003, **3**, 597–603.

10 T. N. Seyfried and L. C. Huysentruyt, *Crit. Rev. Oncog.*, 2013, **18**, 43–73.

11 E. L. Burnham, W. R. Taylor, A. A. Quyyumi, M. Rojas, K. L. Brigham and M. Moss, *Am. J. Respir. Crit. Care Med.*, 2005, **172**, 854–860.

12 S. Nagrath, L. V Sequist, S. Maheswaran, D. W. Bell, P. Ryan, U. J. Balis, R. G. Tompkins and D. A. Haber, *Nature*, 2007, **450**, 1235–1239.

13 M. Cristofanilli, G. T. Budd, M. J. Ellis, A. Stopeck, J. Matera, M. C. Miller, J. M. Reuben, G. V. Doyle, W. J. Allard, L. W. M. M. Terstappen and D. F. Hayes, *N. Engl. J. Med.*, 2004, **351**, 781–791.

14 M. Barclay and Michael, Imperial College London, 2017.

15 D. Di Carlo, K.-H. Jeong and L. P. Lee, *Lab Chip*, 2003, **3**, 287.

16 R. H. Templer and O. Ces, *J. R. Soc. Interface*, 2008, **5 Suppl 2**, S111-2.

17 O. Rinner, L. N. Mueller, M. Hubálek, M. Müller, M. Gstaiger and R. Aebersold, *Nat. Biotechnol.*, 2007, **25**, 345–352.

18 R. Fan, O. Vermesh, A. Srivastava, B. K. H. Yen, L. Qin, H. Ahmad, G. a Kwong, C.-C. Liu, J. Gould, L. Hood and J. R. Heath, *Nat. Biotechnol.*, 2008, **26**, 1373–8.

19 Q. Shi, L. Qin, W. Wei, F. Geng, R. Fan, Y. Shik Shin, D. Guo, L. Hood, P. S. Mischel and J. R. Heath, *Proc. Natl. Acad. Sci.*, 2012, **109**, 419–424.

20 E. Burgin, A. Salehi-Reyhani, M. Barclay, A. Brown, J. Kaplinsky, M. Novakova, M. a a Neil, O. Ces, K. R. Willison and D. R. Klug, *Analyst*, 2014, **139**, 3235–44.

21 A. J. Hughes, D. P. Spelke, Z. Xu, C.-C. Kang, D. V Schaffer and A. E. Herr, *Nat. Methods*, 2014, **11**, 749–55.

22 S. C. Bendall, E. F. Simonds, P. Qiu, E. A. D. Amir, P. O. Krutzik, R. Finck, R. V Bruggner, R. Melamed, A. Trejo, O. I. Ornatsky, R. S. Balderas, S. K. Plevritis, K. Sachs, D. Pe'er, S. D. Tanner and G. P. Nolan, *Science (80-.).*, 2011, **332**, 687–696.

23 K. J. Meaburn, P. R. Gudla, S. Khan, S. J. Lockett and T. Misteli, *J. Cell Biol.*, 2009, **187**, 801–12.

24 P. Rompolas, K. R. Mesa and V. Greco, *Nature*, 2013, **502**, 513–518.

25 C. Giesen, H. A. O. Wang, D. Schapiro, N. Zivanovic, A. Jacobs, B. Hattendorf, P. J. Schüffler, D. Grolimund, J. M. Buhmann, S. Brandt, Z. Varga, P. J. Wild, D. Günther and B. Bodenmiller, *Nat. Methods*, 2014, **11**, 417–422.

26 W. Schubert, B. Bonnekoh, A. J. Pommer, L. Philipsen, R. Böckelmann, Y. Malykh, H. Gollnick, M. Friedenberger, M. Bode and A. W. M. Dress, *Nat. Biotechnol.*, 2006, **24**, 1270–1278.

27 J.-R. Lin, M. Fallahi-Sichani and P. K. Sorger, *Nat. Commun.*, 2015, **6**, 8390.

28 P. Zrazhevskiy and X. Gao, *Nat. Commun.*, 2013, **4**, 1619.

29 R. von Wasielewski, M. Mengel, S. Gignac, L. Wilkens, M. Werner and A. Georgii, *J. Histochem. Cytochem.*, 1997, **45**, 1455–1459.

30 S. L. Stott, C.-H. C.-H. Hsu, D. I. Tsukrov, M. Yu, D. T. Miyamoto, B. a. Waltman, S. M. Rothenberg, A. M. Shah, M. E. Smas, G. K. Korir, F. P. Floyd, A. J. Gilman, J. B. Lord, D. Winokur, S. Springer, D. Irimia, S. Nagrath, L. V. Sequist, R. J. Lee, K. J. Isselbacher, S. Maheswaran, D. a. Haber and M. Toner, *October*, 2010, **107**, 18392–7.

31 A. Palmieri, S. V. Ley, K. Hammond, A. Polyzos and I. R. Baxendale, *Tetrahedron Lett.*, 2009, **50**, 3287–3289.

32 Y. S. Shin, H. Ahmad, Q. Shi, H. Kim, T. a Pascal, R. Fan, W. A. Goddard and J. R. Heath, *Chemphyschem*, 2010, **11**, 3063–9.

33 A. J. Magness, J. Squires, B. Griffiths, K. Khan, A. Swain, K. Willison, D. Cunningham, M. Gerlinger and D. Klug, *Converg. Sci. Phys. Oncol.*, 2017.

34 N. Li Jeon, S. K. W Dertinger, D. T. Chiu, I. S. Choi, A. D. Stroock and G. M. Whitesides, 2000.

35 A. Salehi-Reyhani, S. Sharma, E. Burgin, M. Barclay, A. Cass, M. a a Neil, O. Ces, K. R. Willison and D. R. Klug, *Lab Chip*, 2013, **13**, 2066–74.

36 E. A. Ottesen, J. W. Hong, S. R. Quake and J. R. Leadbetter, *Science (80-.).*, 2006, **314**, 1464–1467.

37 V. Chaitankar, G. Karakülah, R. Ratnapriya, F. O. Giuste, M. J. Brooks and A. Swaroop, *Prog. Retin. Eye Res.*, 2016, 55, 1–31.

38 R. Martins, G. J. Lithgow and W. Link, *Aging Cell*, 2015, 1–12.

39 A. Eijkelenboom and B. M. T. Burgering, *Nat. Rev. Mol. Cell Biol.*, 2013, **14**, 83–97.

40 K. Hannenhalli, Sridhar ; H. Kaestner, *Nat. Rev. Genet.*, 2009, **10**, 233–240.

41 E. Lai, V. R. Prezioso, E. Smith, O. Litvin, R. Costa and J. Darnell J. E., *Genes Dev.*, 1990, **4**, 1427–1436.

42 D. Weigel and H. Jäckle, *Cell*, 1990, **63**, 455–456.

43 S. Kousteni, *Bone*, 2012, 50, 437–443.

44 D. N. Gross, M. Wan and M. J. Birnbaum, *Curr. Diab. Rep.*, 2009, 9, 208–214.

45 J. Zhao, J. J. Brault, A. Schild, P. Cao, M. Sandri, S. Schiaffino, S. H. Lecker and A. L. Goldberg, *Cell Metab.*, 2007, **6**, 472–483.

46 T. Becker, G. Loch, M. Beyer, I. Zinke, A. C. Aschenbrenner, P. Carrera, T. Inhester, J. L. Schultze and M. Hoch, *Nature*, 2010, **463**, 369–73.

47 Z. Li, H. Zhang, Y. Chen, L. Fan and J. Fang, *J. Biol. Chem.*, 2012, **287**, 17737–45.

48 A. K. Brown and A. E. Webb, *Curr. Top. Dev. Biol.*, 2018, **127**, 165–192.

49 D. Calnan and A. Brunet, *Oncogene*, 2008, 2276–2288.

50 K. Siddle, *J. Mol. Endocrinol.*, 2011, **47**, R1-10.

51 K. Okkenhaug, *Annu. Rev. Immunol.*, 2013, **31**, 675–704.

52 R. Fritsch and J. Downward, *Cell*, 2013, **154**, 940-940.e1.

53 T. Yamamori, O. Inanami, H. Nagahata and M. Kuwabara, *Biochem. Biophys. Res. Commun.*, 2004, **316**, 720–30.

54 S. Guo, *J. Endocrinol.*, 2014, **220**, T1–T23.

55 C. J. Vlahos, W. F. Matter, K. Y. Hui and R. F. Brown, *J. Biol. Chem.*, 1994, **269**, 5241–8.

56 X. Zhang, N. Tang, T. J. Hadden and A. K. Rishi, *Biochim. Biophys. Acta - Mol. Cell Res.*, 2011, **1813**, 1978–86.

57 H. Daitoku, J.-I. Sakamaki and A. Fukamizu, *Biochim. Biophys. Acta*, 2011, **1813**, 1954–60.

58 W. Zhang, S. Patil, B. Chauhan, S. Guo, D. R. Powell, J. Le, A. Klotsas, R. Matika, X. Xiao, R. Franks, K. a Heidenreich, M. P. Sajan, R. V Farese, D. B. Stolz, P. Tso, S.-H. Koo, M. Montminy and T. G. Unterman, *J. Biol. Chem.*, 2006, **281**, 10105–17.

59 H. Tran, A. Brunet, J. M. Grenier, S. R. Datta, A. J. Fornace, P. S. DiStefano, L. W. Chiang, M. E. Greenberg, K. Lin, J. B. Dorman, A. Rodan, C. Kenyon, A. J. Fornace, P. S. DiStefano, L. W. Chiang and M. E. Greenberg, *Science*, 2002, **296**, 530–4.

60 S. Guo, G. Rena, S. Cichy, X. He, P. Cohen and T. Unterman, *J. Biol. Chem.*, 1999, **274**, 17184–92.

61 X. Zhang, L. Gan, H. Pan, S. Guo, X. He, S. T. Olson, A. Mesecar, S. Adam and T. G. Unterman, *J. Biol. Chem.*, 2002, **277**, 45276–84.

62 L. Qiang, A. S. Banks and D. Accili, *J. Biol. Chem.*, 2010, **285**, 27396–401.

63 H. Huang and D. J. Tindall, *J. Cell Sci.*, 2007, **120**, 2479–87.

64 H. Matsuzaki and H. Daitoku, *Proc. Natl. Acad. Sci.*, 2003, **100**, 11285–11290.

65 G. Rena, Y. L. Woods, A. R. Prescott, M. Peggie, T. G. Unterman, M. R. Williams and P. Cohen, *EMBO J.*, 2002, **21**, 2263–71.

66 X. Zhao, L. Gan, H. Pan, D. Kan, M. Majeski, S. A. Adam and T. G. Unterman, *Biochem. J.*, 2004, **378**, 839–49.

67 H. Lu, P. Liu, Y. Pan and H. Huang, *Neoplasia*, 2011, **13**, 854–863.

68 A. Brunet, L. Sweeney, J. Fitzhugh Sturgill, K. Chua, P. Greer, Y. Lin, H. Tran, S. Ross, R. Mostoslavsky, H. Cohen, L. Hu, H. Cheng, M. Jedrychowski, S. Gygi, D. Sinclair, F. Alt and M. Greenberg, *Science (80-.).*, 2004, **303**, 2011–2015.

69 Y. I. Kitamura, T. Kitamura, J.-P. Kruse, J. C. Raum, R. Stein, W. Gu and D. Accili, *Cell Metab.*, 2005, **2**, 153–63.

70 M. A. G. Essers, S. Weijzen, A. M. M. De Vries-smits, N. D. De Ruiter and L. Johannes, *EMBO J.*, 2004, **23**, 4802–4812.

71 M. M. Brent, R. Anand and R. Marmorstein, *Structure*, 2008, **16**, 1407–16.

72 J. Sunayama, F. Tsuruta, N. Masuyama and Y. Gotoh, *J. Cell Biol.*, 2005, **170**, 295–304.

73 J. D. Graves, Y. Gotoh, K. E. Draves, D. Ambrose, D. K. M. Han, M. Wright, J. Chernoff, E. A. Clark and E. G. Krebs, *EMBO J.*, 1998, **17**, 2224–34.

74 B. Shen, L. Chao and J. Chao, *Am. J. Physiol. Heart Circ. Physiol.*, 2010, **298**, H1048-54.

75 L.-O. O. Klotz, C. Sánchez-Ramos, I. Prieto-Arroyo, P. Urbánek, H. Steinbrenner and M. Monsalve, *Redox regulation of FoxO transcription factors*, Elsevier, 2015, vol. 6.

76 T. N. Schachter, T. Shen, Y. Liu and M. F. Schneider, *Am. J. Physiol. Cell Physiol.*, 2012, **303**, C977-90.

77 A. Brunet, L. B. Sweeney, J. F. Sturgill, K. F. Chua, P. L. Greer, Y. Lin, H. Tran, S. E. Ross, R. Mostoslavsky, H. Y. Cohen, L. S. Hu, H.-L. Cheng, M. P. Jedrychowski, S. P. Gygi, D. A. Sinclair, F. W. Alt and M. E. Greenberg, *Science*, 2004, **303**, 2011–5.

78 Y. S. Hori, A. Kuno, R. Hosoda and Y. Horio, *PLoS One*, 2013, **8**, e73875.

79 T. B. Dansen, L. M. M. Smits, M. H. van Triest, P. L. J. de Keizer, D. van Leenen, M. G. Koerkamp, A. Szypowska, A. Meppelink, A. B. Brenkman, J. Yodoi, F. C. P. Holstege and B. M. T. Burgering, *Nat. Chem. Biol.*, 2009, **5**, 664–672.

80 H. Daitoku, M. Hatta, H. Matsuzaki, S. Aratani, T. Ohshima, M. Miyagishi, T. Nakajima and A. Fukamizu, *Proc. Natl. Acad. Sci. U. S. A.*, 2004, **101**, 10042–7.

81 Y. S. Mao, B. Zhang and D. L. Spector, *Trends Genet.*, 2011, **27**, 295–306.

82 H. Matsuzaki, H. Daitoku, M. Hatta, H. Aoyama, K. Yoshimochi, A. Fukamizu and P. K. Vogt, .

83 T. Furuyama, H. Yamashita, K. Kitayama, Y. Higami, I. Shimokawa and N. Mori, *Microsc. Res. Tech.*, 2002, **59**, 331–334.

84 A. van der Horst, B. M. T. Burgering, F. Baluška, A. Hlavacka, D. Volkmann, D. Menzel, Y. S. Hori, A. Kuno, R. Hosoda, Y. Horio, J. W. Hwang, H. Yao, S. Caito, I. K. Sundar, I. Rahman, H. Matsuzaki, H. Daitoku, M. Hatta, K. Tanaka, A. Fukamizu, A. van der Horst, A. M. M. de Vries-Smits, A. B. Brenkman, M. H. van Triest, N. van den Broek, F. Colland, M. M. Maurice, B. M. T. Burgering, F. Seiler, J. Hellberg, P. M. Lepper, A. Kamyschnikow, C. Herr, M. Bischoff, F. Langer, H.-J. Schafers, F. Lammert, M. D. Menger, R. Bals, C. Beisswenger, E. L. Greer, A. Brunet, H. Huang, K. M. Regan, Z. Lou, J. Chen, D. J. Tindall, X. Zhang, N. Tang, T. J. Hadden and A. K. Rishi, *Nat. Cell Biol.*, 2013, **8**, 1064–1073.

85 M. E. Giannakou and L. Partridge, *Trends Cell Biol.*, 2004, **14**, 404–8.

86 E. L. Greer and A. Brunet, *Oncogene*, 2005, **24**, 7410–25.

87 M. C. Motta, N. Divecha, M. Lemieux, C. Kamel, D. Chen, W. Gu, Y. Bultsma, M. McBurney and L. Guarente, *Cell*, 2004, **116**, 551–563.

88 T. F. Liu and C. E. McCall, *Genes Cancer*, 2013, **4**, 135–47.

89 H. Matsuzaki, H. Daitoku, M. Hatta, K. Tanaka and A. Fukamizu, *Insulin*, 2003, **100**, 11285–11290.

90 M. Aoki, H. Jiang and P. K. Vogt, 2004.

91 A. van der Horst, A. M. M. M. de Vries-Smits, A. B. Brenkman, M. H. van Triest, N. van den Broek, F. Colland, M. M. Maurice and B. M. T. T. Burgering, *Nat. Cell Biol.*, 2006, **8**, 1064–73.

92 T. Obsil and V. Obsilova, *Oncogene*, 2008, 27, 2263–2275.

93 Y. Furukawa-Hibi, Y. Kobayashi, C. Chen and N. Motoyama, *Antioxid. Redox Signal.*, 2005, **7**, 752–760.

94 K.-L. Tsai, Y.-J. Sun, C.-Y. Huang, J.-Y. Yang, M.-C. Hung and C.-D. Hsiao, *Nucleic Acids Res.*, 2007, **35**, 6984–94.

95 J. Weigelt, I. Climent, K. Dahlman-Wright and M. Wikström, *Biochemistry*, 2001, **40**, 5861–9.

96 S. C. Martinez, C. Cras-Méneur, E. Bernal-Mizrachi and M. A. Permutt, *Diabetes*, 2006, **55**, 1581–1591.

97 R. S. Streeper, C. A. Svitek, S. Chapman, L. E. Greenbaum, R. Taub and R. M. O'Brien, *J. Biol. Chem.*, 1997, **272**, 11698–701.

98 T. Obsil and V. Obsilova, *Biochim. Biophys. Acta*, 2011, **1813**, 1946–53.

99 E. Boura, J. Silhan, P. Herman, J. Vecer, M. Sulc, J. Teisinger, V. Obsilova and T. Obsil, *J. Biol. Chem.*, 2007, **282**, 8265–75.

100 M. Doucet, A. Dubé, D. R. Joanisse, R. Debigaré, A. Michaud, M.-È. Paré, R. Vaillancourt, E. Fréchette and F. Maltais, *Thorax*, 2010, **65**, 963–70.

101 A. S. Gershon, L. Warner, P. Cascagnette, J. C. Victor and T. To, *Lancet*, 2011, **378**, 991–996.

102 J. Vestbo, S. S. Hurd, A. G. Agustí, P. W. Jones, C. Vogelmeier, A. Anzueto, P. J. Barnes, L. M. Fabbri, F. J. Martinez, M. Nishimura, R. A. Stockley, D. D. Sin and R. Rodriguez-Roisin, *Am. J. Respir. Crit. Care Med.*, 2013, **187**, 347–365.

103 B. Yawn, D. Mannino, T. Littlejohn, G. Ruoff, A. Emmett, I. Raphiou and G. Crater, *Curr. Med. Res. Opin.*, 2009, **25**, 2671–2677.

104 Y. R. Chen, J. M. Leung and D. D. Sin, *PLoS One*, 2016, **11**, e0158843.

105 P. J. Barnes, P. G. J. Burney, E. K. Silverman, B. R. Celli, J. Vestbo, J. A. Wedzicha and E. F. M. Wouters, *Nat. Rev. Dis. Prim.*, 2015, **1**, 15076.

106

107 T. Ingebrigtsen, S. F. Thomsen, J. Vestbo, S. van der Sluis, K. O. Kyvik, E. K. Silverman, M. Svartengren and V. Backer, *Respir. Med.*, 2010, **104**, 1890–5.

108 A. Agusti, M. Decramer, B. Celli, R. Chen, G. Criner, P. Frith, D. Halpin, M. Nishimura, R. Rodriguez-Roisin and C. Vogelmeier, *POCKET GUIDE TO COPD DIAGNOSIS, MANAGEMENT, AND PREVENTION - A Guide for Health Care Professionals*, 2017.

109 D. H. Kim, J. Y. Kim, B. P. Yu and H. Y. Chung, *Biogerontology*, 2008, **9**, 33–47.

110 D. Lee and A. L. Goldberg, *J. Biol. Chem.*, 2013, **288**, 30515–26.

111 S. F. Van Eeden and D. D. Sin, *Can. Respir. J.*, 2013, **20**, 27–29.

112 Y. Nakamaru, C. Vuppusetty, H. Wada, J. C. Milne, M. Ito, C. Rossios, M. Elliot, J. Hogg, S. Kharitonov, H. Goto, J. E. Bemis, P. Elliott, P. J. Barnes and K. Ito, *FASEB J.*, 2009, **23**, 2810–2819.

113 et al. Griffiths AJF, Miller JH, Suzuki DT, *An Introduction to Genetic Analysis. Bacterial conjugation.*, W.H. Freeman, 2000.

114 A. Alimonti, C. Nardella, Z. Chen, J. G. Clohessy, A. Carracedo, L. C. Trotman, K. Cheng, S. Varmeh, S. C. Kozma, G. Thomas, E. Rosivatz, R. Woscholski, F. Cognetti, H. I. Scher and P. P. Pandolfi, *J. Clin. Invest.*, 2010, **120**, 681–93.

115 N. Huang, I. Lee, E. M. Marcotte and M. E. Hurles, *PLoS Genet.*, 2010, **6**, 1–11.

116 J. Nakae, T. Kitamura, Y. Kitamura, W. H. Biggs, K. C. Arden and D. Accili, *Dev. Cell*, 2003, **4**, 119–29.

117 J. Nakae, W. H. Biggs, T. Kitamura, W. K. Cavenee, C. V. E. Wright, K. C. Arden and D. Accili, *Nat. Genet.*, 2002, **32**, 245–253.

118 A. Salehi-Reyhani, J. Kaplinsky, E. Burgin, M. Novakova, A. J. deMello, R. H. Templer, P. Parker, M. a a Neil, O. Ces, P. French, K. R. Willison and D. Klug, *Lab Chip*, 2011, **11**, 1256–61.

119 A. J. Magness, Imperial College London.

120 G. M. Whitesides, *Nature*, 2006, **442**, 368–73.

121 Y. Xia and G. Whitesides, *Annu. Rev. Mater. Sci.*, 1998, **28**, 153–184.

122 B. Huang, H. Wu, D. Bhaya, A. Grossman, S. Granier, B. K. Kobilka and R. N. Zare, *Science*, 2007, **315**, 81–4.

123 A. Khademhosseini, R. Langer, J. Borenstein and J. P. Vacanti, *Proc. Natl. Acad. Sci. U. S. A.*, 2006, **103**, 2480–7.

124 K. Ren, J. Zhou and H. Wu, *Acc. Chem. Res.*, 2013, **46**, 2396–2406.

125 Y. Zheng, W. Dai, D. Ryan and H. Wu, *Biomicrofluidics*, 2010, **4**, 36504.

126 C.-W. Tsao and D. L. DeVoe, *Microfluid. Nanofluidics*, 2008, **6**, 1–16.

127 K. N. Ren, Y. Z. Zheng, W. Dai, D. Ryan, C. Y. Fung and H. K. Wu, 2010, 554–556.

128 M. W. Tibbitt and K. S. Anseth, *Biotechnol. Bioeng.*, 2009, **103**, 655–63.

129 A. W. Martinez, S. T. Phillips, M. J. Butte and G. M. Whitesides, *Angew. Chem. Int. Ed. Engl.*, 2007, **46**, 1318–20.

130 M. Goebel-Stengel, A. Stengel, Y. Taché, J. R. Reeve and Jr., *Anal. Biochem.*, 2011, **414**, 38–46.

131 R. Lamichhane, A. Solem, W. Black and D. Rueda, *Methods*, 2010, **52**, 192–200.

132 X. Zhu and A. Guo, *Funct. Protein Microarrays Drug Discov.*, 2006, 53–72.

133 A. L. Mattheyses, S. M. Simon and J. Z. Rappoport, *J. Cell Sci.*, 2010, **123**, 3621–8.

134 S. Shashkova and M. C. Leake, *Biosci. Rep.*, 2017, **37**.

135 G. V. Casquillas, *Elveflow*.

136 J. A. Squires, 2017.

137 U. Sauer, *Methods Mol. Biol.*, 2011, **785**.

138 R. Wacker, H. Schröder and C. M. Niemeyer, *Anal. Biochem.*, 2004, **330**, 281–7.

139 M. Fuentes, B. C. C. Pessela, J. V Maquiese, C. Ortiz, R. L. Segura, J. M. Palomo, O. Abian, R. Torres, C. Mateo, R. Fernández-Lafuente and J. M. Guisán, *Biotechnol. Prog.*, 2004, **20**, 1134–9.

140 E. Michelini, L. Cevenini, L. Mezzanotte, A. Coppa and A. Roda, *Anal. Bioanal. Chem.*, 2010, **398**, 227–38.

141 F. Diehl, S. Grahlmann, M. Beier and J. D. Hoheisel, *Nucleic Acids Res.*, 2001, **29**, E38.

142 P. R. T. Jess, V. Garcés-Chávez, D. Smith, M. Mazilu, L. Paterson, a Riches, C. S. Herrington, W. Sibbett and K. Dholakia, *Opt. Express*, 2006, **14**, 5779–91.

143 A. Ashkin and J. Dziedzic, *Science (80-.).*, 1987, **235**, 1517–1520.

144 K. R. Rau, P. a Quinto-Su, A. N. Hellman and V. Venugopalan, *Biophys. J.*, 2006, **91**, 317–29.

145 V. Ho, *Making cell microscopy quantitative by creating a secondary standard BSc Chemistry*, London, 2016.

146 A. Herbert, .

147 D. G. Altman, M. Altman and J. M. Bland, *BMJ Br. Med. J. Br. Med. J. BMJ*, 1995, **310**, 29828–3317.

148 P. J. Barnes, *J. Allergy Clin. Immunol.*, 2016, **138**, 16–27.

149 V. M. Keatings, D. J. Evans, B. J. O'Connor and P. J. Barnes, *Thorax*, 1997, **52**, 372–374.

150 S. D. H. Chan, G. Luedke, M. Valer, C. Buhlmann and T. Preckel, *Cytometry. A*, 2003, **55**, 119–25.

151 M. J. Holtzman, D. E. Byers, J. Alexander-Brett and X. Wang, *Nat. Rev. Immunol.*, 2014, **14**,

686–698.

152 P. Saviranta, R. Okon, A. Brinker, M. Warashina, J. Eppinger and B. H. Geierstanger, *Clin. Chem.*, 2004, **50**, 1907–20.

153 P. Peluso, D. S. Wilson, D. Do, H. Tran, M. Venkatasubbaiah, D. Quincy, B. Heidecker, K. Poindexter, N. Tolani, M. Phelan, K. Witte, L. S. Jung, P. Wagner and S. Nock, *Anal. Biochem.*, 2003, **312**, 113–24.

154 M. F. Berger and M. L. Bulyk, *Nat. Protoc.*, 2009, **4**, 393–411.

155 R. Wacker and C. M. Niemeyer, *Chembiochem*, 2004, **5**, 453–9.

156 M. Kimoto, R. Yamashige, K. Matsunaga, S. Yokoyama and I. Hirao, *Nat. Biotechnol.*, 2013, **31**, 453–7.

157 R. Bailey and G. Kwong, *J. Am. Chem. Soc.*, 2007, **129**, 1959–1967.

158 M. L. Bulyk, X. Huang, Y. Choo and G. M. Church, *Proc. Natl. Acad. Sci. U. S. A.*, 2001, **98**, 7158–63.

159 Y. Zhao, W. Shao, H. Wei, J. Qiao, Y. Lu, Y. Sun, K. Mitchelson, J. Cheng and Y. Zhou, *J. Proteome Res.*, 2008, **7**, 1315–25.

160 D. Juncker, P.-S. Lo, H. Li, V. Laforte and S. Bergeron, *Anal. Bioanal. Chem.*, 2015, **407**, 8451–8462.

161 H. F. Liu, J. Ma, C. Winter and R. Bayer, *MAbs*, 2010, 2, 480–499.

162 W. Liu, S. Wang, L. Gao, F. Zhang and J. Xu, *J. Chem. Inf. Comput. Sci.*, 2003, **43**, 2014–2018.

163 C. C. Chou, C. H. Chen, T. T. Lee and K. Peck, *Nucleic Acids Res.*, 2004, **32**, e99.

164 R. M. Simon, *Design and analysis of DNA microarray investigations*, Springer, 2003.

165 A. Sidhu, P. Miller, K. Johanson and A. Hollenbach, *Biochemistry*, 2008, 6809–6818.

166 A. M. Sochaj, K. W. Świderska and J. Otlewski, *Biotechnol. Adv.*, 2015, 33, 775–784.

167 D. Di Carlo, L. Y. Wu and L. P. Lee, *Lab Chip*, 2006, **6**, 1445–9.

168 C.-P. Jen, J.-H. Hsiao and N. a Maslov, *Sensors (Basel).*, 2012, **12**, 347–58.

169 M. Berrar, Daniel P., Dubitzky, Werner, Granzow, *A Practical Approach to Microarray Data Analysis*, 2003.

170 E. Berglund, C. Borrebaeck, P. Delfani, A. Gerdtsson, L. Dexlin-Mellby and C. Wingren, *Microarrays*, 2016, **5**, 16.

171 J. E. Lee, J. H. Seo, C. S. Kim, Y. Kwon, J. H. Ha, S. S. Choi and H. J. Cha, *Korean J. Chem. Eng.*, 2013, **30**, 1934–1938.

172 A. Makaraviciute and A. Ramanaviciene, *Biosens. Bioelectron.*, 2013, **50**, 460–71.

173 B. Hua, K. Y. Han, R. Zhou, H. Kim, X. Shi, S. C. Abeysirigunawardena, A. Jain, D. Singh, V. Aggarwal, S. A. Woodson and T. Ha, *Nat. Methods*, 2014, **11**, 1233–1236.

174 P. Pollheimer, B. Taskinen, A. Scherfler, S. Gusenkov, M. Creus, P. Wiesauer, D. Zauner, W. Schöfberger, C. Schwarzinger, A. Ebner, R. Tampé, H. Stutz, V. P. Hytönen and H. J. Gruber, *Bioconjug. Chem.*, 2013, **24**, 1656–68.

175 J. M. Baskin, J. A. Prescher, S. T. Laughlin, N. J. Agard, P. V Chang, I. A. Miller, A. Lo, J. A. Codelli and C. R. Bertozzi, *Proc. Natl. Acad. Sci.*, 2007, **104**, 16793–16797.

176 N. J. Agard, J. M. Baskin, J. A. Prescher, A. Lo and C. R. Bertozzi, *ACS Chem. Biol.*, 2006, 1, 644–648.

177 S. a Omori, M. H. Cato, A. Anzelon-Mills, K. D. Puri, M. Shapiro-Shelef, K. Calame and R. C. Rickert, *Immunity*, 2006, **25**, 545–57.

178 A. Bilancio, K. Okkenhaug, M. Camps, J. L. Emery, T. Ruckle, C. Rommel and B. Vanhaesebroeck, *Blood*, 2006, **107**, 642–50.

179 H. S. Dengler, G. V Baracho, S. A. Omori, S. Bruckner, K. C. Arden, D. H. Castrillon, R. A. DePinho and R. C. Rickert, *Nat. Immunol.*, 2008, **9**, 1388–1398.

180 S. Furukawa, L. Wei, S. M. Krams, C. O. Esquivel and O. M. Martinez, *Am. J. Transplant*, 2013, **13**, 2035–43.

181

182 A. M. Shore, P. C. White, R. C.-Y. Hui, A. Essafi, E. W.-F. Lam, M. Rowe and P. Brennan, *J. Virol.*, 2006, **80**, 11191–11199.

183 E. Lakatos, A. Salehi-Reyhani, M. Barclay, M. P. H. Stumpf and D. R. Klug, *PLoS One*, 2017, **12**.

184 D. Kong and T. Yamori, *Cancer Sci.*, 2007, **98**, 1638–1642.

185 S. I. Yaguchi, Y. Fukui, I. Koshimizu, H. Yoshimi, T. Matsuno, H. Gouda, S. Hirono, K. Yamazaki and T. Yamori, *J. Natl. Cancer Inst.*, 2006, **98**, 545–556.

186 P. S. Swain, M. B. Elowitz and E. D. Siggia, *Proc. Natl. Acad. Sci. U. S. A.*, 2002, **99**, 12795–800.

187 M. Soltani, C. A. Vargas-Garcia, D. Antunes and A. Singh, *PLOS Comput. Biol.*, 2016, **12**, e1004972.

188 A. D. Kohn, S. A. Summers, M. J. Birnbaum and R. A. Roth, *J. Biol. Chem.*, 1996, **271**, 31372–8.

189 R. L. Elstrom, D. E. Bauer, M. Buzzai, R. Karnauskas, M. H. Harris, D. R. Plas, H. Zhuang, R. M. Cinalli, A. Alavi, C. M. Rudin and C. B. Thompson, *Cancer Res.*, 2004, **61**, 7349–7355.

190 R. B. Robey and N. Hay, *Semin. Cancer Biol.*, 2009, **19**, 25–31.

191 D.-I. Kim, S.-K. Lim, M.-J. Park, H.-J. Han, G.-Y. Kim and S. H. Park, *Life Sci.*, 2007, **80**, 626–632.

192 J. F. Clarke, P. W. Young, K. Yonezawa, M. Kasuga and G. D. Holman, *Biochem. J.*, 1994, **300 (Pt 3)**, 631–5.

193 A. Barthel, S. T. Okino, J. Liao, K. Nakatani, J. Li, J. P. Whitlock and R. A. Roth, *J. Biol. Chem.*, 1999, **274**, 20281–6.

194 S. Miyamoto, A. N. Murphy and J. H. Brown, *Cell Death Differ.*, 2008, **15**, 521–529.

195 F. Das, N. Ghosh-Choudhury, N. Dey, A. Bera, M. M. Mariappan, B. S. Kasinath and G. Ghosh Choudhury, *J. Biol. Chem.*, 2014, **289**, 32703–16.

196 E. J. Williams and P. Doherty, *Mol. Cell. Neurosci.*, 1999, **13**, 272–80.

197 G. L. G. L. Rosano and E. A. Ceccarelli, *Recombinant protein expression in Escherichia coli: Advances and challenges*, Frontiers Media SA, 2014, vol. 5.

198 L. A. Palomares, S. Estrada-Mondaca and O. T. Ramírez, in *Recombinant Gene Expression*, Humana Press, New Jersey, 2004, pp. 015–052.

199 A. Vera, N. González-Montalbán, A. Arís and A. Villaverde, *Biotechnol. Bioeng.*, 2007, **96**, 1101–1106.

200 G. L. Rosano and E. A. Ceccarelli, *Front. Microbiol.*, 2014, **5**, 172.

201 M. Putker, H. Vos, K. Van Dorenmalen, H. De Ruiter, A. G. A. G. Duran, B. Snel, B. M. B. M. T. Burgering, M. Vermeulen and T. B. B. Dansen, *Antioxid. Redox Signal.*, 2014, **22**, 15–28.

202 C. Holohan, S. Van Schaeybroeck, D. B. Longley and P. G. Johnston, *Nat. Rev. Cancer*, 2013, **13**, 714–726.

203 H. D. Soule, J. Vazquez, A. Long, S. Albert and M. Brennan, *J. Natl. Cancer Inst.*, 1973, **51**, 1409–1413.

204 R. L. Dillon, D. E. White and W. J. Muller, *Oncogene*, 2007, **26**, 1338–1345.

205 O. Padovan-Merhar, G. P. Nair, A. G. Biaesch, A. Mayer, S. Scarfone, S. W. Foley, A. R. Wu, L. S. Churchman, A. Singh and A. Raj, *Mol. Cell*, 2015, **58**, 339–352.

206 M. Yamamoto, N. A. Patel, J. Taggart, R. Sridhar and D. R. Cooper, *Int. J. Cancer*, 1999, **83**, 98–106.

207 F. Zhao and W. T. Klimecki, *J. Appl. Toxicol.*, 2015, **35**, 945–951.

208 R. R. Reddel, Y. Ke, B. I. Gerwin, M. G. McMenamin, J. F. Lechner, R. T. Su, D. E. Brash, J. B. Park, J. S. Rhim and C. C. Harris, *Cancer Res.*, 1988, **48**, 1904–1909.

209 P. H. Michelson, M. Tigue, R. J. Panos and P. H. Sporn, *Am. J. Physiol.*, 1999, **277**, L737–L742.

210 S. D. Jayasena, *Clin. Chem.*, 1998, **44**, 86–91.

211 A. Chen and S. Yang, *Biosens. Bioelectron.*, 2015, 71, 230–242.

212 Y. L. Jeyachandran, J. A. Mielczarski, E. Mielczarski and B. Rai, *J. Colloid Interface Sci.*, 2010, **341**, 136–142.

213 A. Klug, *Annu. Rev. Biochem*, 2010, **79**, 213–31.

214 C. Sissi and M. Palumbo, *Nucleic Acids Res.*, 2009, **37**, 702–711.

215 G. Gould and A. Pearce, *Contin. Educ. Anaesth. Crit. Care Pain*, 2006, **6**, 97–100.

216 R. G. Tieleman, Y. Plantinga, D. Rinkes, G. L. Bartels, J. L. Posma, R. Cator, C. Hofman and R. P. Houben, *Europace*, 2014, **16**, 1291–5.

217 J. Durán-Cantolla, G. Zamora Almeida, O. Vegas Diaz de Guereñu, L. Saracho Rotaeche, M. Hamdan Alkhraisat, J. Durán Carro, C. Egea Santaolalla and E. Anitua, *Respirology*, 2017, **22**, 378–385.

218 S. Ganesan, B. L. Unger, A. T. Comstock, K. a Angel, P. Mancuso, F. J. Martinez and U. S. Sajjan, *Thorax*, 2013, **68**, 131–41.

219 D. G. Altman and J. M. Bland, *BMJ*, 2005, **331**, 903.

220 S. Bozinovski, R. Vlahos, M. Hansen, K. Liu and G. P. Anderson, *Int. J. COPD*, 2006, **1**, 31–38.

221 F. Seiler, J. Hellberg, P. M. Lepper, A. Kamyschnikow, C. Herr, M. Bischoff, F. Langer, H.-J. Schafers, F. Lammert, M. D. Menger, R. Bals, C. Beisswenger, H.-J. Schäfers, F. Lammert, M. D. Menger, R. Bals and C. Beisswenger, *J. Immunol.*, 2013, **190**, 1603–13.

222 S. A. McCarroll and D. M. Altshuler, *Nat. Genet.*, 2007, **39**, S37–S42.

223 J. S. Beckmann, X. Estivill and S. E. Antonarakis, *Nat. Rev. Genet.*, 2007, **8**, 639–646.

224 L. W. MATTHEWS, S. SPECTOR, J. LEMM and J. L. POTTER, *Am. Rev. Respir. Dis.*, 1963, **88**, 199–204.

225 M. T. Lopez-Vidriero, I. Das and L. Reid, *Thorax*, 1979, **34**, 512–517.

226 A. Bhowmik, T. A. Seemungal, R. J. Sapsford, J. L. Devalia and J. A. Wedzicha, *Thorax*, 1998, **53**, 953–6.

227 I. Pin, P. G. Gibson, R. Kolendowicz, A. Girgis-Gabardo, J. A. Denburg, F. E. Hargreave and J. Dolovich, *Thorax*, 1992, **47**, 25–29.

228 R. LOUIS, L. C. K. LAU, A. O. BRON, A. C. ROLDAAN, M. RADERMECKER and R. DJUKANOVIĆ, *Am. J. Respir. Crit. Care Med.*, 2000, **161**, 9–16.

229 P. Lacy, J. L. Lee and D. Vethanayagam, *Ther. Clin. Risk Manag.*, 2005, **1**, 169–79.

230 A. Bhowmik, T. A. Seemungal, R. J. Sapsford and J. A. Wedzicha, *Thorax*, 2000, **55**, 114–20.

231 I. I. Katkov and P. Mazur, *Cell Biochem. Biophys.*, 1999, **31**, 231–245.

232 I. H. Kim, J. D. Yang, D. G. Lee, H. Y. Chung and B. C. Cho, *Aesthetic Surg. J.*, 2009, **29**, 35–39.

233 K. Tatsutani, B. Rubinsky, G. Onik and R. Dahiya, *Urology*, 1996, **48**, 441–447.

234 S. M. Hedrick, R. H. Michelini, A. L. Doedens, A. W. Goldrath and E. L. Stone, *Nat. Rev. Immunol.*, 2012, **12**, 649–661.

235 P. J. Barnes and M. G. Cosio, *PLoS Med*, 2004, **1**, e20.

236 M. C.-T. Hu, D.-F. Lee, W. Xia, L. S. Golfman, F. Ou-Yang, J.-Y. Yang, Y. Zou, S. Bao, N. Hanada, H. Saso, R. Kobayashi and M.-C. Hung, *Cell*, 2004, **117**, 225–37.

237 R. G. Crystal, S. H. Randell, J. F. Engelhardt, J. Voynow and M. E. Sunday, *Proc. Am. Thorac. Soc.*, 2008, **5**, 772–777.

238 Q. Qiu, N. W. Todd, R. Li, H. Peng, Z. Liu, H. G. Yfantis, R. L. Katz, S. A. Stass and F. Jiang, *Cancer*, 2008, **114**, 275–83.

239 J. BELDA, R. LEIGH, K. PARAMESWARAN, P. M. O'BYRNE, M. R. SEARS and F. E. HARGREAVE, *Am. J. Respir. Crit. Care Med.*, 2000, **161**, 475–478.

240 S. H. Randell, *Proc. Am. Thorac. Soc.*, 2006, **3**, 718–725.

11 Appendix:

11.1 Antibody and DNA Capture Agents Sequences

Table 11.1 Tables detailing the vendors of the tested antibodies and the sequences of the oligonucleotide capture agents.

ASSAY REAGENTS	VENDOR
DNA CAPTURE AGENTS (PRE-ANNEALED, HPLC PURIFIED)	IDT DNA
FOXO1 (DU 1071)	MRC Pure Reagents
HUMAN FOXO1/FKHR ANTIBODY MAB5939	R&D Systems
ANTI-FOXO1A ANTIBODY (AB111029)	AbCam
ANTI-FOXO1A [EP927Y] ANTIBODY (AB52857)	AbCam
ANTI-FOXO1A ANTIBODY (AB150059)	AbCam
ANTI-FOXO1A ANTIBODY [3B6] (AB126826)	AbCam
ANTI-FOXO1A [EPR12020] ANTIBODY (AB179450)	AbCam

ANTI-FOXO1A ANTIBODY (AB89433)	AbCam
ANTI-FOXO1A ANTIBODY (AB1102)	AbCam
ANTI-FOXO1A ANTIBODY (AB131206)	AbCam
ANTI-FOXO1A ANTIBODY (AB12161)	AbCam
HUMAN FOXO1/FKHR MAB (CLONE 597554)	Novus Bio
FOXO1 (C29H4) RABBIT MAB #2880	Cell Signalling Technologies
FOXO1 (C29H4) RABBIT MAB #2891	Cell Signalling Technologies
FKHR ANTIBODY (C-9): SC-374427	Santa Cruz

OLIGONUCLEOTIDE LABEL	SEQUENCE
FOXO CAPTURE AGENT 1 (CA1)	TGGGTAAACAACAACATGTTGACATCGCGG
FOXO CAPTURE AGENT 2 (CA2)	AGCGGTGGAGGCCTGTGTCCTTTTTGTTTACATTTTG
FOXO CAPTURE AGENT 3 (CA3)	TGGTGTTGACACAACAGTAAACAATCGCGG
FOXO CAPTURE AGENT 4 (CA4)	TGGTGTTGACACAGCAGTAAACAATTGCGG
FOXO CAPTURE AGENT 5 (CA5)	TGGGTAAACATCAGCAGTAAACAATCTCGG
FOXO CAPTURE AGENT 6 (CA6)	CGCGCGAGCGGTGTCCTTGTTTACATTTTG
FOXO CAPTURE AGENT 7 (CA7)	CGCGCGACGGTGCCTTGTTTACATTTTGC
FOXO CAPTURE AGENT 8 (CA8)	CGCGCGACGGTGCCTTGTTTACATTTTGTT
FOXO CAPTURE AGENT 9 (CA9)	AGCGGAGGCCAGGCCTGCTTGTTTACATTTTG

11.2 Western Blots

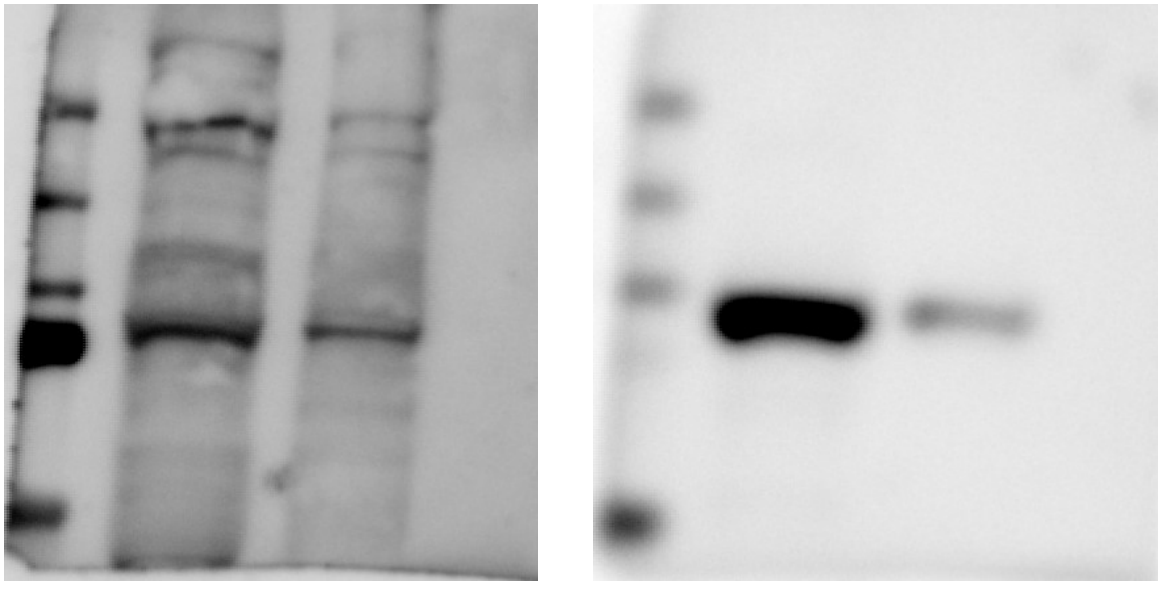


Figure 11.1 Western blots for the two most used antibodies in this project. The left figure shows the Capture antibody, mAb5939 and the right figure shows the secondary detection antibody, EP927Y. Both were run against with a Toledo cell lysate with the middle band being the pure undiluted lysate and the far-right band from a 5x dilution of the Toledo lysate.

11.3 Origin Overlap Function

The origin plugin can be found license free at:

https://www.originlab.com/fileExchange/details.aspx?fid=371